ZANCO Journal of Pure and Applied Sciences
The official scientific journal of Salahaddin University-Erbil
https://zancojournals.su.edu.krd/index.php/JPAS

ISSN (print):2218-0230**, ISSN (online):** 2412-3986**, DOI: http://dx.doi.org/10.21271/zjpas**

RESEARCH PAPER

Allelopathy Index: a new mathematical assessment method for allelopathy studies

Kawa A. Ali

Agricultural Engineering Sciences College,Salahaddin University- Erbil,Kurdistan Region, Iraq

A B S T R A C T:

A lab bioassay was conducted in Agricultural Engineering Sciences College labs to study the allelopathic influence of wild oat (***Avena fatua* L**.) different plant parts shoot, root and seeds aqueous extracts with five concentrations (0, 25%, 50%, 75% and 100%) on three plant species Lettuce, Onion and Tomato seeds. Results indicated significant effect on all studied data, germination percentage, inhibition of germination, radicle length (cm); plumule length(cm); radicle dry weight, plumule dry weight; total seedlings dry weight (mg); radicle and plumule growth inhibition. The best bioassay plant was lettuce seeds for using as indicator in allelopathy studies. The main goal of the study was proposing five mathematical equations to indicate allelopathy index, the best two equations were chosen according to their best manipulation and demonstration based on total seedlings dry weight.

KEY WORDS: Allelopathy Index, Concentration dependent, Mathematical Equations.
DOI: http://dx.doi.org/10.21271/ZJPAS.33.2.1
ZJPAS (2021) , 33(1);1-18 .

1.INTRODUCTION:

Interference between plants divided to two ecological phenomenon competition and allelopathy, the first takes place for environmental resources such as light, nutrient, moisture and space, while in allelopathy phenomenon donor plants excrete chemicals to suppress the growth of plants in vicinity (Ali, 2001). There are many studies that tried to separate between both phenomenon's that may influence plant life either by reducing essential growth needs or by producing chemical compounds that finally both alter the recipient plant metabolism and growth (Fernandez et al., 2016, He et al., 2012, Ali and Sakri, 2010).

Allelopathy interactions may include both harmful or beneficial biochemical relationship between plants and surrounding organisms (Dias et al., 2017).

Plants are non-motile creatures so they developed the ability to adapt their environmental fluctuation periods through different techniques. Plant plasticity which, is defined as (plants ability to adapt to or cope with changes in its environment), it is one of the methods that plants pursued to face their macro and micro environment changes (Karban, 2008). Plants have acquired the capability of biosynthesizing different bioactive natural compounds with definite role to withstand unfavorable environmental challenges (Agrawal et al., 2002, Ali and Aziz, 2002).

The considerable progress of allelopathy studies in different aspects such as crop production, weed management and the importance of sustainable agriculture leads to a huge improvement in food production and it minimizes the environmental damages by establishing eco-friendly agricultural systems (An et al., 2008). Different bioassay techniques were used in allelopathy researches to indicate the effect of different levels of concentration of either water (aqueous) or alcoholic extract of different plant parts (seed, shoot and root) on some selected plant seeds, then quantitative parameters will be recorded to

* **Corresponding Author:**
Kawa A. Ali
E-mail: Kawa.ali@su.edu.krd.
Article History:
Received: 28/05/2020
Accepted: 24/10/2020
Published: 18/04 /2021

interpret the situation, most times the effect may be concentration dependent while some times it will be stimuli in low concentrations and inhibitor in high concentrations or vis versa (Ercoli et al., 2007, Rejila and Vijayakumar, 2011).

Analysis and interpretation of allelopathy studies focuses on plants chemical interaction of donor plant on recipient plant through different characteristics parameters, many attempts had been carried out to present or suggest mathematical models for data manipulation in order to clarify allelopathical effects (An et al., 2002, An et al., 2008, Liu et al., 2003, Pal et al., 2009, Liu et al., 2011, Williamson and Richardson, 1988). Mathematical equations were presented to illustrate the allelopathic effects on recipient plants depending on stimulation and inhabitation effects according to extract concentration as in equation (1) which were proposed by (An et al., 1993) where p is the biological response to the allelochemical and S is the stimulatory or I the inhibitory effect. There was also an attempt to indicate the effect of an allelochemical in the environment as in equation (2) depending on the system of production , transformation and decomposition of allelochemicals (An et al., 2003) where AE is the amount of the allelochemical in the environment and K1 is the rate of allelochemicals release per day and K2 is the rate constant of an allelochemical degradation per day.

$$\boldsymbol{P = 100 + S - I} \qquad \ldots\ldots\ldots(\mathbf{1})$$

$$\mathbf{AE} = \frac{\mathbf{K1\ f\ (t)}}{\mathbf{K2 - K1}}\left(\mathbf{e^{-K1\ t} - e^{-K2\ t}}\right) \qquad \textbf{..... (2)}$$

(Liu et al., 2003) proposed a new mathematical equation based on the relationship between the allelochemical dose and the response of the recipient organism and they assumed that the response will be non-linear as in equation (3) where E(D) is the effect of allelochemical, D is the dose, R is the response and RC is the response in control treatments.

$$\boldsymbol{R = RC + E(D)} \qquad \ldots\ldots\ldots\ldots(\mathbf{3})$$

In this study, some mathematical equations will be presented on the base that allelopathy is regarded as abiotic environmental stress where the donor plant alters the target plants growth and development by producing allelochemical compounds (Pedrol et al., 2006). Data from this work and other papers will be analyzed to suggest the most suitable equation for allelopathy studies to indicate the best allelopathy index. Our proposed equations were based on seedling's dry weight which we think, is the most reliable data for plant growth. We could estimate allelopathy index (AI) on recipient plants as in equation (4) where (DWc) is the dry weight of control treatments, (DWt) is dry weight of treatment. Also allelopathy index (AI) could be estimated according to equation (5) or (6) where (DWgm) is the mean dry weight for all treatments or as in equation (7) and (8) where SDWt is seedlings dry weight in treatment and SDWc is the seedlings dry weight in control. Another equation will be proposed in this study according to the linear relationship between the extract concentration and the response of the recipient plant (8) where (ymax) is y when C = 0, while Co is C at which y=0 and b can be estimated according to the slope of the relative ship between ln (y/ymax) on ordinate and ln (1-Co/C) on abcissia.

$$\mathbf{AS} = \mathbf{DWc - DWt} \qquad \ldots\ldots\ldots\ldots(\mathbf{4})$$

$$\mathbf{AI} = \mathbf{1} - \left(\frac{\mathbf{DWc - DWt}}{\mathbf{DWgm}}\right) \qquad \ldots\ldots\ldots\ldots\ldots(\mathbf{5})$$

$$\mathbf{AI} = \left(\frac{\mathbf{1} - \left(\frac{\mathbf{DWt}}{\mathbf{DWc}}\right)}{\mathbf{1} - \left(\frac{\mathbf{DWmt}}{\mathbf{DWmc}}\right)} \right) \quad \ldots\ldots\ldots\ldots (6)$$

$$\boldsymbol{AI} = \left(\mathbf{1} - \frac{\boldsymbol{SDWt}}{\boldsymbol{SDWc}}\right) \times \mathbf{100} \quad \ldots\ldots\ldots\ldots (7)$$

$$\boldsymbol{AI} = \boldsymbol{ymax}\left(\mathbf{1} - \frac{\boldsymbol{C}}{\boldsymbol{Co}}\right)^{\boldsymbol{b}} \quad \ldots\ldots\ldots\ldots (8)$$

The selected donor plant for this study was wild oat (***Avena fatua*** L.) which was previously reported to cause allelopathic effect on recipient plants (Schumacher et al., 1983, Fragasso et al., 2012, Fay and Duke, 1977). The main goal of the study is proposing five mathematical equations to indicate the best interpretation for allelopathy index.

2.MATERIALS AND METHODS:

The study consists of a completely randomized factorial experiment of three treatments with three replications, first three recipient plant species of recipient plants (Lettuce, Tomato and Onion), second three wild oat plant parts aqueous extract (shoot, root and seeds), third five extract concentration levels (zero, 25, 50, 75 and 100%) zero concentration was considered as control.

2.1Plant Samples: Wild oat plants were collected from the grdarasha field of agricultural engineering sciences college during 2017-2018 agricultural season and separated to three parts (Root, shoot and seeds). First plant parts were cut to small 2-3cm peace's, next it was air dried in a shade place, then it was milled by electrical mill finally it was kept in dark plastic jars and put in () cooler machine -20°C till use.

2.2 Extract Preparation: first 10g of wild oat plant parts and 100ml of distilled water were put in dark bottles, next the bottles were placed in a shaker 120RPM for 24 hours. Then the aqueous solutions passed through four layers of cheese-cloth after that it was filtered by whatman filter paper #1. The final extract aqueous extract was considered as (100 % crude solution), finally different concentrations were prepared as 25, 50, 75 and 100% from the crude extract by adding distilled water, while distilled water was considered as control treatment (Sisodia and Siddiqui, 2010, Ali and Maulood, 2011, Ali et al., 2012).

2.3 Bioassay: seeds of Lattuce (*Lactuca sativa* L.), tomato (*Solanum lycopersicum* L.) and Onion (*Allium cepa* L.) were selected for this study due to their sensitivity and use in plant hormone bioassays (Macías et al., 2000, Sampietro, 2009). First twenty-five seeds of each species were placed between two sheets of whatman filter paper #1 in 9 cm petri-dishes next 8ml of the studied concentrations of aqueous extracts of three wild oat plant parts (shoot, root and seeds) were added to each petri-dish, then each petri-dish were sealed with para-film and placed in a growth chamber under 22 -24°C. finally the experiment was finished after 10 days where seedlings were collected.

2.4 Recorded Data: The recording data were germination rate; radicle length (cm); radicle dry weight (g); plumule length(cm); plumule dry weight (g); seedlings dry weight (mg), inhibition of germination, radicle and plumule growth inhibition measured according to equations shown below (Oliveira et al., 2013, Norsworthy, 2003, Jiang and Lafitte, 2007, Ali and Aziz, 2002).

$$\textbf{Germination } \% = \frac{GS}{TTS} \times 100 \quad \text{..... (9)}$$

$$\textbf{IOG } \% = \frac{GPC - GPT}{GPC} \times 100 \quad \text{... ... . (10)}$$

$$\textbf{RGI or PGI } \% = \left(1 - \frac{WUS}{WNS}\right) \times 100 \quad \text{... ... ... (11)}$$

Where GS = germinated seeds, TTS = Total tested seeds, IOG= Inhibition of germination, GPC= germination percentage of control, GPT= germination percentage of treatment, RGI= radicle growth inhibition, PGI= plumule growth inhibition, WUS= dry weight under stress, WNS= dry weight under non stress conditions.

2.5 Allelopathy Index Equations: proposed equations (4), (5), (6), (7) and (8) were used for indicating the most suitable mathematical equation for studying allelopathical plant relationships.

2.6 Statistical Analysis: all recorded data were subjected to standard analysis of variance and means were compared using Duncan Multiple Range Test (DMRT) at 5% of probability using SPSS computer analysis version (Field, 2013, Weinberg and Abramowitz, 2008).

3. RESULTS AND DISCUSSION

Results of this study could divided to the three main factors and the interactions between them as will be summarized below.

3.1. The effect of tested plant species on germination and some seedling growth characteristics: Table (1) indicates the significant effect of aqueous extracts of wild oat on all recorded data of the three tested plant species in this study. Whereas the highest germination percentage, Plumule and radicle length, Plumule, radical and total dry weight were 95%, 3.81cm, 2.83 cm 1.24g ,0.66 g, 1.91g respectively were recorded with tomato seedlings and the lowest data for mentioned characteristics were recorded for lettuce plants in germination percentage, radicle length, radicle and total dry weight 83.56%, 0.78cm, 0.07g and 0.51g respectively, while onion seedling where at lowest levels for Plumule length and Plumule dry weight 3.08cm and 0.42 g respectively. Data of inhibition of germination, Plumule and radicle growth inhibition indicates the significant differences between the three plant species response to the aqueous extracts of wild oat whereas for inhibition of germination the highest value was 16.44% with lettuce seedlings and the lowest was 4.27% in tomato seeds, while highest data of Plumule and radicle growth inhibition were recorded with tomato seedlings 25.44% and 72.89% respectively, but the lowest data values for both was recoded with lettuce seedlings. This disparity between studied plants species response may be shown because of their genetic variation (Abd-ElGawad et al., 2020, Ali, 2016).

3.2. The Effect of Plant Parts Aqueous Extracts on Germination and Some Seedling Growth Characteristics: The effect of shoot, root and seeds aqueous extracts of wild oat cased significant differences on all recorded data except data of roots dry weight (table- 2). The highest values for germination percentage, Plumule and radicle length, Plumule and total seedling dry weight were 95.02%, 4.62(cm), 2.37(cm), 0.77(g) and 1.05(g) respectively which were observed with root aqueous extracts. Lowest data for germination percentage 84.89% was observed with shoot aqueous extracts. Lowest levels for Plumule and radicle length, Plumule and total dry weight were 2.20 (cm), 0.99(cm), 0.60 (g) and 0.85 (g) respectively reported with seeds aqueous extracts of wild oat.

Inhibition of germination was at highest level with shoot extracts 15.11% and lowest data was 4.98 % recorded with root extracts. Records of Plumule and radicle growth inhibition where at the pick 32.12 % and 66.29% respectively with seeds aqueous extracts and at their minimum levels 4.63% of Plumule growth inhibition under the impact of root extracts and 54.92% for radicle growth inhibition treated with shoot extracts. It seems that shoot plant parts had stronger allelopathic impact comparing to both root and seeds extracts which may be due to its high content of phytochemical compounds which may be photosynthesis byproducts which may kept in cell as compartments or stored in cell vacuoles (Kamal, 2011, Sodaeizadeh et al., 2009).

3.3. The Effect of Aqueous Extracts Concentration levels on Germination and Some Seedling Growth Characteristics: Table-3 indicates the significant effect of concentration levels on all recorded data, highest values for germination percentage, plumule and radicle length, plumule, radicle and total dry weight were 99.85%, 5.40(cm), 3.20(cm), 0.90 (g), 0.96(g) and 1.86 (g) respectively where observed with control treatments. Lowest records were observed with the highest concentration level 100% these data declare the concentration dependent allelopathic effect for aqueous extracts (Ali, 2016, Ali and Aziz, 2002). Data of inhibition of germination, plumule growth inhibition, radicle growth inhibition where in harmony with concentration levels which means they were in lowest levels in control treatments, while they were elevated with highest concentration levels in this study. The phenomenon of utmost impact with higher concenrtation may be due to accumulation of allelochemicals in higher extract concentrations as indicated by (El-Rokiek and Eid, 2009, Bing-Yao et al., 2006).

3.4. The Combination Effect of Tested Plant Species and Wild Oat Plant Part Aqueous Extracts on Germination and Some Seedling Growth Characteristics: The effect of interaction of plant species and extract parts significantly affected all recorded data except radicle dry weight (Table-4). The maximum value for germination percentage was 98.40% in tomato seeds treated with wild oat seed extracts, while minimum value was 73.33% when lettuce seeds treated with wild oat seeds extracts. The peak data of plumule length were (5.12 cm) observed in two sets in tomato seedlings treated with wild oat root extracts and onion seedlings treated with root extracts, while the least value was 1.64 (cm) when onion seedling that was treated with wild oat seed extracts. Tomato seeds when treated with wild oat root extracts had longer radicle length 4.71 (cm) but when lettuce seeds treated with shoot extracts it resulted the shortest radicle length 0.57 (cm). plumule and seedlings total dry weight were at highest levels 1.42 (g) and 2.13(g) respectively when tomato seeds treated with wild oat shoot extracts, while lowest values 0.29 (g) and 0.37 (g) respectively by treating onion seeds with wild oat seed extracts. Inhibition of germination was at highest level 26.67% in lettuce seeds which treated with wild oat seed extracts and in lowest level 3.47% when onion seeds treated with wild oat seed extracts. Records of Plumule and radicle growth inhibition where at the peak 47.30 % and 70.86 % respectively with onion seeds treated with wild oat seed aqueous extracts and at their minimum levels -16.60 % for Plumule growth inhibition when onion seeds treated with wild oat root extracts and 44.41% for radicle growth inhibition for lettuce seeds which treated with wild oat shoot extracts. The goal of studying this combination effect is to indicated the most sensitive plant species that bioassayed under the impact of different wild oat plant part aqueous extractions, it was obvious that genetic variation was the main cause for bioassayed test plants sensitivity to different wild oat plant part extracts and the allelochemical content in wild oat plant parts which had been reported that five allelochemical compounds had been isolated from the shoot parts of wild oats (Liu et al., 2016).

3.5 The Combination Effect of Tested Plant Species and Wild Oat Plant Part Aqueous Extracts on Germination and Some Seedling Growth Characteristics: The combined effect of plant species and wild oat plant part extract caused significant differences on all recorded data as shown in table (5). 100% germination percentage were recorded with lettuce and tomato seedlings under control treatments, while lowest germination percentage was 60.44% in lettuce seeds under 100% concentration of wild oat extracts. The higher plumule length was 7.00 (cm) observed with onion seedlings in control treatment, while the lowest plumule length was 1.58 (cm) in onion seedlings under 100% extract concentration. Maximum data of radicle length was 5.87 (cm) in tomato seedlings treated with distilled water (control), meanwhile minimum data was 0.30 (cm) with onion seedlings under 100% extract concentration. The plumule dry weight peak was 1.67(g) with tomato seedlings in control treatment, while tiniest value was 0.33 (g) in onion seedlings under 100% extract concentration. The radicle dry weight peak was 2.47 (g) with tomato seedlings in control treatment, while lowest value was 0.01 (g) in lettuce seedlings under 100% extract concentration. The highest seedlings total dry weight was 4.14 (g) in tomato under control treatments, while lowest value was 0.38 (g) when lettuce seeds where treated with 100% extract concentration. Inhibition of germination percentage parameters in table (5) indicates highest value in lettuce seeds treated with 100% extract concentration and lowest values where 0.00% in control treatments of lettuce and tomato seeds. Plumule growth inhibition was at highest level 42.35% with tomato seedlings under 100% extraction concentration, while lowest value was -5.70% in lettuce seeds under 25% extract concentration. Highest radicle growth inhibition was 92.37% in tomato seeds under 100% extract concentration, meanwhile lowest values were 0% in two cases of lettuce and onion seeds under control treatments. It had been reported that shoot parts of wild oat contain five allelochemical compounds (syringic acid, tricin, acacetin, syringoside, and diosmetin)(Liu et al., 2016).

3.6 The Combination Effect of Wild Oat Plant Part Aqueous Extracts and The Extract Concentration on Germination and Some Seedling Growth Characteristics: The combination effect of plant part extract and extract concertation imposed significant effect on all recorded data except radicle dry weight (table-6). The germination percentage were in highest levels 100% in control treatments for root and seed aqueous extracts, while lowest value was 65.33% in shoot parts highest concentartion100%. The highest record for plumule length was 5.42 (cm) with the control treatment of shoot aqueous extracts, while the minimum value 0.51 (cm) was observed in seed extracts with 100% concentration. Radicle length were at its highest levels 3.20 (cm) in control treatments for the three plants parts (shoot, root and seeds), meanwhile the lowest level 0.22 (cm) with seeds extracts in 100% concentration. Plumule and total seedlings dry weight were at the peak 0.90 (g) and 1.86 (g) respectively for the three plant parts aqueous extracts (shoot, root and seed) with control treatments, the minimum value for Plumule and total seedlings dry weight were 0.34 (g) and 0.39 (g) respectively in seeds extracts under the highest concentration 100%.

The data of inhibition of germination was at highest level 34.67% in shoot extracts under maximum concentration level 100% and in lowest level 0% in root and seeds control treatments. Records of Plumule and radicle growth inhibition where at the peak 60.68 % and 94.14 % respectively with seeds extract under 100% concentration and at their minimum levels 0% in control treatments for the three plant parts (shoot, root and seed) extracts. It was reported that aerial parts (shoot) of wild oat contains higher amounts of allelochemicals when compared with root or seeds (Liu et al., 2016). The allelopathic effect was concentration dependent (Ali and Aziz, 2002).

3.7 The Triple Effect of tested Plant Species, Wild Oat Plant Part Aqueous Extracts and The Extract Concentration on Germination and Some Seedling Growth Characteristics: The triple effect was significant on all reported data except radicle dry weight (Table-7). The highest germination percentage 100% were reported with lettuce seeds when treated with control treatment for shoot, root and seed parts of wild oat plants and also 25% of root aqueous extracts, while for onion seeds control of root and seeds extracts and also concentration of 25% of root aqueous extracts and 50% of seeds extracts, whereas for tomato seeds for control treatments of shoot, root and seeds of wild oat extracts beside 25 and 75% of seeds aqueous extracts. The lowest value of germination percentage was 37.33% recorded with seeds aqueous extracts of wild oat under 100% concentration. Data of plumule length was at highest level 7.07 (cm) in the triple effect of onion tested seeds treated with control of shoots aqueous extracts, while lowest value was 0.19 (cm) reported in the interaction between onion seeds treated with wild oats seeds aqueous extracts with 100% concentration. Radicle length data indicated highest levels 5.87 (cm) with the combination between tomato tested seeds under the three plant parts (shoot, root and seeds) aqueous extracts with control treatments, meanwhile lowest observed data was 0.09 (cm) when onion seeds treated with seeds aqueous extracts in 100% concentration. Plumule dry weight were at the peak 1.67 (g) with the triple effect of tomato tested seeds treated with control of the three wild oat aqueous extracts while it was at minimum level 0.08 (g) when onion tested seeds treated with wild oat seeds aqueous extract with 100% concentration. Seedling total dry weight were at the highest value 4.14 (g) with the triple effect of tomato tested seeds treated with control of the three wild oat aqueous extracts while it was at lowest level 0.10 (g) when onion tested seeds treated with wild oat seeds aqueous extract

with 100% concentration. Inhibition of germination percentage parameters in table (7) indicates highest value 37.33% in lettuce seeds treated with wild oats seeds extracts with the 100% concentration and lowest values where 0.00% in control treatments of lettuce, onion and tomato seeds beside lettuce treated with root extracts with 25% concentration, onion seeds treated with wild oats root extracts with the concentration 25% and tomato seeds treated with 25% and 75% of seeds aqueous extracts. Plumule growth inhibition was at highest level 84.85% with onion seedlings under 100% extraction concentration of wild oat seeds aqueous extracts, while lowest value was -17.19% in onion seeds under root extracts with concentration level of 75%. Highest radicle growth inhibition was 95.08% in onion seeds under the 100% extract concentration of seeds aqueous extracts, meanwhile lowest values were -5.12% in the triple combination of onion tested seeds, shoot extracts of wild oat and the concentration level of 25%. All these findings explain the importance of indicating the best bioassay plant for allelopathic studies to insure accurate and reliable results that could be manipulated for entire allelopathic researches, it is clear that wild oat plant had allelopathic effect that is concentration dependent and its root, shoot and seeds differ in their allelopathic influence (Iannucci et al., 2012, Liu et al., 2016).

3.8 Allelopathy Index Equations: After conduction the experiment, recording data of germination and seedling growth we estimated the allelopathic index (Table- 8) according to the previously proposed equations and based on seedlings dry weight.

1st Proposed Equation: - Equation (4) which depends on the difference between seedlings dry weight in control treatment and extracts treatments. The data with minus signals represent higher growth than control treatments or stimulatory effect of allelochemicals, while positive data which is above zero means allelochemicals inhibitory effects (figure-1).

2nd Proposed Equation: - This equation depends on the seedlings weight differences between control and treatments divided by general mean of total dry weight, then it will be subtracted from (1) as shown in equation (5). Control treatments will have unity data and then any data above unity will be the result of stimulation allelopathic effect and lower than unity means inhibitory effects that shows severity of allelopathic relation-ship in minus data as shown in figure (2).

3rd Proposed Equation: - This equation is the result of dividing the subtract of average dry weights of control divided by average dry weights of treatments over the subtraction from unity of average of treatments divided by general average of the both as in equation (6). Control treatments result will be zero so any data above zero will be stimulatory allelopathic effect and data below zero will represent inhibitory effects (figure-3).

4th Proposed Equation: - This equation is an attempt to proposed a percentage proportion for allelopathic effect as shown in equation (7). Where seedlings dry weight of treatments will be divided by average of control treatments then it will have subtracted from one and multiplied by 100 to indicate the allelopathic index as percentage. These results could use to compare different treatment sets (figure- 4).

5th Proposed Equation: - this equation is an attempt to represent the linear relation-ship that could manipulate allelopathic effects. In this equation there is data from the natural logarithm of each treatment and the concentration differences between treatments (equation- 8). It is obvious from (figure- 5) that the higher data means stronger allelopathic effect.

3.9 Comparison between equations: - Above equations indicate different manipulation types for instance equation (5) in this study will be the best according to the goal of indicating stimulatory or inhibitory allelopathic effects and the use of three set of averages. Equation (7) will be preferred to use in comparison of different plant species allelopathic potentiality. Both equations demonstrate stimulatory or inhibitory allelopathic effects according to plants dry weight so it will provide a reasonable solution for such studies, beside its simple and accurate bases.

4.CONCLUSION: - From these results we conclude that lettuce plants was the most suitable plant to be used as a bioassay indicator plant comparing to Tomato and Onion plants in allelopathy studies. Wild oat plant parts imposed allelopathic impact that could be classified from stronger to weaker as Shoot – seed- root and the impact was concentration dependent. From This study's analytical findings and equation results it was clear that our proposed equations (5) and (7) were better than other three proposed equations to be used in allelopathy studies as allelopathy index due to their capability to manipulate different allelopathic relationships.

Table 1. The Effect of Plant Species on Germination and Some Seedlings Growth Characteristics

Plant Species	Germination %	Inhibition %	Plumule Length (cm)	Radicle Length (cm)	Plumule Dry Weight (g)	Radicle Dry Weight (g)	Total Dry Weight (g)	Plumule Growth Inhibition %	Radicle Growth Inhibition %
lettuce	83.56 c	16.44 c	3.10 b	0.78 c	0.44 b	0.07 b	0.51 b	6.16 a	50.23 a
Onion	90.05 b	9.96 b	3.08 b	0.98 b	0.42 c	0.12 b	0.54 b	24.28 b	56.34 b
Tomato	95.73 a	4.27 a	3.81 a	2.83 a	1.24 a	0.66 a	1.91 a	25.44 b	72.89 c

Note: Means with the same symbols in one column are not significantly different from each other at alpha = 0.01% based on multiple range test of Duncan

Table 2. The Effect of Plant Part Extracts on Germination and Some Seedlings Growth Characteristics

Wild Oat Plant Part	Germination %	Inhibition %	plumule length (cm)	radicle length (cm)	plumule dry weight (g)	radicle dry weight (g)	total dry weight (g)	plumule Growth Inhibition %	Radicle Growth Inhibition %
Shoot	84.89 c	15.11 c	3.17 b	1.23 b	0.73 b	0.31 a	1.04 a	19.13 b	54.92 a
Root	95.02 a	4.98 a	4.62 a	2.37 a	0.77 a	0.29 a	1.05 a	4.63 a	58.25 a
Seed	89.42 b	10.58 b	2.20 c	0.99 c	0.60 c	0.25 a	0.85 b	32.12 c	66.29 b

Note: Means with the same symbols in one column are not significantly different from each other at

alpha = 0.01% based on multiple range test of Duncan

Table 3. The Effect of Wild Oat Extracts Concentration Levels on Germination and Some Seedlings Growth Characteristics

Extract Concentration	Germination %	Inhibition %	plumule length (cm)	radicle length (cm)	plumule dry weight (g)	radicle dry weight (g)	total dry weight (g)	plumule Growth Inhibition %	Radicle Growth Inhibition %
Control	99.85 a	0.15 a	5.40 a	3.20 a	0.90 a	0.96 a	1.86 a	0.00 a	0.00 a
25%	96.15 b	3.85 b	3.53 b	1.55 b	0.72b	0.15 b	0.87 b	12.64 b	59.97 b
50%	92.30 c	7.70 c	3.10 c	1.43 c	0.67 c	0.12 b	0.79 b	21.85 c	71.62 c
75%	84.89 d	15.11 d	2.63 d	0.86 d	0.65 c	0.10 b	0.76 bc	24.85 c	80.48 d
100%	75.70 e	24.30 e	2.00 e	0.62 e	0.55 d	0.08 b	0.64 c	33.80 d	87.03 e

Note: Means with the same symbols in one column are not significantly different from each other at alpha = 0.01% based on multiple range test of Duncan

Table 4. The Combination Effect of Bioassayed Plant Species and Wild Oat plant part extraction on Germination and Some Seedlings Growth Characteristics

Species	Extract	Germination %	Inhibition %	Plumule length (cm)	radicle length (cm)	Plumule dry weight (g)	radicle dry weight (g)	total dry weight (g)	Plumule Growth Inhibition %	Radicle Growth Inhibition %
Lettuce	Shoot	84.27 d	15.73 d	3.23 c	0.57 f	0.46 e	0.08 b	0.54 d	0.57 f	44.41 c
	root	93.07 bc	6.93 b	3.61 b	1.07 e	0.45 ef	0.07 b	0.51 d	3.40 f	52.96 b
	seed	73.33 f	26.67 f	2.45 d	0.71 f	0.41 f	0.06 b	0.47 d	14.52 e	53.33 b
Onion	Shoot	77.87 e	22.13 e	2.48 d	0.99 e	0.32 g	0.14 b	0.46 d	42.13 b	49.42 bc
	root	95.73 ab	4.27 ab	5.12 a	1.34 d	0.64 d	0.14 b	0.78 c	-16.60 g	48.73 bc
	seed	96.53 a	3.47 a	1.64 e	0.62 f	0.29 g	0.08 b	0.37 d	47.30 a	70.86 a
Tomato	Shoot	92.53 c	7.47 c	3.81 b	2.13 b	1.42 a	0.71 a	2.13 a	14.69 e	70.94 a
	root	96.27 a	3.73 a	5.12 a	4.71 a	1.21 b	0.66 a	1.87 b	27.09 d	73.05 a
	seed	98.40 a	1.60 a	2.51 d	1.65 c	1.09 c	0.62 a	1.71 b	34.54 c	74.68 a

Note: Means with the same symbols in one column are not significantly different from each other at alpha = 0.01% based on multiple range test of Duncan

Table 5. The Combination Effect of Tested Plant Species and Wild Oat extract Concentration Levels on Germination and Some Seedlings Growth Characteristics

plant species	Concentration %	Germination %	Inhibition %	plumule length (cm)	radicle length (cm)	plumule dry weight (g)	radicle dry weight (g)	total dry weight (g)	plumule Growth Inhibition %	Radicle Growth Inhibition %
Lettuce	Control	100.00 a	0.00 a	4.01 cd	1.26 e	0.48 ef	0.14 bc	0.62 de	0.00 a	0.00 a
	25%	94.22 bc	5.78 bc	3.79 d	1.00 ef	0.50 e	0.08 bc	0.58 e	-5.70 a	42.89 b
	50%	88.00 d	12.00 d	3.23 e	0.74 fg	0.43 fg	0.07 bc	0.50 e	7.73 b	48.28 b
	75%	75.11 e	24.89 e	2.70 f	0.59 gh	0.41 g	0.04 bc	0.46 e	8.97 bc	70.10 c
	100%	60.44 f	39.56 f	1.75 h	0.32 h	0.36 hi	0.01 c	0.38 e	19.82 d	89.88 d
Onion	Control	99.56 a	0.44 a	7.00 a	2.46 c	0.55 d	0.27 b	0.82 d	0.00 a	0.00 a
	25%	96.44 ab	3.56 ab	2.58 f	0.97 ef	0.47 ef	0.15 bc	0.62 de	14.93 cd	46.03 b
	50%	94.22 bc	5.78 bc	2.22 g	0.75 fg	0.39 gh	0.06 bc	0.45 e	28.93 e	76.61 c
	75%	84.89 d	15.11 d	2.02 g	0.42 h	0.34 i	0.05 bc	0.39 e	38.31 f	80.22 cd
	100%	75.11 e	24.89 e	1.58 h	0.30 h	0.33 i	0.06 bc	0.39 e	39.22 f	78.84 c
Tomato	Control	100.00 a	0.00 a	5.17 b	5.87 a	1.67 a	2.47 a	4.14 a	0.00 a	0.00 a
	25%	97.78 ab	2.22 ab	4.21 c	2.69 bc	1.19 b	0.21 bc	1.40 b	28.69 e	90.99 e
	50%	94.67 bc	5.33 bc	3.85 d	2.79 b	1.18 b	0.24 bc	1.42 b	28.88 e	89.98 de
	75%	94.67 bc	5.33 bc	3.17 e	1.56 d	1.21 b	0.21 bc	1.42 b	27.27 e	91.13 e
	100%	91.55 c	8.44 c	2.66 f	1.24 e	0.96 c	0.18 bc	1.14 c	42.35 f	92.37 e

Note: Means with the same symbols in one column are not significantly different from each other at alpha = 0.01% based on multiple range test of Duncan

Table 6. The Combination Effect of Wild Oat Part extract and extract Concentration Levels on Germination and Some Seedlings Growth Characteristics

Wild Oat Plant Part	Concentration	Germination %	Inhibition %	plumule length (cm)	radicle length (cm)	plumule dry weight (g)	radicle dry weight (g)	total dry weight (g)	plumule Growth Inhibition %	Radicle Growth Inhibition %
Shoot	Control	99.56 a	0.44 a	5.42 a	3.20 a	0.90 a	0.96 a	1.86 a	0.00 a	0.00 a
	25%	93.78 c	6.22 c	3.61 d	1.03 cd	0.77 b	0.21 b	0.98 b	5.67 ab	41.88 b

	50%	88.44 d	11.56 d	3.06 e	0.79 de	0.69 c	0.16 b	0.84 bcd	23.93 c	59.67 c
	75%	77.33 f	22.67 f	2.35 f	0.68 ef	0.76 b	0.13 b	0.89 bcd	25.67 cd	82.08 de
	100%	65.33 g	34.67 g	1.43 gh	0.45 fg	0.55 e	0.09 b	0.64 cde	40.38 e	90.99 e
Root	Control	100.00 a	0.00 a	5.39 a	3.20 a	0.90 a	0.96 a	1.86 a	0.00 a	0.00 a
	25%	99.11 ab	0.89 ab	4.83 b	2.90 a	0.77 b	0.13 b	0.90 bc	4.73 ab	63.87 c
	50%	95.56 bc	4.44 bc	4.60 b	3.05 a	0.71 c	0.13 b	0.84 bcd	9.77 b	74.19 d
	75%	94.67 c	5.33 c	4.24 c	1.54 b	0.69 c	0.10 b	0.79 bcde	8.34 b	77.21 d
	100%	85.78 de	14.22 de	4.05 c	1.18 c	0.77 b	0.11 b	0.88 bcd	0.33 a	75.97 d
Seed	Control	100.00 a	0.00 a	5.39 a	3.20 a	0.90 a	0.96 a	1.86 a	0.00 a	0.00 a
	25%	95.56 bc	4.44 bc	2.15 f	0.73 ef	0.62 d	0.10 b	0.72 cde	27.52 cd	74.15 d
	50%	92.89 c	7.11 c	1.65 g	0.45 fg	0.61 d	0.08 b	0.69 cde	31.85 d	81.01 de
	75%	82.67 e	17.33 e	1.31 h	0.36 g	0.51 e	0.07 b	0.59 ef	40.54 e	82.16 de
	100%	76.00 f	24.00 f	0.51 i	0.22 g	0.34 f	0.05 b	0.39 f	60.68 f	94.14 f

Note: Means with the same symbols in one column are not significantly different from each other at alpha = 0.01% based on multiple range test of Duncan

Table 7. The Triple Combination Effect of Tested Plant Species, Wild Oat Part extract and extract Concentration Levels on Germination and Some Seedlings Growth Characteristics

plant species	Wild Oat Plant Part	Concentration %	Germination %	Inhibition %	plumule length (cm)	radicle length (cm)	plumule dry weight (g)	radicle dry weight (g)	total dry weight (g)	plumule Growth Inhibition %	Radicle Growth Inhibition %
Lettuce	Shoot	Control	100.00 a	0.00 a	4.01 fg	1.26 e-g	0.48 j-L	0.14 b	0.62 i-m	0.00 c-e	0.00 a
		25%	92.00 b-e	8.00 b-e	4.10 fg	0.61 i-m	0.56 ij	0.08 b	0.64 h-m	-16.86 b	40.68 c
		50%	85.33 e-g	14.67 e-g	3.68 gh	0.40 k-m	0.46 k-m	0.10 b	0.57 i-n	1.92 d-f	20.04 b
		75%	77.33 h	22.67 h	2.79 jk	0.37 k-m	0.43 Lm	0.04 b	0.47 j-o	8.95 e-h	70.63 e-g
		100%	66.67 i	33.33 i	1.55 mn	0.19 m	0.37 m-o	0.01 b	0.38 j-o	8.83 e-h	90.68 h
	Root	Control	100.00 a	0.00 a	4.01 fg	1.26 f-j	0.48 j-L	0.14 b	0.62 i-m	0.00 c-e	0.00 a
		25%	100.00 a	0.00 a	4.05 fg	1.33 e-g	0.50 j-L	0.08 b	0.58 i-m	-8.39 b-d	38.99 c
		50%	96.00 a-d	4.00 a-d	3.41 h	1.23 e-g	0.43 Lm	0.05 b	0.48 j-o	6.03 e-g	63.39 d-f
		75%	92.00 b-e	8.00 b-e	3.33 hi	0.94 f-k	0.41 L-n	0.04 b	0.45 j-o	3.44 d-g	76.19 e-h
		100%	77.33 h	22.67 h	3.24 hi	0.59 i-m	0.40 L-o	0.02 b	0.42 j-o	15.93 g-i	86.21 gh
	Seed	Control	100.00 a	0.00 a	4.01 fg	1.26 e-g	0.48 j-L	0.14 b	0.62 i-m	0.00 c-e	0.00 a
		25%	90.67 c-f	9.33 c-e	3.22 h-j	1.05 f-i	0.44 Lm	0.07 b	0.51 i-o	8.17 e-h	49.01 cd
		50%	82.67 gh	17.33 gh	2.59 k	0.59 i-m	0.41 L-n	0.05 b	0.46 j-o	15.24 g-i	61.41 de
		75%	56.00 j	44.00 j	1.98 lm	0.46 j-m	0.40 L-o	0.05 b	0.45 j-o	14.51 f-i	63.49 d-f
		100%	37.33 l	62.67 l	0.47 op	0.18 m	0.31 op	0.01 b	0.32 k-o	34.70 k-n	92.76 h
Onion	Shoot	Control	98.67 ab	1.33 ab	7.07 a	2.46 d	0.55 i-K	0.27 b	0.82 f-j	0.00 c-e	0.00 a
		25%	93.33 a-d	6.67 a-d	1.85 l-n	1.03 f-j	0.50 j-L	0.31 b	0.81 f-j	8.95 e-h	-5.12 a
		50%	85.33 e-g	14.67 e-g	1.53 mn	0.65 h-m	0.28 pq	0.08 b	0.35 j-o	49.52 o	70.84 e-g
		75%	65.33 i	34.67 i	1.35 n	0.49 i-m	0.17 rs	0.03 b	0.20 m-o	68.54 p	88.86 gh
		100%	46.67 k	53.33 k	0.63 op	0.31 Lm	0.09 st	0.02 b	0.11 no	83.66 q	92.54 h
	Root	Control	100.00 a	0.00 a	6.97 a	2.46 d	0.55 i-k	0.27 b	0.82 f-j	0.00 c-e	0.00 a
		25%	100.00 a	0.00a	5.46bc	1.67 e	0.57 ij	0.10 b	0.67 h-m	-3.23 c-e	61.60 de
		50%	97.33 a-c	2.67 a-c	4.77de	1.43 e-g	0.61 i	0.08 b	0.69 h-L	-11.71 bc	70.37 e-g
		75%	97.33 a-c	2.67 a-c	4.49 ef	0.63 i-m	0.64 i	0.10 b	0.74 h-k	-17.19 b	62.79 d-f
		100%	84.00 f-h	16.00 f-h	3.94 g	0.51	0.83 h	0.14 b	0.97	-50.85 a	48.91 cd

						i-m			e-i		
		Control	100.00 a	0.00 a	6.97 a	2.46 d	0.55 i-k	0.27 b	0.82 f- j	0.00 c-e	0.00 a
		25%	96.00 a-d	4.00 a-d	0.43 op	0.23 m	0.33 n-p	0.05 b	0.38 j-o	39.07 L-o	81.59 f-h
	Seed	50%	100.00 a	0.00 a	0.36 p	0.18 m	0.28 pq	0.03 b	0.31 k-o	48.99 n	88.62 gh
		75%	92.00 b-e	8.00 b-e	0.23 p	0.14 m	0.20 qr	0.03 b	0.23 L-o	63.57 p	89.01 gh
		100%	94.67 a-d	5.33 a-d	0.19 p	0.09 m	0.08 t	0.01 b	0.10 o	84.85 q	95.08 h
		Control	100.00 a	0.00 a	5.17 b-d	5.87 b	1.67 a	2.47 a	4.14 a	0.00 c-e	0.00 a
		25%	96.00 a-d	4.00 a-d	4.89 ef	1.45 ef	1.25 bc	0.23 b	1.48 cd	24.93 i-k	90.09 gh
	Shoot	50%	94.67 a-d	5.33 a-d	3.96 g	1.32 e-g	1.33 b	0.29 b	1.61 bc	20.35 h-j	88.14 gh
		75%	89.33 d-g	10.67 d-g	2.90 i-k	1.17 e-h	1.67 a	0.31 b	1.99 b	-0.49 c-e	86.75 gh
		100%	82.67 gh	17.33 gh	2.11 L	0.86 g-L	1.19 cd	0.25 b	1.43 cd	28.64 j-m	89.74 gh
		Control	100.00 a	0.00 a	5.17 b-d	5.87 b	1.67 a	2.47 a	4.14 a	0.00 c-e	0.00 a
		25%	97.33 a-c	2.67 a-c	4.97 c-e	5.71 b	1.24 c	0.22 b	1.45 cd	25.80 i-L	91.02 h
Tomato	Root	50%	93.33 a-d	6.67 a-d	5.60 b	6.47 a	1.08 ef	0.27 b	1.35 c-e	34.98 k-n	88.80 gh
		75%	94.67 a-d	5.33 a-d	4.90 de	3.04 c	1.02 fg	0.17 b	1.19 c-g	38.77 L-o	92.66 h
		100%	96.00 a-d	4.00 a-d	4.98 c-e	2.45 d	1.07 ef	0.17 b	1.24 c-f	35.92 k-n	92.79 h
		Control	100.00 a	0.00 a	5.17 b-d	5.87 b	1.67 a	2.47 a	4.14 a	0.00 c-e	0.00 a
		25%	100.00 a	0.00 a	2.79 jk	0.91 f-k	1.08 ef	0.19 b	1.27 c- e	35.34 k-n	91.85 h
	Seed	50%	96.00 a-d	4.00 a-d	2.00 Lm	0.59 i-m	1.14 de	0.17	1.31 c-e	31.33 j-n	93.00 h
		75%	100.00a	0.00 a	1.72 L-n	0.47 j-m	0.94 g	0.14 b	1.08 d-h	43.53 no	93.98 h
		100%	96.00 a-d	4.00 a-d	0.88 o	0.39 k-m	0.63 i	0.13 b	0.76 g-k	62.49 p	94.57 h

Note: Means with the same symbols in one column are not significantly different from each other at alpha = 0.01% based on multiple range test of Duncan

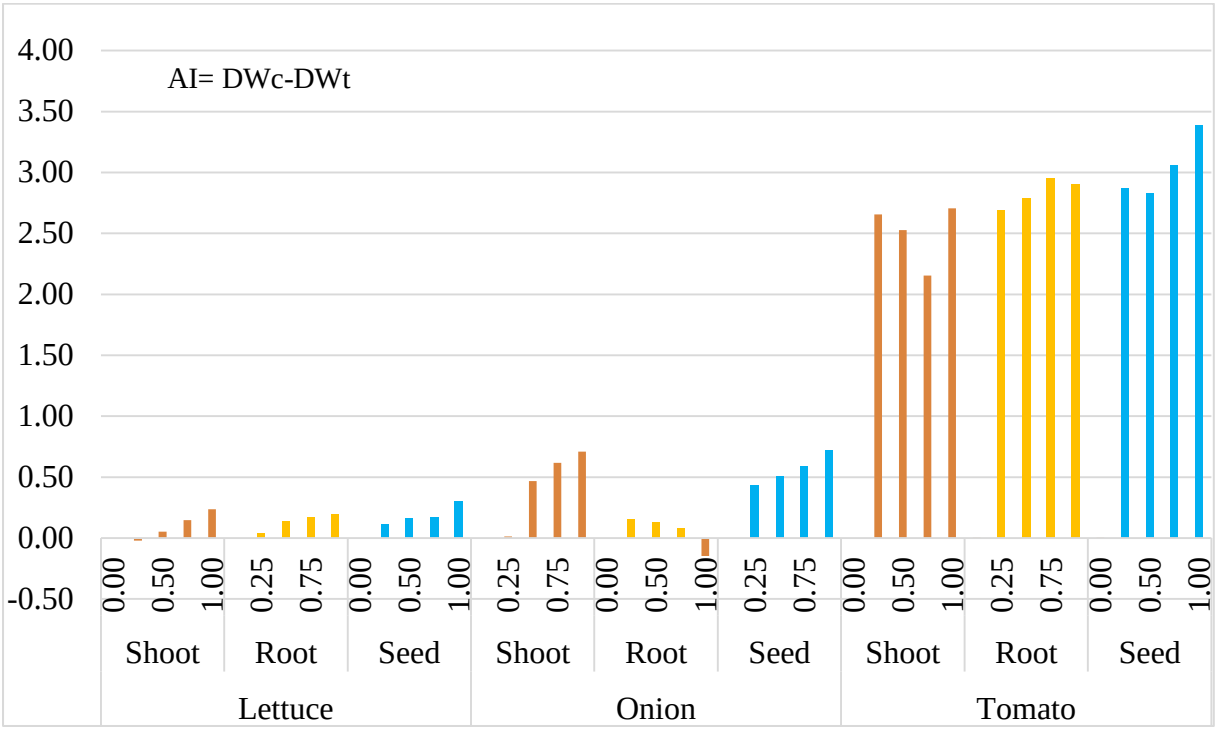

Figure 1 the Allelopathic Index according to Equation Number (4).

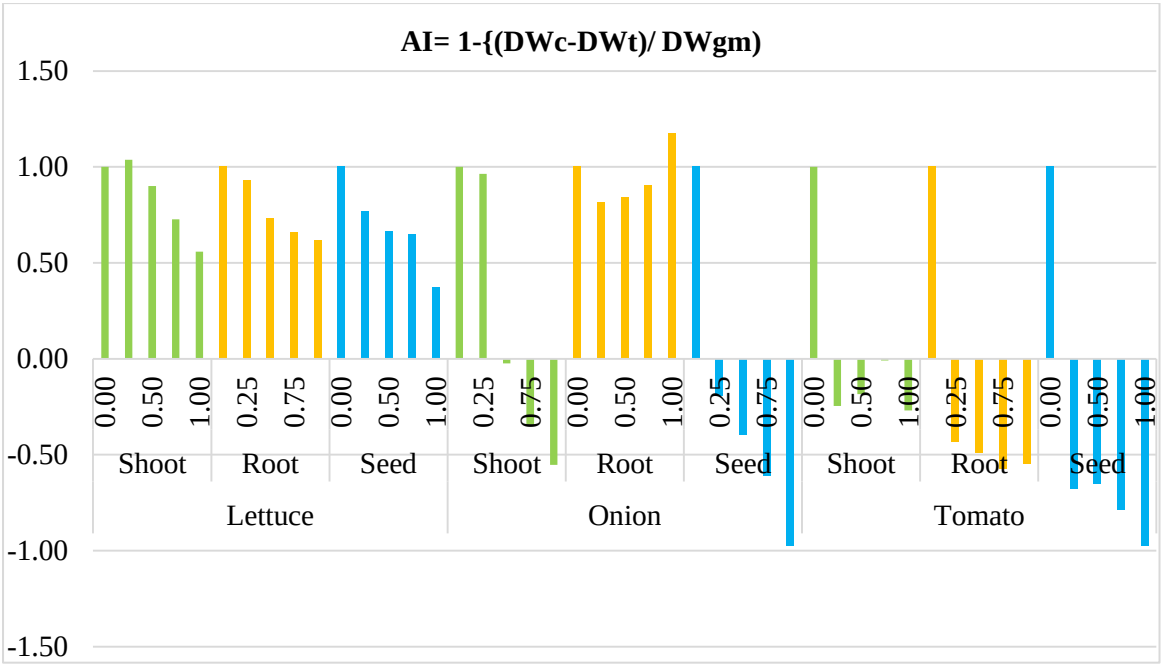

(Figure 2)The Allelopathic Index According to Equation(5)

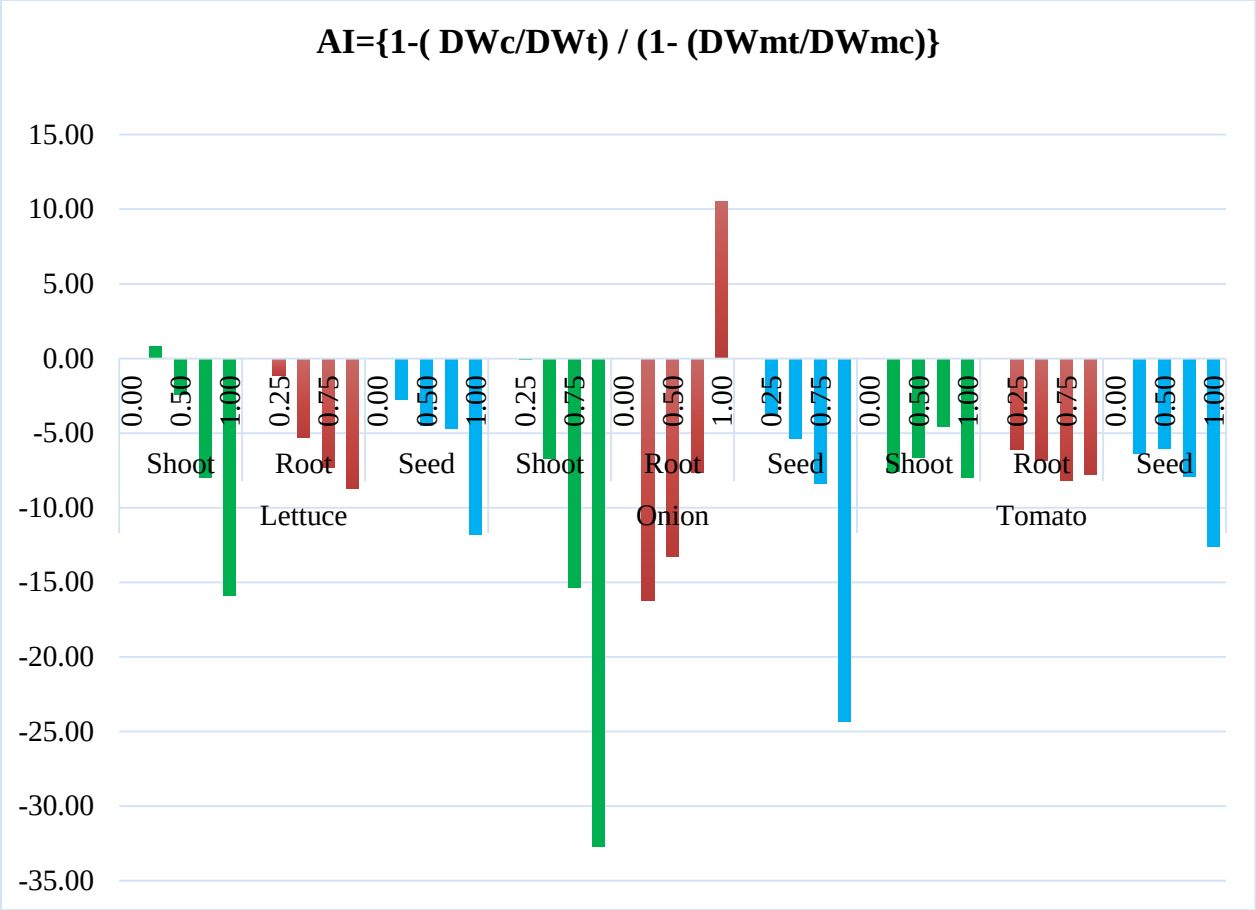

(Figure 3) the Allelopathic Index According to Equation Number (6).

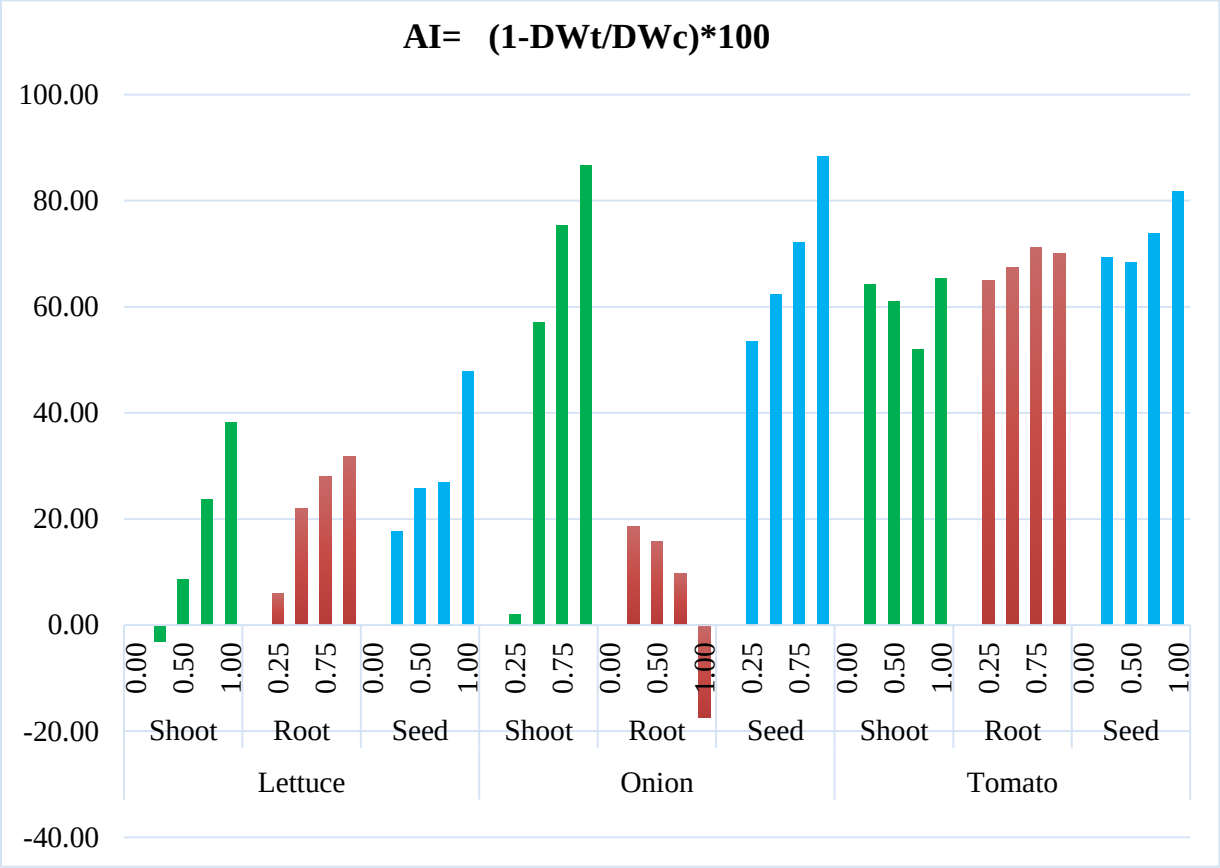

Figure 4 The Allelopathic Index According to Equation Number (7).

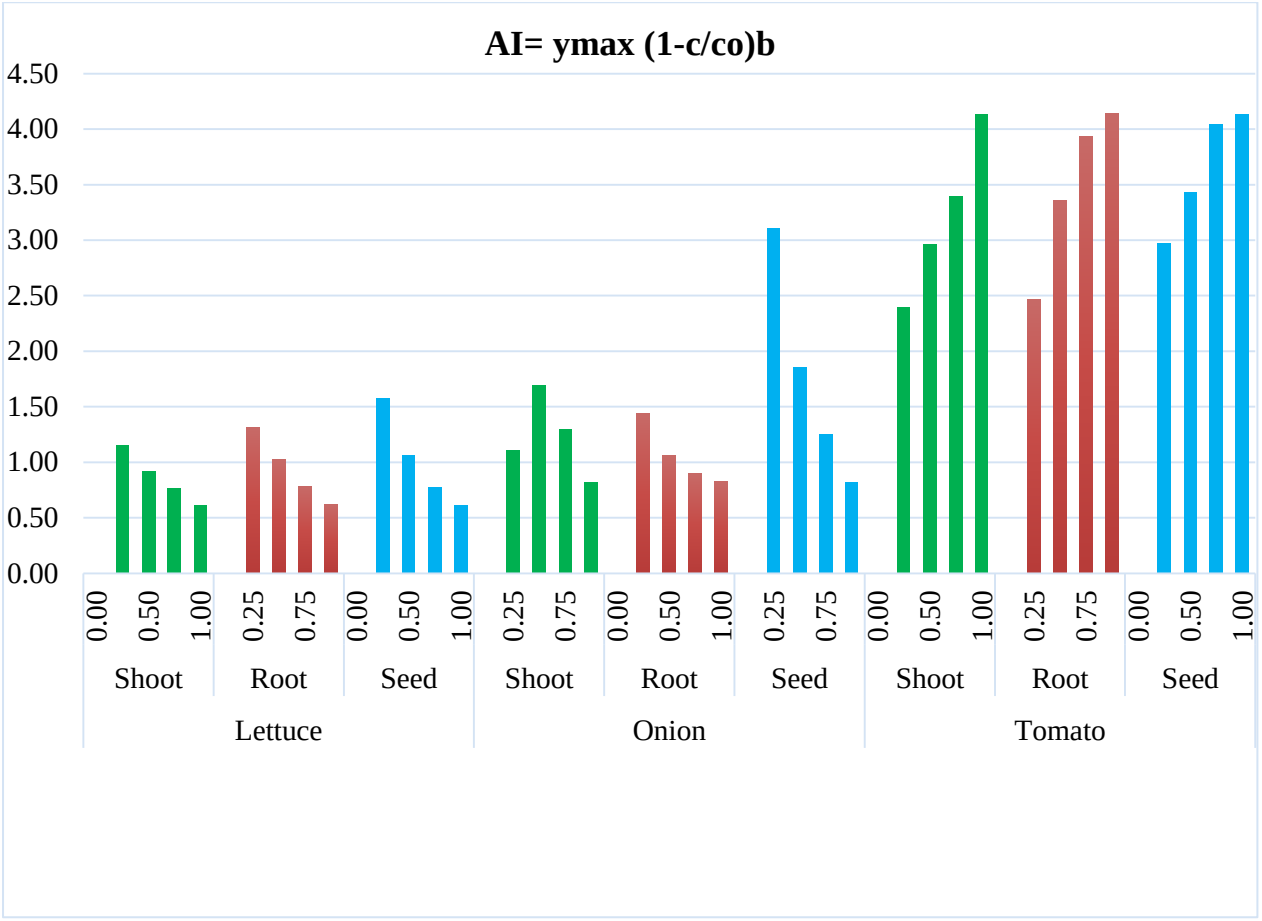

Figure 5 The Allelopathic Index According to Equation Number (8).

REFERENCES: -

ABD-ELGAWAD, A. M., EL-AMIER, Y. A., ASSAEED, A. M. & AL-ROWAILY, S. L. 2020. Interspecific variations in the habitats of Reichardia tingitana (L.) Roth leading to changes in its bioactive constituents and allelopathic activity. *Saudi Journal of Biological Sciences*, 27**,** 489-499.

AGRAWAL, A. A., CONNER, J. K., JOHNSON, M. T. & WALLSGROVE, R. 2002. Ecological genetics of an induced plant defense against herbivores: additive genetic variance and costs of phenotypic plasticity. *Evolution*, 56**,** 2206-2213.

ALI, K. 2001. *Some Ecological Studies on interference between soft wheat and syrian cephalaria Weed* Master of Science, Salahaddin University- erbil.

ALI, K. & AZIZ, F. 2002. Studying the effect of root and shoot extracts of syrian cephalaria (Cephalaria syriaca) extract on wheat seeds (Triticum aestivum) germination properties. *Zanco) journal of pure and applied science.(2002) Vol*, 14**,** 15-24.

ALI, K. A. 2016. Allelopathic potential of radish (Raphanus sativus L.) on germination and growth of some crop and weed plants. *Int. J. Biosci*, 9**,** 394-403.

ALI, K. A. & MAULOOD, P. M. 2011. The allelopathic effect of different species of grapevine berries aqueous extracts on some germination parameters of lettuce. *International Journal of Biosciences (IJB),* (1) 6**,** 70-80.

ALI, K. A. & **SAKRI, F. Q. 2010**. **Influence of Cephalaria syriaca Residue Concentrations on Germination and Growth of Wheat, barley and some companion weeds.** . ***ZANCO Journal of Pure and Applied Sciences*, (22) 5, 122-132**.

ALI, K. A., SAKRI, F. Q. & LI, Q. X. 2012. Isolation and purification of allelochemicals from Cephalaria syriaca plant. *Int J Biosci*, 2**,** 90-103.

AN, M., JOHNSON, I. & LOVETT, J. 1993. Mathematical modeling of allelopathy: biological response to allelochemicals and its interpretation. *Journal of Chemical Ecology*, 19**,** 2379-2388.

AN, M., JOHNSON, I. & LOVETT, J. 2002. Mathematical modelling of residue allelopathy: the effects of intrinsic and extrinsic factors. *Plant and Soil*, 246**,** 11-22.

AN, M., LI LIU, D., WU, H. & LIU, Y. H. 2008. Allelopathy from a mathematical modeling perspective. *Allelopathy in sustainable agriculture and forestry*. Springer.

AN, M., LIU, D., JOHNSON, I. & LOVETT, J. 2003. Mathematical modelling of allelopathy: II. The dynamics of allelochemicals from living plants in the environment. *Ecological Modelling*, 161**,** 53-66.

BING-YAO, S., JIAN-ZHONG, T., ZHI-GANG, W., FU-GEN, G. & MING-DE, Z. 2006. Allelopathic effects of extracts from Solidago canadensis L. against seed germination and seedling growth of some plants. *J. Environ. Sci,* 18**,** 304-309.

DIAS, M., NOZARI, R. & SANTARÉM, E. 2017. Herbicidal activity of natural compounds from Baccharis spp. on the germination and seedlings growth of Lactuca sativa and Bidens pilosa. *Allelopath. J,* 42**,** 21-36.

EL-ROKIEK, K. & EID, R. 2009. Allelopathic effects of Eucalyptus citriodora on amaryllis and associated grassy weed. *Planta daninha,* 27**,** 887-899.

ERCOLI, L., MASONI, A., PAMPANA, S. & ARDUINI, I. 2007. Allelopathic effects of rye, brown mustard and hairy vetch on redroot pigweed, common lambsquarter and knotweed. *Allelopathy Journal,* 19**,** 249.

FAY, P. & DUKE, W. 1977. An assessment of allelopathic potential in Avena germ plasm. *Weed science,* 25**,** 224-228.

FERNANDEZ, C., MONNIER, Y., SANTONJA, M., GALLET, C., WESTON, L. A., PRÉVOSTO, B., SAUNIER, A., BALDY, V. & BOUSQUET-MÉLOU, A. 2016. The impact of competition and allelopathy on the trade-off between plant defense and growth in two contrasting tree species. *Frontiers in plant science,* 7**,** 594.

FIELD, A. 2013. *Discovering statistics using IBM SPSS statistics*, sage.

FRAGASSO, M., PLATANI, C., MIULLO, V., PAPA, R. & IANNUCCI, A. 2012. A bioassay to evaluate plant responses to the allelopathic potential of rhizosphere soil of wild oat (Avena fatua L.). *Agrochimica,* 56**,** 120-128.

HE, H. B., WANG, H. B., FANG, C. X., LIN, Z. H., YU, Z. M. & LIN, W. X. 2012. Separation of allelopathy from resource competition using rice/barnyardgrass mixed-cultures. *Plos one,* 7.

IANNUCCI, A., FRAGASSO, M., PLATANI, C., NARDUCCI, A., MIULLO, V. & PAPA, R. 2012. Dynamics of release of allelochemical compounds from roots of wild oat (Avena fatua L.). *Agrochimica,* 56**,** 185-192.

JIANG, W. & LAFITTE, R. 2007. Ascertain the effect of PEG and exogenous ABA on rice growth at germination stage and their contribution to selecting drought tolerant genotypes. *Asian J. Plant Sci,* 6**,** 684-687.

KAMAL, J. 2011. Quantification of alkaloids, phenols and flavonoids in sunflower (Helianthus annuus L.). *African Journal of Biotechnology,* 10**,** 3149-3151.

KARBAN, R. 2008. Plant behaviour and communication. *Ecology letters,* 11**,** 727-739.

LIU, D. L., AN, M., JOHNSON, I. R. & LOVETT, J. V. 2003. Mathematical modeling of allelopathy. III. A model for curve-fitting allelochemical dose responses. *Nonlinearity in biology, toxicology, medicine,* 1**,** 15401420390844456.

LIU, X., TIAN, F., TIAN, Y., WU, Y., DONG, F., XU, J. & ZHENG, Y. 2016. Isolation and identification of potential allelochemicals from aerial parts of Avena fatua L. and their allelopathic effect on wheat. *Journal of agricultural and food chemistry,* 64**,** 3492-3500.

LIU, Y., CHEN, X., DUAN, S., FENG, Y. & AN, M. 2011. Mathematical modeling of plant allelopathic hormesis based on ecological-limiting-factor models. *Dose-Response,* 9**,** dose-response. 09-050. Liu.

NORSWORTHY, J. K. 2003. Allelopathic Potential of Wild Radish (Raphanus raphanistrum) 1. *Weed Technology,* 17**,** 307-313.

OLIVEIRA, A. K. M. D., RIBEIRO, J. W. F., PEREIRA, K. C. L. & SILVA, C. A. A. 2013. Effects of temperature on the germination of Diptychandra aurantiaca (Fabaceae) seeds. *Acta Scientiarum. Agronomy,* 35**,** 203-208.

PAL, R., BASU, D. & BANERJEE, M. 2009. Modelling of phytoplankton allelopathy with Monod–Haldane-type functional response—A mathematical study. *Biosystems,* 95**,** 243-253.

PEDROL, N., GONZÁLEZ, L. & REIGOSA, M. J. 2006. Allelopathy and abiotic stress. *Allelopathy*. Springer.

REJILA, S. & VIJAYAKUMAR, N. 2011. Allelopathic effect of Jatropha curcas on selected intercropping plants (green chilli and sesame). *Journal of Phytology*.

SCHUMACHER, W. J., THILL, D. C. & LEE, G. A. 1983. Allelopathic potential of wild oat (Avena fatua) on spring wheat (Triticum aestivum) growth. *Journal of Chemical Ecology,* 9**,** 1235-1245.

SISODIA, S. & SIDDIQUI, M. B. 2010. Allelopathic effect by aqueous extracts of different parts of Croton bonplandianum Baill. on some crop and weed plants. *Journal of Agricultural Extension and Rural Development,* 2**,** 22-28.

SODAEIZADEH, H., RAFIEIOLHOSSAINI, M., HAVLÍK, J. & VAN DAMME, P. 2009. Allelopathic activity of different plant parts of Peganum harmala L. and identification of their growth inhibitors substances. *Plant Growth Regulation,* 59**,** 227.

WEINBERG, S. L. & ABRAMOWITZ, S. K. 2008. *Statistics using SPSS: An integrative approach*, Cambridge University Press.

WILLIAMSON, G. B. & RICHARDSON, D. 1988. Bioassays for allelopathy: measuring treatment responses with independent controls. *Journal of chemical ecology,* 14**,** 181-187.

ZANCO Journal of Pure and Applied Sciences
The official scientific journal of Salahaddin University-Erbil
https://zancojournals.su.edu.krd/index.php/JPAS

ISSN (print):2218-0230**, ISSN (online):** 2412-3986**, DOI: http://dx.doi.org/10.21271/zjpas**

RESEARCH PAPER

Assessment of Ground water Quality for Drinking purpose in the Shaqlawa Area, Erbil-KRI

Siraj M. A. Goran [1], Dilshad A. Rasul[2], Dldar S. Ismaeel [3]

[1]Department of Environmental Sciences, College of Science, Salahaddin University-Erbil, Kurdistan Region, Iraq
[2]Department of Medical Laboratory Technology, Soran Technical Institute, Erbil Polytechnic University, Erbil, Kurdistan Region, Iraq
[3]Department of Medical Laboratory Technology, Erbil Medical Technical Institute, Erbil Polytechnic University, Erbil, Kurdistan Region, Iraq

A B S T R A C T:

Physical, chemical and biological properties of some artesian wells in Shaqlawa area were done, through collecting water samples for 12 artesian wells seasonally (Spring, summer, autumn and winter) during 2016, which distributed in Shaqlawa, Harir and Permam area.

In ground water samples of study areas, electric conductivity was range between 252-2300 µS/cm, with mean values for all 12 wells were range between 474.8-1575.5 and overall mean was 689.3.The pH of study samples is neutral or around neutrality and ranged between 7.0 and 8.4 With mean values ranged between 7.2-8.2 and the overall mean 7.6 and standard deviation of 0.4 and agreed with WHO guidelines for drinking water purpose. Sodium and potassium levels were ranged from 1 to 310 and 0.1 to 8.18 mg/L. Turbidity is one of the parameters for the acceptability of drinking water quality. WHO, guidelines for turbidity is < 5 NTU.

The overall mean value of total alkalinity in studied water samples was 278.5 mg $CaCO_3$/L.

The levels of sulfate in groundwater samples of the study area ranged between 11.8 to 314 mg/L. The overall mean and STDEV is 72.7 and 71.6 respectively. . Concentration of total hardness in the studied area were ranged between 160 and 560 mg $CaCO_3$/L. Furthermore, calcium dominated magnesium in studied well water.

Nitrate levels in groundwater samples were low. Microbiological analysis of studied water samples was zero, except in two samples. Water quality index or studied parameters in groundwater samples were excellent.

KEY WORDS: Drinking water; Water Quality; Shaqlawa; Kurdistan Region, Iraq
DOI: http://dx.doi.org/10.21271/ZJPAS.33.2.2
ZJPAS (2021) , 33(1);19-27 .

1. INTRODUCTION :

Groundwater (GW) is important source of drinking water and its quality relies upon many factors including the composition of interaction of

Assessment of physical and chemical characteristics groundwater is important to estimate its uses. The interaction of mineral in soil and ground water processes will affect the water quality, The chemical composition of water is based primarily on the minerals which have dissolved in it. In addition, the chemical composition of water is modified by ion-exchange equilibrium. There are some environmental conditions affecting on the water chemistry such

* **Corresponding Author:**
Dilshad Abdulkhaliq Rasul
E-mail: dilshad.rasul@epu.edu.iq

Article History:
Received: 09/02/2020
Accepted: 08/11/2020
Published: 18/04/2021

as type of rock, climate, relief, vegetation and time (Rajmohan 2004).

Physical and concoction prepare influencing ground water (Fittes 2002). General physical, chemical and biological parameters are temperature, pH, alkalinity, hardness, solids, turbidity (Zuane, 2010).

In this work an endeavor has been made to evaluate the physical and chemical parameters of ground water like pH, electrical conductivity, hardness, total dissolved solids, alkalinity, phosphate, sulfate, nitrate, chloride and so on., the gathered information were contrasted and standard qualities suggested by WHO (Rao 2013).

Hydrochemical evaluation of groundwater systems is usually based on the availability of a large amount of information concerning groundwater chemistry (Hossien 2004). Quality of groundwater is equally important to its quantity owing to the suitability of water for various purposes (Subramani et.al., 2005). Groundwater chemistry, in turn, depends on a number of factors, such as general geology, degree of chemical weathering of the various rock types, quality of recharge water and inputs from sources other than water rock interaction. Such factors and their interactions result in a complex groundwater quality (Guler and Thyne 2004).

Groundwater is an important water resource for drinking, agriculture and industrial uses in study area. The present study was conducted to investigate certain physical, chemical and biological characteristics of artesian wells in Shaqlawa city, Harir and Permam area to determine its suitability for drinking purpose.

2. MATERIALS AND METHODS

Physical, chemical and biological properties of 4 Artesian wells situated in each of Shaqlawa city, Harir and Permam sub-districts were focused on through water sampling for a year seasonally (Spring, Summer, Autumn and Winter) particularly for ground water that used for drinking during 2016.

Water samples were gathered in polyethylene container and taking after standard methods portrayed by (APHA, 1998 and Parsons, *et al*., 1984) for water examination, all water samples were tested within first 4-6 hour. Alkalinity, chloride, magnesium and calcium were measured by titration technique, while total hardness measured by formulation. pH, EC and TDS were measured utilizing (pH-EC-TDS meter, HI 9812, Hanna instrument).

Sulfate was controlled by turbidimetric technique as indicated by (APHA, 1998). Sodium and potassium cations measured utilizing flame Photometer instrument. Turbidity was measured utilizing Turbidimeter (HF logical, inc. show BRF-15 CE). Most Probable number (MPN) was conducted according to (APHA, 1998).

WQI (Water quality index) for drinking water was used to evaluate groundwater samples according to WHO, (2004) for its suitability for drinking purpose through using the following formula:

$$WQI = \Sigma WIQI / \Sigma WI$$

All analyzed parameters of studied water groundwater samples were considered for WQI calculation except the bacteriological parameter.

2.1 Description of study area

a- Kurdistan covers about 65,000 km² in Iraq at 36.4103° N, 44.3872° E, The Region is geographically diverse, from hot and dry plains to cooler mountainous areas with natural springs and snowfall in the winter.

b- Erbil is a capital of Kurdistan of Iraq. Erbil covers about 18170 square kilometers. It is bounded to the north-west by Greater Zab River and to the south-east by Lesser Zab River. Located at 36.5571° N, 44.3851° E. The climate of the area is characterized by a wide diurnal and annual range of temperature (Figure 1 A).

c- Shaqlawa lies 51 km to the northeast of Erbil, at the bottom of Safeen mountain. Shaqlawa is situated between Safeen mountain and Sork mountain, and sits 1066 m above sea level. The city is known for its waterfalls, trees, and greenery.

In this review, 12 wells were secured through gathering information and data about water quality

evaluation in the zone under review. All wells were dispersed in the area. Four wells situated in each of Shaqlawa districts located in Erbil Province, Harir and Permam sub-districts located in Erbil-Kurdistan Region of Iraq (Figure 1 A).

Erbil Province is the capital of Iraq Kurdistan district of and arranged in the north east of Iraq. Erbil region is the capital of Iraqi Kurdistan with around one million population and arranged in the upper east of Iraq. Its limits reached out from longitude 43° 15` E to 45° 14` E and from scope 35° 27` N to 37° 24` N (Goran, 2006, Shareef and Muhamad, 2012).

Study area is a memorable city and a Hill station in the Erbil Governorate in the Kurdistan area of Iraq (Toma, 2010)

Shaqlawa is sitting 56 km to north-east of Erbil city and situated in versant of Safeen mountain. Permam and Harir located 27 and 47km respectively and the atmosphere in the area has a place with the semi-parched Mediterranean type. It is described by cool, blustery winters from one viewpoint and long, hot, dry summers. Study areas describe by a prolific soil and presence of many water asset like snow and precipitation wellsprings of winter precipitation. The principle hydrogeological attributes are looked like by yearly precipitation run between 800-1000 mm/year, many springs are streaming in contemplated territory, these springs are spill out of Aqra-Bekhme and Pila Spi Formations. The primary hotspot for these springs are identified with aquifers fissured, fissured (Seeyan and Mirkel, 2014).

Kurdistan area of Iraq is a rocky land finds, where, Syria, Turkey and Iran meet. It has chains of high mountains, for example, Toros and Zagros mountains, which frames a couple of incredible curves of around 3000-4000 meters height. The topography of Kurdistan region extended from longitudinal of 43°15` E to 45° 14` E and from latitudinal of 37°27` N to 36° 34` N and spreads a territory of roughly 165 000 square kilometers (Maulood and Hinton, 1978).

Contemplate territory is situated at the High Folded Zone (support by figure of High folded zone in Erbil). The topographic zone reflected the geological structures straightforwardly which affected by nature of these developments, and difference in the imperviousness to degree for disintegration. In study zone see high and ridged area which is spoken to by most established development is Qamchuqa Formation furthermore to Bekhme and Pila Spi Formations, however in low help regions speaks to by clastic formations which is Kolosh, Gercus, Lower Fars and Upper Fars Formations. Khurmala arrangement was happened as a tongue in Kolosh Formation, and Avanah Formation happened in Gercus Formation. Limit of Pila Spi Formation was unconformable over Gercus Formation stores, limit of Pila Spi Formation was unconformable with Lower Fars Formation and limit of Upper Fars Formation was comparable with Lower Fars Formation. The primary hydrogeological attributes are looked like by yearly precipitation run between 800-1000 mm/year, many springs are streaming in contemplated zone, these springs are spill out of Aqra-Bekhme and Pila Spi Formations. The principle hotspot for these springs are identified with aquifers fissured, fissured (Sissakian and Youkhanna, 1978).

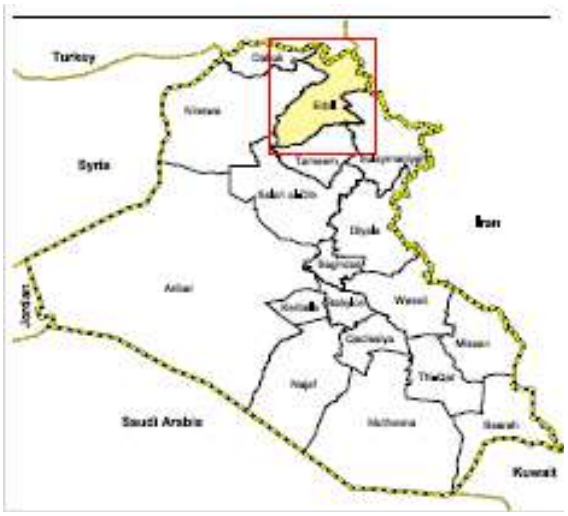

Figure 1: A - Map of Iraq.

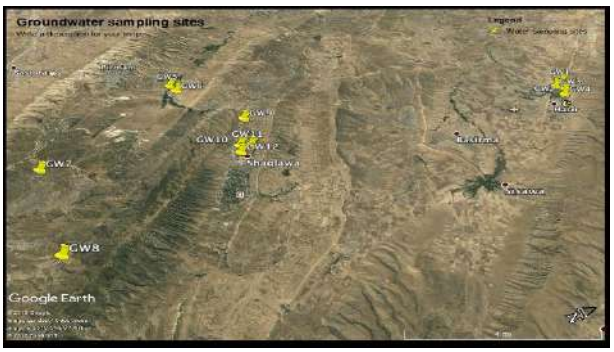

Figure 1: B - Study area

3. RESULTS AND DISCUSSION

According to WHO standards (2011) and IQS, Iraqi Standard (2009) EC value should not exceeded 1500 μS/cm^{-1}. In study areas, EC value was ranged between 252-2300 μS/cm^{-1}, with mean values for all 12 (Wells or GW) were range between 474.8-1575.5 and overall mean was 689.3. (as shown in table 1) and came in agreement with work done by (Toma 2010) on Shaqlawa water wells. Water with high mineral content tends to have higher conductivity, which is a general indication of high dissolved solid concentration of the water. Therefore, conductivity measurements can be used as a quick way to locate potential water quality problems (Mohsin *et al*., 2013)

The pH of water is referring to the measure of hydrogen ions concentration in water. It ranges from 0 to 14. In general, water with a pH of 7 is considered neutral while lower of it referred acidic and a pH greater than 7 known as basic. According to WHO standards pH of water should be 6.5 to 8.5 (Table 1). It is noticed that water with low pH is tend to be toxic and with high degree of pH it is turned into bitter taste. The pH is neutral or close to it as they all range from 7 to 8.4 with mean 7.6 and standard deviation of 0.4 and agreed with (WHO, 2006) standards for drinking water. Correlation coefficients were found between pH, EC, TDS, Alkalinity and SO_4.

Turbidity is one of the parameters for the acceptability of drinking water quality. WHO, guidelines for turbidity is < 5 NTU. All natural waters are turbid but generally surface more than ground water (APHA, 1998). The observed values in studied samples for turbidity were varied from 0.1 to 7.6 NTU, with mean values for all 12 Wells were range between 0.23-3.13 and overall mean was 1.0 (As shown in table 1), the high turbidity in drinking-water may be due to the presence of inorganic particulate matter and rainfall season, this came in agreement with (Toma, 2010) who worked on drinking water of Shaqlawa.

The term total dissolved solids refer mainly to the inorganic substances that are dissolved in water. The effects of TDS on drinking water quality depend on the levels of its individual components; excessive hardness, taste, mineral depositions and corrosion are common properties of highly mineralized water (Shivaprasad *et al.,* 2014) The overall mean of TDS was ranged from 308.6 to 1024.1 (As shown in table 1), according to the WHO standards (1000 mg/L) it is a natural range and its mean and standard deviations is 448 and 230.2 respectively. Alkalinity is the chemical measurement of a water's ability to neutralize acids, is the ability to resist changes in pH with respect to the addition of acid in water provides an idea of natural salts present in water upon the addition of acids or bases. Alkalinity of natural waters is due primarily to the presence of weak acid salts although strong bases may also contribute in extreme environments. Bicarbonates represent the major form of alkalinity in natural waters. Its standard level is 300 mg $CaCO_3$/L, the minimum limit of alkalinity in potable water is 200 mg/L. The maximum level is 755 mg/L which it is a high level. The mean value of alkalinity in the ground water of the study area was 278.5 mg/L with standard deviation of 117.4. This fluctuation in alkalinity level is normal for Kurdistan groundwater systems, this agreed with (Goran 2006) on the natural spring and surface water of Kasnazan and Dilope spring.

Hardness of water is caused by the presence of multivalent metallic cations and is largely due to calcium, Ca^{++}, and magnesium, Mg^{++} ions. Hardness is reported in terms of $CaCO_3$ (WHO, 2004). The maximum acceptable level of total hardness in drinking water according to WHO guideline is 500 mg $CaCO_3$/L (Toma, 2010). Concentration of total hardness in the studied area ranged between 160-560 mg $CaCO_3$/L with a mean and standard deviation is 311.5 and 91.7 respectively.

Calcium and magnesium are the two most common minerals that can cause alkalinity in water and the degree may increase as calcium and magnesium ion increases. This causes water to be hard and leads to aesthetic problems and bitter

taste (Napacho *et al*., 2010). Its standard range is 200 mg $CaCO_3$/L. The maximum acceptable limit of calcium for domestic use is 75ppm and minimum range is 30 (Table 1), most hard-water ions originate from calcium carbonate, levels of water hardness are often referred to in terms of hardness as $CaCO_3$. The content of magnesium in the groundwater was significantly different and it ranged from 11 to 86 and its mean is 41.2 and its STDEV is 17.8, its affect the total hardness. Correlation coefficient were found between hardness, Ca, Mg, SO_4, NO_3

Sodium and potassium are chemicals commonly found in soils and rocks. Sodium is more mobile in soil than potassium and so it is used often as an indicator of human impacts to shallow ground water. Sodium is also a common chemical in minerals. Like potassium, sodium is gradually released from rocks. They belong to a group of chemicals called the "alkali earth metals, they readily dissolve in water. Mean concentrations of sodium and potassium from the Ground Water wells were 22.8 and 1 mg/L (Table 1) respectively, moreover, sodium and potassium were ranged from 1 to 310 and 0.1 to 8.18 mg. l^{-1} with STDEV of 57 and 1.3 respectively (APHA 1998). Sodium correlated significantly ($P<0.05$) with pH, EC, TDS, SO_4, Cl^{-1} and alkalinity.

Sulfate (SO_4) occurs naturally in groundwater. At high levels, sulfate can give water a bitter or astringent taste and can have laxative effects. As a precaution, water with a sulfate level exceeding 400 mg/L should not be used in the preparation of infant formula. The level of sulfate in groundwater in study area is low, between 11.8 milligrams per liter (mg/L) to 314 mg/L, its mean and STDEV are 72.7 and 71.6 respectively (APHA 1998).

Sodium and chloride are substances naturally exist in groundwater at low levels. They are commonly known as salt, or 'table salt. Sodium and chloride are substances that occur naturally in groundwater. They are also substances used by the human body to help it work well. But, certain human activities, such as salting roads, can increase levels in well water so that water taste or quality are impacted. Water containing 350 mg/L of chloride may have a detectable salty taste if the chloride came from sodium chloride (Maiti 2004). The recommended maximum level of chloride in study ground water is 494 and the minimum level is 2.31 mg/L, with a mean of 42.1 and the mean concentrations of sodium from the Ground Water wells is 22.8 mg/L (Table 1).

Natural nitrate levels in groundwater are generally very low (typically less than 10 mg/L NO_3), but nitrate concentrations grow due to human activities, such as agriculture, industry, domestic effluents and emissions from combustion engines. Its standard level is 50 mg/L, in the study area NO_3 levels ranged between 2 to 38, and its mean is 11.9 with STDEV of 9.9. The nitrate concentration in ground water under aerobic condition is 10 mg/L and depends strongly on soil type and the geological conditions (Gray, 1994).

Fecal coliform bacteria originate from intestinal tracts of animal and human indicate the possible presence of pathogenic organisms. In the present study, the recorded value for coliform bacteria (fecal coliform bacteria) values were ranged from 0 to 16 MPN/100ml, the indicated values 16 MPN/ 100ml mean that water is considered unsatisfied for drinking at GW1 during winter 2016 according to WHO guidelines (WHO, 2011). While in other sites have 2.2 MPN.100 mL or less (zero) and in the safe side for drinking purposes due to the chlorination effects (WHO, 2004). (Fripp *et al*., 2015 and Edberg *et al*., 2000).

It was observed that WQI values were ranged from 16.36 at GW3 during Spring season to 47.52 at GW11 during Spring season and ground water samples can be categorized into excellent water quality (Table 1 and Table 3), The mean value of WQI is 21.27 and considered safe for drinking purpose according to WHO, 2004 and Garcia-Avila *et al*., 2018. The "good" quality of studied water samples of Harir and Shaqlawa can be related to the measured parameters that was below maximum standards for drinking water purpose. Same results were obtained by Garcia-Avila *et al*., 2018 in Ecuador water systems.

Table 1: Physical and chemical properties of survived groundwater in Shaqlawa district-Erbil

Location	*Well No.*	*Season*	*Turbidity*	*pH*	*EC*	*TDS*	*T. Alkalinity*	*T. Hardness*	*Ca*	*Mg*	*Na*	*K*	*Cl*	*NO_3*	*SO_4*	*MPN*	*Mean*	*WQI*
Standard			5NTU	6.5-8	400 µS.cm	1000 mg. l-1	300mg $CaCO_3$/L	500 mg $CaCO_3$/L	100mg $CaCO_3$/L	100mg. l-1	200mg. l-1	20mg. l-1	250mg. l-1	50 mg. l-1	250mg. l-1	0/100ml		
Harir 2	GW1	Spring	4.7	7.1	616	400.4	230	250	45	33.5	4	0.6	20	24	64	0	130.7	35.13
		Summer	0.6	8.1	462	300.3	180	175	48	13.5	2.6	0.6	15	7.5	61	0	98.1	19.59
		Autumn	0.2	7.9	581	377.65	220	300	80	24.5	5	0.7	25	26	59	0	131.3	19.00
		Winter	5.6	7.8	473	307.45	262	276	84	16.2	4.4	0.7	15	14	55	16	117.0	39.83
	Mean		2.78	7.7	533.0	346.5	223.0	250.3	64.3	21.9	4.0	0.7	18.8	17.9	59.8	4.0	119.3	
Harir 9	GW2	Spring	0.1	7.4	452	293.8	208	270	63	27.5	1.7	0.2	11	5.6	51	0	106.9	16.41
		Summer	3.3	7.8	475	308.75	260	245	75	14.2	2	0.4	10	6	49	0	112.0	30.09
		Autumn	0.4	7.3	500	325	210	220	40	29.3	2	0.3	15	5	56	0	108.5	17.24
		Winter	0.5	7.4	538	349.7	236	237	43	31.6	2.2	0.4	19	6	54	0	117.3	18.02
Mean			1.08	7.5	491.3	319.3	228.5	243.0	55.3	25.7	2.0	0.3	13.8	5.7	52.5	0.0	111.2	
Harir 16	GW3	Spring	0.2	7.3	516	335.4	240	210	52	19.6	1.8	0.2	13	2	58	0	111.8	16.36
		Summer	0.4	7.1	564	366.6	200	210	45	23.8	2	0.1	15	3	53	0	114.6	16.75
		Autumn	0.5	7.1	580	377	175	250	32	41.4	3	0.4	20	3	50	0	118.4	17.28
		Winter	2.3	7.1	692	449.8	250	320	32	58.4	4	0.4	20	12	49	0	145.9	25.20
Mean			0.85	7.2	588.0	382.2	216.3	247.5	40.3	35.8	2.7	0.3	17.0	5.0	52.5	0.0	122.7	
Harir 19	GW4	Spring	0.1	7.2	515	334.75	220	160	64	11	2.7	0.5	14	20	54	0	106.9	16.55
		Summer	0.3	7.0	592	384.8	220	245	52	28.1	3	1.3	20	28	59	0	126.2	17.65
		Autumn	0.5	7.3	604	392.6	231	267	61	28.0	4	1.2	23	32	68	0	132.3	19.29
		Winter	1.5	7.4	646	419.9	290	340	30	64.5	2	0.3	18	6.3	61	0	145.1	22.39
Mean			0.60	7.2	589.3	383.0	240.3	253.0	51.8	32.9	2.9	0.8	18.8	21.6	60.5	0.0	127.6	
Kore 6	GW5	Spring	0.1	7.9	923	599.95	275	425	94	46.4	18.5	1.4	41	27	108	0	196.0	19.66
		Summer	0.2	7.5	803	521.95	315	350	82	35.4	41	0.9	20	5	53	0	171.9	17.93
		Autumn	0.5	7.4	1003	651.95	350	560	160	39.3	24	1.8	55	38	65	0	227.4	21.60
		Winter	0.1	7.9	926	601.9	280	500	96	63.4	20.4	1.5	45	30	113	0	204.9	20.05
Mean			0.23	7.7	913.8	593.9	305.0	458.8	108.0	46.1	26.0	1.4	40.3	25.0	84.8	0.0	200.1	
Kore 3	GW6	Spring	0.1	7.2	252	163.8	220	400	96	39.1	11.8	1.8	45	5	141	0	105.3	17.00
		Summer	0.3	7.3	600	390	265	280	49	38.4	40	0.8	15	5	54	0	134.2	17.39
		Autumn	0.2	7.8	830	539.5	280	520	128	48.9	17	1.4	40	4	91	0	192.9	19.26
		Winter	1.47	7.9	757	492.05	260	450	112	41.6	15.6	1.7	40	4	104	2.2	174.6	24.29
Mean			0.52	7.6	609.8	396.3	256.3	412.5	96.3	42.0	21.1	1.4	35.0	4.5	97.5	0.6	151.8	
Qirzha	GW7	Spring	1.4	8.2	2100	1365	755	184	17.8	34.0	310	8.18	494	17.8	123.5	0	416.8	28.60
		Summer	0.4	8.2	985	640.25	351	456	40	86.6	77	2.5	36	26	288	0	230.5	22.09
		Autumn	0.52	8.1	917	596.05	378	426	36	81.8	72	2.3	34	33	295	0	221.5	22.49
		Winter	1.01	8.4	2300	1495	674	408	45.7	71.5	244	4.78	494	12.8	314	0	467.2	27.30
Mean			0.83	8.2	1575.5	1024.1	539.5	368.5	34.9	68.5	175.8	4.4	264.5	22.4	255.1	0.0	334.0	
Khoran	GW8	Spring	0.5	7.9	421	273.65	503	256	62.2	24.6	41.85	0.73	2.31	2.29	51.2	0	126.7	19.31
		Summer	0.2	8.2	516	335.4	256	312	40	51.6	4	0.6	16	6	195	0	133.9	18.82
		Autumn	0.3	7.9	532	345.8	238	319	36.5	55.5	55.3	0.52	21.4	11	185		139.1	18.95
		winter	0.6	8.1	430	279.5	529	269	65.8	25.6	1.87	0.682	2.31	2	11.8	0	125.1	19.99
Mean			0.40	8.0	474.8	308.6	381.5	289.0	51.1	39.3	25.8	0.6	10.5	5.3	110.8	0.0	131.2	
Shaqlawa kawaniyan	GW9	Spring	0.9	7.7	626	406.9	321	378	46	64.0	2.3	0.4	21	11	23	0	146.8	20.91
		Summer	0.5	7.9	685	445.25	275	267	42	39.5	3.4	0.5	21	2	14	0	138.7	19.00
		Autumn	0.2	7.5	593	385.45	220	238	45	30.6	4	0.4	25	12	31	0	122.5	17.25
		Winter	0.6	7.6	659	428.35	330	390	48	65.8	2	0.2	15	4	15	0	151.2	19.24
Mean			0.55	7.7	640.8	416.5	286.5	318.3	45.3	50.0	2.9	0.4	20.5	7.3	20.8	0.0	139.8	
Shaqlawa -16	GW10	Spring	0.25	7.4	593	385.45	193	251	36	39.2	1.75	0.2	10	14	15	0	118.9	17.21
		Summer	0.3	7.2	618	401.7	190	290	38	47.5	3	0.4	20	6	27	0	126.9	16.93
		Autumn	0.37	7.2	638	414.7	198	311	45	48.4	1.2	0.5	18	10	40	0	133.3	17.52
		Winter	0.1	7.6	625	406.25	200	260	48	34.2	1	0.3	12	3	19	0	124.3	16.69
Shaqlawa -13	GW11	Spring	7.6	7.3	831	540.15	320	450	48	80.3	18	0.9	82	9	47	0	187.8	47.52
		Summer	2.8	7.6	684	444.6	264	293	51	40.4	3.14	0.5	22	9	28	0	142.3	28.03
		Autumn	2	7.9	662	430.3	237	311	54	42.9	3.75	0.6	26	11	32	0	140.0	25.54
		Winter	0.1	7.8	535	347.75	200	260	48	34.2	1	0.3	12	3	18	0	112.9	17.00
Mean			3.13	8	678	441	255	329	50	49	6	1	36	8.0	31	0	146	
Shaqlawa -20	GW12	Spring	2.3	7.3	597	388.05	220	280	45	40.8	2.8	0.6	15	4.1	27	0	125.4	25.10
		Summer	0.6	7.5	538	349.7	241	289	49	40.6	2.2	0.5	14	18	25	0	121.2	19.23
		Autumn	0.87	7.5	545	354.25	249	314	51	45.5	1.8	0.7	19	21	16	0	125.0	20.57
		Winter	0.1	7.6	555	360.75	150	280	56	34.2	2	0.3	13	4	20	0	114.1	16.72
Mean			0.97	7.5	558.8	363.2	215.0	290.8	50.3	40.3	2.2	0.5	15.3	11.8	22.0	0.0	121.4	
Mean			1.0	7.6	689.3	448.0	278.5	311.5	57.4	41.2	22.8	1.0	42.1	11.9	72.7	0.4		
SD			1.5	0.4	354.2	230.2	117.4	91.7	26.7	17.8	57.0	1.3	96.3	9.9	71.6	2.4		

Table 2: Correlations between studied samples and sites

Correlation		Turbidity	pH	EC	TDS	Alkalinity	Hardness	Ca	Mg	Na	K	Cl	NO_3	SO_4	MPN
Turbidity	Pearson Correlation	1	-.088	.049	.049	.079	.059	-.048	.110	-.004	.008	.075	.001	-.104	.447**
	Sig. (2-tailed)		.551	.739	.739	.594	.690	.744	.458	.980	.955	.614	.995	.483	.002
	N	48	48	48	48	48	48	48	48	48	48	48	48	48	47
pH	Pearson Correlation	-.088	1	.448**	.448**	.564**	.250	.070	.235	.491**	.461**	.407**	.065	.527**	.101
	Sig. (2-tailed)	.551		.001	.001	.000	.086	.637	.107	.000	.001	.004	.659	.000	.497
	N	48	48	48	48	48	48	48	48	48	48	48	48	48	47
EC	Pearson Correlation	.049	.448**	1	1.000**	.762**	.291*	-.046	.399**	.905**	.870**	.929**	.283	.538**	-.087
	Sig. (2-tailed)	.739	.001		.000	.000	.045	.758	.005	.000	.000	.000	.051	.000	.559
	N	48	48	48	48	48	48	48	48	48	48	48	48	48	47
TDS	Pearson Correlation	.049	.448**	1.000**	1	.762**	.291*	-.046	.399**	.905**	.870**	.929**	.283	.538**	-.087
	Sig. (2-tailed)	.739	.001	.000		.000	.045	.758	.005	.000	.000	.000	.051	.000	.559
	N	48	48	48	48	48	48	48	48	48	48	48	48	48	47
Alkalinity	Pearson Correlation	.079	.564**	.762**	.762**	1	.181	-.037	.254	.837**	.794**	.783**	.115	.430**	-.025
	Sig. (2-tailed)	.594	.000	.000	.000		.218	.803	.082	.000	.000	.000	.435	.002	.867
	N	48	48	48	48	48	48	48	48	48	48	48	48	48	47
Hardness	Pearson Correlation	.059	.250	.291*	.291*	.181	1	.589**	.695**	.080	.187	.073	.331*	.414**	-.026
	Sig. (2-tailed)	.690	.086	.045	.045	.218		.000	.000	.590	.202	.624	.021	.003	.862
	N	48	48	48	48	48	48	48	48	48	48	48	48	48	47
Ca	Pearson Correlation	-.048	.070	-.046	-.046	-.037	.589**	1	-.168	-.176	-.001	-.136	.247	-.019	.185
	Sig. (2-tailed)	.744	.637	.758	.758	.803	.000		.253	.231	.997	.358	.090	.899	.213
	N	48	48	48	48	48	48	48	48	48	48	48	48	48	47
Mg	Pearson Correlation	.110	.235	.399**	.399**	.254	.695**	-.168	1	.255	.230	.210	.200	.531**	-.204
	Sig. (2-tailed)	.458	.107	.005	.005	.082	.000	.253		.080	.115	.151	.172	.000	.170
	N	48	48	48	48	48	48	48	48	48	48	48	48	48	47
Na	Pearson Correlation	-.004	.491**	.905**	.905**	.837**	.080	-.176	.255	1	.939**	.945**	.172	.581**	-.048
	Sig. (2-tailed)	.980	.000	.000	.000	.000	.590	.231	.080		.000	.000	.243	.000	.749
	N	48	48	48	48	48	48	48	48	48	48	48	48	48	47
K	Pearson Correlation	.008	.461**	.870**	.870**	.794**	.187	-.001	.230	.939**	1	.898**	.320*	.559**	-.022
	Sig. (2-tailed)	.955	.001	.000	.000	.000	.202	.997	.115	.000		.000	.027	.000	.886
	N	48	48	48	48	48	48	48	48	48	48	48	48	48	47
Cl	Pearson Correlation	.075	.407**	.929**	.929**	.783**	.073	-.136	.210	.945**	.898**	1	.129	.469**	-.042
	Sig. (2-tailed)	.614	.004	.000	.000	.000	.624	.358	.151	.000	.000		.383	.001	.777
	N	48	48	48	48	48	48	48	48	48	48	48	48	48	47
NO_3	Pearson Correlation	.001	.065	.283	.283	.115	.331*	.247	.200	.172	.320*	.129	1	.346*	.015
	Sig. (2-tailed)	.995	.659	.051	.051	.435	.021	.090	.172	.243	.027	.383		.016	.920
	N	48	48	48	48	48	48	48	48	48	48	48	48	48	47
SO_4	Pearson Correlation	-.104	.527**	.538**	.538**	.430**	.414**	-.019	.531**	.581**	.559**	.469**	.346*	1	-.023
	Sig. (2-tailed)	.483	.000	.000	.000	.002	.003	.899	.000	.000	.000	.001	.016		.881
	N	48	48	48	48	48	48	48	48	48	48	48	48	48	47
MPN	Pearson Correlation	.447**	.101	-.087	-.087	-.025	-.026	.185	-.204	-.048	-.022	-.042	.015	-.023	1
	Sig. (2-tailed)	.002	.497	.559	.559	.867	.862	.213	.170	.749	.886	.777	.920	.881	
	N	47	47	47	47	47	47	47	47	47	47	47	47	47	47

**. Correlation is significant at the 0.01 level (2-tailed).
*. Correlation is significant at the 0.05 level (2-tailed).

Table 3. Water quality classification ranges and types of water based on WQI values

No.	Type of groundwater	Range
1	Excellent water	< 50
2	Good water	50.1–100
3	Poor Water	100.1–200
4	Very poor water	200.1–300
5	Unsuitable for drinking/Human consumption purpose	≥ 300.1

4. CONCLUSIONS

4.1 Conclusions:

1. Our conclusion of the present study revealed that the quality assessment of physico-chemical parameters obtained not exceeded and in compliance with permissible limits recommended by WHO Standards and remain in the safe side and considered suitable for drinking consumption.
2. Total alkalinity and Total hardness in studied samples were high due to the geological formation of the area.
3. Studied water samples were satisfactory for drinking purpose physically and chemically except at GW7 during winter and spring season
4. Bacteriologically, water wells were satisfied for drinking except GW1 during winter 2016.
5. Water quality index for studied water samples are excellent and at safe values for drinking purpose.

4.2 Recommendations

1. Monitoring of artesian wells should be done in regular state at least quarterly by government.
2. Chlorination of water is of great important.

References

Al-Khashman O. A. 2008. Assessment of the spring water quality in The Shoubak area, Jordan. Environmentalist 28:203–215

American Public Health Association (A.P.H.A). 1998. Stander Methods for the examination of water & wastewater, 20th Edition. A.P.H.A., 1015 fifteenth street, NW, Washington , DC. 2005-2605.

Damo R. and Icka P. 2013. Evaluation of Water Quality Index for Drinking Water. Pol. J. Environ. Stud. 22 (4):1045-1051

Edberg S.C., Rice E.W., Karlin R.J. and Allen M.J. 2000. Escherichia coli: the best biological drinking water indicator for public health protection. Journal of Applied Microbiology, 88: 1068-1168

Fittes C. R. 2002. Ground Water Science. An imprint of Elsevier Science Lt.168pp

Fripp W, Woodyard C.D., and Hanna M. 2015. Fecal Coliform Contamination of Drinking Water An Evaluation of World Field Assessment Techniques. EWB-USA, 104: 1-13.

García-Ávila F., Ramos- Fernández L., Pauta D., Quezad D. 2018. Evaluation of water quality and stability in thedrinking water distribution network in the Azogues city, Ecuador. Elsevier Inc., 18: 111–123.

Goran, S. M. A. 2006. Limnological & non diatom phytoplankton composition of Dilope spring & Kasnazan impoundment. M.Sc. Thesis, Univ. of Salahaddin-Erbil. Iraq.

Gray, N. F. 1994. Drinking Water Quality: problems and solutions, 2nd Cambridge university press. 522pp

Guler C. and Thyne G. D. 2004. Hydrologic and geologic factors controlling surface and groundwater chemistry in Indian Wells-Owens Valley area, southeastern California, USA," Journal of Hydrology, 285: 177–198.

Hossien M. T. 2004. "Hydrochemical evaluation of groundwater in the Blue Nile Basin, eastern Sudan, using conventional and multivariate techniques," Hydrogeology Journal, 12: 144–158.

IQS, Iraqi Standard (2009) Iraqi Standard of Drinking Water (417), 2nd modification

Lorenz, F. and Erickson, E. J. 2013. Strategic Water Iraq and Security Planning in the Euphrates-Tigris Basin. Marine Corps University Press Quantico, Virginia. 310pp.

Maiti, S. K. 2004. Handbook of Methods in Environmental Studies Vol. 1: Water & Wastewater Analysis. 2nd edition, ABD Publisher, Distribution by Oxford Book Company. 307pp

Maulood, B. K. & Hinton G. C. F. 1978. An ecological study on Serchinar water-chemical & physical aspects. Zanco J., 4(3): 93-117.

Mohsin, M., Safdar S., Asghar, F., Jamal, F. 2013. Assessment of Drinking Water Quality and its Impact on Residents Health in Bahawalpur City. International Journal of Humanities and Social Science, 3 (15): 114-128.

Napacho, Z. A. and Manyele, S. V. 2010. Quality assessment of drinking water in Temeke District (part II): Characterization of chemical parameters. African Journal of Environmental Science and Technology Vol. 4(11), pp. 775-789.

Parsons, T.R.; Maita, Y.; and Lalli, C. M. 1984. A Manual of chemical and Biological Methods for seawater Analysis. Pergamon International Library. Robert Maxwell publisher, M.C. Oxford, U.K. 171pp.

Rajmohan, N. and Elango, E. L. 2004. Identification and evolution of hydrogeochemical processes in the groundwater environment in an area of the Palar and Cheyyar River Basins, Southern India. Environ. Geol., 46, 47–61.

Rao, J. H. 2013. Physico-Chemical Characteristics of Ground Water of Vuyyuru, 3 (2): 225-23.

Seeyan, S. and Merkel, B. 2014. Determination Of Recharge By Means Of Isotopes And Water Chemistry In Shaqlawa-Harrir Basin,

Kurdistan Region, Iraq. Hydrol Current Res 5: 179.

Shareef, K. M. and Muhamad, S. G. 2012. Natural and Drinking Water Quality In Erbil, Kurdistan, Review Article, 3(2), 227-238,

Shivaprasad, H., Nagarajappa, D. P. and Sham Sundar K. M. 2014. A Study on Physico-Chemical Characteristics of Borewell Water In Sugar Town, Mandya City, Karnataka State, India. Journal of Engineering Research and Applications, Vol. 4, Issue 7 (1): pp.112-123

Sissakian, V. k. and Youkhanna, R. Y. 1978. Regional geological mapping of Erbil, Shaqlawa – KoisanjaqRaidar area. Report No. 975, Som library, Baghdad.

Subramani, T., Elango, L. and Damodarasamy, S. R. 2005. "Groundwater quality and its suitability for drinking and agricultural use in Chithar River Basin, Tamil Nadu, India," Environmental Geology, Vol. 47, pp. 1099–1110.

Technology Integration Division (TID). 2011. Iraq in Perspective, an orientation guide.Defence Language Institute Foreign language center. 79pp.

Tomas, J. J. 2010. Evaluation of Trace Metals In Shaqlawa Wellwater. Arbil-Kurdistan Region Of Iraq, Journal Of Duhok University.13(1) Salahaddin University – Erbil, Retrieved On: 16 January 2016)

World Health Organization (WHO). 2004. Guideline for Drinking - Water Quality. 3rd Edition Vol.1 Recommendation Geneva

World Health Organization (WHO). 2006. Guideline for Drinking-Water Quality. 3rd Edition. Vol. 1, Recommendation. World Health Organization Press. Geneva. 562p.

World Health Organization (WHO). 2011. Guidelines for Drinking-Water Quality. 3rd Edition. Vol. 1, Recommendations. World Health Organization WHO. Geneva.

Zekster, I. S. 2000. Groundwater and the environment. CRC Press LLC, Boca Raton London New York Washington, D.C. 410pp

Zuane, J. D. 2007. Handbook of Drinking Water Quality,2nd edition, John Wiley & Sons, Inc. 325pp

ZANCO Journal of Pure and Applied Sciences
The official scientific journal of Salahaddin University-Erbil
https://zancojournals.su.edu.krd/index.php/JPAS

ISSN (print):2218-0230**, ISSN (online):** 2412-3986**, DOI: http://dx.doi.org/10.21271/zjpas**

RESEARCH PAPER

Influence of *Vitis vienefera* L. Cultivars on Some Physicochemical Characters and Enzyme Activities of Soil

Shakar Jamal aweez [1] Sakar Abdulqadr Saheed[1] Snowber Muhamad Ahmed[2]

1Department of environmental science, College of Science, Salahaddin University- Erbil,Kurdistan Region, Iraq
2Department of general science,college of Basic Education, Salahaddin University- Erbil,Kurdistan Region, Iraq

A B S T R A C T:

This study was carried out in order to evaluate the impacts of grape (*Vitis vienfera* L.) cultivars on soil physicochemical and enzyme activity.The soilsamples at root zones of various grape cultivars (Kamala, Kshmishy, Rashmiry, Doshawe, Halwany, Rashme and Bedenka) were collected in four different farm conditions. The experiment was designed in a completely randomized design (CRD) with three replicates. The results revealed non-significant variation ($p \leq 0.01$) among grape cultivars for(pH, organic matter% and water content%)of soil the total mean value (7.50, 16.55% and 11.41% were recorded respectively while Bedenka cultivar has recorded a highest porosity cultivars and the total mean value of all cultivars was (23.31%)However there was a significant variance among cultivars in soil electrical conductivity the total mean of all cultivars is(222.14µS.cm^{-1}) which not cause soil salinity .there was not significant variance recorded in soil enzymes among the grape cultivars for each (urease µgN.g^{-1} soil ,dehydrogenase **µ**gTPF.g^{-1}and catalase). Rashme cultivar has a highest dehydrogenases value of soil statistically compared to other cultivars and the total mean value of all cultivars is (116.67 **µ**gTPF.g^{-1},).

KEY WORDS: grape, cultivars, soil enzyme.
DOI: http://dx.doi.org/10.21271/ZJPAS.33.2.3
ZJPAS (2021) , 33(1);28-33 .

1.INTRODUCTION:

Grape (*Vitis vinifera* L.) belong to family Vitaceae. itis one of the commercial fruit in world as well as in Kurdistan there are numerous cultivars and clones in the country. The latest statistic which provide by Food and Agriculture Organization in Kurdistan region there are more than 46 varieties of grapes.(Ahmed *et al.*, 2015,Atrushy *et al.*, 2016 and Mariappan *et al.*,2017).Soil is a dynamic system in which continuous interaction takes place between soil minerals, organisms and organic matter(Khudhur ,2018).

Falling plants' leaves are the most important plant residues that generate organic soil matter, improve physical properties of the soil, preserve organic carbon content increase nutrient availability and provide microbial activity and growth with nutrients and energy, as they contain more than 60% cellulose, decomposition of cellulose is a fundamental action for soil bacteria. (Killum and Jim, 2015).The tests of soil enzyme may give information about the potential of soils carrying out some biochemical processes in the height of enzymatic action is one of the for most not worthy pointers of the characteristics and the quality of soil . Urease enzyme is an extracellular enzyme that catalyzes the hydrolysis of the urea forming ammonia and CO_2, which is retained by organic and inorganic colloids of the soil. Catalase enzyme is an enzyme that is a result of metabolic events and respiratory evets of living organisms that separates cytotoxic hydrogen peroxide (H_2O_2)

* **Corresponding Author:**
Shakar Jamal aweez
E-mail: sakarsaheed83@gmail.com
Article History:
Received: 07/09/2020
Accepted: 12/01/2021
Published: 18/04 /2021

into water and oxygen. (Kuscu *et al.*, 2018).Dehydrogenases play a significant role in the biological oxidation of soil organic matter by transferring hydrogen from organic substrates to inorganic acceptors (Wolinska and Stepniewska, 2014). This study aimed to assessment Influence of *Vitis vienefera* L. Cultivars on Some Physicochemical Characters and Enzyme activities of Soil effects of grape (*Vitis vienfera*) cultivars on soil enzyme activity.

2.Materials and Methods:

2.1 Description area:

In general,Iraqi Kurdistan region is consists of a mountains and the foothills. The area primarily amplified over the Zagross mountain up to the Taurus mountains in Turkey. The region shores areborders are Iran in the East, Syria in the West and Turkey in the North.The locations of the studied areas (chnarok) is located at a distance of 95 kilometers from Erbil and 15 kilometers northeast of koya.Chnarok summer resort is located next to Haibat sultan mountain (1260 meter)on the old road between Koya and Dokan.

2.2 Description of grape varieties

Grapes wide spread in the area of mid and north of Iraq, the vineyard under study were (9±1) years old. The cultivars are grown on its own root with conical cluster shape, ranged from small to large sizes, leaves arranged from three to five lobes depending on types of grape varieties, the flowers are hermaphrodite (perfect), the fruits start to ripens in the end of July and into August (Atrushy,etal.,2016).

2.3Soil sampling

Two soil samples were collected from farm of grape varieties; Kamalay and Kshmishy.The second two samples from the farm of Rashmiry and Doshawe. As well as one soil sample collected from Halwany.Finally,two soil samples had been collected from Rashme and Bedenka farm.The soil samples were taken by using auger from surface layer 0 – 30 cm at different location as shown in table (1) and figure (1).

Table 1. Soil samples geographical locations

Site No.	Site name	Coordination Location	
		North	East
S1	Farm 1	36° 06' 50"	44° 39' 46 "
S2	Farm 2	36° 06' 51"	44° 39' 59"
S3	Farm3	36° 06' 46 "	44° 39' 42"
S4	Farm4	36° 06' 45 "	44° 39' 51"

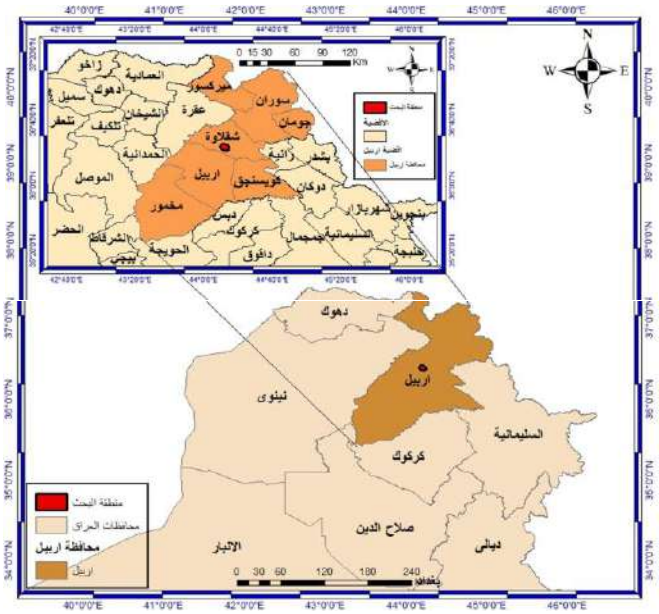

Figure (1): Soil samples collection areas of Iraqi Kurdistan region

2.2. Determination of soil physicochemical properties

Hydrometer method was used for particle size distribution and determination of soil textural classes using ISSS triangle. The pH and EC of the soils were determined in 1:5 (soil: water suspension) using a calibrated pH-meter (JENWAY 3505) and an electrical conductivity meter (JENWAY 4510) according to the method given in (Rayan *et al*., 2001). Gravimetric method was used for soil moisture content determination as described by (Jaiswal, 2003). Soil porosity was determined by placing samples into the core weighing and then putting them oven at 105 for 24hrs rather that, the dried samples were weighed again, then put it in water bath until they were dried, later the samples were weighed according to (Allen, 1974).Walkly-Black procedure 1934 was followed for determination of soil organic matter as given by (Pansu and Gautheyrou, 2006).

2.3.Estimation of soil enzyme activity

Estimation of dehydrogenase

The dehydrogenase activity was determined by the modified procedure of Casida 1977 given by (Anjaneyulu et al.,2011). For 5g of soil in a test tube 2.5 ml sterile distilled water and 1ml of 3% aqueous solution of triphenyl tetrazolium chloride (TTC) was added and incubated at 30^0C for 24 hours.The triphenyl tetrazolium formazan end product was measured at 485 nm. The results expressed as µg TPF g-1 dry weight soil.

Estimation of urease

Urease activity was determined by modified method of Hoffmann and Teicher 1961 described by (Uzun and Uyanoz,2011).For1g of soil,0.25 ml toluene,0.75 ml citrate buffer (pH 6.7) and 1ml of 10% urea substrate solution were incubated for 3 hours at 37^0C .Formation of ammonium was found out spectrophotometrically at 636 nm (Bashour and Sayeg,2007).Results expressed us µg N g-1 dry soil.

Estimation of catalase

The catalase activity was determined by $KMnO_4$ titration method as described by (Kumar, 2004).Two grams of oven -dried soil was mixed with 40 ml of distilled water and put in a rotary shaker. Then 5ml of 0.3 % H_2O_2 was added and the slurry was shaken for 20 minutes at 150rpm.The remaining peroxide was stabilized by adding 5ml 3N H_2SO_4 and 25 ml filtered aliquots which were titrated with 0.1 N $KMnO_4$. Results were expressed as ml of 0.1 N $KMnO_4$dry soil.20 min^{-1}, equivalent to peroxide decomposed per gram of oven – dry soil.

2.4. Statistical Analysis

This study was carried out according to Completely Randomized Design (CRD) with three replicates. Data were analyzed statically using Statistical Package for Social Science (SPSS version 24). Duncan's Multiple Range Test was used for the comparison of treatment means at 1%for laboratory parameters (AL-Rawi and KHalafulla,1980).

3. Results and discussions:

Data presented in table (2) indicate the effects of grape (*vitisvienfera*) cultivars on some physical and chemical properties of soil Kamala, Kshishy, Rashmiry, Halwany,Rashme and Bednka; onphysical and chemical soil enzyme activity. The results indicate the non-significant variation ($p \leq 0.01$) among the grape cultivars in pH, organic matter% and water content % of soil, the total means value (7.50, 16.55% and 11.41%) for (pH, organic matter% and water content%) respectively. The minimum and maximum mean value of (pH, organic matter %, and water content %) were ranged between (7.18-7.75, 8,9-27.61% and 6.42-14.77%) respectively. While the Bedenka cultivar has a highest porosity % which is superior significantly to other

cultivars General means of porosity for all cultivars is (23.31%), the minimum and maximum mean value of (porosity%) was ranged between (16.56-35.50%).The results revealed significant variance($p \geq 0.01$) among cultivars in soil electrical conductivity, the general mean of all cultivars was (222.14µS.cm^{-1}) Which indicates that the soils do not reach salinity, while minimum and maximum value ranged between (162.15-287.42 µS.cm^{-1})Electric conductivity (EC)is measurement of total amount of soluble salts present in soil, this amount revealed that organic residues contain soluble salts and the presence of more exchangeable calcium, magnesium and potassium in the soil, When rich- nutrient, plant residues decompose, salts and ions in the soil and in its liquid phase are increased. Such changes exert and influence on soil EC, which is regulated by several soil fertility attributes, such as pH, P, K, Ca, Mg, OM, cation exchange capacity (CEC)and by the contents of other soluble salts and organic ligands.This result agreed with (Carmo, *et al*.,2016)who showed that EC-soil property

interactions are not easily identified, since the magnitude of the interactions regulating soil EC levels are complex and dynamic, thus, it's important to investigate the change in EC in soils treated with different wastes, bearing in mind that EC reflects that the sum of salts and ions in the soil solution, the levels of which are regulated by the type, composition and the amount of waste added to the soil. While for other physicochemical properties' farms have the same climatic condition such as temperature and precipitation which cause some different soil properties while weathering in pedogenesis process and soil formation also have a great role effects on chemical and physical properties of soil. The chemical and physical nature of the carbonates(e.g.,particle size and mineralogy (carbonates exerts a major effect on soil chemical properties in calcareous soils, such as nutrient availability.This result similar to the result of (Killum and Jim,2015) notice that the fall leaves of grape plant is most important plant residues in which provide soil organic matter, improve physical properties of soil, sustain organic carbon content and can also enhance the availability of nutrient and provide the nutrient and energy for microbial activity and growth because contain more than 60 % cellulose the decomposition of cellulose is a key activity for soil bacteria

Data present in table (3) and figure (1) indicate the effects of grape (*vitisvienfera*) cultivars on soil enzyme activity (urease µgN.g^{-1} soil ,dehydrogenase **µ**gTPF.g^{-1}, and catalase) of soil cultivated by various grape cultivars (Kamala, Kshmishy, Rashmiry, Doshawe, Halwany, Rashme and Bedenka).The result show that there was non-significant variation ($p \leq 0.01$) among the grape cultivars on urease µgN.g^{-1} soil ,dehydrogenase **µ**gTPF.g^{-1}, and catalase of soil, the total means value (161.19, 116.67 and1.14**)** of (urease µgN.g^{-1} soil ,dehydrogenase **µ**gTPF.g^{-1}, and catalase)respectively, as well as the minimum and maximum mean values of (urease µgN.g^{-1} soil ,dehydrogenase **µ**gTPF.g^{-1}, and catalase were ranged between (78.60-243.00, 67.30, -222.40, and 0.07-1.83**)** respectively. The result indicate that the Rashme cultivar has a highest dehydrogenases value of soil compared to other cultivars and the total mean value of all cultivars was (116.67**),** the minimum and maximum mean value of (dehydrogenase) is ranged between (67.30-222.40). These results indicate enzyme activity of soil linked with mineral and organic matter occurring in the soil and the amendment, on the other hand the present of microbial activity. Furthermore, it contains essential micro and macronutrients for plant growth, (The reason might be due to fact that the application organic residues in soils is useful source of plant nutrients, particularly nitrogen and phosphorous and also potentially improve soil biological activity, physical and chemical properties. This result similar to the result (Akmal et al., 2012) who showed that the activity of soil enzymes is also affected by different biotic factors such as temperature, moisture, soil pH, and oxygen content. Kujar et al., 2012)reported that the variation in soil enzymes activity was significantly attributed to differences in soil texture.C, N,P content,bulk density,water holding capacity,moisture content and soil pH.Comparative analysis of soil enzyme revealed that there was gradual increase in amylase,invertase, protease and dehydrogenase activity from a nutrient deficient situation (fresh mine soil) compared to an enriched soil (fresh soil).(Berber *et al.*2014*)*,reported that the relationship between urease enzyme activity was not related significantly to pH, organic matter(O.M) electrical conductivity (EC) and calcium carbonate (CaCo3)is not statistically significant.(Kuscu et al., 2018) the relationship between urease and pH was found to be statistically significant.

Table 2.infleunce of *vitisyvienefera* L. cultivars on some physicochemical characters of soil farms .

Grapes cultivars	pH	ECµS.cm^{-1}	Organic matter%	Water content%	Porosity%
Kamalay	7.44a	198.13dc	17.71a	11.72a	20.30b
Kshmishy	7.67a	177.76d	16.43a	11.13a	21.50b

Rashmiry	7.52a	200.17c	12.37a	11.97a	22.92b
Doshawe	7.49a	249.73b	17.60a	12.03a	20.91b
Halwany	7.48a	277.54a	18.52a	11.91a	24.72b
Rashme	7.50a	246.54b	13.63a	11.14a	22.32b
Bedenka	7.39a	205.13c	19.56a	9.98a	30.53a
Total means	**7.50**	**222.14**	**16.55**	**11.41**	**23.31**
Minmum	**7.18**	**162.15**	**8.09**	**6.42**	**16.56**
Maximum	**7.75**	**287.42**	**27.61**	**14.77**	**35.50**

Table 3. infleunce of *vitisyvienefera* L. cultivars on enzymes activity of soil farms

Grapes cultivars	Urease	Dehydrogenase	Catalase
Kamalay	162.17a	96.47b	0.85a
Kshmishy	158.20a	104.53b	1.10a
Rashmiry	186.37a	90.73b	1.25a
Doshawe	142.03a	126.37b	1.19a
Halwany	159.67a	122.83b	1.37a
Rashme	140.63a	185.93a	1.18a
Bedenka	179.28a	89.83b	1.05a
Total means	**161.19**	**116.67**	**1.14**
Minmum	**78.60**	**67.30**	**0.07**
Maximum	**243.00**	**222.40**	**1.83**

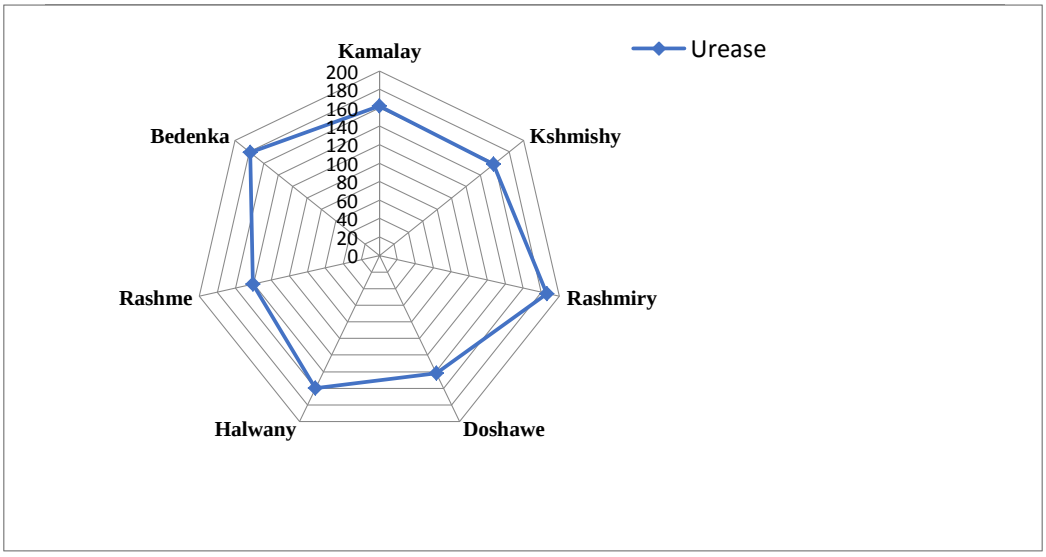

Figure (2):Influence of *Vitisvienefera*L.cultivars on urease activity of soil farms

4. Conclusion

The study was mainly focusing on the effects of grape (*vitisvienfera*) cultivars on physicochemical and enzyme activity of soil in 4 different farms cultivated various grape ;(Kamala, Kshmishy, Rashmiry, Doshawe, Halwany, Rashme and Bedenka). The results revealed the non-significant variation among the grape cultivars in pH, organic matter and water content of soils, while Bedenka cultivar recorded the highest porosity of soil which is superior significantly to other cultivars .Also there is non-significant variation among the grape cultivars for (urease µgN.g^{-1} soil dehydrogenase **µ**gTPF.g^{-1}, and catalase of soil

respectively ,but Rashme cultivar has a highest dehydrogenases value of soil statistically compared to other cultivars.

5.References

Ahmed A.M.N, D.A.Ibrahim andS. P.Uzun.(2015). Invitromicropropagation of VitisVinifera L.In Kurdistan Reagion of Iraq.Journal of university of zakho, 3(1), Pp 55-66.

Akmal, M.; M. S Altaf.; R. Hayat.; F.U. Hassan and M. Islam. (2012).Temporal Changes in Soil Urease, Alkaline Phosphatase and Dehydrogenase Activity in Rain Fed Wheat Field of Pakistan**.** Journal of Animal and Plant Sciences. 22(2): Pp 457-462

Allen, S.E. (1974). Chemical Analysis of Ecological Materials. Black well Scientific Publication Osney Mead, Oxford, p 565 .

Al-Rawi K.M. and A.A.M. Khalafulla. (1980). Design and analysis of agriculture experiment .univercity chemical of Mousle ministry of high education and scientific research . Mousl.Iraq.Pp488.(In Arabic)

Anjaneyulu,E., M.Ramgopal , G. Narasimha and M. Balaji . (2011).Effect of pig iron slag particles on soil physico-, biological and enzyme activities.Iranica J. Energy & Environment, 2(2):Pp 161-165.

AtrushySM ,S. A.Mustafa and F. K.Ahmad.(2016).Evaluation of some seeded cultivars of grape in different location of Kurdistan-region, Iraq. Kufa journal for agricultural Sciences. 8(2):Pp279-266

Bashour II and A. H. Sayegh. (2007). Methods of Analysis for Soils of Arid and Semi-Arid Regions.Food and Agriculture Organization of the United Nations, Rome.

Berbar, K. A.S.,S. Farasat.,A. Namli.(2014.) Afforestatıon Effects on Soil Biochemical Properties.Eurasian Journal of Forest Science, 1 (1),p 25,

Carmo D. L. L.B. de Lima and C. A. Silva.(2016).Soil Fertility and Electrical Conductivity Affected by Organic Waste Rates and Nutrient Inputs.Soil Fertility and Plant Nutrition.

Jaiswal PC. (2003). Soil, Plant and Water Analysis.Kalyani Publisher.

Khudhur, N.S.(2018). Effect of Kawrgosk Oil Refinery on Some Physicochemical Characteristics, Microbial Population and Biochemical Properties of Surface Soils.ZankoJournal of Pure and Applied Science: 30(1):Pp 1-13

Killum K.and I.P Jim.(2015).The bacteria and archaea.soil microbiology, ecology and biochemistry. Fourth edition.

Kujur, M.; S. K. Gartia and A. K. Patel. (2012).Quantifying the Contribution of Different Soil Properties on Enzyme Activities in Dry Tropical Ecosystems. Asian Research Publishing Network Journal of Agricultural and Biological Science.7 (9): Pp1-10

Kumar A. (2004). Industrial pollution and management, In, Study of correlation of physical, chemical and biological characteristics with catalase activity in industrially polluted and unpolluted soils of Warangal (D.T.) A.P. by Kumari BL and Charya MA, APH Publishing. New Delhi, Pp. 134-138.

Kuscu I.S.K., M. Cetin.N. Yigit , G. Savaci and H. Sevik.(2018). Rwlation ship between enzyme activity (urease-catalase) and nutrient element in soil use.pol .Journal of Environmental.Study.Vol.27, No. 5.Pp 2107-2112.

Mariappan V.N, V.S Pooja, B. P.D.Batvari, R. Indirani. (2017). Grape cultivation and many meat approaches by Geospatial tools-areview. J Adv Res Geosci Rem Sens. 4(1&2):17-28, ISSN:Pp 2455-3190.

Pansu M and J. Gautheyrou. (2006). Handbook of Soil Analysis: Mineralogical, Organic and Inorganic Methods. Springer-Verlag Berlin Heidelberg.

Ryan J, G. Estefan and A. Rashid.(2001). Soil and Plant Analysis Laboratory Manual.2nd edition.International Center for Agricultural Research in the Dry Areas (ICARDA), Aleppo, Syria.

Uzun N and R.Uyanoz. 2011. Determination of urease catalase activities and CO2 respiration in different soils obtained from in semi-arid region Konya, Turkey. Trends Soil Science Plant NutritionJournal., 2(1): Pp1-6.

ZANCO Journal of Pure and Applied Sciences
The official scientific journal of Salahaddin University-Erbil
https://zancojournals.su.edu.krd/index.php/JPAS

ISSN (print):2218-0230**, ISSN (online):** 2412-3986**, DOI: http://dx.doi.org/10.21271/zjpas**

RESEARCH PAPER

Synthesis, *in vitro* Antimicrobial assay and Molecular Docking Studies of some new Symmetrical Bis-Schiff Bases and their 2-Azetidinones.

Sangar Ali Hassan[1], Media Noori Abdullah[2], Dara Muhammed Aziz[3]

[1,3]Department of Chemistry, College of Science, Raparin University-Sulaymaniyah, Kurdistan Region, Iraq
[2]Department of Chemistry, College of Science, Salahaddin University - Erbil, Kurdistan Region, Iraq

A B S T R A C T:
Four membered cyclic amides that are a broadly utilized class of antimicrobial agents up to now. Moreover, Symmetrical Bis-Schiff bases constitute an extraordinary class of strained compounds with varied applications and building blocks for the synthesis of 2-Azetidinones antibiotics. Because of those over biological significance, this study concludes a versatile synthetic precursor for the synthesis of the new Symmetrical Bis-Schiff bases and 2-Azetidinones in an exceedingly high yield. 2-Azetidinones were synthesized through [2+2] dichloroketene-imine cycloaddition reaction. The structures of the synthesized compounds were characterized by FT-IR, ^{1}H-NMR, and ^{13}C-NMR. Additionally, the products were assayed against two antibacterial types Gram-positive (*S. aureus*) and Gram-negative (*E. coli*) microorganisms and two varieties of fungal strains *A. niger*, *T. mentagrophytes* by broth microdilution method. As a result, all synthesized compounds displayed good antimicrobial activities against resistant strains. Finally, molecular docking studies were explained the inhibitory activities for the new products with the target (PDB ID: 1MWU) methicillin acyl-Penicillin binding protein 2a from methicillin-resistant *Staphylococcus aureus* strain 27r at 2.60 Å resolution.

KEY WORDS: Symmetrical Bis-Schiff Base, 2-Azetidinone, Antimicrobial assay, and Molecular Docking Studies.
DOI: http://dx.doi.org/10.21271/ZJPAS.33.2.4
ZJPAS (2021), 33(2);34-50 .

1. INTRODUCTION:

The development of new antimicrobial organic compounds might afford further opportunities for the treatment of diverse microorganism infections that uncountable folks worldwide affected (Kumar et al., 2017). Conversely, heterocyclic Schiff bases are well-known to human treatment when illnesses are affecting for a protracted time (Azzawi and Al-Obiadi). For that reason, researchers and pharmaceuticals are synthesizing and studying Schiff bases that are one of the most significant synthetic usages in organic chemistry which is used as intermediate for the synthesis of different compounds (Ali et al., Shockravi et al., 2009).

Schiff bases are known as imines or azomethines which had been discovered by Hugo Schiff in 1864 (Ahmad et al., 2020). The functional group of (C=N) is the functional group of Schiff base which are commonly synthesized through the condensation of active carbonyl groups and primary amines (Bhuyar et al., 2013, Sharma et al., 2012). Symmetrical bis-azomethines (Ar-N=CH-Ar-CH=N-Ar) have a similar synthetic mono Schiff base's pathway but by using the different molar ratio (Ozdemir Gungor, 2017). Schiff bases have broad variability applications in a medicinal field that possess a wide spectrum of biological activities such as antibacterial (Ziwar and Musheer), antioxidant (Hassan, 2019), antifungal (Noori et al., 2019), anti-inflammatory,

* **Corresponding Author:**
Sangar Ali Hassan
E-mail: sangar.ali@uor.edu.krd
Article History:
Received: 16/09/2020
Accepted: 28/10/2020
Published: 18/04 /2021

analgesic, anticancer (Kajal et al., 2013), antitumor (Ibrahim, 2015), anticonvulsant antimalarial, anti-tubercular (Khdur and Zimam, 2018a), and antidiabetic (Al-Masoudi et al., 2016).

The chemistry of 2-Azetidinone has involved a crucial site in organic chemistry, it is four-membered heterocyclic amides (Singh and Sudheesh, 2014, Van Brabandt et al., 2005). The (N) atom is linked to the 2-carbon atom neighboring to the carbonyl so it referred to Azetidin-2-one. Staudinger had synthesized 2-Azetidinone in 1907 for the first time through [2+2] ketene-imine cycloaddition reaction (Khdur and Zimam, 2018a). Azetidin-2-one is based on the varieties of the important antibiotics on an individual basis human and varied medicines (Singh and Sudheesh, 2014). Azetidin-2-one antibiotics action by inhibiting the microorganism cytomembrane in each gram-positive and gram-negative microorganism caused by their sturdy binding affinity to energetic penicillin-binding proteins (PBPs) (Piens, 2017). To date, researchers still improvements and discovering new drugs as a result of vying a vital role in the therapeutic field owing to their broader spectrum of biological activities (Jurčík et al., 2011) such as antibacterial, antifungal (Mehta et al., 2006), antioxidant (Hassan, 2019), anticancer, analgesic and antiviral activities (Deep et al., 2016), anti-inflammatory (Ayyash, 2019), antimalarial (Borazjani et al., 2020).

In a read of that overhead biotic importance, the current study has been focused on the synthesis of the Bis-Schiff bases and their 2-Azetidinone. All the synthesized compounds were tested for antibacterial and antifungal activities and additionally the screened activities supported by their Molecular Docking studies.

2. MATERIALS AND METHODS

Chemical compounds were bought from Sigma-Aldrich, Fluka, and Merck chemical companies and used without further purification. Melting points were determined by electrothermal melting point apparatus (Stuart, normal power 75 W, model: ST15 OSA at Raparin University/ Kurdistan/Iraq) in capillaries and were uncorrected. Thin-layer chromatography (TLC) on pre-coated SiO_2 gel (HF254, 200 mesh) aluminum plate was used to check the progress of the reactions, a mixture of n-hexane: ethyl acetate (7:3) was used as eluent. TLC plates were visualized by UV light (CSL-MDOCBASIC at Raparin University/ Kurdistan/Iraq). The Ultrasonic cleaner was used for sonication (DIGITAL PRO+, 40 kHz, and a standard power 180 W at Raparin University/ Kurdistan/Iraq). FT-IR spectra were recorded on the Thermo Scientific Spectrometer (Model: Nicolet iS 10 at Raparin University/ Kurdistan/Iraq). ^{1}H-NMR and ^{13}C-NMR spectra were carried out on a Bruckner (400 MHz at Tehran University/ Iran), DMSO-d_6 was used as a solvent with TMS as an inner standard), data were reported as chemical shift in ppm, apparent multiplicity (s = singlet, d = doublet, t = triplet, br= broad, *J*= coupling constant, Hz = Hertz). A microplate reader (BioTek-ELx808 at Raparin University) was used for the detection of antimicrobial activity of the synthesized compounds.

2.1. A general synthetic method for the synthesis of symmetrical Bis-Schiff bases (2-8)

All the symmetrical Schiff bases were synthesized via the condensing between amines and terephthaldehyde. An appropriate synthetic method was used with a slight modification (Turan and Sekerci, 2009). An amine ethyl alcohol solution (2 mmol in ethanol 5 mL) was added to a warm ethyl alcohol solution of terephthaldehyde (1 mmol in 5 ml ethanol). A catalytic amount of glacial acetic acid was used (10 mol %). The reaction mixture was sonicated for 35-75 minutes. The completion of the reaction was checked by TLC plates. The precipitate was collected through filtration. The products were recrystallized several times from absolute ethanol to obtain pure products (**2-8**), the reaction conditions are shown in the (Scheme 1).

2.1.1. 4,4'-(1,4-phenylenebis(methaneylylidene))bis(azaneylylidene)bis(*N*-(thiazol-2-yl) benzene sulfonamide) (2)

Pale yellow color solid, m.p. = 254-255 ^{0} C, yield= 83%, time= 40 minutes. FT-IR (cm^{-1}): 3194 ($NH_{str.}$), 3010 ($CH_{Ar.\ Str.}$), 1620 ($C{=}N_{str.\ imine}$), 1578 ($C{=}C_{Ar.\ Str.}$), 1303 ($SO_{2\ asym.\ str.}$), 1146 ($SO_{2\ sym.str.}$). ^{1}H-NMR (DMSO-d_6): δ 12.680 (s, br, 2H (NH)), 8.101 (s, 2H (CH=N)), 8.731 (s, 4H (H2, H3, H5, H6)), 7.891 (d, 4H (H3', H5'), *J*= 8

Hz), 7.436 (d, 4H (H2', H6'), *J*= 8 Hz), 7.297 (d, 2H (H4''), *J*= 7.6 Hz), 6.875 (d, 2H (H5''), *J*= 8.4 Hz). ^{13}C-NMR (DMSO-d_6): δ 169.37 (2C (C2'')), 162.55 (2C (C=N)), 154.79 (2C (C1')), 140.88 (2C (C1, C4)), 140.30 (2C (C4')), 138.86 (2C (C4'')), 130.49 (4C (C2, C3, C5, C6)), 129.98 (4C (C3', C5')), 121.94 (4C (C2', C6')), 112.92 (2C (C5'')).

2.1.2. 8,8'-(1,4-phenylenebis(methaneylylidene))bis(azaneylylidene))bis(naphthalene-2-sulfonic acid) (3)

Dark gray color solid, m.p. >300℃, yield= 75%, time= 75 minutes. FT-IR (cm^{-1}): 3382 (OH $_{str.}$), 3029 (CH $_{Ar. Str.}$), 1612 (C=N $_{str. imine}$), 1574 (C=C $_{Ar. Str.}$), 1347 (SO_2 $_{asym.str.}$), 1181 (SO_2 $_{sym. str.}$). ^{1}H-NMR (DMSO-d_6): δ 8.713 (s, 2H (CH=N)), 8.481 (s, 2H (OH)), 8.382 (d, 2H (H4'), *J*= 8.4 Hz), 7.985 (d, 2H (H7'), *J*=8 Hz), 7.961 (s, 4H (H2, H3, H5, H6)), 7.883 (d, 2H (H5'), *J*= 7.6 Hz), 7.812 (s, 2H (H1')), 7.781 (d, 2H (H3'), *J*=8.4 Hz), 7.487 (t, 2H (H6'), *J*= 7.6 Hz, J= 8 Hz). ^{13}C-NMR (DMSO-d_6): δ 161.03 (2C (C=N)), 151.43 (2C (C8')), 142.78 (2C (C2')), 137.18 (2C (C1, C4)), 132.92 (2C (4'a)), 130.11 (2C (C6')), 129.99 (2C (C4')), 129.06 (4C (C2, C3, C5, C6)), 126.91 (2C (C5')), 126.66 (2C (C8'a)), 124.64 (2C (C1')), 121.46 (2C (C3')), 116.78 (2C (C7')).

2.1.3. 4,4'-((1,4-phenylenebis(methaneylylidene))bis(azaneylylidene))bis(*N*-phenylaniline) (**4**)

Dark green color solid, m.p. = 122-123 ^{0} C, yield= 78%, time= 65 minutes. FT-IR (cm^{-1}): 3415 (NH $_{str.}$), 3049 (CH $_{Ar. Str.}$), 1617 (C=N $_{str. imine}$), 1588 (C=C $_{Ar. Str.}$). ^{1}H-NMR (DMSO-d_6): δ 8.753 (s, 2H (CH=N)), 8.392 (s, 2H (NH)), 8.043 (s, 4H (H2, H3, H5 , H6)), 7.383 (d, 4H (H2', H6'), *J*= 7.2 Hz), 7.285 (t, 4H (H3'', H5''), *J*= 8 Hz, *J*= 7.6 Hz), 7.154 (d, 4H (H3', H5'), *J*= 8 Hz), 7.135 (d, 4H (H2'', H6''), *J*= 7.2 Hz), 6.878 (t, 2H (H4''), *J*= 7.2 Hz, *J*= 7.2 Hz). ^{13}C-NMR (DMSO-d_6): δ 159.39 (2C (C=N)), 143.52 (2C (C1'')), 143.09 (2C (C1')), 143.04 (2C (C4')), 138.91 (2C (C1, C4)), 129.73 (4C (C3'', C5'')), 129.04 (4C (C2, C3, C5, C6)), 123.43 (4C (C2', C6')), 123.16 (4C (C3', C5')), 120.48 (2C (C4'')), 117.75 (4C (C2'', C6'')).

2.1.4. 1,4'-(1,4-phenylene)bis(*N*-(4-(phenyldiaze nyl)phenyl)methanimine) (5)

Orange color solid, m.p. = 191-192 ^{0} C, yield= 76%, time= 70 minutes. FT-IR (cm^{-1}): 3037 (CH $_{Ar. Str.}$), 1615 (C=N $_{str. imine}$), 1581 (C=C $_{Ar. Str.}$). .). ^{1}H-NMR (DMSO-d_6): δ 8.575 (s, 2H (CH=N)), 8.121 (s, 4H (H2, H3, H5, H6)), 7.377 (d, 4H (H2'', H6''), *J*= 8 Hz), 7.297 (d, 4H (H3', H5'), *J*= 7.6 Hz), 7.257 (t, 4H (H3'', H5''), *J*= 6.8 Hz, *J*= 7.6 Hz), 7.146 (t, 2H (H4''), *J*= 8.8 Hz, *J*=8 Hz), 6.491 (d, 4H (H2', H6'), *J*= 8.4 Hz). ^{13}C-NMR (DMSO-d_6): δ 159.53 (2C (C=N)), 153.77 (2C (C1'')), 148.62 (2C (C1')), 145.78 (2C (C4')), 137.19 (2C (C1, C4)), 131.72 (2C (C4'')), 129.51 (4C (C2, C3, C5, C6)), 128.96 (4C (C3'', C5'')), 122.51 (4C (C2'', C6'')), 121.43 (4C (C2', C6')), 118.66 (4C (C3', C5')).

2.1.5. 4,4'-((1,4-phenylenebis(methaneylylidene))bis(azaneylylidene))bis(*N*-(pyrimidin-2-yl) benzenesulfonamide) (6)

Pale green color solid, m.p. = 297-298 ^{0} C, yield= 81%, time= 45 minutes. FT-IR (cm^{-1}): 3226 (NH $_{str.}$), 3041 (CH $_{Ar. Str.}$), 1626 (C=N $_{str. imine}$), 1578 (C=C $_{Ar. Str.}$), 1335 (SO_2 $_{asym. str.}$), 1155 (SO_2 $_{sym.str.}$). ^{1}H-NMR (DMSO-d_6): δ 11.830 (s, br, 2H (NH)), 8.777 (s, 2H (CH=N)), 8.523 (d, 4H (H3'', H5''), *J*= 8.4 Hz), 8.075 (s, 4H (H2, H3, H5, H6)), 7.648 (d, 4H (H3', H5'), *J*= 8.4 Hz), 7.477 (d, 4H (H2', H6'), *J*= 7.6 Hz), 7.049 (t, 2H (H4''), *J*= 7.6 Hz, *J*=8 Hz). ^{13}C-NMR (DMSO-d_6): δ 171.01 (2C (C1'')), 162.07 (2C (C=N)), 159.87 (4C (C3'', C5'')), 155.51 (2C (C1')), 137.95 (2C (C1, C4)), 137.10 (2C (C4')), 130.40 (4C (C2, C3, C5, C6)), 129.92 (4C (C3', C5')), 122.27 (4C (C2', C6')), 115.32 (2C (C4'')).

2.1.6. 4,4'-((1,4-phenylenebis(methaneylylidene))bis(azaneylylidene))bis(1',5'-dimethyl-2'-phenyl-1',2'-dihydro-3*H*-pyrazol-3'-one) (7)

Yellow color solid, m.p. = 167-168 ^{0} C, yield= 80%, time= 60 minutes. FT-IR (cm^{-1}): 3041 (CH $_{Ar. Str.}$), 2984, 2935 (CH $_{Aliph. Str.}$), 1640 (C=O $_{str.}$), 1610 (C=N $_{str. imine}$), 1589 (C=C $_{Ar. Str.}$). ^{1}H-NMR (DMSO-d_6): δ 9.676 (s, 2H (CH=N)), 8.034 (s, 4H (H2, H3, H5, H6)), 7.571 (t, 4H (H3'', H5''), *J*= 8 Hz, *J*= 7.6 Hz), 7.513 (d, 4H (H2'', H6''), *J*= 8.4 Hz), 7.396 (t, 2H (H4''), *J*= 7.2 Hz, J= 7.4 Hz), 3.362 (s, 6H (N-CH_3)), 2.525 (s, 6H (C-CH_3)). ^{13}C-NMR (DMSO-d_6): δ 162.16 (2C (C=N)), 159.54 (2C (C3')), 151.31 (2C (C5')), 137.19 (2C (C1, C4)), 132.42 (2C (C1'')), 130.11 (4C (C2, C3, C5, C6)), 129.54 (4C (C3'', C5'')), 123.78 (4C (C2'', C6'')), 121.64 (2C (C4'')), 111.91 (2C (C4')), 36.96 (2C (N-$\underline{C}H_3$)), 19.07 (2C (C-$\underline{C}H_3$)).

2.1.7. 4,4'-((1,4-phenylenebis(methaneylylidene))bis(azaneylylidene))bis-2'-benzothiazol (8)

Green color solid, m.p. = 181-182 ^{0} C, yield= 85%, time= 35 minutes. FT-IR (cm^{-1}): 2999 (CH $_{Ar. Str.}$), 1622 (C=N $_{str. imine}$), 1588 (C=C $_{Ar. Str.}$). ^{1}H-NMR (DMSO-d_6): δ 8.865 (s, 2H (CH=N)), 7.951 (d, 2H (H4'), *J*= 8.4 Hz), 7.767 (s, 4H (H2, H3, H5, H6)), 7.503 (d, 2H (H7'), *J*= 8 Hz), 7.140 (t, 2H (H5'), *J*= 8 Hz, *J*= 8 Hz), 6.954 (t, 2H (H6'), *J*= 8.4 Hz, *J*= 8 Hz). ^{13}C-NMR (DMSO-d_6): δ 169.10 (2C (C2')), 159.74 (2C (C=N)), 149.41 (2C (C3'a)), 137.34 (2C (C1, C4)), 129.70 (4C (C2, C3, C5, C6)), 126.89 (2C (C7'a)), 124.98 (2C (C5')), 122.55 (2C (C6')), 121.41 (2C (C7')), 120.84 (2C (C4')).

2.2. A general synthetic method for the synthesis of 2-Azetidinones (10-16)

A convenient synthetic pathway was used (Turan et al., 2016). A solution was prepared from the mixing trichloroacetyl chloride (2 mmol) and activated zinc (0.04 g) in 50 mL of diethyl ether, the mixture was sonicated for 30 minutes at 25 °C. The Schiff base (1 mmol) was added to the mixture and refluxed for 8-12 hours under a nitrogen atmosphere. A TLC plate was used to monitor the progress of the reaction. The excess zinc was filtered off. The solvent was evaporated via a rotary evaporator and washed products in absolute ethanol to remove zinc salt. The products were purified by column chromatography silica gel (n-hexane: ethyl acetate 65:35) to obtain the pure 2-Azetidinones. The reaction conditions are illustrated in (Scheme 2).

2.2.1. 4,4'-(1,4-phenylenebis-(3,3-dichloro-4-oxoazetidin-1,4-diyl))bis(-*N*-(thiazol-2-yl) benzenesulfonamide) (10)

Brown color solid, m.p. = 231-232 ^{0} C, yield= 78%, time= 8.5hrs. FT-IR (cm^{-1}): 3202 (NH $_{str.}$), 3009 (CH $_{Ar. Str.}$), 1745 (C=O $_{str. 2\text{-}Azetidinone ring}$), 1593 (C=C $_{Ar. Str.}$), 1326 (SO_2 $_{asym. str.}$), 1135 (SO_2 $_{sym. str.}$). ^{1}H-NMR (DMSO-d_6): δ 12.767 (s, br, 2H (NH)), 7.904 (d, 4H (H3', H5'), *J*= 8.4 Hz), 7.704 (d, 4H (H2', H6'), *J*= 8.8 Hz), 8.549 (s, 4H (H2, H3, H5, H6)), 7.302 (d, 2H (H4", *J*= 8.4 Hz)), 7.024 (d, 2H (H5"), *J*= 7.6 Hz), 5.774 (s, 2H (CH $_{2\text{-}Azetidinone ring}$)). ^{13}C-NMR (DMSO-$d_6$): δ 169.64 (2C (C2")), 161.20 (2C (C=O $_{2\text{-}Azetidinone ring}$)), 150.54 (2C (C1')), 140.58 (2C (C1, C4)), 136.91 (2C (C4")), 133.09 (2C (C4')), 129.81 (4C (C3', C5')), 125.03 (4C (C2, C3, C5, C6)), 122.74 (4C (C2', C6')), 111.33 (2C (C5")), 94.95 (2C (C-Cl_2 $_{2\text{-}Azetidinone ring}$)), 75.47 (2C (CH $_{2\text{-}Azetidinone ring}$)).

2.2.2. 8,8'-(1,4-phenylenebis(3,3-dichloro-2-oxoazetidine-4,1-diyl))bis(naphthalene-2-sulfonic acid) (11)

Soil color solid, m.p. = 290-291 ^{0} C, yield= 65%, time= 12 hrs. FT-IR (cm^{-1}): 3324 (OH $_{str.}$), 3041 (CH $_{Ar. Str.}$), 1704 (C=O $_{str. 2\text{-}Azetidinone ring}$), 1597 (C=C $_{Ar. Str.}$), 1331 (SO_2 $_{asym. str.}$), 1143 (SO_2 $_{sym. str.}$). ^{1}H-NMR (DMSO-d_6): δ 8.548 (d, 2H (H4'), *J*= 8.8 Hz), 8.506 (s, 2H (OH)), 8.185 (s, 2H (H1')),8.156 (d, 2H (H5'), *J*=7.6 Hz), 8.078 (d, 2H (H7'), *J*= 7.2 Hz), 7.597 (d, 2H (H3'), J=8 Hz), 7.493 (t, 2H (H6'), *J*= 8 Hz, *J*= 7.6 Hz), 7.083 (s, 4H (H2, H3, H5, H6)), 5.461 (s, 2H (CH $_{2\text{-}Azetidinone ring}$)). ^{13}C-NMR (DMSO-$d_6$): δ 158.80 (2C (C=O $_{2\text{-}Azetidinone ring}$)), 147.84 (2C (C8')), 146.95 (2C (C1, C4)), 141.40 (2C (C2')), 138.46 (2C (4'a)), 130.50 (2C (C4')), 129.51 (2C (C6')), 124.55 (4C (C2, C3, C5, C6)), 124.10 (2C (C3')), 121.84 (2C (C8'a)), 118.21 (2C (C1'), 117.99 (2C (C5')) 108.62 (2C (C7')), 94.77 (2C (C-Cl_2 $_{2\text{-}Azetidinone ring}$)), 79.11 (2C (CH $_{2\text{-}Azetidinone ring}$)).

2.2.3. 4,4'-(1,4-phenylenebis(3,3-dichloro-2-oxoazetidine-4,1-diyl))bis(*N*-phenylaniline) (12)

Dark brown color solid, m.p. = 108-109 ^{0} C, yield= 70%, time= 10.5 hrs. FT-IR (cm^{-1}): 3431 (NH $_{str.}$), 3028 (CH $_{Ar. Str.}$), 1725 (C=O $_{str. 2\text{-}Azetidinone ring}$), 1594 (C=C $_{Ar. Str.}$). ^{1}H-NMR (DMSO-d_6): δ 8.818 (s, 2H (NH)), 8.535 (t, 4H (H3", H5"), *J*= 5.6 Hz, *J*= 6 Hz), 8.288 (s, 4H (H2, H3, H5, H6)), 7.771 (d, 4H (H3', H5'), *J*= 8. Hz), 7.079 (d, 4H (H2", H6"), *J*= 7.6 Hz), 7.032 (t, 2H (H4"), *J*= 7.6 Hz, *J*= 8 Hz). 6.902 (d, 4H (H2', H6'), *J*= 8.8 Hz), 5.866 (s, 2H (CH $_{2\text{-}Azetidinone ring}$)). ^{13}C-NMR (DMSO-$d_6$): δ 159.25 (2C (C=O $_{2\text{-}Azetidinone ring}$)), 143.15 (2C (C1"), 138.16 (2C (C1, C4)), 137.02 (2C (C4')), 132.65 (4C (C2', C6')), 129.56 (4C (C3", C5")), 128.20 (2C (C1')), 125.31 (4C (C2, C3, C5, C6)), 122.35 (2C (C4")), 121.73 (4C (C2", C6")), 120.16 (4C (C3', C5')), 92.17 (2C (C-Cl_2 $_{2\text{-}Azetidinone ring}$)), 75.94 (2C (CH $_{2\text{-}Azetidinone ring}$)).

2.2.4. 4,4'-(1,4-phenylene)bis(3,3-dichloro-1-(4-(phenyldiazenyl)phenyl)azetidin-2-one) (13)

Oily color solid, m.p. = 154-155 ^{0} C, yield= 67%, time= 11 hrs. FT-IR (cm^{-1}): 3038 (CH $_{Ar. Str.}$), 1740 (C=O $_{str. 2-Azetidinone ring}$), 1595 (C=C $_{Ar. Str.}$). ^{1}H-NMR (DMSO-d_6): δ 8.380 (d, 4H (H3', H5'), *J*= 8 Hz), 8.070 (d, 4H (H2", H6"), *J*= 8.4 Hz), 7.848 (t, 4H (H3", H5"), *J*= 8 Hz, *J*= 7.2 Hz), 7.466 (s, 4H (H2, H3, H4, H5)), 7.086 (t, 2H (H4"), *J*= 7.6 Hz, *J*=8 Hz), 6.883 (d, 4H (H2', H6'), *J*= 8 Hz), 5.537 (s, 2H (CH $_{2-Azetidinone ring}$)). ^{13}C-NMR (DMSO-d_6): δ 159.87 (2C (C=O $_{2-Azetidinone ring}$)), 151.06 (2C (C1")), 149.93 (2C (C4')), 139.81 (2C (C1')), 138.95 (2C (C1, C4)), 131.11 (2C, (C4")), 130.32 (4C (C2', C6')), 129.51 (4C (C3", C5")), 126.72 (4C (C2, C3, C5, C6)), 124.57 (4C (C3', C5')), 123.63 (4C (C2", C6")), 90.53 (2C (C-Cl_2 $_{2-Azetidinone ring}$)), 74.60 (2C (CH $_{2-Azetidinone ring}$)).

2.2.5. 4,4'-(1,4-phenylenebis(3,3-dichloro-2-oxoazetidine-4,1-diyl))bis(*N*-(pyrimidin-2-yl)benzenesulfonamide) (14)

Deep brown color solid, m.p. = 261-262 ^{0} C, yield= 75%, time= 9 hrs. FT-IR (cm^{-1}): 3254 (NH $_{str.}$), 3021 (CH $_{Ar. Str.}$), 1722 (C=O $_{str. 2-Azetidinone ring}$), 1593 (C=C $_{Ar. Str.}$), 1326 (SO_2 $_{asym.str.}$), 1134 ($SO_{2sym.str.}$). ^{1}H-NMR (DMSO-d_6): δ 11.938 (s, br, 2H (NH)), 8.545 (d, 4H (H3", H5"), *J*= 7.2 Hz), 8.070 (d, 4H (H3', H5'), *J*= 8 Hz), 7.562 (d, 4H (H2', H6'), *J*= 8 Hz), 7.288 (s, 4H (H2, H3, H5, H6)), 7.147 (t, 2H (H4"), *J*= 8.4 Hz, *J*=7.6 Hz), 5.615 (s, 2H (CH $_{2-Azetidinone ring}$)). ^{13}C-NMR (DMSO-d_6): δ 170.19 (2C (C1")), 160.81 (2C (C=O $_{2-Azetidinone ring}$)), 158.88 (4C (C3", C5")), 143.40 (2C (C1')), 142.08 (2C (C1, C4)), 135.66 (2C (C4')), 129.61 (4C (C3', C5')), 124.29 (4C (C2, C3, C5, C6)), 122.34 (4C (C2', C6')), 116.93 (2C (C4")), 92.99 (2C (C-Cl_2 $_{2-Azetidinone ring}$)), 76.65 (2C (CH $_{2-Azetidinone ring}$)).

2.2.6. 4,4'-(1,4-phenylenebis(3,3-dichloro-2-oxoazetidine-4,1-diyl))bis(1,5-dimethyl-2-phenyl-1,2-dihydro-3*H*-pyrazol-3-one) (15)

Coffey color solid, m.p. = 129-130 ^{0} C, yield= 72%, 10 hrs. FT-IR (cm^{-1}): 3035 (CH $_{Ar. Str.}$), 2808, 2941 (CH $_{Aliph. Str.}$), 1731 (C=O $_{str. 2-Azetidinone ring}$), 1672 (C=O $_{str.}$), 1580 (C=C $_{Ar. Str.}$). ^{1}H-NMR (DMSO-d_6): 7.696 (t, 4H (H3", H5") *J*= 7.2 Hz, *J*= 8 Hz), 7.506 (d, 4H (H2", H6"), *J*= 8.8 Hz), 7.454 (t, 2H (H4"), *J*= 8.8 Hz, J= 8.4 Hz), 7.311 (s, 4H (H2, H3, H5, H6)), 5.153 (s, 2H (CH $_{2-Azetidinone ring}$)), 3.261 (s, 6H (N-CH_3)), 2.077 (s, 6H (C-CH_3)). ^{13}C-NMR (DMSO-d_6): δ 162.65 (2C (C3')), 159.09 (2C (C=O $_{2-Azetidinone ring}$)), 145.97 (2C (C1, C4)), 136.94 (2C (C1")), 134.05 (2C (C5')), 129.71 (4C (C3", C5")), 124.56 (4C (C2, C3, C5, C6)), 122.18 (4C (C2", C6")) , 121.70 (2C (C4")), 105.43 (2C (C4')), 94.56 (2C (C-Cl_2 $_{2-Azetidinone ring}$)), 73.81 (2C (CH $_{2-Azetidinone ring}$)), 35.72 (2C (N-$\underline{C}H_3$)), 21.10 (2C (C-$\underline{C}H_3$)).

2.2.7. 4,4'-(1,4-phenylene)bis(1-(benzothiazol-2-yl)-3,3-dichloroazetidin-2-one) (16)

Bronzy color solid, m.p. = 145-146 ^{0} C, yield= 79%, time= 8 hrs. FT-IR (cm^{-1}): 3033 (CH $_{Ar. Str.}$), 1715 (C=O $_{str. 2-Azetidinone ring}$), 1593 (C=C $_{Ar. Str.}$). ^{1}H-NMR (DMSO-d_6): δ 7.879 (d, 2H (H4'), *J*= 8.4 Hz), 7.811 (d, 2H (H7'), *J*= 8.8 Hz), 7.503 (t, 2H (H5'), *J*= 8 Hz, *J*= 8.4 Hz), 6.479 (t, 2H (H6'), *J*= 8 Hz, *J*= 8.4 Hz), 7.024 (s, 4H (H2, H3, H5, H6)), 5.519 (s, 2H (CH $_{2-Azetidinone ring}$). ^{13}C-NMR (DMSO-d_6): δ 162.85 (2C (C2'), 159.71 (2C (C=O $_{2-Azetidinone ring}$)), 149.77 (2C (C3'a)), 141.36 (2C (C1, C4)), 130.42 (2C (C7'a)), 123.88 (2C (C5')), 124.56 (4C (C2, C3, C5, C6)), 121.45 (2C (C6')), 120.33 (2C (C7')), 119.04 (2C (C4'), 89.11 (2C (C-Cl_2 $_{2-Azetidinone ring}$)), 73.23 (2C (CH $_{2-Azetidinone ring}$)).

2.3. *In Vitro* Antimicrobial (antibacterial and antifungal) assay

The broth microdilution method was utilized to test the antibacterial and antifungal assays. The synthesized compounds **(2-8)** and **(10-16)** were screened a great capacity to inhibition strains against gram-positive strain (*S. aureus*), and gram-negative strains (*E. coli*) of bacterial and *A. niger* (natural isolates) and *T. mentagrophytes*. A common medication, Amoxicillin and, Penicillin were used as standard drugs (Aziz and Azeez, 2020).

2.4. Molecular docking software

PubChem (https://pubchem.ncbi.nlm.nih.gov/) and ChemDraw Professional 16.0 were used to design of the synthesized compounds (ligands) as the SDF type file format, Protein Data Bank (https://www.rcsb.org/), online tools were used for download of a protein (ID code: 1MWU). The zinc (http://zinc.docking.org/) website was used for the design and download of standard drugs (amoxicillin and penicillin G). PyRx (AutoDockTools-1.5.6) and BIOVIA Discovery Studio 2020 were employed to imagine and adapt receptor and ligand structures (Beg and Athar, 2020, My et al., 2011).

3. RESULTS AND DISCUSSION

3.1. Chemistry

3.1.1. Symmetrical Bis-Schiff bases (2-8)

A convenient synthetic method was applied for the preparation of symmetrical Bis-Schiff base compounds that are depicted in (Scheme **1**). Terephthaldehyde was preferred for the synthesis of new Symmetrical Bis-Schiff bases as the starting material. Symmetrical Bis-Schiff bases (**2-8**) were synthesized via a condensation reaction of terephthaldehyde (**1**) with seven various aromatic primary amines. Acetic acid was used as an acid catalyst (Shinde et al.). The ultrasonic technique was used for a few purposes such as reducing the time of the reactions, utilizing the least amounts of ethanol dissolvable and, getting a good product yields (Bendale et al., 2011).

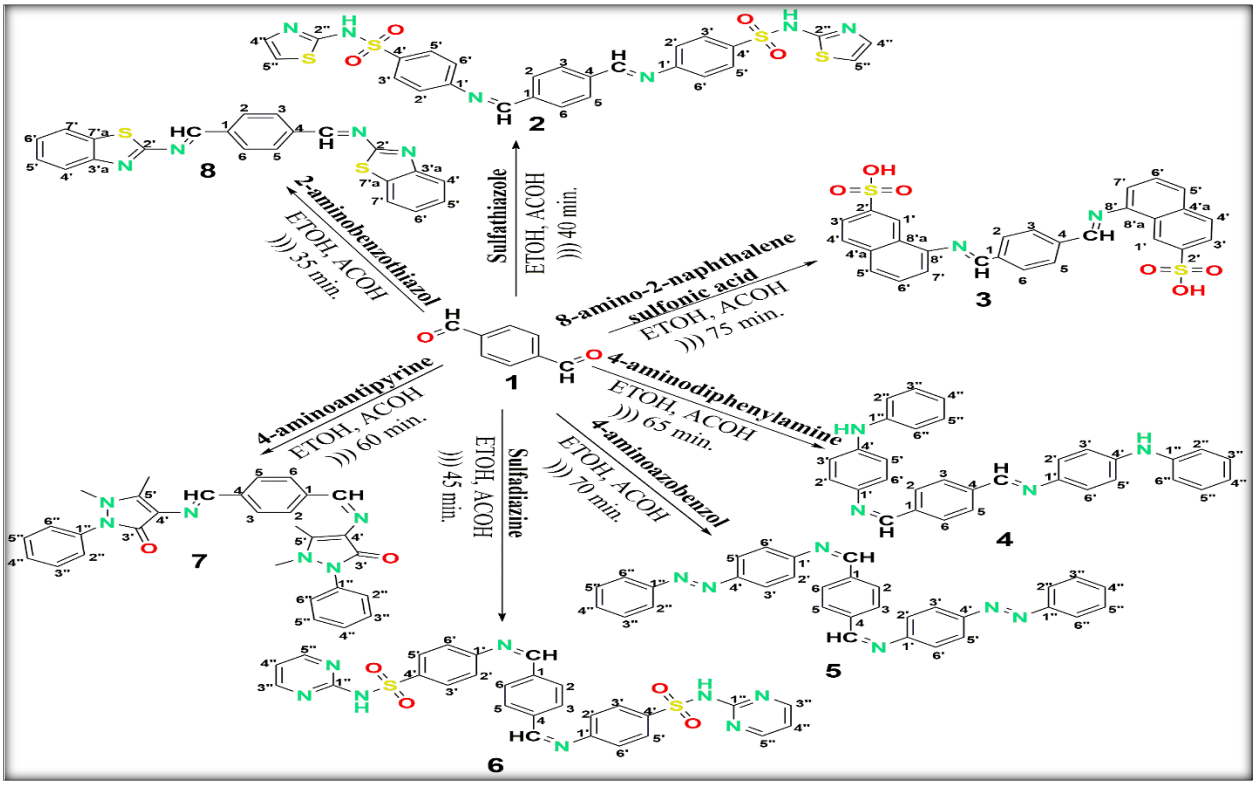

Scheme 1. Symmetrical Bis-Schiff bases synthesis **(2-8)**

Within the spectrum of Bis-Schiff bases, the characteristic absorption around 1610-1626 cm^{-1} can be related to stretching vibration of (-C=N) Schiff bases, which could be a sensible affirmation to the synthesis of Bis-Schiff bases, the vanishing of a carbonyl (C=O) of the terephthaldehyde around 1700 cm^{-1}, and two peaks of primary amines (NH_2) at 3300 and 3400 cm^{-1} were implied that the pure Bis-Schiff bases were formed (Shaygan et al., 2018). Moreover, a carbonyl peak showed up at 1640 cm^{-1} for compound (**7**) but it is not carbonyl of aldehyde, this carbonyl group is a portion of the 4-aminoantipyrine compound. Within the compounds (**2**, **4**, and **6**) a band NH stretching vibration seemed at 3194, 3415 and 3226 cm^{-1} respectively (Hamdan et al., 2018). A broad hydroxide (OH) peak showed up at 3382 cm^{-1} for the compound (**2**) (Singh et al., 2018).

In the ^{1}H-NMR spectrums, singlet peaks appeared at 8.10-9.67 ppm for an identical to two protons of (H-C=N) Schiff bases. A singlet and broad singlet bands did not appear for the proton of (CH=O) of terephthaldehyde and protons of (NH_2) amines, meaning the pure symmetrical Bis-Schiff bases were formed without any reactants (Mohammed and Taha, 2017). The broad singlet band was shown for every (NH) protons of compounds (**2**, **6**, and **4**) at 12.680, 8.392, and 11.830 ppm, separately (Elsayed et al., 2014). A single peak appeared at 8.481 ppm that is doled out to the (O–H) groups of compound (**2**). The equivalence

aromatic protons were shown at 8.777-6.491 ppm. Also, two corresponding singlet peaks at 3.362 and 2.525 ppm were conjointly displayed due to the CH_3 groups of the compound (**7**). ^{13}C-NMR spectrums are shown with these next data. The carbon of (C=N) of symmetrical Schiff bases is recorded at 162.55-159.39 ppm. The aromatic carbons are seen at 171.01-111.91 ppm (Krátký et al., 2017). The two lowest signals appeared at 36.97 and 19.07 ppm due to the CH_3 groups of the compound (**7**). The two symmetrical carbons of carbonyl groups of compound (**7**) are shown at 159.54 ppm, high chemical shift due to neighboring oxygen atoms. Because of electronegativity the neighbor atom is influenced by the linkage of carbons. Those carbon atoms that are linked to two nitrogen atoms or nitrogen and sulfur atoms were shown the most elevated chemical shift as the compounds (**6** and **2**) (Anacona et al., 2015, Krátký et al., 2012).

3.1.2. 2-Azetidinones (10-16)

The synthetic method for the synthesis of 2-Azetidinones is based on [2+2] dichloroketene-imine cycloaddition reaction. The conditions of the reactions are shown in (Scheme 2), and mechanism of the reaction is illustrated in (Scheme 3). One mole of symmetrical Bis-Schiff bases (**2-8**) was reacted with two moles with trichloroacetyl chloride (**9**). Activated zinc was as a catalyst, diethyl ether as solvent (Turan et al., 2016).

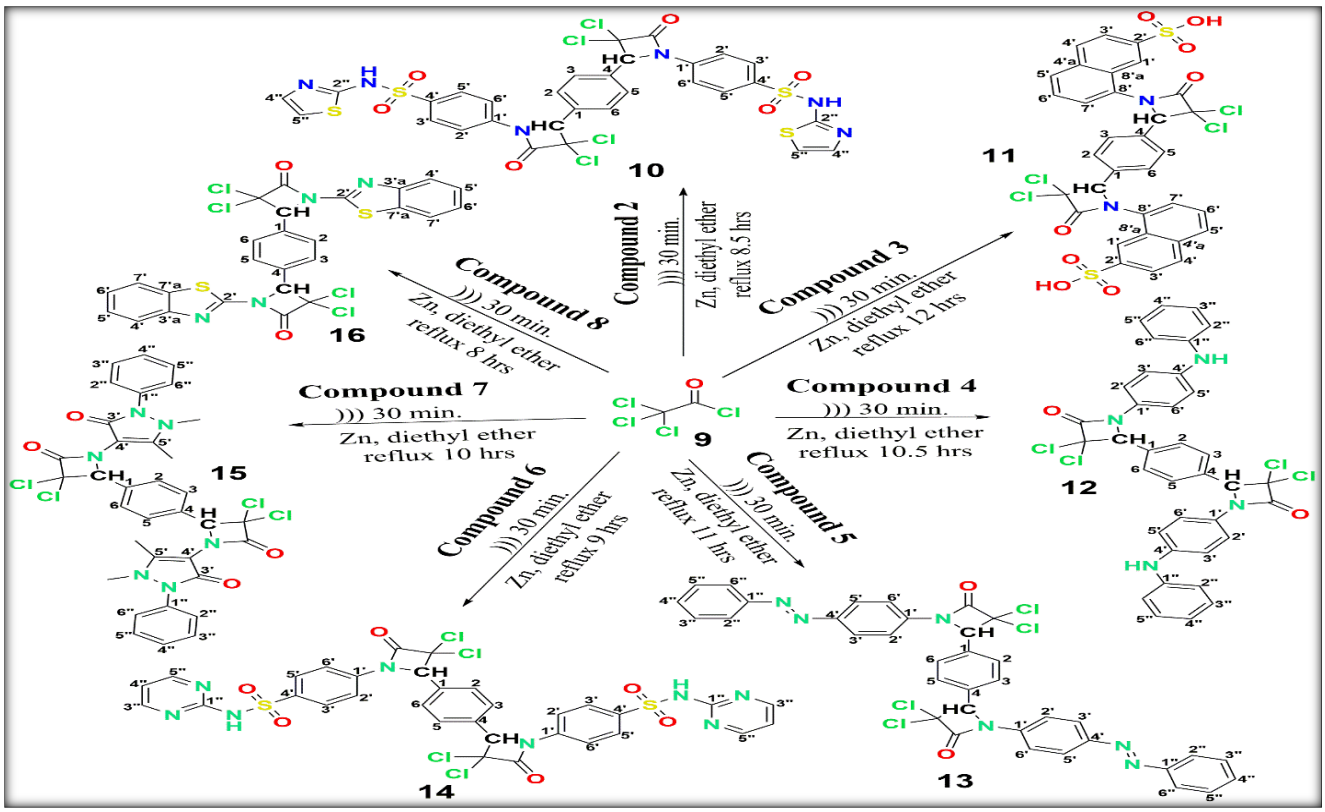

Scheme 2. 2-Azetidinones synthesis **(10-16)**

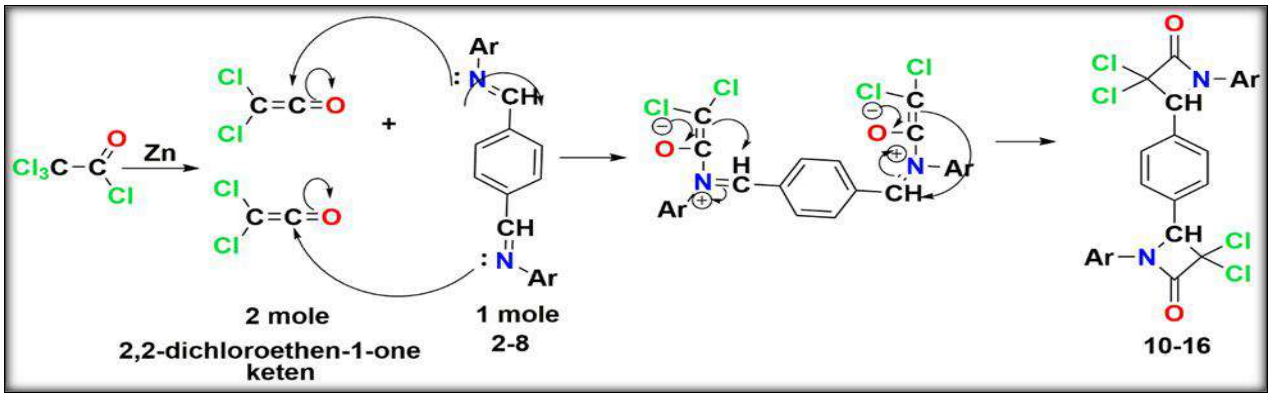

Scheme 3. Mechanism of the synthesis 2-Azedidinones (**10-16**) (Khdur and Zimam, 2018b, Turan et al., 2016)

In the view of spectrums of 2-Azetidinones, the most effective instructive to indicate the formation of 2-Azetidinones by FT-IR is that the vanished of imine vibrational stretching (C=N) groups of symmetrical bis-Schiff bases and appeared of carbonyl (C=O) group of 2-Azetidinones at 1745-1704 cm^{-1}. Concealed the peak of imine groups is good evidence for the formation of pure 2-Azetidinones without bis-Schiff bases reactant (Ayyash, 2019). A vibrational stretching peak appeared at 1672 cm^{-1} for the ketone carbonyl group of the compound (**7**). The NH stretching vibrational peak appeared at 3202, 3431, and 3254 cm^{-1} for the compounds (**10**, **12**, and **14**), severally (Mehta et al., 2014). A broad vibrational stretching peak appeared at 3324 cm^{-1} for the hydroxide (OH) compound (**11**). ^{1}H-NMR spectrums were shown the properties of the protons band. An identical two singlet bands appeared at 5.774-5.53 ppm for (CH) protons of the 2-Azetidinone ring and disappeared the singlet band of imine (CH=N) groups (Khajavi, 1998, Turan et al., 2016). The broad singlet band of NH protons of compounds (**10**, **12**, and **14**) were shown at 12.767, 8.818, 11.938 ppm, individually. A single band appeared for (O–H) protons of the compound (**2**) at 8.506 ppm. The equivalence aromatic protons are shown at 8.548-6.883 ppm. Two singlet bands seem at 3.261 and 2.077 ppm due to CH_3 groups of the compound (**7**). Within the ^{13}C-NMR spectrums of 2-Azeidinones, carbon of the carbonyl of 2-Azetidinone rings seemed at 161.20-158.80 ppm. The aromatic carbons appeared at 170.19-105.43 ppm (Khdur and Zimam, 2018a). Two signals appeared for the carbons of (C-Cl_2 and CH) 2-Azetidinone rings at 79.11-73.23 ppm and 94.95-89.11 ppm, respectively. Two signal bands appeared at 35.72 and 21.10 ppm because of the CH_3 groups of the compound (**15**).

3.2. *In vitro* Antimicrobial assay

All synthesized compounds were evaluated for their *in vitro* antibacterial activities against gram-positive strain, *Staphylococcus aureus* (ATCC 9144), and gram-negative *Escherichia coli* (ATCC 8739), and surveyed for their antifungal activity against *Aspergillus niger* and *Trichophyton mentagrophytes* (Sharma et al., 2012). The antimicrobial of the synthesized compounds assessed through the broth microdilution technique, the results were detailed by the (MIC) minimum inhibitory concentration, and the results are shown in (**Table 1**).

Table 1. *In vitro* antimicrobial assay of the synthesized compounds (MIC µg/mL)

Compounds	MIC for Microorganisms (µg/ml)			
	Bacterial strains		Fungal strains	
	S.aureus	***E.coli***	***A.niger***	***T. mentagrophytes***
2	1.5	1.8	2.5	2.7
3	0.8	0.7	1.8	2.3
4	3	4	4	3.3
5	4	3.5	3	3.5
6	2	1.5	2.7	2.9
7	4.5	4	4.5	5

8	5	4.5	4	4.5
10	1	1.2	3	3.1
11	0.5	0.6	1.6	2.2
12	2.5	2	3.3	3.4
13	2.8	4	3.8	3.6
14	1.9	2.2	2.9	3.2
15	4	3	2	2.6
16	4	3.5	3.2	3.7
Amoxicillin	0.100	0.065	-	-
Penicillin G	0.120	0.075	-	-
Nystatin	-	-	1.5	2

All synthesized compounds screened good antibacterial and antifungal activities as compared to standard amoxicillin, penicillin, and nystatin drugs. As inspected the antibacterial of the synthesized compounds higher than their antifungal. The 2-Azetidinones possessed higher antimicrobial activity than Schiff bases. The compound (**11**) exhibited the most elevated antibacterial activity against *Escherichia coli* and *Staphylococcus aureus* bacteria and showed the most noteworthy activity against *Aspergillus niger* and *Trichophyton mentagrophytes* fungi. The compound (**8**) exhibited the lowest antibacterial activity against *Escherichia coli* and *Staphylococcus aureus* bacteria. The compound (**7**) displayed the lowest antifungal *Aspergillus niger* and *Trichophyton mentagrophytes* fungi. The P values are equal to 0.00512 and 0.00399 for Schiff bases (2-8) and 2-Azetidinones (10-16) against Staphylococcus aureus, respectively. They are less than 0.05 and statistically significant.

3.3. Molecular docking study

To provision the *in vitro* antimicrobial activity of the synthesized compounds a molecular docking study was applied to identify binding affinities and interactions between synthesized compounds and the target protein. For this purpose, methicillin acyl-Penicillin binding protein 2a (PDB ID: 1MWU) was selected as a fitting molecular docking target (My et al., 2011). The minimum binding energy value reflects affinity and high stability of ligands to tie with the receptor (Abbas et al., 2018). Corresponding to the docking studies, the synthesized compounds showed good interactions and binding energy as compared to drug references (Amoxicillin and Penicillin G), which shown in (**Table 2**).

Table 2. Docking studies results of synthesized compounds docked into methicillin acyl-Penicillin binding protein 2a (PDB ID: 1MWU)

Compound	**Binding energy (kcal/mol)**	**Interactions**			
		H-bond	van der Walls	Pi-alkyl	Other Interactions
2	-5.10	GLU^{189}, GLU^{379} SER^{191}, SER^{376} ASP^{221}	-	VAL^{217}	LYS^{215} (Pi-cation)
3	-6.00	LYS^{247}, LYS^{215}	TYE^{366}	LEU^{383}L YS^{382} PRO^{370} VAL^{217}	-
4	-4.40	GLU^{379}	ASP^{221} LYS^{218}	VAL^{217} PRO^{370} LEU^{224}	LYS^{215} (Pi-cation) MET^{375} (Pi-sulfer) TYR^{223} (pi-pi)
5	-4.10	ASP^{367}	LYS^{219}	LEU^{383} PRO^{370} LYS^{382}	LYS^{219} (Pi-cation) GLU^{379} (Pi-anion)
6	-4.90	MET^{375}, PHE^{371}	PRO^{258} TYR^{196} GLY^{257}	PRO^{258}	LYS^{280} (Pi-cation)
7	-5.00	ASP^{552}	LYS^{290}	LEU^{155} LYS^{322} LYS^{319}	LYS^{289} (Pi-amide) ASP^{323} (Pi-anion) GLU^{161} (Pi-anion)

				LYS^{290}	
8	-4.00	GLU^{239}, SER^{240}	THR^{165}	LYS^{215}	TYR^{373} (pi-pi)
10	-7.00	GLU^{189}, SER^{191} LYS^{215}	SER^{376}	PRO^{370} VAL^{217}	GLU^{379} (Pi-anion) GLU^{189} (Pi-anion) LEU^{383} (Pi-sigma) ASP^{367} (Halogen)
11	-8.20	TYR^{269}, TYR^{496}, TYR^{499}, GLN^{396}	GLN^{396} ASN^{393}	LYS^{280} LYS^{281}	LYS^{281} (Pi-cation)
12	-7.30	GLU^{239}	ASP^{295}	LYS^{317} LYS^{318} LEU^{147} ARG^{151} ARG^{241}	LYS^{148} (Pi-cation) ARG^{298} (Pi-cation) VAL^{277} (Pi-sigma) SER^{240} (Pi-amaid)
13	-6.50	SER^{193}	TYR^{196}	PRO^{258}	LYS^{280} (Pi-cation)
14	-7.00	SER^{193}, MET^{375}	PHE^{371} TYR^{255} GLY^{257}	PRO^{258}	TYR^{380} (pi-pi)
15	-7.70	TYR^{380}, ASN^{393}	GLN^{396} HIS^{251}	PRO^{497} LEU^{286} LEU^{391}	-
16	-6.80	MET^{372}, THR^{216}	PRO^{258}	MET^{372} PRO^{258} VAL^{277}	-
Amoxicillin	-7.4	LYS^{148}, THR^{165} SER^{149}, GLY^{239} VAL^{256}	SER^{240}	PRO^{258} MET^{372}	TYR^{373} (pi-pi)
Penicillin G	-7.2	GLU^{396}, GLY^{282} TYR^{496}, ASN^{393}	LEU^{391} TYR^{396} TYR^{499} LYS^{281}	LYS^{285}	LEU^{286} (Pi-sigma)

All synthesized compounds screened a good binding score (-4.00 to -8.20 kcal/mole) as compared to standard drugs. As shown in the table (**2**), the 2-Azetidinones exhibited the lower binding energy than Schiff bases, meaning 2-Azetidinone more stable than Schiff bases whereas it interacted with the active site of the protein. Commonly, the number of the interactions was expanded while the Schiff bases were converted to the 2-Azetidinonedue to chlorine atoms and oxygen atoms of 2-Azetidinone rings as seen in the compound (**11**) figure (**2** and **6**), two hydrogen bond were formed with amino acid residues TYR496, GLN396 due to oxygen atom of the 2-Azetidinone's carbonyl, and chlorine formed hydrogen and halogen bonds in a few of the synthesized compounds such as compound (**10**). Because of the best orientation seen in compound (**11**) as presented better docking scores (-8.20 kcal/mole) and more interactions with amino acid residues, which formed as four hydrogen bonds with these active receptor sites TYR269, TYR496, TYR499, and GLN396, two van der Waals forces with GLN396 and ASN393, two pi-alkyl interactions (LYS280 and LYS281) and a pi-cation interaction LYS281. For Schiff bases, the compound (**3**) showed the lowest binding energy of Schiff bases (-6.00 kcal/mole), the interactions shown in the figure (1 and 5). The lower binding affinities were taken note for compounds (**8** and **16**)**.**

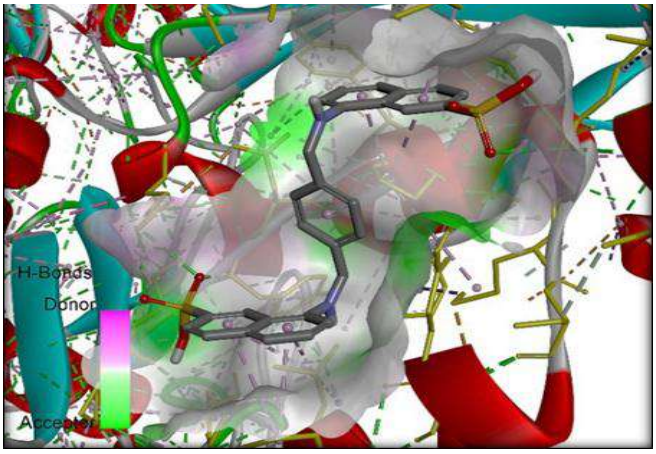

Fig. 1. Three dimension binding model of compound **(3)** docked into the active sites of protein (ID: 1MWU), surface is acceptor hydrogen bond of active sites).

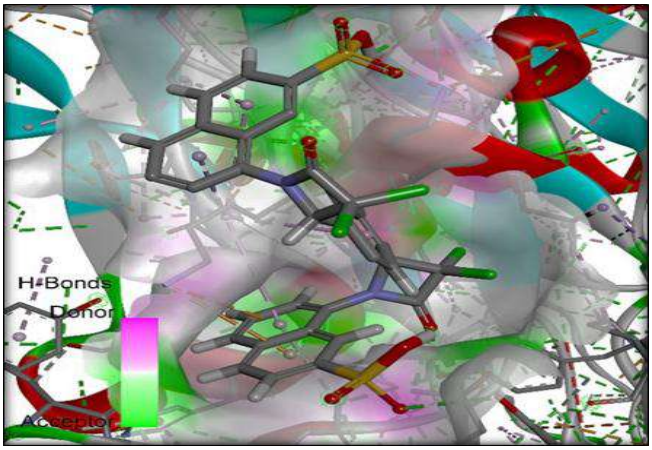

Fig. 2. Three dimension binding model of compound (**11)** docked into the active sites of protein (ID: 1MWU), surface is acceptor hydrogen bond of active sites).

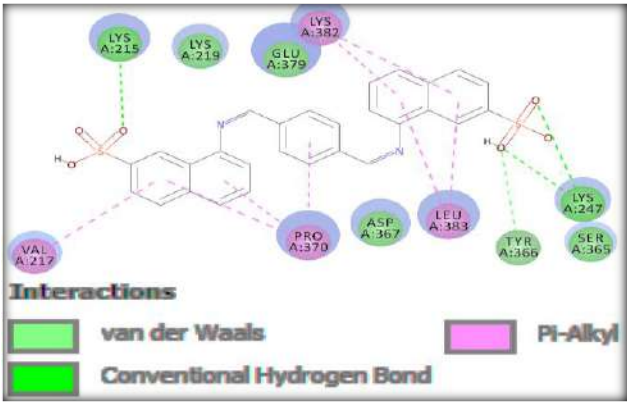

Fig. 3. Three dimension binding model of compound (**3)** docked into the ligand active sites of protein (ID: 1MWU).

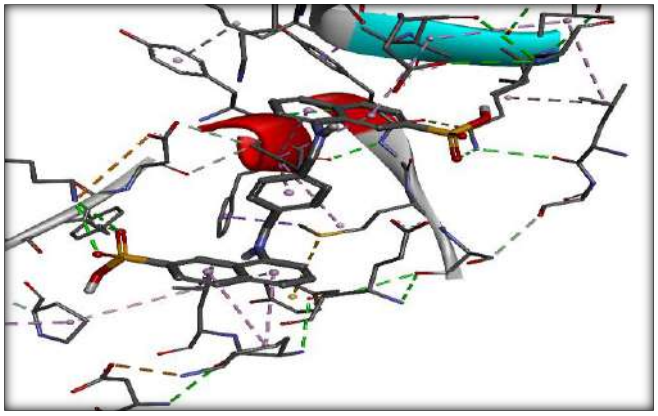

Fig. 4. Three dimension binding model of compound (**11)** docked into the ligand active sites of protein (ID: 1MWU).

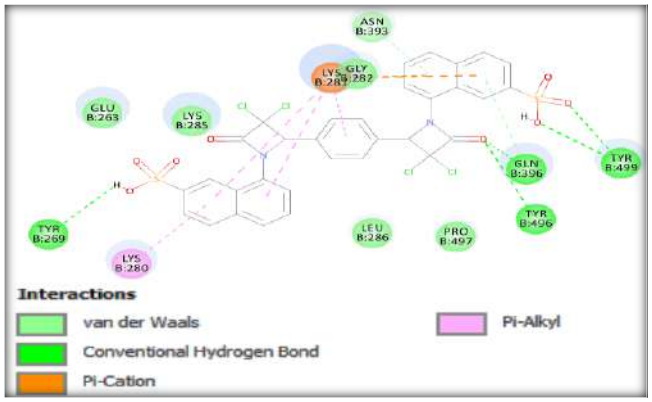

Fig. 5. Two dimensions ligand compound (**3**) interactions, docked into the active sites of the protein (ID: 1MWU)

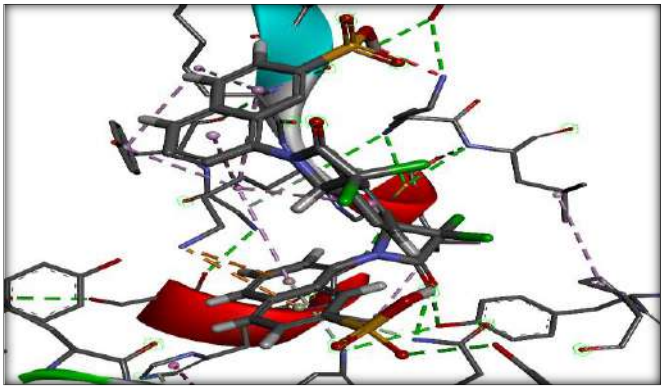

Fig. 6. Two dimensions ligand compound (**11**) interactions, docked into the active sites of the protein (ID: 1MWU).

4. CONCLUSIONS

Within the current investigation, helpful synthetic methods were applied for the synthesis of seven new symmetrical Bis-Schiff bases and 2-Azetidinones in good yield. The structures of synthesized compounds were fully characterized by FT-IR and NMR. Antimicrobial activities were assessed for all synthesized compounds. All the synthesized compounds showed good antimicrobial activity as compared to reference drugs. According to the *in vitro* antimicrobial tests, the compound (**3**) for Schiff bases and compound (**11**) for 2-Azetidinones exhibited highest antimicrobial activity. The part of this research study focused on supporting the antimicrobial activity, to affirm the interactions and supporting the antimicrobial activity, a molecular docking study was utilized for this reason, synthesized compounds showed good binding energy and interactions. The compound (**11**) screened better binding energy and most active to create interactions with acceptor sites, which supported to their antimicrobial activity. The binding energy and antimicrobial activity of 2-Azetidinones were better than Schiff bases due to Chlorine and oxygen atoms of 2-Azetidinones rings, which formed the interactions with protein acceptors like, Hydrogen bond, van der Waals forces, and halogen interactions. Sulfonamides (compounds **2**, **6**, **10** and **14**) and hydroxide groups (compounds **3** and **11**) expanded the activity of the compounds for antimicrobial activity and docking studies. Furthermore, the newly synthesized compounds can use in pharmaceutical fields for treatments of some infections afterward some further assessments.

Acknowledgements: The authors are grateful to God, the Research Center at the University of Raparin (RCUOR) and Salahaddin University.

References

ABBAS, S., NASIR, H. H., ZAIB, S., ALI, S., MAHMOOD, T., AYUB, K., TAHIR, M. N. & IQBAL, J. 2018. Carbonic anhydrase inhibition of Schiff base derivative of imino-methyl-naphthalen-2-ol: Synthesis, structure elucidation, molecular docking, dynamic simulation and density functional theory calculations. *Journal of Molecular Structure,* 11 (5)**,** 183-200.

AL-MASOUDI, W. A., FAAZ, R. A., AL-ASADI, R. H. & JABBAR, H. S. 2016. Synthesis, antimicrobial activity and modelling studies of some new metal complexes of Schiff base derived from sulphonamide drug in vitro. *European Journal of Chemistry,* 7 (1)**,** 102-106.

ALI, A., GHANIM, H. T. & SAID, M. H. 2015. Synthesis and Identification of Schiff Bases lidands as derivatives for Terephthaldehyde and studies it is complexes with some elements *Journal of Applied, Physical and Biochemistry Research,* 1 (1), 9-16.

ANACONA, J., NORIEGA, N. & CAMUS, J. 2015. Synthesis, characterization and antibacterial activity of a tridentate Schiff base derived from cephalothin and sulfadiazine, and its transition metal complexes. *Journal of Spectrochimica,* 137 (14)**,** 16-22.

AYYASH, A. N. 2019. A Novel Bioactive Compounds of 2-Azetidinone Derived from Pyrazin Dicarboxylic Acid: Synthesis and Antmicrobial Screening. *Journal of Acta Pharmaceutica Sciencia,* 57 (4), 103-114.

AZIZ, D. M. & AZEEZ, H. J. 2020. Synthesis of new ß-lactam-N-(thiazol-2-yl) benzene sulfonamide hybrids: Their in vitro antimicrobial and in silico molecular docking studies. *Journal of Molecular Structure,* 22 (2)**,** 128-154.

AZZAWI, A. M. A. & AL-OBIADI, K. K. H. 2016. Synthesis and Antimicrobial screening of new Bis-Schiff Bases and their Acetyl Oxadiazole Azetidinone derivatives derived from Pyromellitidiimide. *International Journal of Research in Pharmacy and chemistry,* 6 (1), 1-8.

BEG, M. & ATHAR, F. 2020. Pharmacokinetic and molecular docking studies of Achyranthes aspera phytocompounds to exploring potential anti-tuberculosis activity. *Journal of Bacteriology & Mycology,* 8 (1)**,** 18-27.

BENDALE, A. R., BHATT, R., NAGAR, A., JADHAV, A. G. & VIDYASAGAR, G. 2011. Schiff base synthesis by unconventional route: an innovative green approach. Jornal of *Der Pharma Chemica,* 3 (2)**,** 34-38.

BHUYAR, S., JUNEJA, H. & PAIWAL, L. 2013. Synthesis, spectroscopic and thermal studies of newly synthesized transition metal coordination polymers. *Journal of Pharmaceutical, Biological and Chemical Sciences.Research Res.* 20 (4)**,** 557-564.

BORAZJANI, N., BEHZADI, M., DADKHAH ASEMAN, M., JARRAHPOUR, A., RAD, J. A., KIANPOUR, S., IRAJI, A., NABAVIZADEH, S. M., GHANBARI, M. M. & BATTA, G. 2020. Cytotoxicity, anticancer, and antioxidant properties of mono and bis-naphthalimido β-lactam conjugates. *Journal of Medicinal Chemistry Research***,** 5 (1), 1-21.

DA SILVA, C. M., DA SILVA, D. L., MODOLO, L. V., ALVES, R. B., DE RESENDE, M. A., MARTINS, C. V. & DE FÁTIMA, Â. 2011. Schiff bases: A short review of their antimicrobial activities. *Journal of Advanced research,* 2 (1)**,** 1-8.

DEEP, A., KUMAR, P., NARASIMHAN, B., LIM, S. M., RAMASAMY, K., MISHRA, R. K. & MANI, V. 2016. 2-Azetidinone derivatives: synthesis, antimicrobial, anticancer evaluation and QSAR studies. *Journal of Acta Poloniae Pharmaceutica-Drug Research,* 73 (1)**,** 65-78.

ELSAYED, B. A., ELHENAWY, A. A. & SULTANAH, A. 2014. Synthesis, Characterization, Antimicrobial and Cytotoxic Studies on Some Novel Transition Metal Complexes of Schiff Base Ligand Derived From Sulfadiazine with Molecular Orbital Calculations. *International Journal of Chemistry and Materials Research,* 2 (1)**,** 1-16.

HAMDAN, I. A.-A., HAMDAN, A. A.-A. & ALI, A. J. 2018. Synthesis, characterization and evolution of biological activity for new heterocyclic derivatives Schiff bases. *Journal of Pharmaceutical Sciences and Research,* 10 (7)**,** 1710-1715.

HASSAN, S. A. 2019. Synthesis, Spectroscopic study and Biological activity of some New Heterocyclic compounds derived from Sulfadiazine. *ZANCO Journal of Pure and Applied Sciences,* 31 (6)**,** 92-109.

IBRAHIM, A. R. 2015. Preparation and Characterization of some transition metal complexes of bis Schiff Base Ligand. *International Journal of Advanced Research,* 8 (3)**,** 315-324.

JURCIK, V., SLAWIN, A. M. & O'HAGAN, D. 2011. Single enantiomer synthesis of α-(trifluoromethyl)-β-lactam. *Beilstein journal of organic chemistry,* 7 (1)**,** 759-766.

KAJAL, A., BALA, S., KAMBOJ, S., SHARMA, N. & SAINI, V. 2013. Schiff bases: a versatile pharmacophore. *Journal of Catalysts,* 20 (3), 1-15.

KHAJAVI, M. 1998. Reaction of Imines with Trichloroacetic Esters or Anhydride Promoted by Iron Carbonyl or Microwave Irradiation. Preparation of 3, 3-Dichloro-β-Lactams. *Journal of Chemical Research***,** 2 (1), 724-725.

KHDUR, R. A. & ZIMAM, E. H. 2018. Synthesis and Characterization of some new β-Lactam Derivatives from Azo Sulphadiazine and its Biological Evaluation as Anticancer. *Journal of Oriental Chemistry,* 34 (1)**,** 371-380.

KHDUR, R. A. & ZIMAM, E. H. 2018. Synthesis, characterization and study biological screening of some new azetidinone derivatives from azo-

sulphadiazine. *Journal of Pak Biotechnol.* 15 (2)**,** 201-217.

KRATKY, M., DZURKOVA, M., JANOUSEK, J., KONECNA, K., TREJTNAR, F., STOLARIKOVA, J. & VINSOVA, J. 2017. Sulfadiazine salicylaldehyde-based Schiff bases: Synthesis, antimicrobial activity and cytotoxicity. *Journal of Molecules,* 22 (4)**,** 1573-1588.

KRATKY, M., VINSOVA, J., VOLKOVA, M., BUCHTA, V., TREJTNAR, F. & STOLARIKOVA, J. 2012. Antimicrobial activity of sulfonamides containing 5-chloro-2-hydroxybenzaldehyde and 5-chloro-2-hydroxybenzoic acid scaffold. *European journal of medicinal chemistry,* 50 (12)**,** 433-440.

KUMAR, S., LIM, S. M., RAMASAMY, K., VASUDEVAN, M., SHAH, S. A. A., SELVARAJ, M. & NARASIMHAN, B. 2017. Synthesis, molecular docking and biological evaluation of bis-pyrimidine Schiff base derivatives. *Journal of Chemistry Central,* 89 (11), 1-16.

MEHTA, P., DAVADRA, P., PANDYA, J. R. & JOSHI, H. S. 2014. Synthesis, characterization and antimicrobial activity of 2-azetidinone derivatives of benzimidazoles. *Journal of International Letters of Chemistry, Physics and Astronomy,* 30 (11)**,** 81-88.

MEHTA, P., SENGAR, N. P., SUBRAHMANYAM, E. V. & SATYANARAYANA, D. 2006. Synthesis and biological activity studies of some thiazolidinones and azetidinones. *Indian journal of pharmaceutical sciences,* 68 (1)**,** 103-106.

MOHAMMED, H. A. & TAHA, N. I. 2017. Microwave Preparation and Spectroscopic Investigation of Binuclear Schiff Base Metal Complexes Derived from 2, 6-Diaminopyridine with Salicylaldehyde. *International Journal of Organic Chemistry,* 7 (4)**,** 412-419.

MY, N. H., HIRAO, H., VAN, D. U. & MOROKUMA, K. 2011. Computational studies of bacterial resistance to β-lactam antibiotics: mechanism of covalent inhibition of the penicillin-binding protein 2a (PBP2a). *Journal of chemical information and modeling,* 51 (6)**,** 3226-3234.

NOORI, N. S., ZAIDAN, T. A. & MESHER, M. F. 2019. Synthesis and Characterization of New Complexes for (1e,1'e)-N,N'-(Thiobis (4,1-Phenylene)) Bis(1-Phenylmethanimine) Substituted Ligands with Fe3+. *International Research Journal Of Pharmacy,* 9 (12)**,** 57-63.

OZDEMIR GUNGOR, O. 2017. Intramolecular Proton Transfer Equilibrium in Salicylidene-and Naphthalene-based Tetraimine Schiff Bases. *Journal of Science,* 30 (1), 191-214.

PIENS, N. 2017. *Synthesis of new β-lactam building blocks and their application in heterocyclic chemistry.* Ph.D Dissertation, Ghent University.

SHARMA, R., SAMADHIYA, P., SRIVASTAVA, S. & SRIVASTAVA, S. 2012. Synthesis and pharmaceutical importance of 2-azetidinone derivatives of phenothiazine. *Journal of Chemical Sciences,* 12 (4)**,** 633-637.

SHAYGAN, S., PASDAR, H., FOROUGHIFAR, N., DAVALLO, M. & MOTIEE, F. 2018. Cobalt (II) complexes with Schiff base ligands derived from terephthalaldehyde and ortho-substituted anilines: synthesis, characterization and antibacterial activity. *Journal of Applied Sciences,* 85 (8)**,** 385-397.

SHINDE, A., ZANGADE, S., CHAVAN, S. & TİWDE, S. Yeni. 2015. Synthesis and antioxidant activity of some novel derivatives of bis-2-azetidinones and bis-4-thiazolidinones. *Journal of the Turkish Chemical Society Section,* 2 (4)**,** 22-31.

SHOCKRAVI, A., SADEGHPOUR, M. & OLYAEI, A. 2009. A convenient synthesis of novel symmetrical bis-Schiff bases of 2, 2'-thio-bis [4-methyl (2-aminophenoxy) phenyl ether] in solution and under solvent-free conditions. *Journal of Chemical Research,* 3 (2)**,** 656-658.

SINGH, G. S. & SUDHEESH, S. 2014. Advances in synthesis of monocyclic beta-lactams. *Journal of Arkivoc,* 14 (1)**,** 337-385.

SINGH, M., HAZRA, A., BHARITKAR, Y. P., KALIA, R., SAHOO, A., SAHA, S., RAVICHANDIRAN, V., GHOSH, S. & MONDAL, N. B. 2018. Synthesis of diversely substituted bis-pyrrolizidino/thiopyrrolizidino oxindolo/acenaphthyleno curcuminoids via sequential azomethine ylide cycloaddition. *Royal Society Journal of Chemistry,* 21 (8)**,** 18938-18951.

TURAN, B., ŞENDIL, K., ŞENGÜL, E., GÜLTEKIN, M. S., TASLIMI, P., GULCIN, I. & SUPURAN, C. T. 2016. The synthesis of some β-lactams and investigation of their metal-chelating activity, carbonic anhydrase and acetylcholinesterase inhibition profiles. *Journal of enzyme inhibition and medicinal chemistry,* 31 (1)**,** 79-88.

TURAN, N. & SEKERCI, M. 2009. Metal complexes of Schiff base derived from terephthalaldehyde and 2-amino-5-ethyl-1, 3, 4-thiadiazole synthesis, spectral and thermal characterization. *Journal of Synthesis and Reactivity in Inorganic, Metal-Organic, and Nano-Metal Chemistry,* 39 (10)**,** 651-657.

VAN BRABANDT, W., DEJAEGHER, Y. & DE KIMPE, N. 2005. New reactions of functionalized β-lactams. *Journal of Pure and applied chemistry,* 77 (12)**,** 2061-2071.

ZIWAR, J. B. & MUSHEER, N. 2016. Synthesis of some Heterocyclic Compounds (Oxazepine, Diazepine) using Ultrasound Irradiation. *ZANCO Journal of Pure And Applied Sciences,* 28 (2), 235-239.

Appendix

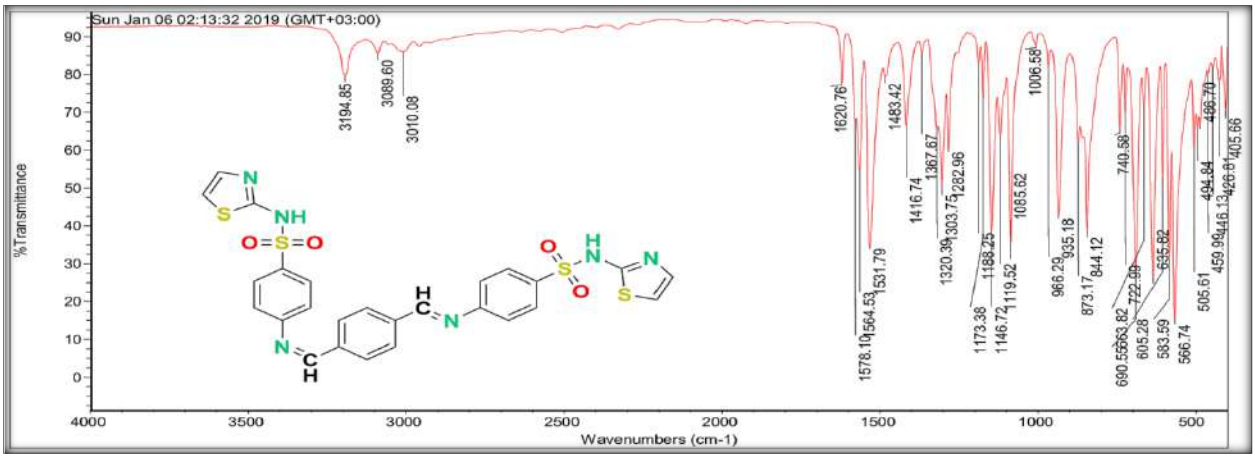

Fig. 7. FT-IR Spectrum of the compound (**2**)

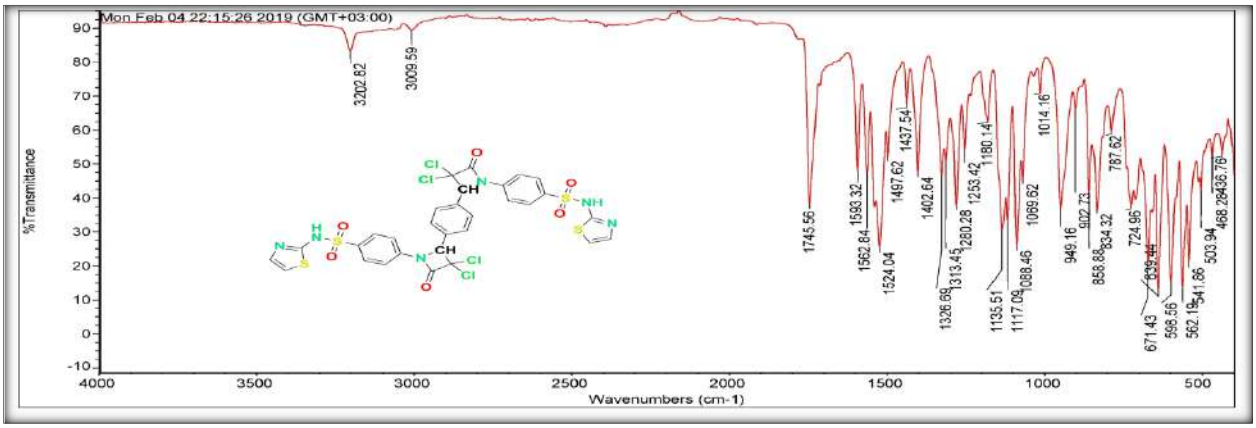

Fig. 8. FT-IR Spectrum of the compound (**10**)

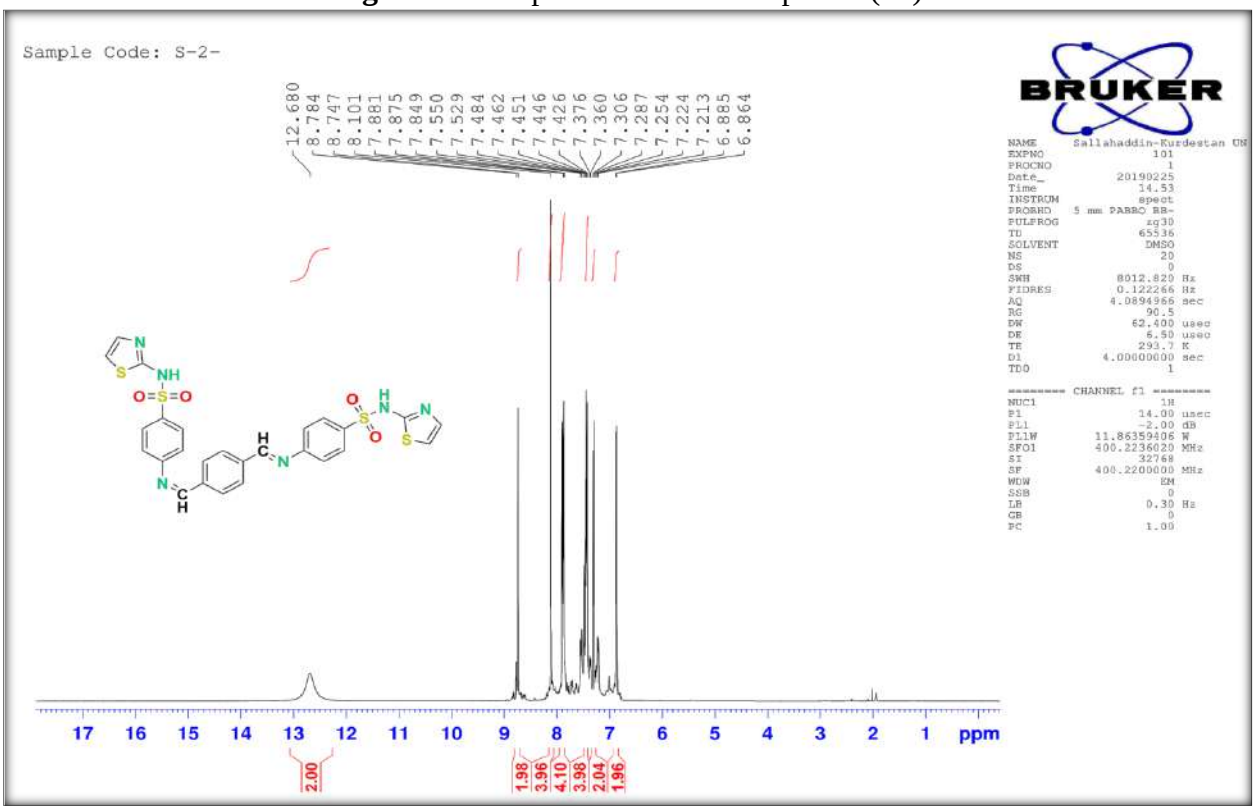

Fig. 9. ^{1}H-NMR spectrum of *the* compound (**2**)

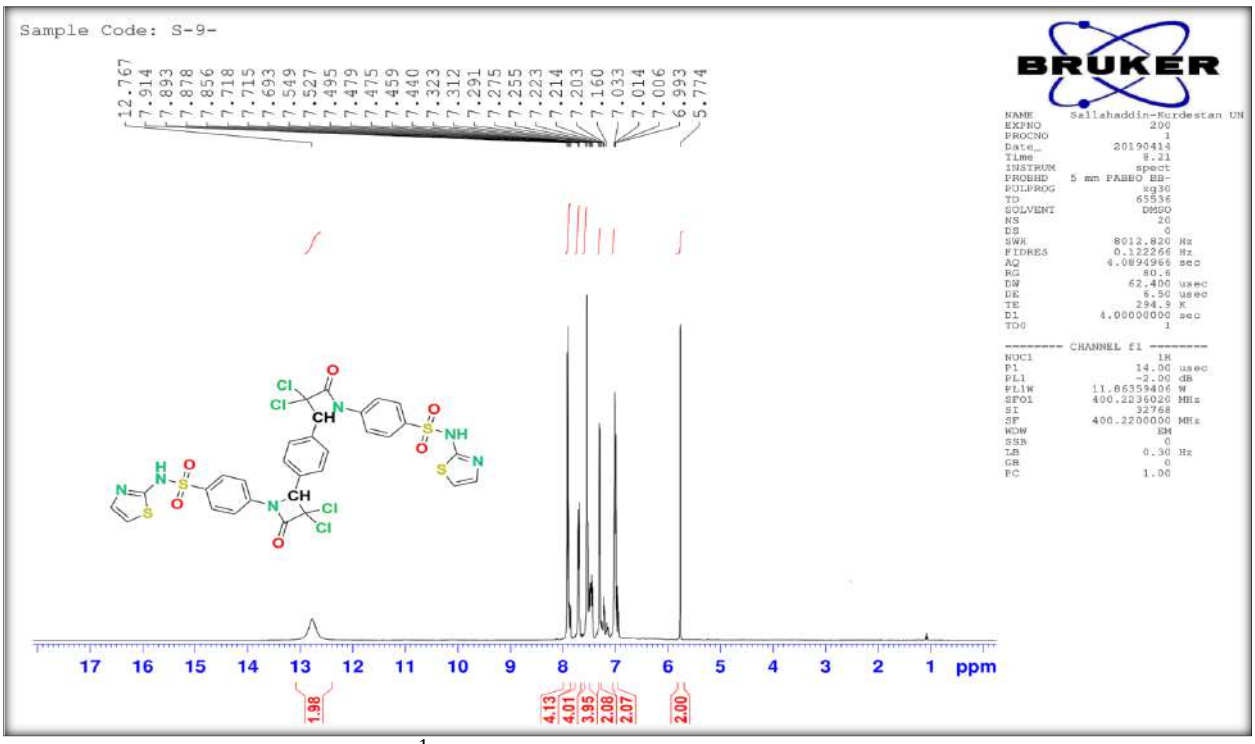

Fig. 10. ^{1}H-NMR spectrum of the compound (**10**)

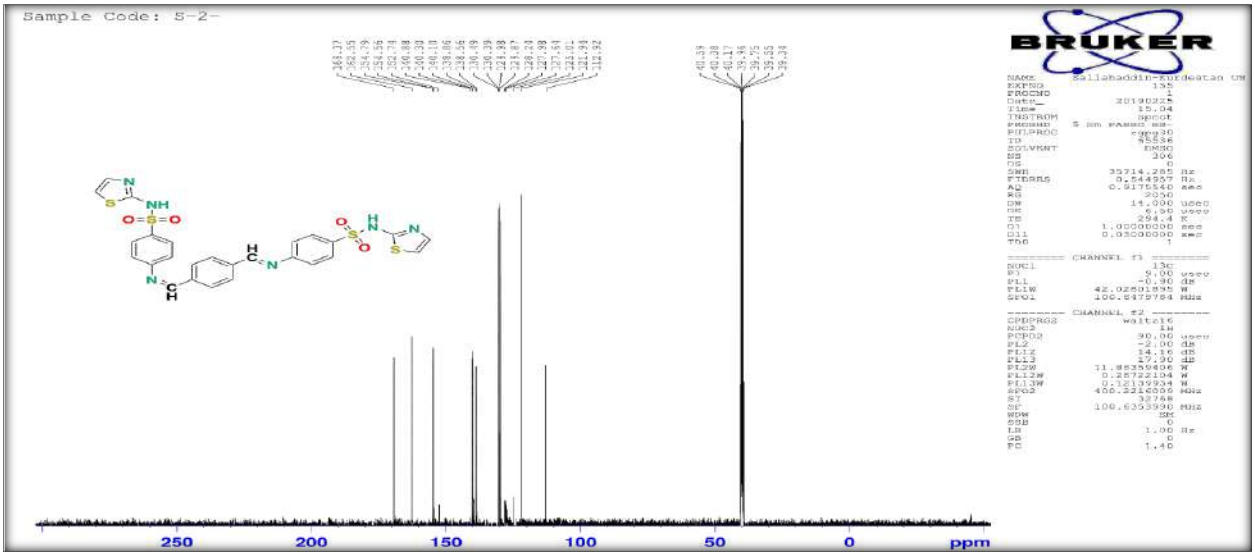

Fig. 11. ^{13}C-NMR Spectrum of the compound (**2**)

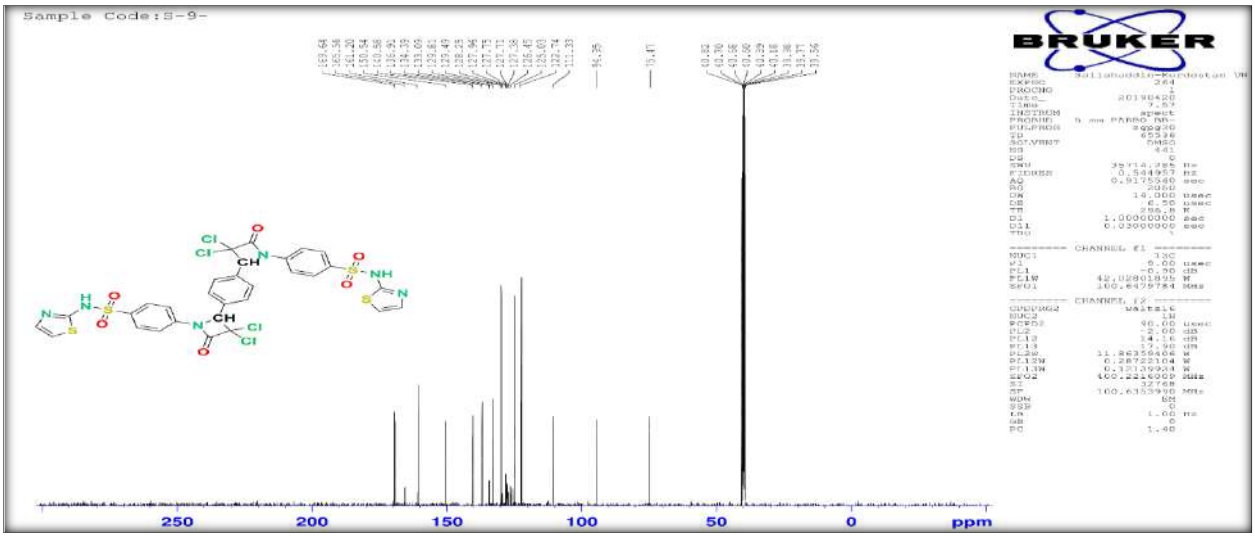

Fig. 12. ^{13}C-NMR Spectrum of the compound (**10)**

ZANCO Journal of Pure and Applied Sciences
The official scientific journal of Salahaddin University-Erbil
https://zancojournals.su.edu.krd/index.php/JPAS

ISSN (print):2218-0230**, ISSN (online):** 2412-3986**, DOI: http://dx.doi.org/10.21271/zjpas**

RESEARCH PAPER

Influence of Solvents on The separation of Water From The bitumen Emulsions Using Alginite.

Sangar S.Ahmed

Department of Chemistry, College of Science, Salahaddin University-Erbil, Kurdistan Region, Iraq

A B S T R A C T:
The impact of various diluents on the removing of water from bitumen emulsions for the distillation feed (bitumen) using alginite as a demulsifier was investigated. Alginite as a natural rock is able to remove water from the bitumen emulsion. The results demonstrated that the alginite can be enhanced by adding solvents. The separation of water without adding diluents using 0.5 wt.% was about 84 %. In contrast, the addition of 2.0 mL 1-butanol can significantly improve the process resulting in water removal of 98.3 %. Furthermore, at the highest volume of hydrocarbon solvent, which was a kerosene fraction (2 mL), this yields an increase in the last water separated from 73.5 % to nearly 81.3 % in the bitumen emulsion. Consequently, the results confirmed that applying toluene, hydrocarbon solvents, and medium-chain alcohols can enhance the destabilization process when they are used together with alginite. Thereafter, changing the physical characteristics of an emulsion with the addition of diluent leads to a decrease in the viscosity of the oil phase and contributes to the coalescence of water droplets.

KEY WORDS: Bitumen, Emulsion, Alginite, 1-butanol, Toluene.
DOI: http://dx.doi.org/10.21271/ZJPAS.33.2.5
ZJPAS (2021) , 33(2);51-58 .

1. INTRODUCTION :

Bitumen (tar sands) consists of a large number of oil resources in Canada. Although, due to oil sands unconsolidated deposits of very heavy hydrocarbon bitumen and this require many stages of processing before refining (Jiang *et al.*, 2007). Bitumen is exploited using in-situ thermal operations corresponding to steam-assisted gravity drainage (SAGD) and cyclic steam stimulation and utilizing surface mining, wherever the bitumen is separated from reservoir sand and clay using hot water and a froth flotation operation.

Due to low mobility and flow which are closed to ambient temperature, the complex composition of heavy crude oil and bitumen would be difficult and expensive to produce and transport through pipelines. Furthermore, their high asphaltene and paraffin contents stimulate pipe clogging, pressure drops, and consequently a lower production rate rather than lighter crude oils (Martínez-Palou et al., 2013) and (Yarranton et al., 2000). Nevertheless, these two operations involve the production of viscous emulsion (Elsayed Abdelfatah *et al.*, 2019). The emulsion is droplets of water or brine which are distributed in an exceedingly continuous phase of crude oil and that they are recognized as water-oil emulsions (W/O) (Saad et al., 2019).

Moreover, high viscosity and enormous contents of resins and asphaltenes contribute to

* **Corresponding Author:**
Sangar Salih Ahmed
E-mail: sangar.ahmad1@su.edu.krd
Article History:
Received: 04/10/2020
Accepted: 09/11/2020
Published: 18/04 /2021

stabilize the water droplets which spread in oil, that making petroleum demulsification harder and also the development of new dehydrating agents is necessary. For the droplets to flocculate and coalesce, the additives should reduce this steric repulsion by softening the rigid skin. Highly interfacially active demulsifiers compared to asphaltene can compete effectively for the interface and soften the interfacial asphaltene film. (Elsayed Abdelfatah *et al.*, 2019) A lot of techniques such as mechanical, chemical, thermal, and electrical have been applied to resolve the emulsion phenomenon. Also, combinations of these methods have been conducted for a good demulsification achievement. (Cendejas *et al.*, 2013)

However, bitumen density is almost the same as the density of water, and without the addition of a light hydrocarbon diluent (e.g., naphtha), froth treatment is not possible. Diluting the froth with a light hydrocarbon decreases the stage of oil density, that making separation of water from diluted possible bitumen. Gravity settlers, centrifuges, and/or cyclones are applied in all operating plants. Therefore, the addition of a diluent reduces the oil phase viscosity, and further support in the removal of the water and solids (Czarnecki and Moran, 2005).

The impact of solvent is also very essential to the stability of diluted water-bitumen emulsion. The stability of the bitumen emulsion was decreased with the rise of the dilution ratio. The diluted bitumen film between water droplets and oil phase, which becomes less stable. Besides, the physical properties of the oil phase such as density, viscosity will affect with using the dilution ratios. (Jiang *et al.*, 2011) Light hydrocarbon such as Naphtha and paraffinic diluent are widely used in froth treatment operations. Hence, a diluent that has the capability of destabilizing the bitumen emulsion would be a breakthrough. Meanwhile, adding conventional demulsifiers requires the addition of volatile organic solvents such as toluene and alcohol as a carrier for the demulsifier. This poses significant environmental issues and complicates the process. Environmentally friendly demulsifiers and diluents are essential for the oil industry. (Salam *et al.*, 2013)

Consequently, the objective of the current work is to go beyond what was performed previously work (Hippmann *et al.*, 2018) and aims to study the influence of various types of solvents on the demulsification of the water-bitumen emulsion prepared with a residual distillation feed oil using alginite as eco-friendly demulsifier. The effects of solvents with alginite on the rheology and water droplets of the bitumen emulsion were also investigated. Alginite is a natural rock out of the oil shale family and it descents from the Gérce mine in- Hungary. The essential ingredients of alginite are high of organic matter (19 %), clay (54 %), and limestone content (22 %) (Hippmann *et al.*, 2018).

2. EXPERIMENTAL SECTION

2.1. EQUIPMENT AND MATERIALS

Vacuum residual distillation feed (bitumen), which was a residue from Khurmala oil field, was utilized to prepare water-bitumen emulsions. It was obtained from Erbil in the (Kurdistan Region of Northern Iraq). All used solvents were of analytical grade and purchased from Fluka (USA).

The density (using the pycnometer), entire sulfur content % (using the X-ray sulfur meter models RX-360SH, Japan), kinematic viscosity (using the SCHOTT CT 52 viscometer), and flash point (using the Automated Cleveland Open cup Flash Point Tester aco-8/8 as) of the bitumen were analyzed. The typical characteristics of bitumen are listed in Table 1. Alginite, which was given by Terra Natural Resources GmbH with a grain size of 3 mm that used as a demulsifier and prepared in powder form of particle size less than 100 µm.

Table 1: Physical properties of bitumen sample.

Test Description	Method	Sample Results
Density g/cm^3	ASTM D-70	0.9937
Sp.gr @ 15.5 °C	ASTM D-1217	0.9935
API Gravity	ASTM D-287	10.93
Total sulphur content wt %	ASTM D-4294	4.8034
Flashpoint °C	ASTM D-92	>120
Viscosity c.St 50 °C	ASTM D-445	2498

Also, the physical properties of diesel and gasoline samples are illustrated in **Table 2** and **Table 3** respectively.

Table 2: Physical properties of diesel sample.

Test description		Unit	Results
Flash point		°C	67
Pour Point		°C	-9
Density at 15.5 °C		g/ml	0.8485
Kinematic Viscosity @40°C		mm^2/sec	3.5
Water content		vol%	0.0
Cetane Number		----	47
Cetane Index		----	50
Total Sulfur Content		mass%	0.645
Initial Boiling Point, IBP		°C	158
Distillation temperature	10% Recovered, vol%	°C	196
	50% Recovered, vol%		272
	90% Recovered, vol%		320
Final Boiling Point, FBP		°C	345
Recovered		vol%	97
Evaporated		vol%	1
Residue		vol%	2
Aniline point		°C	70
Diesel Index		----	55.7

Table 3: Physical properties of gasoline sample.

Test description		Unit	Results
Density at 15 °C		g/ml	0.7312
Specific Gravity@15.5°C		----	0.7320
API Gravity		----	61.78
Water content		vol%	0.0
Initial Boiling Point, IBP		°C	50
Distillation Temperature	10% Recovered, vol%	°C	76
	50% Recovered, vol%		114
	90% Recovered, vol%		192
Final Boiling Point, FBP		°C	200
Recovered		vol%	92
Evaporated		vol%	6.5
Residue		vol%	1.5
Total Sulfur Content		mass%	206
Research octane number, RON		----	92.1
Motor octane number, MON		----	82.9
Antiknock Index, AKI		----	87.5

For preparing the water in oil emulsion, an intensive mixer Citenco F.H.P. motors LC9, (England) was applied. Demulsification experiments were carried out using a magnetic mixer by IKA, Germany. The water content after demulsification was measured by the Karl-Fisher titration using a V20 by Mettler-Toledo, USA. The optical Microscopy was performed using a microscope PrimoStar by Zeiss, Germany, which was equipped with a digital camera DCMC310 and software ScopePhoto (Ver. 3.1.615) by ScopeTek, China. Conversely, the rheology investigations were accomplished by using a rheometer model RN 4.1 with a spindle type Rotor S1 by RHEOTEST, Germany, and a thermostatic bath Alpha RA12 by Lauda, Germany.

2.2.Preparation of water-bitumen emulsion

Making a density difference between bitumen and water, it is better to decrease the viscosity of bitumen, toluene at a volume ratio of 3:1 that was used as a solvent to create the continuous stage. Bitumen was transferred to a beaker and diluent was added. The mixture diluent–bitumen (Dilbit) was stirred to homogenize for 15 minutes at 1500 rpm using a mechanical stirrer (Citenco F.H.P. motors, model LC9, England). Emulsions samples were prepared by slowly adding brine solution (3% NaCl) to diluted bitumen (mass ratio 1:1) and kept mixing at 4500 rpm for 45 minutes. The stability of the prepared emulsion was measured under gravity sedimentation using a test tube at laboratory temperature. The water content of the stable bitumen emulsion was measured over time (more than one year) and the amount of emulsified water remained constant over time in the emulsion. Furthermore, without adding alginite using 2 mL of diluents like toluene, butanol, hexadecyl amine, n-heptane, there was no water separated.

2.3. Demulsification of water-oil emulsion

The demulsification tests of prepared water-bitumen emulsion were carried out as follow:

50 ml of the water-bitumen emulsion was used into a beaker and it was stirred before adding alginite and diluent at constant stirred 1200 rpm for 5 min. using a magnetic stirrer. Then, alginite and diluent were added to the bitumen emulsion at 60 °C temperature and stirred at 1200 rpm for 30 minutes. Then, the influence of solvents on the demulsification process was investigated. After the demulsification process, the water content of the treated bitumen emulsion was measured by the Karl-Fisher method using a Mettler-Toledo V20

(Germany) and reported as a weight percentage. The result was reported as a weight percent and it was calculated by using Equation 1.

$$\text{Water removal } \% = (1 - \frac{\text{Water content of sample}}{\text{Water content of initial emulsion}}) \times 100 \quad \ldots\ldots\ldots\ldots \text{ Equation 1}$$

2.4. Optical microscopy

The optical microscopy technique was utilized to visualize the emulsion droplet sizes. Also, it was used to study the influence of alginite as well as diluents on the size of water droplets in the emulsion. A drop of the emulsion (ca. 50 µL) with a diluent and alginite was placed on a glass slide and followed by a cover slide. The optical microscopy images were captured using a microscope equipped with the digital camera DCMC 310 and a Scope Photo (Ver. 3.1.615) image analysis software.

2.5. Determination of viscosity

Dynamic viscosity of prepared water-bitumen emulsion at a constant speed of rotation (1000 rpm) and temperature (60 °C) using a rheometer was measured. A spindle type Rotor S1 was used to measure the emulsion viscosities with a cell containing 35mL of a sample. The rheometer was connected with a water bath thermostat using a Lauda thermostat. After that, the same procedure was applied to study the effect of alginite and diluents on the viscosity of the water-bitumen emulsion.

3. RESULTS AND DISCUSSION

3.1. Effect of toluene

For the treatment of bitumen emulsion, the solvent was initially applied to form driving forces for the demulsification of water-in-bitumen emulsions by raising the different densities between the oil and water phases and, simultaneously, reducing oil phase viscosity. Since asphaltenes have been recognized as exactly involved in the stabilization of bitumen emulsions, solvent aromaticity should play an essential role in the demulsification of bitumen emulsions, considering that the phase of behavioral asphaltenes depends on solvent aromaticities. (Mullins, 2007) **Figure 1** shows the degree of demulsification of the bitumen emulsion as a function of different amounts of toluene. The experimental evidence shows that when the bitumen emulsion is diluted with 2.0 mL of toluene, more than 87 % of water was separated from the emulsion using 0.5 wt.% of alginite.

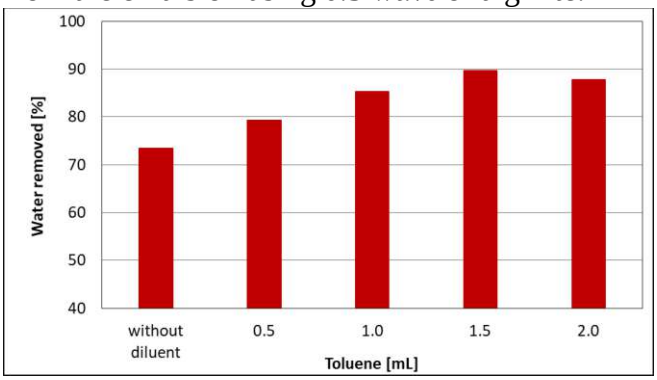

Figure 1: Effect of toluene on water removed using 0.5 wt. % alginite.

The results revealed that the solvent effect was very crucial to the stability of diluted bitumen emulsion. Increasing aromaticity of the emulsion causes enhancing asphaltene solubility allowing asphaltene molecules to be freer to leave their sites at the oil-water interfacial film. This ruptures the film and permits small water droplets to coalescence and grows, eventually separating into an aqueous phase (Zhang *et al.*, 2005).

3.2.Effect of hydrocarbon solvents

Figure 2 shows the impacts of the blending different hydrocarbon solvents with toluene on water removed% from the bitumen emulsion. Depending on diluent blended types with the bitumen emulsion, 78 % of water was separated from the emulsion without using diluents. Moreover, 80.2%, 76.2%, 78.1%, and 78.6% of water were removed from the bitumen emulsions using 2.0 mL of gasoline, n-hexane, n-octane, and n-decane respectively.

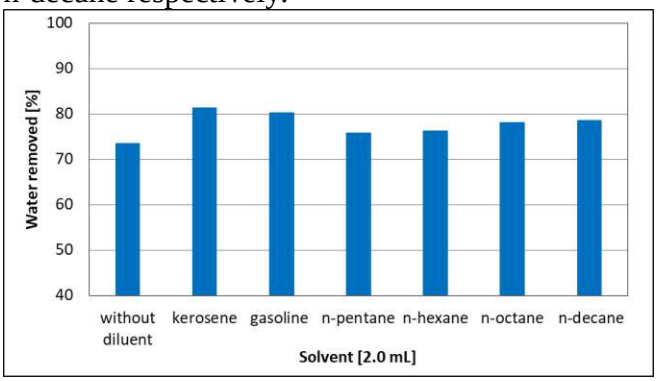

Figure 2: Effect of hydrocarbon solvents on water removed using 0.5 wt. % alginite.

In general, gasoline and kerosene fractions, which include a combination of paraffinic, naphthenic, and aromatic components),

as compared to a light aliphatic solvent, it can achieve more demulsification of bitumen emulsions. Without aromatic and naphthenic constituents, lighter solvents (e.g., n-pentane) were detached water from the emulsion less than heavier solvents (e.g., gasoline and kerosene) with aromatic and naphthenic compounds in their fractions. The same results were observed by (Mullins, 2007). Moreover, the solvent with higher aromaticity (toluene) accelerates water resolution from the oil stage marginally more than the solvent with lower aromaticity (hydrocarbon solvents) (see Figure 1).

3.3.Effect of different type of solvents

Since n-heptane and n-hexane, which have been used in the froth treatment, are greatly volatile solvents, the damage of solvent through the two hours of interface equilibrating should carefully be considered (Czarnecki and Moran, 2005). Consequently, it is important to find and investigate a solvent with high efficiency for destabilizing the water-bitumen emulsion. To study the effect of various solvents on the water-bitumen emulsion, four different solvents such as toluene, butanol, hexadecyl amine, n-heptane were investigated. From **Figure 3**, it is seen that the addition of 2.0 mL of n-heptane destabilizes the water-bitumen emulsions, while with the same amount of butanol more than 98% of water was removed from the emulsion.

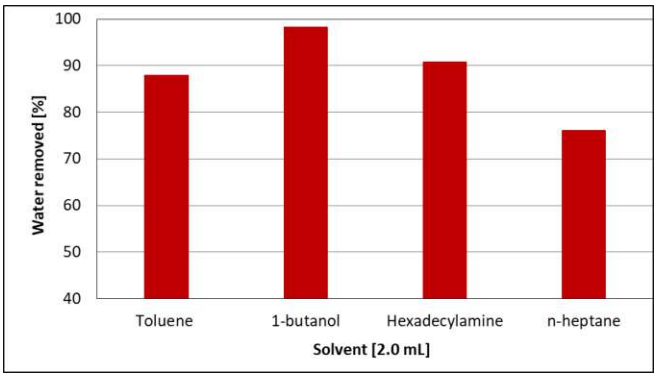

Figure 3: Effect of different solvents on water removed using 0.5 wt. % alginite.

As it can be noticed that from **Figure 3**, extended aromaticity of the bitumen emulsion helps to solubilize the asphaltenes and reduce the emulsion stability. Moreover, most destabilization was achieved when the dispersed phase is diluted with medium-chain alcohols. This attribute to using 1-butanol the asphaltene monolayer becomes more flexible at the interfacial film between water and oil stages. It can be clearly seen that 1-butanol molecules entered the interfacial film and these led to weakening the interfacial film between asphaltene molecules and water, thereby, leading to less-rigid the film. (Abdurahman H. Nour et al., 2007)

On the other hand, the addition of 2.0 mL hexadecylamine results in a separation of 90.8% of the water from the bitumen emulsion. The observation of amine solvent co-demulsifier efficiency was due to the high molecular weight of hexadecylamine, which drives as flocculants in adsorption of amine compounds in the interfacial film and interaction activity. (Abdurahman H. Nour *et al.*, 2007)

3.4. Effect of alcohol solvent

Alcohol solvents contain both hydrophobic and hydrophilic parts in their structure. The alcohol molecules are located at the tail (hydrophobic part) at the surface of the interfacial film, whereas, the tail is penetrating the interfacial film of the bitumen emulsion. Therefore, having alcohol molecules in the monolayer, it diminishes the interactions among asphaltene molecules which may lead to a less-rigid interfacial film. (Zhang *et al.*, 2005)

Figure 4 gives the effect of different blended alcohol solvents on the stability of the bitumen emulsions. It is seen that the highest demulsification efficiency was obtained with 1-butanol was 98 % using 0.5 wt.% of alginite, whereas, with the same amount of ethanol, 1.propanol, 1.hexanol, and 1.decanol, water separation efficiency was 79.5%, 93.0%, 97.4%, and 95.9%, respectively.

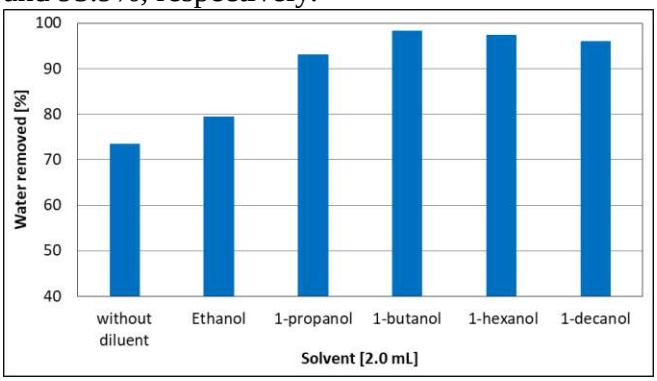

Figure 4: Effect of different alcohol solvents on water removed using 0.5 wt. % alginite.

Furthermore, due to the solubility properties, the water solubility of alcohols can be clarified as; low molecular weights alcohols that are water-soluble such as methanol and ethanol.

Nevertheless, four carbon alcohols and higher, having much lower water solubility. This can be illuminated by considering the way that water molecules can spread solute molecules into a solution. The polar water molecules are attracted to the hydroxyl group by hydrogen bonding that happens between the hydrogen of water molecules and the oxygen in the alcohol molecules. As the hydrocarbon portions of the alcohol become more extensive, they could be in a higher molecular weight (Abdurahman H. Nour et al., 2007). Additionally, medium-chain alcohols such as 1-butanol and 1-hexanol have an entirely different concentration dependence upon destabilization of the bitumen emulsion. The medium-chain alcohols are soluble in both the aqueous phase and the bulk crude oil in the interfacial region. Diffusion/ partitioning between these sites will adjust the interfacial properties of the system in such a way that the film becomes less rigid, and hence more dynamic, allowing more accentuated fluctuations to occur. Such processes will directly improve the possibilities of an effective overlap between dissimilar adjoining droplets, and thus strongly favour coalescences (Sjöblom, H. Söderlund, S. Lindblad, E. J. Johansen and I. M. Skjärvö, 1990).

3.5.Effect of the diluent on the water droplets

To understand more about the effect of diluents specially 1-butanol and alginite on the water-bitumen emulsion, the microscopic technique was applied. As can be distinctly seen from **Error! Reference source not found.**A that without using alginite particles and diluents, the emulsion was stable and no water was separated from the emulsion. On the other hand, as illustrated in **Error! Reference source not found.**C, after mixing alginite with the emulsion, the drops of water start to separate from the emulsion. Also, using 1-butanol with the particles of alginite, the water was separated immediately from bitumen emulsion (see **Error! Reference source not found.**B).

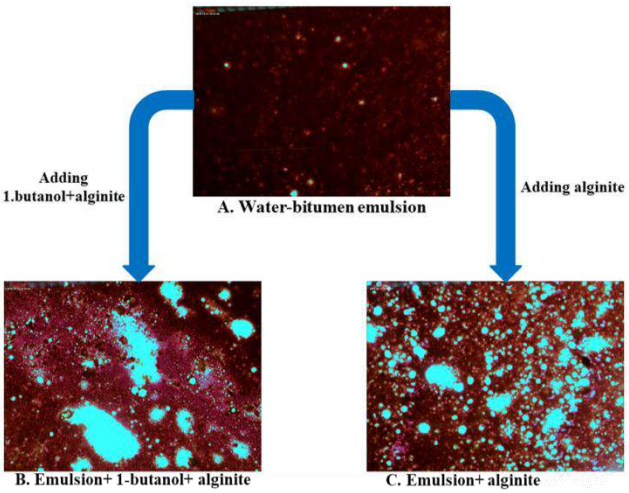

Figure 5A-C: Microscopic images of emulsion C with the addition of alginite at different times.

From the current results, it can be concluded that utilizing 1-butanol besides alginite particles initiates the rise of water droplets in the bitumen emulsion system, thus, extends to an increase in the coalescence of the water droplets.

3.6.Effect of alginite and solvent on the viscosity of the emulsion

The viscosity of the treated and untreated bitumen emulsion was measured to investigate the effect of alginite with diluent and alginite on the rheology of the water-bitumen emulsion. The viscosity test was carried out at temperature 60 °C and constant rotational speed (1000 rpm). As presented in **Figure 6**, the viscosity was reduced after adding alginite to the emulsion immediately. The viscosity of untreated emulsion has remained constant without adding alginite. The result shows that alginite has great power efficiency in decreasing the interfacial tension of the adsorption film in the emulsion, which makes the deformation of the distributed phase easier. Moreover, the viscosity of bitumen emulsion instantly reduced to 10mPa.s after 2 mL of 1-butanol and 0.5 wt.% of alginite was added to the emulsion. This means that water was completely broken from the bitumen emulsion. This can be attributed to the fact that alginite with 1-butanol has the power to split water in the bitumen emulsion. Altering the physical characteristics of an emulsion with the addition of diluents leads to a decrease in the viscosity of the constant stage and provides a coalescence of water droplets. On the other hand, the increase in viscosity of the untreated bitumen emulsion after 600 sec. is mainly due to the increase of interaction bonds,

which is formed between water and functional groups of bitumen. This is leading to reduce in the molecular distances of the emulsion, thereby, a rise of resistance to flow and increase the dynamic viscosity

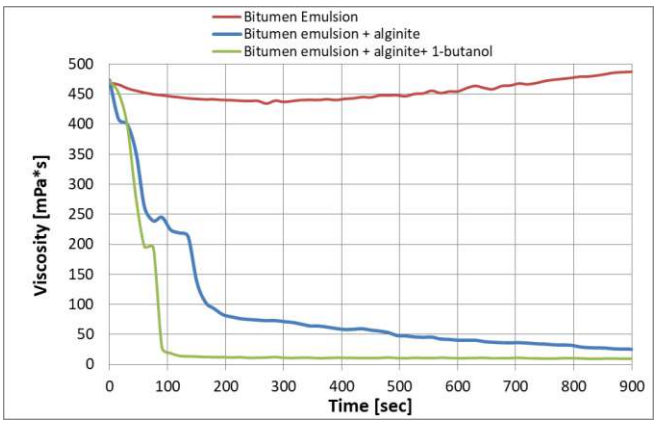

Figure 6: Effect of alginite on the viscosity of water-bitumen emulsion.

From the current results discussed, it can be noticed that 1-butanol made an increase of water droplet sizes and reduce viscosity in the emulsion system after adding to alginite. This demonstrates that the complete distribution of the alginite molecules on the interfacial film is between water and bitumen emulsion.

4. CONCLUSIONS

This work indicates the addition of diluents with alginite was essential to obtain high results. Therefore, alginite can be used as a new powerful demulsifier in both the petroleum industry and the environmental field. The percentage separation of water without adding diluents using 0.5 wt.% was about 84 %. The addition of 2.0 mL 1-butanol can significantly improve the process resulting in water removal becoming 98.3 %. The highest volume of hydrocarbon solvent, which was kerosene fraction (2 mL), this yields an increase in the last water separated from 73.5 % to nearly 81.3 % in the bitumen emulsion. The results revealed that the solvent has a crucial effect on stabilising the diluted bitumen emulsion. Increasing aromaticity of the emulsion with adding toluene to the emulsion can enhance asphaltene solubility while allowing asphaltene molecules to be freer to leave their sites at the W/O interfacial film. This ruptures the film and permits small water droplets to coalescences and grows, and eventually separating into an aqueous phase.

Acknowledgements

The author wishes to thank his advisor, Prof. Dr. rer. Nat. habil. Martin Bertau the head of the Chemical Technology Institute at the Freiberg University of Mining and Technology for his guidance, hospitality, and support throughout this work. Also, thanks to Sebastian Hippmann for his help in performing laboratory experiments. Further thank Terra Natural Resources GmbH, Bonn, Germany for kindly providing alginite material.

References

Abdurahman H. Nour, Rosli Mohd Yunus and Zulkifly Jemaat (2007), "Chemical Demulsification of Water-in-Crude Oil Emulsions", *Journal of Applied Sciences*, Vol. 7 No. 2, pp. 196–207.

Cendejas, G., Arreguín, F., Castro, L.V., Flores, E.A. and Vazquez, F. (2013), "Demulsifying super-heavy crude oil with bifunctionalized block copolymers", *Fuel*, Vol. 103, pp. 356–363.

Czarnecki, J. and Moran, K. (2005), "On the Stabilization Mechanism of Water-in-Oil Emulsions in Petroleum Systems", *Energy & Fuels*, Vol. 19 No. 5, pp. 2074–2079.

Elsayed Abdelfatah, Yining Chen, Paula Berton, Robin D. Rogers and Steven L. Bryant (Eds.) (2019), *Tuning Ionic Liquids for Simultaneous Dilution and Demulsification of Water-In-Bitumen Emulsions at Ambient Temperature*, SPE 193615, SPE Journal, USA.

Hippmann, S., Ahmed, S.S., Fröhlich, P. and Bertau, M. (2018), "Demulsification of water/crude oil emulsion using natural rock Alginite", *Colloids and Surfaces A: Physicochemical and Engineering Aspects*, Vol. 553, pp. 71–79.

Jiang, T., Hirasaki, G., Miller, C., Moran, K. and Fleury, M. (2007), "Diluted Bitumen Water-in-Oil Emulsion Stability and Characterization by Nuclear Magnetic Resonance (NMR) Measurements †", *Energy & Fuels*, Vol. 21 No. 3, pp. 1325–1336.

Jiang, T., Hirasaki, G.J., Miller, C.A. and Ng, S. (2011), "Effects of Clay Wettability and Process Variables

on Separation of Diluted Bitumen Emulsion †", *Energy & Fuels*, Vol. 25 No. 2, pp. 545–554.

Mullins, O.C. (2007), *Asphaltenes, heavy oils, and petroleomics*, Springer, New York.

Saad, M.A., Kamil, M., Abdurahman, N.H., Yunus, R.M. and Awad, O.I. (2019), "An Overview of Recent Advances in State-of-the-Art Techniques in the Demulsification of Crude Oil Emulsions", *Processes*, Vol. 7 No. 7, p. 470.

Salam, K.K., Alade, A.O., Arinkoola, A.O. and Opawale, A. (2013), "Improving the Demulsification Process of Heavy Crude Oil Emulsion through Blending with Diluent", *Journal of Petroleum Engineering*, Vol. 2013 No. 5, pp. 1–6.

Sjöblom, H. Söderlund, S. Lindblad, E. J. Johansen and I. M. Skjärvö (1990), "Water-in-crude oil emulsions from the Norwegian continental shelf', *Colloid & Polymer Science*, Vol. 268, pp. 389–398.

Yarranton, Hussein and Masliyah (2000), "Water-in-Hydrocarbon Emulsions Stabilized by Asphaltenes at Low Concentrations", *Journal of colloid and interface science*, Vol. 228 No. 1, pp. 52–63.

Zhang, L.Y., Lopetinsky, R., Xu, Z. and Masliyah, J.H. (2005), "Asphaltene Monolayers at a Toluene/Water Interface †", *Energy & Fuels*, Vol. 19 No. 4, pp. 1330–1336.

ZANCO Journal of Pure and Applied Sciences
The official scientific journal of Salahaddin University-Erbil
https://zancojournals.su.edu.krd/index.php/JPAS

ISSN (print):2218-0230**, ISSN (online):** 2412-3986**, DOI: http://dx.doi.org/10.21271/zjpas**

RESEARCH PAPER

Association between HOMA-IR with ketoacidosis and lipid profile markers in diabetic nephropathy patients

Zrar Saleem Kareem Almarzany
Department of Biology, Faculty of Science and Health, Koya University Koya KOY45, Kurdistan Region – F.R. Iraq

A B S T R A C T:

The study designed to study the relationship between the homeostatic model assessment of insulin resistance (HOMA-IR) with ketoacidosis markers and hyperlipidemia in patients with non-insulin-dependent diabetes mellitus (NIDDM) and chronic kidney disease at end-stage renal disease (ESRD). Disturbance of the mechanisms which maintain normal blood pH and lipid profiles is a defining feature of chronic metabolic diseases such as diabetes and kidney failure. The present research included 90 patients and 30 healthy subjects. Serum insulin, fasting blood sugar (FBS), glycated hemoglobin % (HbA1c %) and HOMA-IR levels, lipid profile parameters and ketoacidosis markers were estimated in all groups. Statistical analysis showed that high HOMA-IR was significantly associated with lipid profiles and ketoacidosis markers in patients' groups when compared with control. Receiver operating characteristic (ROC) curve analysis investigated HOMA-IR as a significant risk factor for diabetic nephropathy (DN) in ESRD patients. The present finding regarding ROC curve analysis observed that IR is dependently associated with ketoacidosis and lipid profile abnormalities in NIDDM, ESRD and DN patients. Also, the study suggested HOMA-IR as a consequence and risk factor in DN at ESRD.

Keywords:

KEY WORDS: Insulin resistance, ketoacidosis, hyperlipidemia, NIDDM, ESRD, Diabetic nephropathy.
DOI: http://dx.doi.org/10.21271/ZJPAS.33.2.6
ZJPAS (2021) , 33(2);59-66 .

1. INTRODUCTION

NIDDM is the most common form of diabetes in which the primary problem is due to insulin resistance (Shekhane and Muslih, 2019). T2DM can damage kidneys by hyperglycemia that makes the kidneys filter blood hardly resulting in diabetic nephropathy (DN), (Zhou *et al.*, 2015). The pathophysiology of DN is difficult and incompletely understood. Whereas hyperglycemia is clearly essential, the role of IR is increasingly recognized (Filippone *et al.*, 2014).

* **Corresponding Author:**
Zrar Saleem Kareem Almarzany
E-mail: zrar.saleem@koyauniversity.org
Article History:
Received: 06/10/2020
Accepted: 29/11/2020
Published: 18/04 /2021

focused on IR which is presented in chronic renal failure and recent evidence proposes the presence of IR in the early renal disease stages. DN patients have increased cardiovascular mortality rates due to the IR which is proposed as a contributing factor, this is emphasizes the importance of IR mechanisms on DN (Schrauben *et al.*, 2019). However, the precise mechanisms of IR on the lipids profile and ketoacidosis markers remains poorly understood. Till now it is unclear if IR alone contributes to an elevated risk of essential clinical outcomes in kidney failure (Shang *et al.*, 2019). The study aimed to study the association between IR and DN and to investigate the potential mechanisms linking IR with lipid profile and ketoacidosis markers.

MATERIAL AND METHOD

The study included 120 age and sex-

matched persons and classified into the following groups: Group 1 (control group): This group included 30 healthy persons (16 males and 14 females) whose mean age range in years (50.40 ± 5.1). Group 2 (NIDDM): This group included 30 patients with T2DM under medical treatment and have normal GFR level (15 males and 15 females) with ages range in years (55.5 ± 4.82). Group 3 (ESRD patients): 30 patients with end-stage renal disease (17 males and 13 females) under medical treatment and hemodialysis (twice a week with 3 hours dialysis every time) with mean age ranged in years (50.70 ± 2.27 years). Group 4 (NIDDM+ ESRD): 40 patients with diabetic nephropathy at ESRD (14 males and 16 females) under medical and on hemodialysis treatment with their mean age range in years (53.90 ± 4.75). All the studied groups had normal CRP level and were subjected to personal interview through a specifically designed questionnaire form. Standard current criteria were applied for the diagnosis of T2DM in differentiating the diabetic types.

Blood samples were obtained after overnight fasting. Samples of venous blood (3 ml) were collected by sterile disposable syringes and transferred into a disposable plastic test tube. Serum was separated by the centrifugation at (1000g for 15 minutes). The separated serum was investigated for serum glycated hemoglobin (HbA1c), fasting blood glucose (FBS), (Majeed *et al.*, 2019), Lipid profile parameters included (total cholesterol (TC), high-density lipoprotein (HDL), low-density lipoprotein (LDL) and triglycerides (TG)), ketoacidosis markers included (pH, amylase, ketones, HCO3, anion gap, osmolality) by using the biochemical KENZA analyzer diagnostic kit (4 KENZA 240TX /Hitachi-USA) with a full automated biochemical analyzer, French. Insulin resistance (IR) was calculated by the homeostatic model assessment of IR (HOMA-IR) formula.

$$\mathbf{HOMA-IR} = (\mathbf{fasting\ serum\ glucose} \times \mathbf{fasting\ serum\ insulin})/\mathbf{22.5}$$

Consideration of Ethics and written informed consent

Approval of the study was obtained from Koya University/Faculty of science and health/ Department of Biology, office of the Academic Ethical Committee with ethics study number (49). All patients had signed informed written consent as an acceptance for the study project.

RESULTS

Table (1) showed that serum insulin levels were markedly elevated (P<0.001) in all groups when related to the control group. There was a significant increase (P<0.001) in serum insulin of the group of NIDDM+ESRD when related to the group of ESRD. While serum insulin level in ESRD was markedly low (P<0.001) when compared with NIDDM. The serum level of FBS was markedly increased at (P<0.001) in all groups when correlated with the control subjects. The FBS was elevated in a significant way at (P<0.001) group of NIDDM+ESRD when related to both ESRD and NIDDM groups. FBS level in ESRD was significantly (P<0.001) low when compared with NIDDM. Statistical analysis revealed significant elevation in HbA1c % at (P<0.001) in groups of NIDDM and NIDDM+ESRD in relation with the control group. There was a significant increase (P<0.001) in HbA1c % in group of NIDDM+ESRD when related to ESRD group. Also HbA1c level was highly significantly at (P<0.001) in the group of NIDDM when compared with the ESRD group. HOMA-IR significantly elevated at (P<0.001) in groups of NIDDM, ESRD and NIDDM+ESRD in relation to the group of control. HOMA-IR was significantly high (P<0.001) in NIDDM+ESRD when compared with both ESRD and NIDDM groups. Also, HOMA-IR of NIDDM was significantly increased at (P<0.001) when compared with ESRD (P<0.001).

Some biochemical parameters related to ketoacidosis markers in the present study revealed that pH did not change in groups of NIDDM, ESRD and NIDDM+ESRD when correlated with the control group. Anion gap was markedly elevated at (P<0.001) in groups of NIDDM, ESRD and NIDDM+ESRD as correlated with the control group. In NIDDM+ESRD anion gap was elevated at level (P<0.01) in comparison with NIDDM group. Serum HCO3 level was markedly decreased at (P<0.001) in NIDDM, ESRD and NIDDM+ESRD groups when compared with the control. HCO_3 was markedly decreased at (P<0.001) in NIDDM and ESRD groups when compared with the NIDDM+ESRD group. Osmolality in serum was markedly decreased in NIDDM group (P<0.001) and NIDDM+ESRD

group at (P<0.01) when correlated with the control group. There was a significant elevation at (P<0.001) in the osmolality of group of ESRD in comparison to NIDDM+ESRD groups at (P<0.001). Furthermore, osmolality of ESRD group showed significant elevation at (P<0.001) in relation to NIDDM group. Ketonemia was significantly increased in NIDDM, ESRD and NIDDM+ESRD subjects at (P<0.001) when compared with the control subjects. Ketonemia was markedly decreased in groups of NIDDM and ESRD at (P<0.001) when compared with the NIDDM+ESRD group.

Lipid profile tests observed a marked increase in TC level in NIDDM (P<0.01), ESRD (P<0.01) and NIDDM+ESRD at (P<0.001) when compared with the control group. The serum level of TG was markedly elevated in groups of NIDDM, ESRD and NIDDM+ESRD at (P<0.001) when correlated with the control group. TG was slightly low in the group of NIDDM at (P<0.05) as compared with the NIDDM+ESRD group. The level of HDL was low in groups of NIDDM (P<0. 05), ESRD (P<0.001) and NIDDM+ESRD at (P<0.001) in comparison with control group. HDL was high in NIDDM group at (P<0.001) when compared with the group of NIDDM+ESRD. Also a significant increase at (P<0.001) in HDL was shown in NIDDM group when compared with group of ESRD. Serum LDL level was significantly increased at (P<0.001) in NIDDM, ESRD and NIDDM+ESRD when compared with control group.

Receiver characteristics curve for HOMA-IR in the studied patient groups

Biomarkers and risk factors for NIDDM, ESRD and NIDDM+ESRD, were performed by ROC curves. ROC for HOMA-IR as shown in figure (1) was (1.000, 0.981 and 1.000) at (P<0.001) respectively, in groups of NIDDM, ESRD and NIDDM+ESRD. The result indicated HOMA-IR as a major marker for diabetic nephropathy.

Correlation between HOMA-IR with pH, anion gap, HCO3, osmolality and ketonemia in NIDDM group, ESRD group and NIDDM+ESRD group

Pearson's correlation analysis as observed in table (2) for NIDDM group, showed that HOMA-IR significantly correlated with anion gap (r= -0.599, p= 0.001), HCO3 (r=0.696, p= 0.001), Ketonemia (r=-0.437, p= 0.001), Osmolality (r= 0.475, p= 0.001) and pH (r=0.522, p=0.001). In ESRD group, HOMA-IR significantly correlated with anion gap (r= 0.509, p= 0.001), HCO3 (r=-0.669, p= 0.001), Ketonemia (r=0.448, p= 0.001), Osmolality (r= 0.156, p= NS) and pH (r=--0.601, p=0.001). In DN at ESRD group, HOMA-IR significantly correlated with anion gap (r= -0.712, p= 0.001). HCO3 (r=0.811, p= 0.001), Ketonemia (r= -0.730, p= 0.001), Osmolality (r= 0.290, p= 0.005) and pH (r=0.779, p=0.001).

Correlation analysis in table (3) in NIDDM group indicated that HOMA-IR significantly correlated with TG at (r= -0.400, p=0.001), Cholesterol at (r= -0.411, p=0.001), HDL at (r= 239, p=0.02) and LDL at (r= -0.700, p=0.001). ESRD group showed significant correlation between HOMA-IR with TG at (r= 0.672, p=0.001), Cholesterol at (r= 0.465, p=0.001). HDL at (r= -0.527, p=0.001) and LDL at (r= -0.464, p=0.001). Furthermore, NIDDM+ESRD group, showed that HOMA-IR significantly correlated with TG at (r= -0.599, p=0.001), Cholesterol at (r= -0.311, p=0.002), HDL at (r= 0.567, p=0.001) and LDL at (r= -0.770, p=0.001).

Table (1): Mean values (Mean ± S.E) of some assayed biochemical parameters for control group and patients in groups of NIDDM, ESRD and diabetic nephropathy

Parameters	Control N=30	NIDDM N=30	ESRD N=30	NIDDM+ESRD N=30
insulin (pmol/L)	10.000 ± 1.362	39.150±1.000 *** +++	26.750±2.014 *** ###	48.217 ± 1.018 ***
FBS (mg/dl)	118.010±4.031	257.530±7.730 *** ### +++	130.140±5.110 *** ###	294.340 ±4.111 ***

HbA1C (%)	5.850±0.260	7.900±0.180 *** +++	6.583±0.237 ###	8.000±0.258 ***
HOMA-IR	0.91±0.250	3.741±0.291 *** ### +++	1.999±1.051 * ###	5.359±1.090 ***
Blood pH	7.394 ± 0.006	7.265 ± 0.005	7.298 ± 0.004	7.260 ± 0.003
Anion gap (mmol/L)	17.29 ± 0.581	30.920 ± 1.118 *** ##	33.380 ± 1.630 ***	37.020 ± 1.230 ***
HCO_3 mmol/L)	23.090 ± 0.262	15.230 ± 0.205 *** ###	14.760±0.224 *** ###	13.200 ± 0.190 ***
Osmolality(mOsmol/Kg)	292.0 ± 1.024	269.6 ± 2.565 *** +++	295.8±5.585 ###	273.4 ± 5.094 **
Ketonemia(mmol/L)	0.419 ± 0.020	1.530 ± 0.140 *** ###	1.563±1.182 *** ###	2.466 ± 0.112 ***
TC (mg/dl)	178.800±1.637	238.800±10.190 **	241.300±10.990 **	253.9 ± 15.100 ***
TG (mg/dl)	127.800±7.000	281.000 ± 27.640 *** #	322.600 ± 8.372 ***	359.500 ± 16.420 ***
HDL-C (mg/dl)	57.410 ± 2.200	48.610 ± 2.273 * ### +++	30.690 ± 0.953 ***	37.150 ± 2.024 ***
LDL-C (mg/dl)	76.600 ± 4.258	172.600 ± 3.416 ***	175.200 ± 4.208 ***	174.300 ± 3.690 ***

Statistical changes between groups of NIDDM, ESRD and NIDDM+ESRD in comparison with control group is expressed with star (*) symbol (* P<0.001) while statistical changes between NIDDM+ESRD with NIDDM and ESRD groups are expressed as hash (#) symbol (# # #P<0.001), while statistical changes between NIDDM and ESRD subjects are shown with cross (+) symbol (+++ P<0.001).**

Table (2): Correlation between HOMA-IR with pH, anion gap, HCO3, osmolality and ketonemia in NIDDM group, ESRD group and NIDDM+ESRD group

Parameters		HOMA-IR (NIDDM)	HOMA-IR (ESRD)	HOMA-IR (NIDDM+ESRD)
Anion gap	**r**	-0.599	0.509	-0.712
	p	0.001	0.001	0.001
HCO3	**r**	0.696	-0.669	0.811
	p	0.001	0.001	0.001
Ketonemia	**r**	-0.437	0.448	-0.730
	p	0.001	0.001	0.001
Osmolality	**r**	0.475	0.156	0.290
	p	0.001	0.151	0.005
pH	**r**	0.522	-0.601	0.779
	p	0.001	0.001	0.001

Table (3): Correlation between HOMA-IR with cholesterol, TG, HDL, LDL in NIDDM group, ESRD group and NIDDM+ESRD group

Parameters		HOMA-IR (NIDDM)	HOMA-IR (ESRD)	HOMA-IR (NIDDM+ESRD)
TG	**r**	-0.400	0.672	-0.599
	p	0.001	0.001	0.001
Cholesterol	**r**	-0.411	0.465	-0.311
	p	0.001	0.001	0.002
HDL	**r**	0.239	-0.527	0.567
	p	0.021	0.001	0.001
LDL	**r**	-0.700	0.464	-0.770
	p	0.001	0.001	-0.599

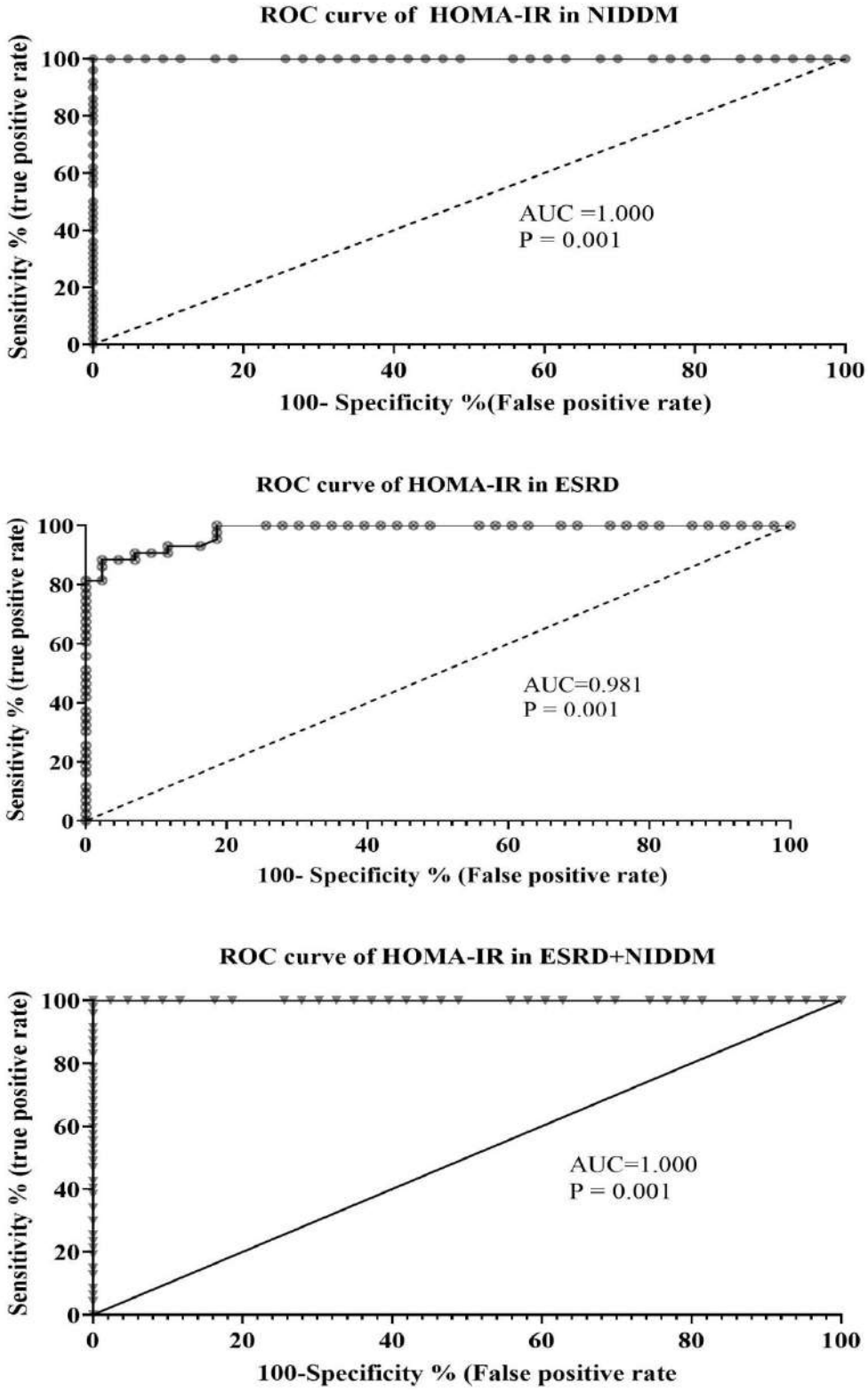

Figure (1): ROC curve shows the sensitivity and specificity of HOMA-IR in NIDDM groups, ESRD groups and NIDDM+ESRD groups.

DISCUSSION

Effects of HOMA-IR on Serum lipids markers in NIDDM, ESRD and NIDDM+ESRD groups

Serum lipids were significantly altered when compared with control. Serum lipids may be independent risk factors in both NIDDM and ESRD. Some previous studies results are inconsistent with the current result (Chen *et al.*, 2013) which revealed that component of metabolic syndrome like hypertriglyceridemia does not relate with serum lipoproteins and indicated them as an independent risk factor of developing metabolic syndrome.

However, there are few studies on the correlation of lipid profile levels in serum with IR in patients NIDDM and ESRD in the Kurdistan region. Therefore, the association of serum lipids and diabetic nephropathy requires to be explored more in our population. The major finding of this study was that high levels of cholesterol, TG, LDL with low HDL was correlated with increased risk of NIDDM and ESRD in both sex in accordance with Zhang *et al.,* (2014) study who showed that serum lipids and lipid ratios in both men and women were associated with CKD and diabetes.

Furthermore, several previous studies showed that high levels of cholesterol and triglyceride might play an essential role in the pathogenesis of diabetic nephropathy by preceding in the genesis of glomerulosclerosis (Chen *et al.*, 2013).

A study was done by Domingueti *et al.*, (2016) showed that LDL, TC, and TG-rich apoB- containing lipoproteins may relate to decreasing in kidney function in kidney failure at ESRD. Another potential confounder such as high serum glucose and insulin is presented. Low HDL level is another component of metabolic syndrome which was in accordance with results of Zhang *et al.*, (2014) study which stated that elevated metabolic syndrome components are related to CKD and diabetes. IR in DM patients and ESRD predict subsequent events of cardiovascular mortality which results from both environmental and genetic factors and contributes to type 2 diabetes mellitus and dyslipidemia (Bianchi *et al.*, 2016). Abnormalities of lipoprotein metabolism occur as a result of the apolipoproteins alterations, lipid transfer proteins, lipolytic enzymes, and receptors of lipoprotein from the early disease stages. However, recently, the main cause is due to the aggravate in IR which promotes atherogenic dyslipidemia (Mikolasevic *et al.,* 2017). The interaction between IR and triglyceride levels is bidirectional. Hypertriglyceridemia and increased free fatty acids contribute to IR, but the relative contribution is not known till now (Guthoff *et al.*, 2017).

Effects of HOMA-IR on metabolic ketoacidosis markers in NIDDM, ESRD and NIDDM+ESRD groups

Ketoacidosis results from rapid changes in blood glucose and insulin responsiveness which alter serum tonicity and osmolality. Variations in insulin kinetics in patients with NIDDM and ESRD present researchers with an additional challenge determining the mechanism of IR outcomes of patients with ESRD and those without significant kidney disease (Rosenstock and Ferrannini, 2015).

IR inhibits the ability of glucose to enter cells, the result becomes an increased reliance on fat oxidation for energy production. Blood will turn to an acidic medium since hyperketonemia causes accumulation of glucose in the blood and urine. Although diabetic ketoacidosis occurs mainly in patients with type 1 diabetes, it is not surprising in some patients with NIDDM which was in accordance with (Yu *et al.*, 2018 and Mottalib *et al.,* 2019). The current study showed that metabolic acidosis is another consequence in NIDDM and ESRD that has been associated with the development of IR. The main cause is the disability to excrete acid and production of excess acid in the setting of progression of IR in NIDDM and chronic renal failure (Chen and Abramowitz, 2014 and Dobre *et al.*, 2015).

Furthermore, acidosis with an increased anion gap observed in all studied groups of both NIDDM and ESRD in agreement with studies of Chen and Abramowitz, (2014) and Schaapveld-Davis *et al.*, (2017). Anion gap elevation is related to low serum bicarbonate. Some factors have been supposed to affect metabolic acidosis which progress diabetes and kidney disease such as activation of ammonia-induced complement, increased endothelin (ET) and aldosterone production due to IR (Chen and Abramowitz, 2014). Some researchers proposed that ammonia reacted biochemically in order to activate the alternative complement pathway. Therefore, progressive kidney injury could further instigate

the compensatory elevation in single-nephron ammonia genesis which was observed in diabetes and ESRD (Schaapveld-Davis *et al.*, 2017).

Elevated aldosterone can also act to decrease GFR caused by acidosis, by its pro-fibrotic and hemodynamic mechanisms. Aldosterone mediates increased acidification of distal nephron in the metabolic acidosis setting, and kidney disease prevention with alkali in the rat remnant kidney model which was related to decreased aldosterone production in kidney cortex (Schembolan *et al.*, 2011).

Conclusion

Lipid profile and ketoacidosis markers showed significant correlation with the studied HOMA-IR. Regarding ROC curve analysis, the result indicated HOMA-IR as an essential biomarker for diabetes and ESRD.

Ethical Requirements enforcement

- Declaration of the author that there are no potential conflicts of interest associated with this manuscript.
- The research involved human participants with informed consent.
- Informed consent: The respondents have received an informat ive consent form and the objective of the research was clarif ied to them.
- Ethical approval: All procedures undertake n in studies involving human subjects is in compliance with the ethical guidelines of t he institutional and/or national study com mittee at which the studies were conducted with IRB and Ethics Committee approval has been obtained.

REFERENCES

BIANCHI, S., BARONTI, A., COMINOTTO, R. & BIGAZZI, R. 2016. Lipid metabolism abnormalities in Chronic Kidney Disease. Giornale italiano di nefrologia. *organo ufficiale della Societa italiana di nefrologia.* 33(68).40-47.

CHEN, S., CHEN, Y., LIU, X., LI, M., WU, B., LI, Y., LIANG, Y., SHAO, X., HOLTHOFER, H. & ZOU, H. 2013. Association of insulin resistance with chronic kidney disease in non-diabetic subjects with normal weight. *Plos One*. 8 (9): 58-66.

CHEN, W. & ABRAMOWITZ, M.K. 2014. Metabolic acidosis and the progression of chronic kidney disease. *BMC Nephrology*. 15 (1): 55-61.

DOBRE, M., RAHMAN, M. & HOSTETTER, T.H. 2015. Current status of bicarbonate in CKD. *Journal of the American Society of Nephrology*. 26 (3): 515 - 523.

DOMINGUETI, C.P., DUSSE, L.M.S.A., DAS-GRACAS, S., CARVALHO, M., DE-SOUSA, L.P., GOMMES, K.B. & FRNANDES, A.P. 2016. Diabetes mellitus: the linkage between oxidative stress, inflammation, hypercoagulability and vascular complications. *Journal of Diabetes and Its Complications*. 30 (4): 738-745.

FILIPPONE, E.J., GUPTA, A. & FARBER, J.L. 2014. Normoglycemic diabetic nephropathy: the role of insulin resistance. *Case Reports in Nephrology and Dialysis*. 4(2): 137-143.

GUTHOFF, M., WAGNER, R., VOSSELER, D., PETER, A., NADALIN, S., HARIMG, H.U., FRITSCHE, A. & HEYNE, N. 2017. Impact of end-stage renal disease on glucose metabolism-a matched cohort analysis. *Nephrology Dialysis Transplantation*.32 (4): 670-676.

MAJEED, Z.R., FIRAS, K. Q., & HEDY, A. H. 2019. Hypotensive action of pomegranate seed extract and zinc chloride in hypertensive rats. The official scientific journal of Salahaddin University-Erbil. *ZANCO Journal of Pure and Applied Sciences*. 31(5):44-52.

MIKOLASEVIC, I., ZUTELIJA, M., MAVRINAC, V. & ORLIC, L. 2017. Dyslipidemia in patients with chronic kidney disease: etiology and management. *International Journal of Nephrology and Renovascular Disease*. 10 (3): 35-46.

MOTTALIB, A., TOMAH, S., HAFIDA, S., ELSEAIDY, T., KASETTY, M., ASHRAFZADEH, S. & HAMDY, O. 2019. Intensive multidisciplinary weight management in patients with type 1 diabetes and obesity: A one- year retrospective matched cohort study. Diabetes, *Obesity and Metabolism*. 21 (1): 37-42.

ROSENSTOCK, J. & FERRANNINI, E. 2015. Euglycemic diabetic ketoacidosis: a predictable, detectable, and preventable safety concern with SGLT2 inhibitors. *Diabetes Care*. 38 (9): 1638-1642.

SCHAAPYELD-DAVIS, C.M., NEGRETE, A.L., HUDSON, J.Q., SAIKUMAR, J., FINCH, C.K., KOCCAK, M., HU, P. & VAN-BERKEL, M.A. 2017. End-Stage Renal Disease Increases Rates of Adverse Glucose Events When Treating Diabetic Ketoacidosis or Hyperosmolar Hyperglycemic State. *Clinical Diabetes*.35 (4): 202-208.

SCHEMBOLAN, M., KATUNA, B.A. & ARTEAGA, E. 2011. Aldosteronel hormone secretory response to chronic NH4Cl-stimulated acidosis. *American Journal physiology*.294 (5): 324–331.

SCHRAUBEN, S.J., JEPSON, C., HSU, J.Y., WILSON, F.P., ZHANG, X., LASH, J.P., ROBINSON, B.M., TOWNSEND, R.R., CHEN, J., FOGELFELD, L. & KAO, P. 2019. Insulin resistance and chronic kidney disease progression, cardiovascular events, and death: findings from the chronic renal insufficiency cohort study. *BMC Nephrology*. 20(1), pp.1-11.

SHANG, J., YU, D., CAI, Y., WANG, Z., ZHAO, B., ZHAO, Z. & SIMMONS, D. 2019. The triglyceride glucose index can predict newly diagnosed biopsy-proven diabetic nephropathy in type 2 diabetes: A nested case control study. *Medicine*. 98(46).

SHEKHANE, B. S. I. & MUSLIH, A. I. 2019. The Influence of carbimazole on serum leptin hormone and insulin resistance in patients with hyperthyroidism. The official scientific journal of Salahaddin University-Erbil. *ZANCO Journal of Pure and Applied Sciences*. 31 (4): 23-35

YU, X., ZHANG, S. & ZHANG, L. 2018. Newer perspectives of mechanisms for euglycemic diabetic ketoacidosis. *International Journal of Endocrinology*. 16 (6): 323-332.

ZHANG, L., YUAN, Z., CHEN, W., CHEN, S., LIU, X., LIANG, Y., SHAO, X. & ZOU, H. 2014. Serum lipid profiles, lipid ratios and chronic kidney disease in a Chinese population. *International Journal of Environmental Research and Public Health*. 11 (8): 7622-7635.

ZHOU, C., MOORE, L., YOOL, A., JAUNZEMS, A. & BYARD, R.W. 2015. Renal tubular epithelial vacuoles-a marker for both hyperlipidemia and ketoacidosis at autopsy. *Journal of Forensic Sciences*. 60(3), pp.638-641.

ZANCO Journal of Pure and Applied Sciences
The official scientific journal of Salahaddin University-Erbil
https://zancojournals.su.edu.krd/index.php/JPAS

ISSN (print):2218-0230**, ISSN (online):** 2412-3986**, DOI: http://dx.doi.org/10.21271/zjpas**

RESEARCH PAPER

Open Cholecystectomy in Respiratory and Cardiovascular disease patients under Lumbar combined Spinal-Epidural Anesthesia

Haidar N. Mohammed: Anesthiologist, Anesthesia Department, College of Health Sciences, University of Duhok, Kurdistan Region, Iraq.
Ayad Ahmad Mohammed: General Surgeon, Department of Surgery, College of Medicine, University of Duhok, Kurdistan Region, Iraq.
Mohammed Abdulameer Algumrawi: Anesthiologist, Department of anesthesia, Duhok Directorate General of Health, Kurdistan Region, Iraq.

A B S T R A C T:

Background and Aims: Regional anesthesia gained popularity over the last three decades due to the technical advances across subdisciplines, better understanding of the physiology, the advances in the field of anesthetic drugs, and the better approach in training for such techniques. The technique is currently used in many anatomical levels and most surgical procedures can be performed using the combined spinal epidural type.
The aim of this study is to evaluate the feasibility of the combined spinal-epidural anesthesia in patients with respiratory and cardiovascular diseases who underwent open cholecystectomy.
Patients and methods: This prospective cross sectional study which was done on patients undergoing elective open cholecystectomy (n=119) for whom the general anesthesia was contraindicated due to major cardiovascular and pulmonary diseases, under lumber combined spinal-epidural anesthesia.
Results: The mean age of our patients was 64.33(SD: 12.085) years; females constituted 73 of them (61.3%) and males 46 (38.7%). Most patients (73) were complaining from the cardiovascular diseases (61.34%). In most patients the onset of the action of the anesthesia was between 10-12 minutes. In 55 patients (46.2%) no extra-drugs were required, and in the rest of patients intravenous mediations were given to relieve anxiety, pain, or both. In 81 patients (68.1%) no intraoperative complications were reported, the most common intraoperative complication was hypotension in 31 patients (26.1%), post-operatively no complications were reported in 86 patients (72%), and hypotension was reported in 12 patients (10.1%), nausea & vomiting in 11 patients (9.2%). The surgeon's satisfaction was excellent in 73.11% of the surgeries, as was good in 23.53%. Most patients gained the lower limb movement within 2 hours. There was a significant correlation between the need for extra drugs and both comorbid diseases and the development of intraoperative complications (P values 0.022 & 0.000) respectively and no significant correlations with other parameters such as the gender, postoperative complications and the surgeon's satisfaction (P values 0.707, 0.522, and 0.056) respectively.
Conclusion:
The technique of the combined spinal epidural anesthesia is safe and very effective when used for American Society of Anesthesiologist (ASA) patient classification class III and IV patients who need open cholecystectomy. This technique should be used by expert anesthetists who are well trained and gained skill in this technique, and it may be used in fields other than surgery such as trauma victims and for cancer patients.

KEY WORDS: open cholecystectomy, combined lumbar spinal-epidural anesthesia, patients with respiratory morbidity, patient with cardiovascular morbidity.

List of abbreviations:
AF: Atrial fibrillation
ASA: American Society of Anesthesiologist.
COPD: Chronic obstructive pulmonary disease
CVA: Cerebrovascular accident
HF: Heart failure
IHD: Ischemic heart disease
MI: Myocardial infarction

*** Corresponding Author:**
Haidar N. Mohammed
E-mail: haider.mohammed@uod.ac
Article History:
Received: 26/09/2020
Accepted: 07/12/2020
Published: 18/04 /2021

TAP: Transversus abdominus plane.
DOI: http://dx.doi.org/10.21271/ZJPAS.33.2.7
ZJPAS (2021) , 33(2);67-75 .

1. INTRODUCTION :

Regional anesthesia gained tremendous popularity over the last three decades, which is attributed to advancement in the technology, better understanding of the physiology, the advancement in the anesthetic drugs, and the better training in such techniques. In some centers the regional anesthesia procedure may reach up to 40% of the anesthetic treatment.(Clemente & Carli, 2008)

The technique is currently used for many anatomical levels and most surgical procedures can be performed using the combined spinal epidural type. Jonnesco, described the feasibility of this technique at various anatomical levels, such as the head and neck, upper limbs, and the thoracic levels. (M. Ellakany, 2013)

This technique is used not only in surgery, but also may be adopted for trauma patients, in obstetric practice, and for patients with cancer who suffered from severe pain. (Clemente & Carli, 2008)

Patients with severe cardiovascular and pulmonary diseases present a very significant challenge to the surgeons and the anesthetists due to the high morbidity and mortality rates which follow general anesthesia. (Gramatica et al., 2002; Kumar Ashish, Koshire Alka, & Bharadwaj Deepti; Van Zundert et al., 2006)

The respiratory function remains intact during the regional anesthesia, the diaphragm and the respiratory muscles remains functioning which will maintain the ventilation and causing minimum CO2 retention, with resultant normal ventilator measurements.(Kumar Ashish et al.)

Most of the inotropic and the chronotropic actions of the heart are mediated by the afferent and efferent nerve fibers carried through reflex neuronal arches. Blocking these pathways by the mean of regional anesthesia, may abolish many of these affects. (Clemente & Carli, 2008)

There are many types of regional anesthesia that are used for various surgical procedures such as the spinal, paravertebral and the celiac plexus block, the combined spinal epidural anesthesia is a relatively easier technique with a relatively lower learning curve and is effective with lower dose of anesthetic drugs. Ultrasound guided block is usually performed to guide for the injection of the anesthetic medications. (Ortiz et al., 2012; Tulgar et al., 2018; Van Zundert et al., 2006)

Segmental epidural anesthesia has some benefits over the spinal one in that the incidence of cardiopulmonary suppression, easier titration of the anesthetic dose, urinary retention is very low and the earlier regain of the movements and activities, it may be done on day case bases. (J. H. Lee et al., 2010; R. Lee, Van Zundert, Visser, Lataster, & Wieringa, 2008) Lee, R., et al., 2008]

Pain is the most common complain after surgery and it spikes within the first hour after surgery, the use of regional anesthesia have been shown to be very effective in reducing the postoperative pain. (Bisgaard et al., 1999; Mehta, Chavda, Wadhwana, & Porecha, 2010)

Patients must be assessed very carefully and frequently during the procedure and any adverse events must be well documented, and when indicated an appropriate intervention must be carried out. Also careful assessment of the postoperative complications should be done in order to assess the safety of the procedure. (Hamad & El-Khattary, 2003; J. H. Lee et al., 2010; Van Zundert et al., 2006) Lee, J.H., et al., 2010 & Hamad, M. and O.I. El-Khattary, 2003]

As gall stone diseases are very common and many patients require surgical removal of the gall bladder, patients with no comorbidities and when general anesthesia is not contraindicated, the surgery can be done easily, but the main concern is that in patients who are ASA class III and IV and they require surgical intervention, this will make the need for an alternative for such patients. The laparoscopic technique has many effects on both the cardiovascular and the pulmonary physiology, this is mainly due to the effects of pneumoperitoneum which cause raise in the intra-abdominal pressure and the CO2 retention. The technique of surgery doesn't require any change whether it is performed adopting general or regional anesthetic technique. [Mehta, N., et al., 2015, Mohammed, A.A. and S.H. Arif, 2019, Khetarpal, R., et al., 2016, Tzovaras, G., et al.,

2008, Sinha, R., A. Gurwara, and S. Gupta, 2009 & Saliminia, A., et al., 2015]

The aim of this study is to evaluate the feasibility of the combined spinal-epidural anesthesia in patients with respiratory and cardiovascular diseases who underwent open cholecystectomy.

2.Patients and methods:

After the approval of Institutional Ethical Committee and taking written informed consent, this prospective observational study involved a total number of 119 patients, who were complaining from major cardiovascular and pulmonary diseases and in whom the general anesthesia was contraindicated.

The data collected from 2 medical centers, Gulan General Governmental and Azadi Teaching Hospitals in the time between 1st of June, 2016 to the 20th of February, 2019. The anesthesia was given by two specialist anesthetists and the operations were performed by one specialist general surgeon. Patients' enrollment followed a consecutive manner.

Inclusion criteria: American Society of Anesthesiologists (ASA) class III and IV patients who underwent open cholecystectomy were included.

Exclusion criteria: Patients with emergency operations, having contraindications of regional anesthesia and patients who refused to be included in this study were excluded.

The patients were informed during the preoperative visit that any anxiety, pain or discomfort occurring during surgery would be dealt with intravenous medications or if they wished. During and after the procedure, the patients were informed to report any dyspnea, abdominal discomfort or pain, nausea and vomiting. In the preoperative room an 18 G IV line secured and all patients received adequate preloading with 15 ml/kg of Ringer's lactate solution over 30 min. The patients were then shifted to the operation theatre and all routine monitors namely, noninvasive blood pressure, peripheral oxygen saturation by pulse oximetry (SpO_2) and electrocardiogram were attached and after obtaining baseline vital signs, oxygen at 5 L/min was commenced through a face mask.

The patients were positioned in sitting position, and under strict aseptic precautions the L_4–L_5 epidural space was accessed using an 18G Tuohy needle and loss-of-resistance technique and spinal anesthesia was then performed with 2 ml that is, 10 mg of 0.5% heavy bupivacaine by a set combined 27G Quincke 15 cm long spinal needle through the already inserted epidural needle after free flow of cerebrospinal fluid, figures 1, 2a & 2b.

The accompanied epidural catheter was threaded cephalad through the Tuohy needle after spinal needle removal and fixed at 4 cm within the epidural space, figure 2c. Patients were turned to the supine position and a 10-degree Trendelenburg tilt was given to achieve the required level of block.

Heart rate, blood pressure, and SpO_2 were recorded every minute for the first 15 min and every 5 min thereafter. The level of sensory (pinprick) block was assessed and recorded every 2 minutes until the start of surgery and every 15 min thereafter. Once the block was considered adequate (minimum block T5—as assessed by pinprick), the surgery was commenced by Kocher (right subcostal) incision.

Pain was treated with meperdine 50 mg or fentanyl 5 mcg/kg/dose initially and then 1-2 mcg/kg/hr. as a maintenance infusion dose, anxiety with midazolam 2 mg and hypotension with ephedrine 30 mg, all as IV boluses as and only when required during the intraoperative period separated or in combined. Only one patient needed TAP block while other one needed spinal adjuvant. The systemic analgesic drugs were administered only if epidural injections were ineffective in controlling pain. Surgeons were free to ask for general anesthesia if they felt that the anesthetic technique was adding technical difficulty for the surgical procedure. An orogastric tube was inserted to decompress the stomach only if the surgeon demanded it. They were also requested to rank the associated technical difficulty after the procedure.

The surgical procedure of open cholecystectomy was carried out according to standard protocol. Operative time as well as any intraoperative or postoperative events was recorded include (hypotension, hypertension, nausea & vomiting, anxiety, dyspnea, shivering).

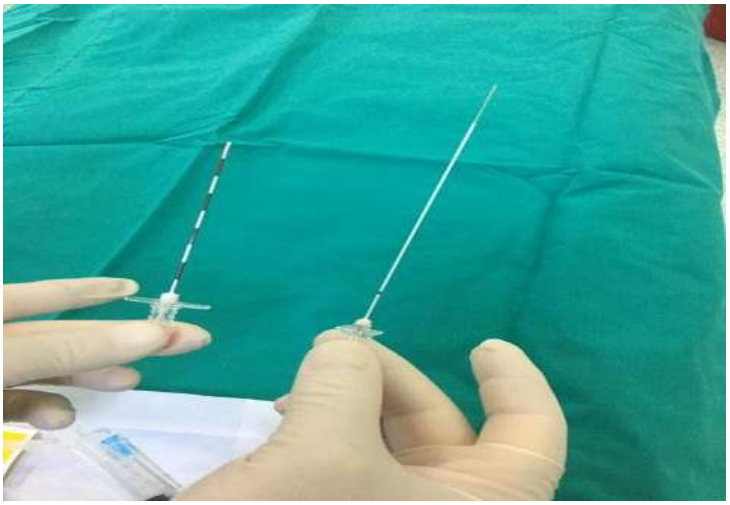

Figure 1: Touhy needle and spinal needle.

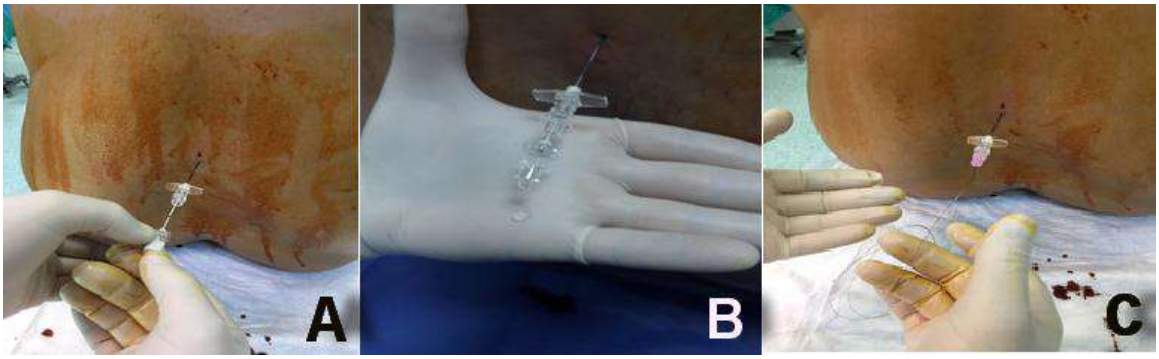

Figure 2: Showing the method of the needle insertion; A: spinal needle through epidural needle, B: CSF dropped through spinal needle, C: epidural catheter in place.

3.Results:

A total number of 119 patients were included in this study; the mean age of our patients was 64.33 (12.085 SD) years and females constituted the majority of them. Most patients were complaining from the cardiovascular diseases, table 1 and figure 3.

In most patients the onset of the action of the anesthesia was between 10-12 minutes; however in some patients it started much earlier or later. In most surgeries the operating surgeon reported a good muscle relaxation with no pain within a feasible time, figure 4.

In more than 50% of patients there was indication for further administration of medications to relieve anxiety, pain, or both, table 2.

The rate of intra and post-operative complications were not very high, making this technique relatively safe and effective. Hypotension was the commonest one both intraoperatively and postoperatively, other types of complications were reported less frequently, table 3.

The surgeon's satisfaction was excellent in the majority of surgeries, and was accepted in only 3.36%, figure 5.

Most patients gained the lower limb movement within 2 hours (the mean time was 117 minutes: Std. deviation 25 minutes), however in some patients this period was extended to 3 hours, figure 6.

Correlations were made between the need for extra drugs or not and various parameters. There was a significant correlation between the need for extra drugs and both comorbid diseases and the development of intraoperative complications (P values 0.022 & 0.000) respectively and no significant correlations with other parameters, table 4.

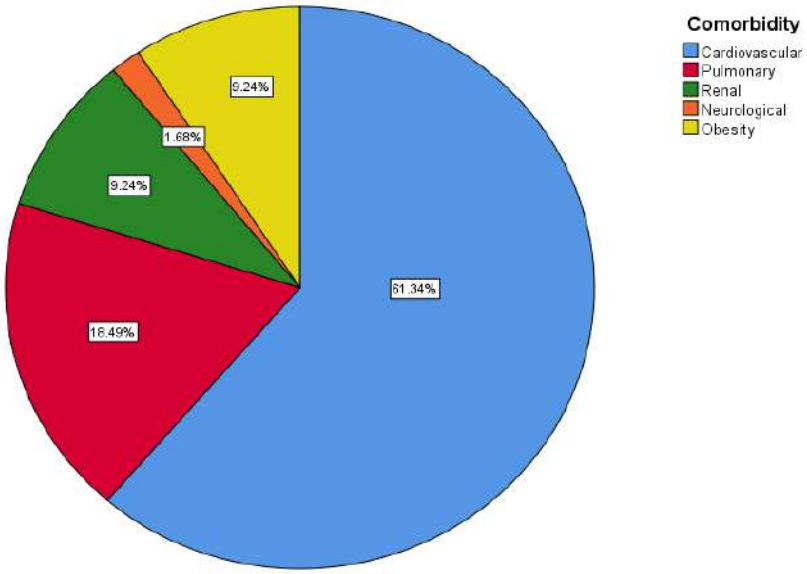

Figure 3: A simple pie chart showing the comorbidities of the patients.

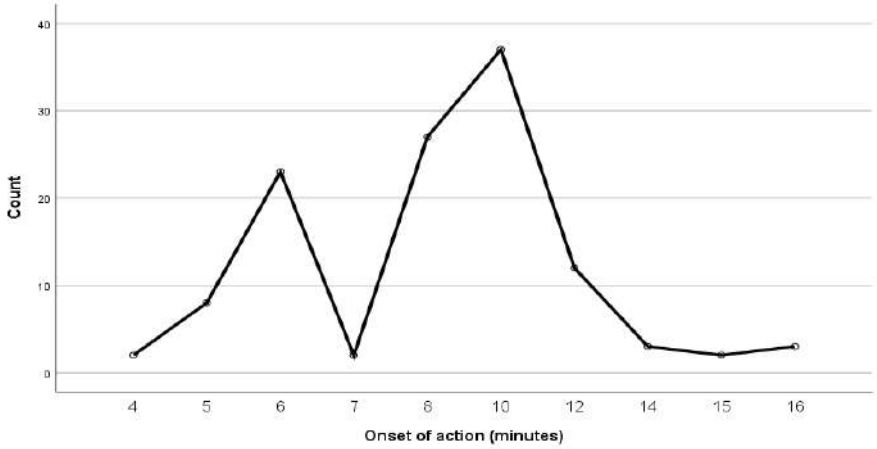

Figure 4: A simple line graph showing the onset of action of the anesthesia.

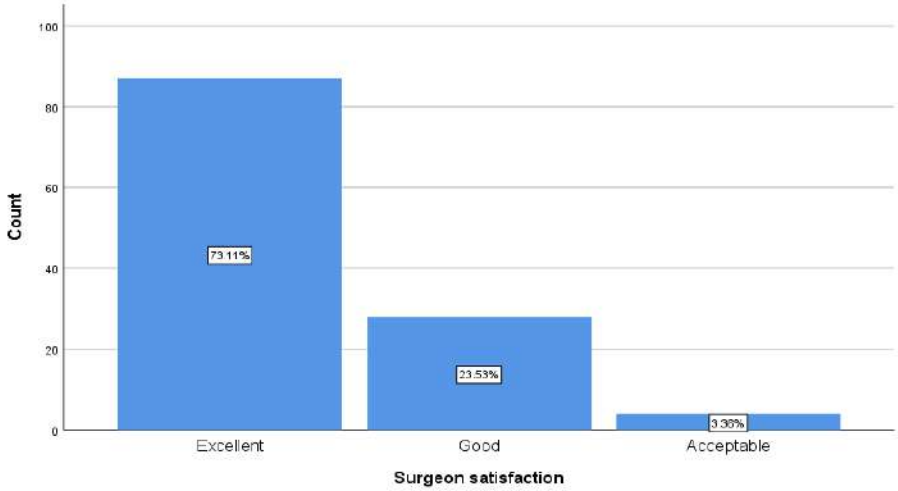

Figure 5: A simple bar chart showing the level of the surgeon satisfaction during surgery.

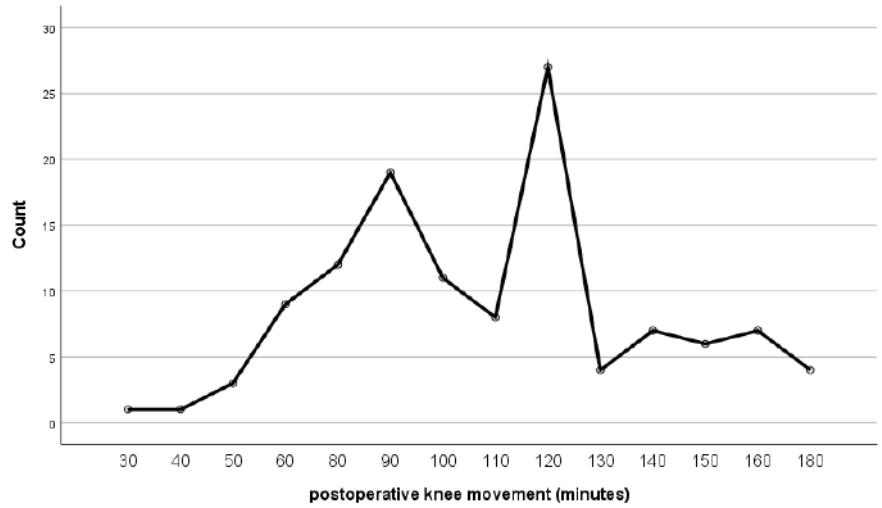

Figure 6: A simple line chart showing the time of return of the lower limb movement after the surgery.

Table 1: The patient's characteristics.

Main category	Subcategories	Frequency	Percentage
Age* **Range: 43-90 years**		64.33	8.799
Gender	Male	46	38.7
	Female	73	61.3
Comorbid diseases	HF+IHD	33	27.7
	HF	14	11.8
	ESRD	11	9.2
	Morbid obesity	11	9.2
	AF+IHD	8	6.7
	Uncontrolled hypertension	8	6.7
	COPD	7	5.9
	Chronic bronchitis	5	4.2
	Bronchial asthma	5	4.2
	HF+ Valvular heart disease	4	3.4
	Complete heart block	3	2.5
	IHD+ Recent CVA	3	2.5
	Pulmonary fibrosis	3	2.5
	Recent MI	2	1.7
	Respiratory failure	1	.8
	Pneumonectomy	1	.8
***The age is presented as mean and standard deviation**			

Table 2: The need for extra drugs during surgery.

Need for extradrugs	Frequency	Percentage
No need for extra-drugs	55	46.2
50 Mg fentanyl	10	8.4
2 mg midazolam	11	9.2
30 mg ephidrene	29	24.4
30 mg ephidrene + 50 Mg fentanyl	2	1.7
2 mg midazolam + 50 Mg fentanyl	7	5.9
Spinal adjuvant	1	.8
2 mg midazolam + TAP block	1	.8
2 mg midazolam + 50 Mg fentanyl + 30 mg ephidrene	1	.8
50 mg meperidine	2	1.7

Table 3: The intra and the post-operative complications.

Main category	Subcategories	Frequency	Percentage
Intraoperative complications	No complications	81	68.1
	Hypotension	31	26.1
	Dyspnea	5	4.2
	Anxiety	1	0.8
	Nausea	1	0.8
Postoperative complications	No complications	86	72.3

Hypotension	12	10.1
Nausea & vomiting	11	9.2
Shivering	6	5.0
Hypertension	2	1.7
Dyspnea	2	1.7

Table 4: The correlation between the need for extra drugs and various parameters using the Chi Square test.

Categories	Need for extra drugs		Sig. (2-sided)
	No (n=55)	Yes (n=64)	
Gender			
Male	20(36.4%)	26(40.6%)	0.707
Female	35(63.6%)	38(59.4%)	
Comorbidities	30(54.5%)	43(67.2%)	
Cardiovascular	13(23.6%)	9(14.1%)	
Pulmonary	3(5.5%)	8(12.5%)	**0.022**
Renal	0(0.0%)	2(3.1%)	
Neurological	9(16.4%)	2(3.1%)	
Obesity			
Intraoperative complications	43(78.2%)	38(59.4%)	
No complications	1(1.8%)	0(0.0%)	
Anxiety	0(0.0%)	1(1.6%)	0.000
Nausea	6(10.9%)	25(39.1%)	
Hypotension	5(9.1%)	0(0.0%)	
Dyspnea			
Postoperative complications	43(78.2%)	43(67.2%)	
No complications	3(5.5%)	9(14.1%)	
Hypotension	0(0.0%)	2(3.1%)	
Hypertension	1(1.8%)	1(1.6%)	0.522
Dyspnea	5(9.1%)	6(9.4%)	
Nausea & vomiting	3(5.5%)	3(4.7%)	
Shivering			
Surgeon satisfaction	45(81.8%)	42(65.6%)	
Excellent	9(16.4%)	19(29.7%)	0.056
Good	1(1.8%)	3(4.7%)	
Acceptable			

4.Discussion:

General anesthesia is usually adopted for patients who need open cholecystectomy because it provides effective and satisfactory muscle relaxation, but it has many adverse effects especially in patients with major comorbidities particularly cardiovascular and pulmonary diseases. The intubation may have many negative impacts on the pulmonary function due to laryngeal spasm and edema.(M. H. Ellakany, 2014; Khan, Ashraf, & Khan, 2013)

Despite the effectiveness of combined spinal-epidural anesthesia in the surgical practice, there are some limitations that block practicing this technique, this may include the lack of the organized training courses and the fear that this technique may not work sufficiently. (Clemente & Carli, 2008)

The mean age of the patients who were involved in the study was 64.33 years (SD: 12.085). Female patients constituted 61.3% (73 patients) and males constituted 38.7% (43 patients), 61.34% of patients (73) had cardiovascular comorbidities and 18.49% had pulmonary ones (22). Table1 & Figure3. Patients experience anxiety at different levels starting from the insertion of the spinal needle, and during the whole surgical procedure, however anxiety was reported in the minority of our patients, only 0.8% of our patients experience anxiety during the procedure as shown in table3. (Van Zundert et al., 2006)

Most patients experienced an onset of action within 10-12 minutes, others experienced earlier onset of action within 6-7 minutes. The loss of the stress related sympathetic efferent pathways, may result in lack of the normal homeostatic response to stress and injury, together with the loss of the sympathetic vasoconstriction, resulting in hypotension. Figure4. In our study the rate of intra and postoperative hypotension was 26.1% and 10.1% respectively, in most of the published literature hypotension is one of the well

documented adverse events, this is due reduction in the mean arterial pressure, hypotension is easily controlled with ephedrine. (Clemente & Carli, 2008), (Clemente & Carli, 2008; Donmez et al., 2017; J. H. Lee et al., 2010)

Respiratory difficulties and dyspnea were among the other reported complications both intra and postoperatively in 4.2% and 1.7% respectively. This complication is well documented by most authors who reported higher rates (12%), this may be managed by assisted mask ventilation with oxygen. When more invasive monitoring is done many patients may have academia. Dyspnea during surgery may be explained by the stress of the anesthesia and the intra-abdominal manipulation, most patients may have associated cardiac and pulmonary disorders causing dyspnea. The segmental block may result in loss of the appropriate muscle function and blockage of the efferent or the afferent intercostal nerve roots pathways, this impairing effective respiration. About 46.2% (55 patients) required no extra-medications during the procedure, the rest of patients required extra-medications to alleviate pain, nausea, or other symptoms during the procedure. Intraoperatively, 68.1% of our patients (81 patients) had no intraoperative complications, and the most frequent intraoperative complication was hypotension which was reported in 26.1% of patients (31 patients). (Das et al., 2015; J. H. Lee et al., 2010; Mohammed & Arif, 2019)

The reported rate of postoperative nausea and vomiting may reach 20% in most cases, this is mostly centrally mediated, in our study 72.3% of patients reported no postoperative complications and the remaining percentage of patients reported postoperative complications, 10.1% (12 patients) developed postoperative hypotension, 9.2% of our patients (11 patients) had postoperative nausea and vomiting, this is relatively lower that the reported rate in most articles. (J. H. Lee et al., 2010). Table3.

The major concern of the operating surgeon was the inadequate muscle relaxation during the procedure, in our study in most of the performed surgeries (73.11%) the surgeon's satisfaction was excellent, and was just acceptable in 3.38% of the surgeries.(Khan et al., 2013). Figure 5

Local complications are reported to be associated with this type of anesthesia, these may include; hematoma formation at the site of injection, pain at the site of catheter insertion, and infection. Intrathecal spread may also occur; inadvertent vascular or pleural puncture have also been reported. (Naja & Lönnqvist, 2001)

Postoperatively, the majority of our patients started lower limbs movement after 120 minutes, few patients started to move their lower limbs within less than 60 minutes. The lower limb motor block is usually minor and transient and resolves with time, this is caused by the spread of the anesthetic drugs to the lumbar and the sacral motor nerve roots.(Van Zundert et al., 2007). Figure 6

In our study we included patients who underwent open cholecystectomy, however recently in many center they use this technique for patients with laparoscopic cholecystectomy, which is proved to be safe and very effective. This may be difficult for complicated cases such as the acute cholecystitis, tumors or cases who are ASA class III and IV. (Van Zundert et al., 2007)

There was a significant correlation between the need for extra drugs and both comorbid diseases and the development of intraoperative complications (P values 0.022 & 0.000) respectively and no significant correlations with other parameters such as the gender, postoperative complications and the surgeon's satisfaction (P values 0.707, 0.522, and 0.056) respectively. Table 4

5.Conclusion:

The technique of the combined spinal epidural anesthesia is safe and very effective when used for ASA class III and IV patients who need open cholecystectomy. This technique should be used by specialist anesthetists who are well trained in this technique, and it may be used in fields other than surgery such as trauma victims and for cancer patients.

Declaration section:

Ethics approval and consent to participate: Ethical committee approval is granted from the research registration unit at the Duhok Directorate General of Health.

Consent for publication: A written consent was obtained from all the participants.

Availability of data and materials: Not applicable.

Funding: The authors are the source of funding.

Acknowledgements: Not applicable.

References

Bisgaard, T., Klarskov, B., Kristiansen, V. B., Callesen, T., Schulze, S., Kehlet, H., & Rosenberg, J. (1999). Multi-regional local anesthetic infiltration during laparoscopic cholecystectomy in patients receiving prophylactic multi-modal analgesia: a randomized, double-blinded, placebo-controlled study. *Anesthesia and Analgesia, 89*(4), 1017.

Clemente, A., & Carli, F. (2008). The physiological effects of thoracic epidural anesthesia and analgesia on the cardiovascular, respiratory and gastrointestinal systems. *Minerva Anestesiol, 74*(10), 549-563.

Das, W., Bhattacharya, S., Ghosh, S., Saha, S., Mallik, S., & Pal, S. (2015). Comparison between general anesthesia and spinal anesthesia in attenuation of stress response in laparoscopic cholecystectomy: A randomized prospective trial. *Saudi journal of anaesthesia, 9*(2), 184.

Donmez, T., Erdem, V. M., Uzman, S., Yildirim, D., Avaroglu, H., Ferahman, S., & Sunamak, O. (2017). Laparoscopic cholecystectomy under spinal-epidural anesthesia vs. general anaesthesia: a prospective randomised study. *Annals of surgical treatment and research, 92*(3), 136-142.

Ellakany, M. (2013). Comparative study between general and thoracic spinal anesthesia for laparoscopic cholecystectomy. *Egyptian Journal of Anaesthesia, 29*(4), 375-381.

Ellakany, M. H. (2014). Thoracic spinal anesthesia is safe for patients undergoing abdominal cancer surgery. *Anesthesia, essays and researches, 8*(2), 223.

Gramatica, L., Brasesco, O., Luna, A. M., Martinessi, V., Panebianco, G., Labaque, F., . . . Rosenthal, R. (2002). Laparoscopic cholecystectomy performed under regional anesthesia in patients with chronic obstructive pulmonary disease. *Surgical Endoscopy and Other Interventional Techniques, 16*(3), 472-475.

Hamad, M., & El-Khattary, O. I. (2003). Laparoscopic cholecystectomy under spinal anesthesia with nitrous oxide pneumoperitoneum: a feasibility study. *Surgical Endoscopy and Other Interventional Techniques, 17*(9), 1426-1428.

Khan, M. N., Ashraf, M. N., & Khan, H. D. (2013). Spinal anesthesia versus general anesthesia for open cholecystectomy: comparison of postoperative course. *Ann Pak Inst. Med Sci, 9*, 95-98.

Kumar Ashish, M., Koshire Alka, M., & Bharadwaj Deepti, D. (2016). A case series of use of combined spinal epidural anesthesia for laparoscopic appendectomy in adults. *Age (in years), 33*, 22-45.

Lee, J. H., Huh, J., Kim, D. K., Gil, J. R., Min, S. W., & Han, S. S. (2010). Laparoscopic cholecystectomy under epidural anesthesia: a clinical feasibility study. *Korean Journal of Anesthesiology, 59*(6), 383.

Lee, R., Van Zundert, A., Visser, W. A., Lataster, L. A., & Wieringa, P. A. (2008). Thoracic combined spinal-epidural (CSE) anaesthesia. *Southern African Journal of Anaesthesia and Analgesia, 14*(1), 63-69.

Mehta, P. J., Chavda, H. R., Wadhwana, A. P., & Porecha, M. M. (2010). Comparative analysis of spinal versus general anesthesia for laparoscopic cholecystectomy: A controlled, prospective, randomized trial. *Anesthesia, essays and researches, 4*(2), 91.

Mohammed, A. A., & Arif, S. H. (2019). Midline gallbladder makes a challenge for surgeons during laparoscopic cholecystectomy; case series of 6 patients. *Annals of Medicine and Surgery, 40*, 14-17.

Naja, Z., & Lönnqvist, P. A. (2001). Somatic paravertebral nerve blockade incidence of failed block and complications. *Anaesthesia, 56*(12), 1181-1201.

Ortiz, J., Suliburk, J. W., Wu, K., Bailard, N. S., Mason, C., Minard, C. G., & Palvadi, R. R. (2012). Bilateral transversus abdominis plane block does not decrease postoperative pain after laparoscopic cholecystectomy when compared with local anesthetic infiltration of trocar insertion sites. *Regional Anesthesia and Pain Medicine, 37*(2), 188-192.

Tulgar, S., Kapakli, M. S., Senturk, O., Selvi, O., Serifsoy, T. E., & Ozer, Z. (2018). Evaluation of ultrasound-guided erector spinae plane block for postoperative analgesia in laparoscopic cholecystectomy: a prospective, randomized, controlled clinical trial. *Journal of Clinical Anesthesia, 49*, 101-106.

Van Zundert, A., Stultiens, G., Jakimowicz, J., Peek, D., Van der Ham, W., Korsten, H., & Wildsmith, J. (2007). Laparoscopic cholecystectomy under segmental thoracic spinal anaesthesia: a feasibility study. *British journal of anaesthesia, 98*(5), 682-686.

Van Zundert, A., Stultiens, G., Jakimowicz, J., Van den Borne, B., Van der Ham, W., & Wildsmith, J. (2006). Segmental spinal anaesthesia for cholecystectomy in a patient with severe lung disease. *BJA: British Journal of Anaesthesia, 96*(4), 464-466.

ZANCO Journal of Pure and Applied Sciences
The official scientific journal of Salahaddin University-Erbil
https://zancojournals.su.edu.krd/index.php/JPAS

ISSN (print):2218-0230**, ISSN (online):** 2412-3986**, DOI: http://dx.doi.org/10.21271/zjpas**

RESEARCH PAPER

Heavy metal ions removal from wastewater using various low-cost agricultural wastes as adsorbents: a survey

Bnar M. Ibrahim

Department of Chemistry, College of science, University of Raparin, Iraq.

A B S T R A C T:
Toxic heavy metals have an important role in water pollution. Because of their toxicity and non-biodegradability which affects humans, animals, and also plants. Researchers in the field of environment used various heavy metal removal methods, such as ion exchange, precipitation, evaporation, membrane filtration and adsorption. Low cost, high efficiency and easy regeneration make the adsorption process as an effective technique in the heavy metal removal. The purpose of this review is to gather sufficient information about various agricultural waste adsorbents and their removal capacity for heavy metals.

KEY WORDS: heavy metals, adsorption, agricultural waste adsorbents.
DOI: http://dx.doi.org/10.21271/ZJPAS.33.2.8
ZJPAS (2021) , 33(2);76-91 .

1. INTRODUCTION :

Elements that have atomic masses between 63.5 - 200.6, and a density higher than five are considered heavy metals. In developing countries because of more industries such as metal plating, mining processes, fertilizer industries, tanneries, batteries, paper industries and pesticides, etc., heavy metals released into the environment directly or indirectly. Organic contaminants are biodegradable and do not accumulate in living organisms unlike heavy metals, which are toxic or carcinogenic. Industrial wastewaters need treatment when contaminated with toxic heavy metals such as zinc, copper, nickel, mercury, cadmium, lead and chromium (Fu and Wang, 2011).

* **Corresponding Author:**
Bnar Mahmoud Ibrahim
E-mail: bnar.mahmoud@uor.edu.krd
Article History:
Received: 13 / 12 /2020
Accepted: 30/01/2021
Published: 18 /04 /2021

Various diseases considered due to exposure to heavy metal ions such as birth problem, kidney damage, skin infections and cancer (Hokkanen et al, 2018). Because of their health problems the World Health Organization (WHO) are recommended their removal from wastewater (Mara, 2003).

Chromium has various oxidation numbers, chromium (VI) and chromium (III) are mostly used in industrial sewage (Mohhan and Pitman, 2006). Chromium (III) is safer than Cr (VI) and Cr (VI) is an oxidising agent, carcinogenic in nature and is also has a negative impact on plants and living organisms (Renu et al, 2017). Chromium (VI) exposure causes cancer in the lungs, abdomen pain, nausea, and severe diarrhoea, throw up and haemorrhage (Mohanty et al, 2006).

International Agency for Research on Cancer (IARC) listed cadmium as a Category-I carcinogen and its major sources include smelting, mining, plastic industry, metal refinery and

photographic industry (Ghare et al, 2013). Copper is important for enzyme synthesis, tissue and bone maturity but Cu (II) is carcinogenic and poison when it is taken in high concentration and causes head acke, vomiting, nausea, liver and kidney failure and inhaling disorders (Lan et al, 2013). Important sources of copper are smelting, drilling, electroplating, surface finishing, electric devices, electronic pieces (Bilal et al, 2013). Nickel is considered as human carcinogen and causes various health effects including renal and lung disorders, abdominal pain and skin irritation. (Borba et al, 2006). Zinc is also important for human's body but high intake amount of zinc causes skin infections, belly contraction, vomiting and anaemia (Oyaro et al, 2007). More importantly, lead and mercury have adverse effects on human health and can affect nervous system, kidney damage, brain, liver and reproductive system (Ding et al, 2010, Namasivayam and Kadirvelu, 1999). Arsenic may also cause pain in the skin, lung, kidney, muscles, lack of appetite and nausea (Mohan and Pittman, 2007).

Various methods have been utilized for eliminating toxic heavy metals from wastewater like physical, chemical, biological and a combination of several techniques (Zhou et al, 2004). In recent years, adsorption as an effective and inexpensive water remedy has been used (Stephen et al, 2011).

For the first time activated carbon was used as an efficient and standard adsorbent for waste water remediation from toxic metal ions as a result, of its small fragment sizes and active free valences (Kurniawan et al, 2006). But high cost and difficult regeneration of activated carbon restricted its use, regeneration of AC need expensive chemicals and high temperature (Babel and Kurniawan, 2003).

As a substitute for existing expensive methods of r emoving heavy metals from solutions, the use of l ow-cost sorbents has been studied.

Recently, various types of natural materials or wastes and biopolymers have been utilized as adsorbents for the adsorption process due to their efficient adsorption capacities; either used naturally or with some modifications (Abas et al, 2013).

The increasing number of publications on adsorption using low cost adsorbents concludes increasing interest in finding suitable adsorbents for the adsorption process. In this article, an overview of the adsorption process using low cost adsorbents for heavy metal removal is presented by highlighting the applicability of adsorbents and adsorption capacity.

The main objective of this survey is to display information about adsorption process and reusing agricultural waste as adsorbents for heavy metal removal.

2. Adsorption operation

In recent times, the adsorption system has an important technique in metal ions removal and it used for a long time. Today adsorption is a basic method because of its adaptability in design and easy process instead of getting to perform adsorptions, which are perceived as impractical employing most conventional techniques.

The "adsorption" process can be defined as a weight transfer technique by way that a material is moved from the liquid segment to the floor of a stable and linked by using physiochemical reactions (Babel and Kurniawan, 2003).

The benefits of the adsorption operation in casting off or minimising the heavy metals even at low concentration enhance the utility of adsorption as one practical treatment. The efficacy of the adsorption method is specifically affected by the form of the solution in which the pollutants are dispersed, the molecular size and the pollutant polarity, as well as the kind of adsorbent used. Adsorption is also present due to the appealing interactions among a floor and the species being adsorbed at certain molecular level (Monser and Adhoum, 2002).

In addition, Adsorption can be categorised into two; physical and chemical adsorption. Physical adsorption is a reversible process as a consequence of intermolecular forces of enchantment among molecules of the adsorbent and the adsorbate. Chemical adsorption is an irreversible phenomenon and its a consequence of the chemical reaction between the solid and the material adsorbed (Yadla et al, 2012).

High physical adsorption occurs at a temperature s imilar to the critical temperature of a given gas in t erms of temperature, even though chemical adsorp tion occurs at temperatures much higher than the c

ritical temperature. Both processes may occur concurrently under certain conditions (Dabrowski, 2001).

3. Mechanism of adsorption

Adsorption mechanisms are not easy and there is no theory that completely explains how metal ions adsorb on the external part of the adsorbent. Various models have been described as mechanism between the adsorbate and the adsorbent. In order to explain the sorption isotherms both Langmuir and Freundlich models are mostly utilized while sorption kinetics is presented by using pseudo first order and pseudo second order kinetic models (Abas et al, 2013).

3.1Adsorption isotherm

Isotherms are mathematical equations used to explain the behaviours of adsorption of a particular adsorbent-adsorbate combination (Al-Madhoun et al, 2005).

The adsorption isotherm shows how the adsorbed molecules, when the adsorption cycle enters equilibrium state are dispersed among the liquid state and the solid state. Analysing isothermic data by appropriating them into various isothermic models is an essential way of identifying the right rule that can be utilized for layout purpose (Nawabanne and Igbokwe, 2008). There are several simple isothermic models including: Langmuir, Freundlich, Temkin, BET, D-R model and others (Otun et al, 2006). The adsorption models Langmuir and Freundlich are commonly used because they are easy to explain experimental findings in a wide range of concentrations (Peric et al, 2004).

3.1.1 Langmuir isotherm

The simplest physically possible isotherm is depended on three hypotheses:

(i) Adsorption cannot extend beyond monolayer cover.

(ii) All sites are identical and have a uniform surface area.

(iii) The molecules capability to adsorb at a provided site does not depend on the occupation of adjacent sites (i.e., there are no reactions among adsorbed particles) (Atkin and Paula, 2006).

Langmuir isotherm model can be written in the following (Hussain et al, 2009, Mehdi and Mehdi, 2014, Zawaniz et al, 2009):

$$\frac{C_e}{Q_e} = \frac{C_e}{Q_{max}} + \frac{1}{K_L Q_{max}} \qquad \text{----------(1)}$$

Where,

Q_{max} (mg/g) refers to maximum monolayer coverage adsorption,

K_L (L/mg) refers to Langmuir constant related to sorption strength,

Ce is the metal ions quantity in the solution (mg L^{-1}) and

qe is the metal ions quantity on the adsorbent sites (mg g^{-1}) at equilibrium.

3.1.2 Freundlich isotherm

Freundlich isotherm rule states that the adsorbed molecules heterogeneously cover the adsorbent surfaces. This isotherm is widely utilized to characterize the adsorption on a wide variety of adsorbents of organic and inorganic compounds (Febrianto et al, 2009).

For Freundlich equation, it is written as:

$$\ln q_e = \ln K_F + 1/n \ln C_e \qquad \text{----------(2)}$$

While K_f is the Freundlich isotherm constant whereas 1/n is the diversity factor that is described the adsorption capability and strength and C_e is the equilibrium concentration (mg L^{-1}). This model states that when the adsorbate quantity increase, also the quantity of adsorbate on the adsorbent surface will be increase and thus sorption intensity decreases exponentially with the accomplishment of the adsorbent sorption centre (Karakaya, 2011). Langmuir and Freundlich isotherm rules are also applied to explain the short term, single-element adhesion of metal ions by various materials (Zhang et al, 2000).

4. Adsorption kinetics

In terms of kinetic energy, contacting time from practical data's can be applied to research the rate-limiting stage in the adsorption operation. The adsorption action can be managed by one or more stages such as pore diffusion, surface diffusion or more than one phase combination. The first order statement of Lagergen's and the second order equation of Ho's are some examples of kinetic models widely used to characterize certain kinetic models of adsorption (Ho, 2006).

The Lagergren models first-order kinetic pseudo-equation is given as such equations:

$$\ln (q_e - q_t) = \ln q_e - K_1 t \quad \text{----------(3)}$$

While q_e and q_t are the quantity of adsorbed waste (mg/g) in equilibrium and at any time *t* (min) and k_1 is the constant rate of pseudo first order adhesion (min ^{1}) (Deng et al, 2015). First order Pseudo statement refers to the concept of the rate of change in the uptake of solute over time that is directly proportional in concentration of saturation and the quantity of solid take over time (Khaled et al, 2009). The kinetic statement of second order pseudo is given as (Yang and Jiang, 2014,Wang et al, 2015):

$$\frac{t}{q_t} = \frac{1}{k_2 qe^2} + \frac{t}{q_e} \quad \text{----------(4)}$$

The second order pseudo rule is depending on the hypothesis that the rate limiting stage that drive from chemisorption including valence powers by exchanging electrons among the adsorbent and the adsorbate molecules (Ho and McKay, 1999).

Adsorption capacity qe was calculated using the following equation (Katsumata et al, 2003):-

$$q_e = \frac{C_0 - C_e}{m} V \quad \text{----------5}$$

While C_0 and C_e are the initial and equilibrium metal ions quantity (mg L^{-1}), respectively. *V* (L) is the volume of solution and *m* (g) is the adsorbent mass.

5. Factors affecting the adsorption capacity

There are various factors, which affect adsorption capacity such as temperature, shaking time, adsorbent dose and pH. Among the above-mentioned factors pH has been described as the most significant variable concerning metal adsorption on adsorbent (Srivastava et al, 2006).

The solutions pH influences the surface charge of the adsorbents as well as the degree of ionization and speciation of the various contaminants, the change of the pH affects the adsorptive mechanism by dissociating the reactive groups on the adsorbents surface active sites.

This contributes to improvements in the adsorptio n system's reaction kinetics and equilibri um characteristics (Katsumata et al, 2003).

This is partially because adsorbate competes intensely with hydrogen ions themselves (Ozcan et al, 2005). Various anionic and cationic species adsorption on the adsorbents surface can be explained on the basis of the competitive adsorption of $H3O^+$ and OH^- ions with the adsorbate. It is commonly observed that the surface adsorbs anions at lower pH due to presence of $H3O^+$ ions, while the adsorbent surface is active for the adsorption of cations at higher pH due to the deposition of hydroxyl ions (Katsumata et al, 2003).

Metal uptake depends on both the active sites and the composition of the solutions metal ions. $H3O^+$ predominates and occupies the binding sites of the adsorbent at low pH while the concentration of $H3O^+$ decreases at elevated pH and that of hydroxyl ions increases on the adsorbent surface. Thus the adsorbents surface charge changes to negatively charged sites, resu lting in greater cation attraction (Chakravarty et al, 2008,Kailani et al, 2009).

6. Adsorption on Agricultural Wastes

Recently, an incredible deal of interest in the research for the elimination of heavy metals from commercial effluent has been focused on the use of agricultural wastes as adsorbents (Barakat, 2011). The use of agricultural wastes in bioremediation of heavy metallic ions, is known as bio-sorption. Bio sorption is a physiochemical method that occurs naturally in po sitive biomass, which lets in it to passively listen and bind contaminants onto its cellular structure. Many researchers agree with that this phenomenon will offer an economical opportunity for putting off poisonous heavy metals from industrial wastewater and resource in environmental remediation (Wang and chen, 2009)

The elimination of metal ions from sewage water by applying agricultural fabric is refers to bio

sorption (Renu et al, 2016). Bio sorption method has a sorbent and solvent and this solvent include species, which have to be adsorbed on sorbent surface. These sorbents have affinity for metal ions species. These ions are attracted through sorbent and bound in complicated manner. Agricultural waste substances consist of cellulose and lignin and other components are hemicellulose, lipid, protein, water, starch, ash etc and many extra compounds. Cellulose is an organic compound, a polysaccharide together with linear chain of numerous hundred to many thousand of β related D-glucose units (Demirbas, 2008). However, Lignin is a complex polymer of fragrant alcohols called monolignols.

It is maximum usually derived from wooden and it's far an integral part of the secondary cell partitions of flora and a few algae. These compounds includes functional organizations such as, carbonyl, amido, amino, phenolic, carboxyl group, alchohols, ester and sulphydryl (Gupta and Ali, 2000). These functional groups have ability of complicated formation. Table 1 displays various agricultural waste substances which have been used for heavy metals removal.

Table 1 Various biomass of plant origin for removal of poisonous metal ions from wastewater

Biomass	**Adsorption capacity (mg/g)**	**Optimum pH**	**Adsorption isotherm**	**Reference**
Spent green tea	Pb^{2+} 90.10	------	L	Zuorro and Lavecchia, 2010
Tea waste	Pb^{2+}65.00	5-6	L,F	Amarasinghe and Williams, 2007
Mango peel	Pb^{2+}99.05	5.0	L	Iqbal et al, 2009b
Banana peel	Pb^{2+}2.18	5.0	L	Anwar et al, 2010
Moringa oleifera bark	Pb^{2+}34.60	5.0	L	Reddy et al, 2010
Rhizophoraapiculata tannin	Pb^{2+}31.32	5.0	L, F, S	Oo et al, 2009
Shell carbon	Pb^{2+}30.00	-----	-------	Sekhar, 2008
Hazelnut shell	Pb^{2+}28.18	6,7	L	Pehlivan et al, 2009
Cicerarientinum	Pb^{2+}20.00	6.0	L	Mohammad et al, 2010
Almond shell	Pb^{2+} 8.08	6,7	L	Pehlivan et al, 2009
Wheat bran	Pb^{2+}87.00	4-7	L	Bulut and Baysal, 2006
Coir pith waste	Pb^{2+}263.00	5.0	L	Kadirvelu and Namasivayam, 2000
Spent black tea	Pb^{2+}129.90	-----	L	Zuorro and Lavecc

				hia, 2010
Maize cope and husk	Pb^{2+}456	------	-------	Igwe et al, 2005
Cocoa shells	Pb^{2+}6.2	2.0	-----	Meunier et al, 2003
Orange Lemon Banana Water melon	Pb^{2+}91% Pb^{2+}94% Pb^{2+}92% Pb^{2+}96%	2.0	L	Jena and Sahoo, 2017
Rise husk modified with orthophosphoric acid	Pb^{2+}138.89	-----	L	Dada et al, 2013
Lemon peel modified with Citric acid	Pb^{2+}93.83%	6.0	F	Tovar et al, 2018
Acacia leucocephala bark	Ni^{2+}294.10	5.0	L	Subbaiah et al, 2009
Orange peel	Ni^{2+}158.00	6.0	L	Ajmal et al, 2000
Pomegranate peel	Ni^{2+}52.00	5.5-6.5	L	Bhatnagar and Minocha, 2010
Mango peel	Ni^{2+}39.75	5-6	L	Iqbal et al, 2009a
Activated carbon prepared from Cicer arietinum	Cu^{2+}18.05 Zn^{2+}18 Pb^{2+}20	7.0 7.0 6.0	F	Ramana et al, 2010
Coir pith	Ni^{2+}15.95	5.3	L	Parab et al, 2006
Tea waste	Ni^{2+}73.00	-----	L,F	Ahluwalia and Goyal, 2005
Tea waste	Ni^{2+}15.26	4.0	L	Malkoc and Nuhoglu, 2005
Cicerarientinum	Zn^{2+}20.00	6.0	L	Mohammad et al, 2010
Wheat bran	Zn^{2+}16.40	6.5	L	Dupont et al, 2005
Tea waste	Zn^{2+}8.90	4.2	-----	Wasewar et al, 2009
Mango peel	Zn^{2+}28.21	5-6	L	Iqbal et al, 2009a
Maize cope and husk	Zn^{2+}495.9	------	------	Igwe et al, 2005

Natural rice husk	Cd $^{2+}$73.96	6.0	L,F,D-R	Akhtar et al, 2010
Maize cope and husk	Cd $^{2+}$493.7	-----	-----	Igwe et al, 2005
Rice husk modified with Sulphuric acid	Cd $^{2+}$101	5.4	L	Ozer, and Pirinc, 2006
Wheat bran	Cd $^{2+}$15.82–22.78	5.0	L	Nouri et al, 2007
Wheat straw	Cd $^{2+}$11.60–39.22 Cd $^{2+}$0.1032 mmol/g	6.0 5.0	L	Farooq et al, 2001,Tan and Xiao, 2009
Puresorbe	Cd $^{2+}$285.70	7.0	L, F	Pino et al, 2006
Coir pith	Cd $^{2+}$93.40	5.0	L	Kadirvelu and Namasivayam, 2003
Copra meal	Cd $^{2+}$4.99	5.0	L	Ho and Ofomaja, 2006
Orange peel	Cd $^{2+}$47.60	7.0	L	Sha et al, 2009
Mango peel	Cd $^{2+}$68.92	5.0	L	Iqbal et al, 2009b
Banana peel	Cd $^{2+}$5.71–35.52 Cd $^{2+}$2.18	8.0 3.0	L	Memon et al, 2008a, Anwar et al, 2010
Pomelo peel	Cd $^{2+}$21.83	5.0	L	Saikaew et al, 2009
Raw date pit	Cd $^{2+}$35.90	4.0	-----	Kahraman et al, 2008
Raw coffee powder	Cd $^{2+}$15.65	7.0	L	Azouaou et al, 2010
Tea waste	Cd $^{2+}$11.29	5.5	F	Cay et al, 2004
Pinus roxburghii bark	Cd $^{2+}$3.01	7.0	L	Padmini and Sridhar, 2007
Rice husk ash	Cd $^{2+}$3.04	6.0	F	Srivastava et al, 2008
Coffee residues blended with clay	Cd $^{2+}$ 17.5–17.9	7-9	L	Boonamnuayvitaya et al, 2004
Coffee husks	Cd $^{2+}$6.9	6.0	L	Oliveira et al, 2008
Coffee beans	Cd $^{2+}$3.80	8.0	L	Kaikake et al, 2007
Apple pomace modified with	Cd^{2+}4.45,91.74	5-6	L	Chand et al, 2014

Succinic anhydride				
Apple pomace modified with xanthate	Cd^{2+}112.35	4.0	L	Chand et al, 2015
Olive stone modified with zinc chloride	Cd^{2+}95%	> 6	L,F	Kula et al, 2008
Rice husk modified with Sulphuric acid	Cd^{2+}41.15 and 38.76	6.0	L	El-Shafey, 2007
Melon husk modified with H2SO4, NaHCO3	Cd^{2+}96.8%	------	F	Giwa et al, 2013
Rice husk	Cr^{6+} 0.79	2.0	F	Bishnoi et al, 2003
Egg shell	Cr^{6+} 1.45	5.0	L,F	Daraei et al, 2015
Wheat straw	Cr^{6+} 21.34	1.0	F	Wang et al, 2010
Banana peel	Cr^{6+} 131.56	2.0	L	Memon et al, 2009
Bael fruit	Cr^{6+} 17.27	2.0	L	Anand kumar and Mandal, 2009
Groundnut husk	Cr^{6+} 7.00	3.0	F	Dubey and Gopal, 2007
Almond shell	Cr^{6+} 3.40	3.5	L	Pehlivan and Altun, 2008
Hazelnut shell	Cr^{6+} 8.28	3.5	L	Pehlivan and Altun, 2008
Walnut shell	Cr^{6+} 8.01	3.5	L	Pehlivan and Altun, 2008
Pinus roxburghii bark	Cr^{6+} 4.15	2.0	F	Sarin and Pant, 2006
Banana peel	Cr^{6+} 93.35%	3.0	------	Tejada-Tovar et al, 2018
Coconut coir pith modified with hexadecyltrimethyl ammonium bromide surfactant	Cr^{6+} 76.3	2.0	L, F, D-R	Namasivayam and Suresh kumar, 2008
Silica derived from rice	Cr^{6+} 63.69	2.0	L	Oladoja et al,

husk modified with Iron oxide				2013
Rice husk modified with Ozone	Cr^{6+} 8.7–13.1	2.0	F	Sugashini and Begum, 2015
Orange peel modified with potassium carbonate	Cr^{3+} 80%	3.0	L	Arslan et al, 2017
Wheat bran	Cu^{2+} 6.85–17.42	6.0	L,F	Aydın et al, 2008
Orange peel	Cu^{2+}50.94	7.0	L	Sha et al, 2009
Mango peel	Cu^{2+}46.09	5-6	L	Iqbal et al, 2009a
Peanut hull	Cu^{2+}9.00–21.25	5.5	L	Zhu et al, 2009
Peanut hull pellet	Cu^{2+}12.00	5-7.5	L	Johnson et al, 2002
Cicerarientinum	Cu^{2+}18.00	6.0	L	Mohammad et al, 2010
Chestnut shell	Cu^{2+}12.56	5.0	L	Yao et al, 2010
Casuarina	Cu^{2+}16.58	5.0	L, F	Mohan and
equisetifolia bark				Sumitha, 2008
Rhizophoraapiculata tannin	Cu^{2+}8.78	5.0	L, F, S	Oo et al, 2009
Tobacco fibre	Cu^{2+}10.5	----	L, F	Demirbas, 2008
Cotton boll	Cu^{2+}11.4	5.0	L	Ozcoy and Kumbur, 2006
Pomegranate peel	Cu^{2+}1.31 Pb^{2+}13.87	5.8 5.6	L	EL-ASHTOUKHY et al, 2008
Tea waste	Cu^{2+}8.64–48.00	5.5	F	Cay et al, 2004
Banana peel	Cu^{2+}20.37	6.5	L	Hossain et al, 2012
Corn stalk modified with: 1. nitric acid 2. diethylenetriamine 3. phosphoric acid 4. corn cob silica with alginate	Cu^{2+} 20.65 Cr^{6+} 200 Zn^{2+}79.21 Cu^{2+}4.73, Cd^{2+}4.60	4.5 2.4 ----- 7.0	F L L L	Vafakhah et al, 2014 Chen et al, 2011 Buasri et al, 2012 Shim et al, 2014

Orange peel waste modified with methyl acrylate	Cu^{2+}289	7.0	L	Feng et al, 2009
Orange peel waste modified with methyl acrylate	Pb^{2+}476.1 Ni^{2+}162.6 Cd^{2+}293.3	5.0	L	Feng et al, 2011
Orange peel modified with KCl	Cu^{2+}59.77 Cd^{2+}125.63 Pb^{2+}141.84 Zn^{2+}45.29 Ni^{2+}49.14	5.0-5.5	L	Xueyi et al, 2011
Orange peel	Cu^{2+} 3.65 Co^{2+}1.82 Ni^{2+}6.01 Zn^{2+}5.25 Pb^{2+}7.75	6.0-8.0	F	Annadurai et al, 2002
Banana peel	Cu^{2+}4.75 Co^{2+}2.55 Ni^{2+}6.88 Zn^{2+}5.8 Pb^{2+}7.97	6.0-8.0	F	Annadurai et al, 2002
Calcined banana peel	Cu^{2+}49.5 Pb^{2+}45.6 Cd^{2+}30.7 Cr^{6+} 25.2	4.0	L	Li et al, 2016
Sugarcane bagasse modified with succinic anhydride	Cu^{2+}114 Pb^{2+}189 Cd^{2+}196	5.5 5.0 6.0	L	Karnitz et al, 2007
Maize husk Maize husk modified with EDTA	Cd^{2+}−151.51 Pb^{2+}−217.39 Zn^{2+}−3330.0 Cd^{2+}833.3 Pb^{2+}714.29 Zn^{2+}769	7.5 --------	F F	Igwe and Abia, 2007
Suger beet pulp	Pb^{2+}5.60	5-5.5	F	Pehlivan, et al,

	Cd^{2+}7.16			2008
Rose waste	Pb^{2+}151.51 Co^{2+} 27.62	5.0 6.0	F	Javed et al, 2007
Phosphorylated orange waste	Cu^{2+}67.35 Pb^{2+}251	4.5 4.4	L	Ghimire et al, 2008
Grape bagasse	Cd^{2+}53.84 Pb^{2+}42.27	7.0 3.0	L	Farinella et al, 2007

7. Conclusions

Toxic metal ions, which pollute wastewater, considered as a major essential nature issues at some point of the globe. Various, remedy technology have been used for heavy metal elimination from sewage water. In this review we demonstrate adsorption as a more effective technique depending on the published articles. It is shown from this review that most of research's indicated that the adhesion or removal with the aid of inexpensive polymer adsorbents is identified as a powerful and thrift technique for the contaminate water treatment than expensive activated carbon.

Reference

Azouaou, N., Sadaoui, Z., Djaafri, A., Mokaddem, H. 2010. Adsorption of cadmium from aqueous solution onto untreated coffee grounds: equilibrium, kinetics and thermodynamics. J. Hazard. Mater. 184, 126–134

Arslan,Y., Kendüzler, E., Kabak, B., Demir, K., Tomul, F. 2017. Determination of Adsorption Characteristics of Orange Peel Activated with Potassium Carbonate for Chromium(III) Removal, JOTCSA. 4, 51-64.

Aydın, H., Bulut, Y., Yerlikaya, C. 2008. Removal of copper (II) from aqueous solution by adsorption onto low-cost adsorbents. J. Environ. Manage. 87, 37–45.

Akhtar, M., Iqbal, S., Kausar, A., Bhanger, M., Shaheen, M. A. 2010. An economically viable method for the removal of selected divalent metal ions from aqueous solutions using activated rice husk. Colloids Surf. B Interfaces. 75, 149–155.

Amarasinghe, B., Williams, R. 2007. Tea waste as a low cost adsorbent for the removal of Cu and Pb from wastewater. Chem. Eng. J. 132, 299–309.

Anwar, J., Shafique, U., Salman, M., Dar, A., Anwar, S. 2010. Removal of Pb (II) and Cd (II) from water by adsorption on peels of banana. Bioresour. Technol. 101,1752–1755.

Ahluwalia, S., Goyal, D. 2005. Removal of heavy metals by waste tea leaves from aqueous solution. Eng. Life Sci. 5, 158–162.

Anandkumar, J., Mandal, B. 2009. Removal of Cr (VI) from aqueous solution using Bael fruit (Aegle marmelos correa) shell as an adsorbent. J. Hazard. Mater. 168, 633–640.

Al-Madhoun, W. A., Isa, M. H., Ramli, N. A., Adlan, M. N., Hameed, B. H., Farooqi, I, H. 2005. International Conference-Water: Values & Rights, Palestine Academy for Science and Technology and Palestinian Water Authority, Palestine, 1-11.

Abas, S. N. A., Ismail, M. H. Sh., Kamal, M. L., Izhar, Sh. 2013 Adsorption Process of Heavy Metals by Low-Cost Adsorbent: A Review, World Applied Sciences Journal. 28 (11), 1518-1530.

Atkin, P., De Paula, J. 2006.Atkins Physical Chemistry, 8th Edition, W. H. Freeman and company, 917.

Annadurai, G., Juang, R. S., Lee, D. J. 2002. Adsorption of heavy metals from water using banana and orange peels, water science and technology. 47 (1),185–190.

Ajmal, M., Rao, R. A. K., Ahmad, R., Ahmad, J. 2000. Adsorption studies on Citrus reticulata (fruit peel of orange): removal and recovery of Ni (II) from electroplating wastewater. J. Hazard. Mater. 79,117–131.

Anwar, J., Shafique, U., Salman, M., Dar, A., Anwar, S. 2010. Removal of Pb (II) and Cd (II) from water by adsorption on peels of banana. Bioresour. Technol. 101, 1752–1755.

Boonamnuayvitaya, V., Chaiya, C., Tanthapanichakoon, W., Jarudilokkul, S. 2004. Removal of heavy metals by adsorbent prepared from pyrolyzed coffee residues and clay. Separation and Purification Technology 35 (1),11–22.

Bhatnagar, A. Minocha, A. 2010. Biosorption optimization of nickel removal from water using Punica granatum peel waste. Colloids Surf. B Interfaces 76 , 544–548.

Bulut, Y., Baysal, Z. 2006. Removal of Pb (II) from wastewater using wheat bran. J. Environ. Manage. 78 ,107–113.

Babel, S., Kurniawan, T. A. 2003. Cost adsorbents for heavy metals uptake from contaminated water: a review, Journal of Hazardous Materials .97, 219- 243.

Bilal, M., Shah, J. A., Ashfaq, T., Gardazi, S. M. H., Tahir, A. A., Pervez, A., Haroon, H., Mahmood, Q. 2013. Waste biomass adsorbents for copper removal from industrial wastewater – A review, Journal of

Hazardous Materials. 263 , 322–333.

Borba, C. E., Guirardello, R., Silva, E. A., Veit, M. T., Tavares, C. R. G. 2006. Removal of nickel (II) ions from aqueous solution by biosorption in a fixed bed column: experimental and theoretical breakthrough curves. Biochemical Engineering Journal. 30 (2) ,184–191.

Babel, S., Kurniawan, T. A. 2003. Various treatment technologies to remove arsenic and mercury from contaminated groundwater: an overview. In: Proceedings of the First International Symposium on Southeast Asian Water Environment, Bangkok, Thailand. ,433-440.

Buasri, A., Chaiyut, N.,Tapang, K., Jaroensin, S., Panphrom, S.2012. Equilibrium and kinetic studies of biosorption of Zn (II) ions from wastewater using modified corn cob. Apcbee Procedia. 3,60-64.

Bishnoi, N. R., Bajaj, M., Sharma, N., Gupta, A. 2003. Adsorption of Cr(VI) on activated rice husk carbon and activated alumina. Bioresour. Technol. 91 (3) , 305–307.

Barakat, M. A. 2011. New trends in removing heavy metals from industrial wastewater, Arabian Journal of Chemistry. 4, 361–377.

Cay, S., Uyanık, A., Özası, K. A. 2004.Single and binary component adsorption of copper (II) and cadmium (II) from aqueous solutions using tea-industry waste. Sep. Purif. Technol. 38, 273–280.

Chand, P., Shil, A. K., Sharma, M., Pakade, Y. B. 2014. Improved adsorption of cadmium ions from aqueous solution using chemically modified apple pomace: mechanism, kinetics, and thermodynamics. International Biodeterioration & Biodegradation 90, 8–16.

Chand, P., Bafana, A., Pakade, Y. B. 2015. Xanthate modified apple pomace as an adsorbent for removal of Cd (II), Ni (II) and Pb (II), and its application to real industrial wastewater. International Biodeterioration & Biodegradation 97, 60–66.

Chakravarty, S., Pimple, S., Chaturvedi, H. T.,Singh, S. 2008. Removal of copper from aqueous solution using newspaper pulp as an adsorbent, Journal of Hazardous Materials, 159, 396-403.

Chen, S.,Yue, Q., Gao, B., Li, Q., Xu, X.2011. Removal of Cr (VI) from aqueous solution using modified corn stalks: Characteristic, equilibrium, kinetic and thermodynamic study. Chemical Engineering Journal, 168(2), 909-917.

Daraei, H., Mittal, A., Noorisepehr, M., Mittal, J.2015. Separation of chromium from water samples using eggshell powder as a low-cost sorbent: kinetic and thermodynamic studies. Desalination and Water Treatment 53 (1) , 214–220.

Dubey, S. P., Gopal, K. 2007. Adsorption of chromium (VI) on low cost adsorbents derived from agricultural waste material: a comparative study. J. Hazard. Mater. 145, 465–470.

Ding, N., Cao, Q., Zhao, H., Yang, Y., Zeng, L.,He, Y., Xiang, K., Wang, G. 2010. Colorimetric Assay for Determination of Lead (II) Based on Its Incorporation into Gold Nanoparticles during Their Synthesis, *Sensors. 10* ,11144-11155.

Dabrowski, A. 2001. Adsorption, from theory to practice. Advances in Colloid and Interface Science. 93, 135-224.

Deng, S., Zhang, G., Wang, X., Zheng, T., Wang, P. 2015.Preparation and performance of polyacrylonitrile fiber functionalized with iminodiacetic acid under microwave irradiation for adsorption of Cu(II) and Hg(II), Chemical Engineering Journal. 276, 349–357.

Demirbas, A. 2008. Heavy metal adsorption onto agro-based waste materials: A review. J. Hazard. Mater. 157, 220.

Demirbas, A. 2008. Heavy metal adsorption onto agro-based waste materials: a review. Journal of hazardous materials. 157(2), 220-229.

Dada, A. O., Ojediran, J. O., Olalekan, A. P. 2013. Sorption of Pb from Aqueous Solution unto Modified Rice Husk: Isotherms Studies, Advances in Physical Chemistry.

Dupont, L., Bouanda, J., Dumonceau, J., Aplincourt, M.2005. Biosorption of Cu (II) and Zn (II) onto a lignocellulosic substrate extracted from wheat bran. Environ. Chem. Lett. 2,165–168.

El-Ashtoukhy, E.-S. Z., Amin, N. K., Abdelwahab, O. 2008. Removal of lead (II) and copper (II) from aqueous solution using pomegranate peel as a new adsorbent. Desalination, 223, 162-173.

El-Shafey, E. I. 2007. Sorption of Cd (II) and Se (IV) from aqueous solution using modified rice husk. Journal of Hazardous Materials 147 (1), 546–555.

Feng, N., Guo, X., Liang, S.2009. Adsorption study of copper (II) by chemically modified orange peel. Journal of Hazardous Materials, 164(2) ,1286-1292.

Feng, N., Guo, X., Liang, S., Zhu, Y., Liu, J.2011. Biosorption of heavy metals from aqueous solutions by chemically modified orange peel. Journal of Hazardous Materials,185(1), 49-54.

Febrianto, J., Kosasih, A. N., Sunarso, J., Ju, Y., Indraswati, N., and Ismadji, S. 2009. Equilibrium and kinetic studies in adsorption of heavy metals using biosorbent: A summary of recent studies, Journal of Hazardous Materials. 162, 616-645.

Fu, E.,Wang, Q. 2011. Removal of heavy metal ions from wastewaters A review, Journal of Environmental Management. 92, 407-418.

Farinella, N. V., Matos, G. D., Arruda, M. A. Z. 2007. Grape bagasse as a potential biosorbent of metals in effluent treatments, Bioresource Technology, 98, 1940–1946.

Farooq, U., Khan, M. A., Athar, M., Kozinski, J. A. 2011. Effect of modification of environmentally friendly biosorbent wheat (Triticum aestivum) on the biosorptive removal of cadmium (II) ions from aqueous solution. Chem. Eng. J. 171, 400–410.

Ghimire, K. N., Inoue, J., Inoue, K., Kawakita, H., Ohto, K. 2008. Adsorptive separation of metal ions onto phosphorylated orange waste, Separation Science and Tech- nology, 43, 362–375.

Ghare, A. A., Kamble, G. S., Anuse, M. A., Kolekar, S. S. 2013. Development and Optimization of Analytical

Method for Synergistic Extraction and Spectrophotometric Determination of Cadmium(II) by using 1-(2',4'- dinitroaminophenyl)-4,4,6-trimethyl-1,4-dihydropyrimidine-2-thiol: Analysis of Alloys, Thin Film and Biological Material, Columbia International Publishing, Journal of Trace Element Analysis. 2 (1), 1-20.

Gupta, V. K., Ali, I. 2000. Utilisation of bagasse fly ash (a sugar industry waste) for the removal of copper and zinc from wastewater. Separation and Purification Technology. 18(2),131-140.

Giwa, A. A., Bello, I. A., Oladipo, M. A., Adeoye, D. O. 2013. Removal of cadmium from waste-water by adsorption using the husk of melon (Citrullus lanatus) Seed. Int. J. Basic Appl. Sci., 2(1),110-123.

Hossain, M. A., Ngo, H. H., Guo W. S., and Nguyen, T. V. 2012. Biosorption of Cu(II) from water by Banana peel based biosorbent: Experiments and models of adsorption and desorption. Journal of Water Sustainability. 2(1),87-104.

Ho, Y. S., McKay, G. 1999. Pseudo-second order model for sorption processes. Process Biochemistry. 34, 451-465.

Ho, Y.-S., Ofomaja, A. E. 2006. Biosorption thermodynamics of cadmium on coconut copra meal as biosorbent. Biochem. Eng. J. 30, 117–123.

Hokkanen, S., Bhatnagar, A., Srivastava,V., Suorsa, V., Sillanpaa, M. 2018. Removal of Cd^{2+}, Ni^{2+} and PO_4^{3-} from aqueous solution by hydroxyapatite-bentonite clay-nanocellulose composite, International Journal of Biological Macromolecules.118 ,903-912.

Hussain, M. A., Salleh, A., Millow, P. 2009. Characterization of the Adsorption of the Lead (II) by the Nonliving Biomass. Amirican Journal of Biochemistry and Biotechnology. 5, 75-83.

Ho, Y. S. 2006. Review of second-order models for adsorption systems, Journal of Hazardous Materials. 136, 681-689.

Iqbal, M., Saeed, A., Zafar, S. I. 2009b. FTIR spectrophotometry, kinetics and adsorption isotherms modeling, ion exchange, and EDX analysis for understanding the mechanism of Cd^{2+} and Pb^{2+} removal by mango peel waste. J. Hazard. Mater. 164, 161–171.

Igwe, J. C., Abia, A. A.2007. Equilibrium sorption isotherm studies of Cd(II), Pb(II) and Zn(II) ions detoxification from waste water using unmodified and EDTA- modified maize husk, Electronic Journal of Biotechnology 10, 536–548.

Igwe, J. C., Ogunewe, D. N., Abia, A. A. 2005. Competitive adsorption of Zn(II), Cd(II) and Pb(II) ions from aqueous and non-aqueous solution by maize cob and husk. Afr. J. Biotechnol. 4 (10) ,1113– 1116.

Iqbal, M., Saeed, A., Kalim, I. 2009a. Characterization of adsorptive capacity and investigation of mechanism of Cu^{2+}, Ni^{2+} and Zn^{2+} adsorption on mango peel waste from constituted metal solution and genuine electroplating effluent. Separ. Sci. Technol. 44 ,3770–3791.

Jena, S., Sahoo, R. K. 2017. Removal of Pb(II) from Aqueous Solution Using Fruits Peel as a Low Cost Adsorbent, International Journal of Science, Engineering and Technology, 5 .

Johnson, P., Watson, M., Brown, J., Jefcoat, I. 2002 Peanut hull pellets as a single use sorbent for the capture of Cu (II) from wastewater. Waste Manag. 22, 471–480.

Javed, M. A., Bhatti, H.N., Hanif, M.A., Nadeem, R.2007. Kinetic, Equilibrium modeling of Pb(II) and Co(II) sorption onto rose waste biomass, Separation Science and Technology 42, 3641–3656.

Kurniawan, T. A., Chan, G, Y, S., Lo, W. H., Babel, S. 2006. Physico–chemical treatment techniques for wastewater laden with heavy metals, Chemical Engineering Journal. 118, 3–98.

Karakaya, A. 2011. *Purification Of Polyphenolic Compounds From Crude Olive Leaf Extract.* MSc., Izmir Institute of Technology.

Karnitz, O., Gurgel, L. V. A., De Melo, J. C. P., Botaro, V. R., Melo, T. M. S., de Freitas Gil, R. P. L., Gil, F.2007. Adsorption of heavy metal ion from aqueous single metal solution by chemically modified sugarcane bagasse. Bioresource Technology, 98(6),1291-1297.

Katsumata, H., Kaneco, S., Inomata, K., Itoh, K., Funasaka, K., Masuyama, K., Suzuki, T., Ohta, K. 2003. Removal of heavy metals in rinsing wastewater from plating factory by adsorption with economical viable materials, Journal of Environmental Management. 69 ,187–191.

Kadirvelu, K., Namasivayam, C. 2003. Activated carbon from coconut coirpith as metal adsorbent: adsorption of Cd (II) from aqueous solution. Adv. Environ. Res. 7, 471–478.

Khaled, A., Nemr, A. E., El Sikaily, A., Abdelwahab, O.2009. Treatment of artificial textile dye effluent containing Direct Yellow 12 by orange peel carbon. Desalination. 238, 210-232.

Kadirvelu, K., Namasivayam, C. 2000. Agricutural by-product as metal adsorbent: sorption of lead (II) from aqueous solution onto coir pith carbon. Environ. Technol. 21,1091–1097.

Kailani, G., Rao, G. B., Saradhi, B. V., Kumar, Y. P. 2009. ARPN journal of Engineering and Applied Science, 4, 39-49.

Kahraman, S., Dogan, N., Erdemoglu, S. 2008. Use of various agricultural wastes for the removal of heavy metal ions. Int. J. Environ. Pollut. 34, 275–284.

Kaikake, K., Hoaki, K., Sunada, H., Dhakal, R. P., Baba, Y. 2007. Removal characteristics of metal ions using degreased coffee beans: adsorption equilibrium of cadmium (II). Bioresource Technology 98 (15), 2787–2791.

Kula, I., Uğurlu, M., Karaoğlu, H., Celik, A. 2008. Adsorption of

Cd (II) ions from aqueous solutions using activated carbon prepared from olive stone by $ZnCl_2$ activation. Bioresource Technology 99 (3), 492–501.

Li, Y., Liu, J., Yuan, Q., Tang, H., Yu, F., Lv, X.2016. A green adsorbent derived from banana peel for

highly effective removal of heavy metal ions from water, The Royal Society of Chemistry.

Lan, S., Wu, X., Li, L., Li, M., Guo, F., Gan, S. 2013. Synthesis and characterization of hyaluronic acid-supported magnetic microspheres for copper ions removal. Colloids and Surfaces A, Physicochemical and Engineering Aspects .425, 42–50.

Mara, D. D. 2003. Water sanitation and hygiene for the health of developing nations, Public Health. 117, 452-456.

Mohan, D., Pittman, C. U. 2006. Activated carbons and low cost adsorbents for remediation of tri- and hexavalent chromium from water, Journal of Hazardous Materials. 137 (2), 762–811.

Mohan, D., Pittman, C. U. 2007. Arsenic removal from water/ wastewater using adsorbents – a critical review. Journal of Hazardous Materials. 142 (1), 1–53.

Monser, L., Adhoum, N. 2002. Modified activated carbon for the removal of copper, zinc, chromium and cyanide from wastewater. Separation and Purification Technology. 26(2/3),137-146.

Mehdi, R., Mehdi, V. 2014. Langmuir, Freundlich and Temkin adsorption isotherms of propranolol on multi-wall carbon nanotube. *Journal of Modern Drug Discovery and Drug Delivery Research.* 11, 1-3.

Meunier, N., Laroulandie, J., Blais J. F., and Tyagi, R. D. 2003. Cocoa shells for heavy metal removal from acidic solutions. Bioresource Technology. 90(3),255-63.

Mohammad, M., Maitra, S., Ahmad, N., Bustam, A., Sen, T., Dutta, B. K. 2010. Metal ion removal from aqueous solution using physic seed hull. J. Hazard. Mater. 179 ,363–372.

Malkoc, E., Nuhoglu, Y. 2005. Investigations of Ni(II) removal from aqueous solutions using tea factory waste. Journal of Hazardous Materials. 127, 120-128.

Memon, J. R., Memon, S. Q., Bhanger, M., Memon, G. Z., El- Turki, A., Allen, G. C. 2008a. Characterization of banana peel by scanning electron microscopy and FT-IR spectroscopy and its use for cadmium removal. Colloids Surf. B Interfaces. 66,260–265.

Memon, J. R., Memon, S. Q., Bhanger, M. I., El-Turki, A., Hallam, K. R., Allen, G. C. 2009. Banana peel: a green and economical sorbent for the selective removal of Cr (VI) from industrial wastewater. Colloids Surf. B Interfaces 70, 232–237.

Mohan, S., Sumitha, K. 2008. Removal of Cu (II) by adsorption using casuarina equisetifolia bark. Environ. Eng. Sci. 25, 497–506.

Mohanty, K., Jha, M., Meikap, B. C., Biswas, M. N. 2005. Removal of chromium (VI) from dilute aqueous solutions by activated carbon developed from Terminalia arjuna nuts activated with zinc chloride, Chemical Engineering Science. 60 (11), 3049–3059.

Nouri, L., Ghodbane, I., Hamdaoui, O., Chiha, M. 2007. Batch sorption dynamics and equilibrium for the removal of cadmium ions from aqueous phase using wheat bran. J. Hazard. Mater. 149, 115–125.

Namasivayam, C., Kadirvelu, K. 1999.Uptake of mercury (II) from wastewater by activated carbon from an unwanted agricultural solid by-product: coirpith. Carbon . 37 (1) ,79–84.

Nawabanne, J. T., Igbokwe, P. K. 2008. Kinetics and equilibrium modeling of nickel adsorption by cassava peel. Journal of Engineering and Applied Sciences. 3 , 829-834.

Namasivayam, C., Sureshkumar, M. V. 2008. Removal of chromium (VI) from water and wastewater using surfactant modified coconut coir pith as a biosorbent. Bioresource Technology 99 (7), 2218–2225.

Oladoja, N. A., Ololade, I. A., Alimi, O. A., Akinnifesi, T. A., Olaremu, G. A.2013. Iron incorporated rice husk silica as a sorbent for hexavalent chromium attenuation in aqueous system. Chemical Engineering Research and Design 91 (12), 2691–2702.

Oyaro, N., Juddy, O., Murago, E. N. M., and Gitonga, E. 2007. The contents of Pb, Cu, Zn and Cd in meat in Nairobi, Kenya, Journal of Food Agriculture & Environment. 5(3-4), 119-121.

Ozcan, A., Ozcan, S., Tunali, S., Akar, T., Kiran, I. 2005. Journal of hazardous material. B124, 200-208.

Ozcoy, H. D., Kumbur, H.2006. Adsorption of Cu(II) ions on cotton boll. J. Hazard. Mater. 136,911.

Ozer, A., Pirinc , H. B. 2006. The adsorption of Cd(II) ions on sulfuric acid-treated wheat bran, J. Hazard. Mater. 137,849–855.

Otun, J. A., Oka, I. A., Olarinoye, N. O., Adie, D. B., Okuofu, C. A. 2006. Adsorption isotherms of Pb, Ni and Cd ions onto PES, Journal of Applied Sciences. 6 , 2368-2376.

Oo, C.-W., Kassim, M., Pizzi, A. 2009. Characterization and performance of Rhizophora apiculata mangrove polyflavonoid tannins in the adsorption of copper (II) and lead (II). Ind. Crops Prod. 30,152–161.

Oliveira, W. E., Franca, A. S., Oliveira, L. S., Rocha, S. D. 2008. Untreated coffee husks as biosorbents for the removal of heavy metals from aqueous solutions. Journal of Hazardous Materials 152 (3), 1073–1081.

Pehlivan, E., Altun, T., Cetin, S., Bhanger, M. I. 2009. Lead sorption by waste biomass of hazelnut and almond shell. J. Hazard. Mater. 167,1203–1208.

Parab, H., Joshi, S., Shenoy, N., Lali, A., Sarma, U., Sudersanan, M.2006. Determination of kinetic and equilibrium parameters of the batch adsorption of Co (II), Cr (III) and Ni (II) onto coir pith. Process Biochem. 41, 609–615.

Peric, J., Trgo, M., Medvidoovic, N. V. 2004. Removal of zinc, copper and lead by natural zeolite a comparison of adsorption isotherms, Water Research. 38,1893-1899.

Pehlivan, E., Yanik, B. H., Ahmetli, G., Pehlivan, M.2008. Equilibrium isotherm studies for the uptake of cadmium and lead ions onto sugar beet pulp, Bioresource Technology 99, 3520–3527.

Pino, G. H., de Mesquita, L. M. S., Torem, M. L., Pinto, G. A. S. 2006. Biosorption of cadmium by green

coconut shell powder. Miner. Eng. 19, 380–387.

Padmini, E., Sridhar, S. 2007. Effect of pH and contact time on the uptake of heavy metals from industrial effluents by Pongamia pinnata Bark. Asian J. Microbiol. Biotechnol. Environ. Sci. 9, 187–190.

Pehlivan, E., Altun, T. 2008. Biosorption of chromium (VI) ion from aqueous solutions using walnut, hazelnut and almond shell. J. Hazard. Mater. 155, 378–384.

Renu., Agarwal, M., Singh, K. 2017. Heavy metal removal from wastewater using various adsorbents: a review, journal of water reuse and desalination.

Ramana, D., Jamuna, K., Satyanarayana, B., Venkateswarlu , B., Rao, M. M., Seshaiah, K. 2010. Removal of heavy metals from aqueous solutions using activated carbon prepared from Cicer arietinum. Toxicol. Environ. Chem. 92,1447–1460.

Renu, M. Agarwal, K. Singh, A. 2016. survey of modified agricultural wastes for heavy metal removal from waste water, International journal of engineering science and research technology, 5(12).

Reddy, D. H. K., Seshaiah, K., Reddy, A., Rao, M. M.,Wang, M. 2010. Biosorption of Pb2+ from aqueous solutions by Moringa oleifera bark: equilibrium and kinetic studies. J. Hazard. Mater. 174, 831–838.

Sekhar, M. C. 2008. Removal of lead from aqueous effluents by adsorption on coconut shell carbon. J. Environ. Sci. Eng. 50, 137–140.

Sugashini, S., Begum, K. M. M. S. 2015. Preparation of activated carbon from carbonized rice husk by ozone activation for Cr (VI) removal. New Carbon Materials. 30 (3), 252–261.

Srivastava, V. S., Mall, I. D., Mishra, I. M. 2006. Characterization of mesoporous rice husk ash (RHA) and adsorption kinetics of metal ions from aqueous solution onto RHA, Journal of hazardous material. 134, 257-267

Stephen, M., Catherine, N., Brenda, M., Andrew, K., Leslie, P., Corrine, G. 2011. Oxolane-2,5-dione modified electro spun cellulose nano fibers for heavy metals adsorption, Journal of Hazardous Materials. 192 , 922-927.

Shim, J., Lim, J. M., Shea, P. J., Oh, B. T. 2014.Simultaneous removal of phenol, Cu and Cd from water with corn cob silica-alginate beads. Journal of hazardous materials, 272,129-136.

Subbaiah, M. V., Vijaya, Y., Kumar, N. S., Reddy, A. S., Krishnaiah, A. 2009. Biosorption of nickel from aqueous solutions by Acacia leucocephala bark: kinetics and equilibrium studies. Colloids Surf. B Interfaces 74, 260–265.

Srivastava, V. C., Mall, I. D., Mishra, I. M.2008. Removal of cadmium (II) and zinc (II) metal ions from binary aqueous solution by rice husk ash. Colloids and Surfaces A: Physicochemical and Engineering Aspects. 312 (2) ,172–184.

Sha, L., Xueyi, G., Ningchuan, F., Qinghua, T. 2009. Adsorption of Cu^{2+} and Cd^{2+} from aqueous solution by mercapto-acetic acid modified orange peel. Colloids Surf. B Interfaces. 73, 10–14.

Saikaew, W., Kaewsarn, P., Saikaew, W. 2009. Pomelo peel: agricultural waste for biosorption of cadmium ions from aqueous solutions. World Acad. Sci. Eng. Technol. 56, 287–291.

Sarin, V., Pant, K. K. 2006. Removal of chromium from industrial waste by using eucalyptus bark. Bioresour. Technol. 97, 15–20.

Tovar, C. T., Ortiz, A. V., Correa, D. A., Gómez, N. P., Amor, M. O. 2018. Lead (II) Remotion in Solution Using Lemon Peel (Citrus limonum) Modified with Citric Acid, International Journal of Engineering and Technology.10 (1).

Tejada-Tovar, C., González-Delgado, A., Villabona-Ortíz, A. 2018. Comparison of Banana Peel Biosorbents for the Removal of Cr (VI) from Water. Contemporary Engineering Sciences. 11 (21), 1033 – 1041.

Tan, G., Xiao, D .2009. Adsorption of cadmium ion from aqueous solution by ground wheat stems. J. Hazard. Mater. 164, 1359–1363.

Vafakhah, S., Bahrololoom, M. E., Bazarganlari, R., Saeedikhani, M. 2014. Removal of copper ions from electroplating effluent solutions with native corn cob and corn stalk and chemically modified corn stalk. Journal of Environmental Chemical Engineering, 2(1), 356-361.

Wasewar, K. L., Atif, M., Prasad, B., Mishra, I. 2009. Batch adsorption of zinc on tea factory waste. Desalination 244, 66–71.

Wang, J., Chen, C. 2009. Biosorbents for heavy metals removal and their future, Biotechnology Advances. 27(2) ,192 – 226

Wang, X. S., Chen, L. F., Li, F. Y., Chen, K. L., Wan, W. Y., Tang, Y. J. 2010. Removal of Cr (VI) with wheat-residue derived black carbon: reaction mechanism and adsorption performance. J. Hazard. Mater. 175, 816–822.

Wang, Z., Barford, J. P., Hui, C. W., McKay, G. 2015. Kinetic and equilibrium studies of hydrophilic and hydrophobic rice husk cellulosic fibers used as oil spill sorbents, Chemical Engineering Journal. 281,961-969.

Xueyi, G., Sha, L., Qinghua, T. 2011.Removal of Heavy Metal Ions from Aqueous Solutions by Adsorption Using Modified Orange Peel as Adsorbent, Advanced Materials Research. 236-238, 237-240.

Yao, Z.-Y., Qi, J.-H., Wang, L.-H. 2010. Equilibrium, kinetic and thermodynamic studies on the biosorption of Cu (II) onto chestnut shell. J. Hazard. Mater. 174,137–143.

Yadla, S. V., Sridevei, V., Chandana Lakshmi, M. V. V.2012. Adsorption performance of fly ash for the removal of lead. International Journal of Engineering Research & Technology. 1(7).

Y u, B., Zhang, Y., Shukla, A., Shukla, S., and Dorris, K. L. 2000. The removal of heavy metals from aqueous solution by sawdust adsorption- Removal of lead and comparison of its adsorption with copper, Journal of Hazardous Materials. 84(1), 83-94.

Yang, G., Jiang, H. 2014. Amino modification of biochar for enhanced adsorption of copper ions from synthetic wastewater, Water Res. 48, 396-405.

Zawaniz, L. C. A., Thomas, S. Y. 2009. Choong, Equilibrium, Kinetics and Thermodynamic Studies:

Adsorption of Remazol Black 5 on the Palm Kernel Shell Activated Carbon, European Journal of Scientific Research. 37, 67-76.

Zhou, D., Zhang, L., Zhou, J., Guo, S. 2004. Cellulose/chitin beads for adsorption of heavy metals in aqueous solution, Water Research. 38 , 2643-2650.

Zuorro, A., Lavecchia, R. 2010. Adsorption of Pb (II) on spent leaves of green and black tea. Am. J. Appl. Sci. 7,153–159.

Zhu, C.-S., Wang, L.-P., Chen, W.-B. 2009. Removal of Cu (II) from aqueous solution by agricultural by-product: peanut hull. J. Hazard. Mater. 168, 739–746.

Zuorro, A., Lavecchia, R. 2010. Adsorption of Pb (II) on spent leaves of green and black tea. Am. J. Appl. Sci. 7, 153–159.

ZANCO Journal of Pure and Applied Sciences
The official scientific journal of Salahaddin University-Erbil
https://zancojournals.su.edu.krd/index.php/JPAS

ISSN (print):2218-0230**, ISSN (online):** 2412-3986**, DOI: http://dx.doi.org/10.21271/zjpas**

RESEARCH PAPER

Numerical and experimental study of mechanical properties and hydrostatic behavior of PVC-O material for drinking water pipes

Dilshad Azad Mohammed[1], Mohammedtaher M. Saeed Mulapeer[2]

[1]Department of Refrigeration & Air conditioning, Kalar Technical Institute, Sulaimani Polytechnic University, Sulaimani, Iraq

[2] Department of Mechanical & Mechatronics ,College of Engineering, Salahaddin University -Erbil, Iraq

A B S T R A C T:

This study investigates the mechanical properties for oriented polyvinyl chloride PVC-O material from three different directions of stress application. A PVC-O 500 pipe material has been studied in terms of mechanical properties in three different directions (0^o, 45^o, 90^o). Tensile strength at yield and percent elongation at fracture has been determined in all three directions. Two types of end caps (A and B) have been used to evaluate the pipe's hydrostatic strength. Results showed that molecular orientation has a significant impact on the pipe strength and ductility in different directions. Increasing the molecular orientation in the direction of the hoop (90^o direction), the strength increased to 91 MPa compared with 0^o and 45^o direction, which were 49 MPa and 61 MPa, respectively. Results showed that the percentage of elongations was 200%, 76 %, and 61% for 0^o, 45^o, and 90^o directions, respectively. The burst pressure for type A and B end caps was 6.22 MPa. Finite element analysis by SolidWorks 2018 simulation has been employed; the FEA has showed a good agreement with experimental results with a maximum difference of 5.16%. The FE results also showed that end caps affect stress distribution around the pipe during the hydrostatic test specially when using type B end caps. It's also concluded that both types of end caps cause stress concentration near the edges of the caps.

KEY WORDS: Oriented Polyvinyl Chloride; Hoop stress; Hydrostatic strength; Von Mises yield criteria; Finite element analysis.
DOI: http://dx.doi.org/10.21271/ZJPAS.33.2.9
ZJPAS (2021) , 33(2);92-104 .

1. INTRODUCTION :

Pipe materials technology, market requirements, and demand for more potable and waste water supplies have enforced pipe makers to advance developments in the mechanical properties of water pipes. In the late nineteenth century, PVC plastic material has discovered and lead to numerous applications, among those plastic pipes. In the middle of the 1930s, engineers, and scientists in Germany produced a limited amount of PVC pipes (AWWA 2002).

Since then, extreme improvements and developments are made in the plastic pipe field, which includes producing un-plasticized polyvinyl chloride PVC-U, chlorinated polyvinyl chloride PVC-C, Modified polyvinyl chloride PVC-M, and recently oriented polyvinyl chloride PVC-O (Mulapeer et al, 2016).

PVC-O has the same constituents of PVC-U pipes, and both are produced by the extrusion process, but a further process is required to produce PVC-O pipes, off-line or in-line manufacturing processes, in which both processes aimed to activate the molecular orientation in a circumferential direction by increasing the pipe

*** Corresponding Author:**
Mohammedtaher M. Saeed Mulapeer
E-mail: mohammedtaher.mulapeer@su.edu.krd
Article History:
Received: 13 / 09/2020
Accepted: 05/11/2020
Published: 18 /04 /2021

diameter during the manufacturing (ISO:16422, 2006) as shown in figure (1).

Increasing pipe diameter drives the molecules to orientate in the hoop direction and leads to substantial improvement in the mechanical properties, both strength, and toughness (Molecor 2017). PVC-O pipes also have significant resistance against surge pressures and water hammer and are quite capable of withstanding pressure transients over twice their rated working pressure (UK Water Industry 1999).

Since the product is an innovation and is not fully recognized by many academia, research centers, and even pipe manufacturers, there are limited published papers on this product. (Ferrante et al., 2015) presented the results of a study that investigate material rheology of PVC-O. Coupled measures of pressure and strain studied the viscoelastic effects in the strain-stress domain. They found that the rheological behavior of PVC-O is more predominant when pipes are subjected to transient pressure to a factor of 2 compared to UPVC pipes. (Bauer, 1994) studied the mechanical properties of oriented PVC pipes over traditional UPVC pipes, and it has been revealed that hoop stress of approximately 1.75 to 2.0 times higher is required to burst PVC-O that leads to PVC-O pipes requires less wall thickness than UPVC pipe at the same pressure and factor of safety.

Regarding fatigue resistance, studies found that PVC-O sustains more cyclic stress than UPVC; PVC-O demonstrates roughly 50 times greater strength (UK Water indusry1999).

(Purdue ECT Team, 2017) provided the market with the most eco-friendly pipes by eliminating many of the existing disadvantages of thermoplastic pipes. PVC-O provides greater hydraulic capacity between 15% - 40% higher than pipes made of other materials with the same outer diameter, and high chemical resistance, which does not require any coating of the pipes. Furthermore, the pipes can endure internal pressures about twice the nominal pressure of conventional pipes. Before the real emerging of PVC-O into the market, numerous studies have been conducted in order to improve the mechanical properties and hydraulic capacity of the available UPVC pipes. (Awham and Salih, 2011) studied some of the mechanical behavior, including impact, elastic modulus, flexural strength, and compression strength of PVC-U pipes. The results showed that PVC-U pipes have higher impact resistance and flexural strength as well as the compression failure considered suitable compared with other materials. Also, the results showed the presence of notches has a significant influence on such properties; as notch depth increased, the impact strength decreases.

Regarding the elastic modulus, it has been found that such material has a high elastic modulus compared with traditional PVC. (Ahmad et al., 2010) investigated the effects of rice husk and acrylic impact modifiers on the mechanical properties of PVC-U composites. Adding rice husk fillers from (10% - 40%) and 8% acrylic impact modifier has increased the flexural and tensile modulus of the unmodified and modified PVC-U composite. For 20% of rice husk, the flexural strength for both unmodified and modified PVC-U composite was increased. The scanning electron microscopy (SEM) showed that the rice husk fillers agglomerated and unevenly distributed throughout the matrix. The result showed that the impact strength of the filled PVC-U composites at 20% filler increased, but the tensile and flexural properties decreased with increasing impact modifier content. The formulation containing 8% of acrylic impact modifier and 20% of rice husk showed the best balance of stiffness and toughness properties. (Onitiri and Adeniyi, 2015) Studied the transverse compression loading under different temperature effects of recycled and extruded virgin PVC-U materials, the results showed recycled PVC-U exhibits better rigidity for all the temperatures considered except at 40^{o}C where stress at yield of 59.19 MPa and 61.31 MPa for recycled and virgin PVC-U has been recorded respectively. Results also revealed that virgin PVC-U exhibits improved plasticity while recycled PVC-U showed improved rigidity from 85^{o}C to 130^{o}C. (Nirmala and Rajkumar, 2016) investigated the behavior of buried PVC-U pipes under the ground soil; several parameters were considered. It has been concluded that the depth of embedment of pipe, type of backfill, thickness of pipe and surcharge loads are the prime factors that affects the behavior of buried pipes.

This study aims to investigate the mechanical properties and hydrostatic strength of PVC-O

pipes using experimental and numerical tools to understand material behavior under different loading conditions.

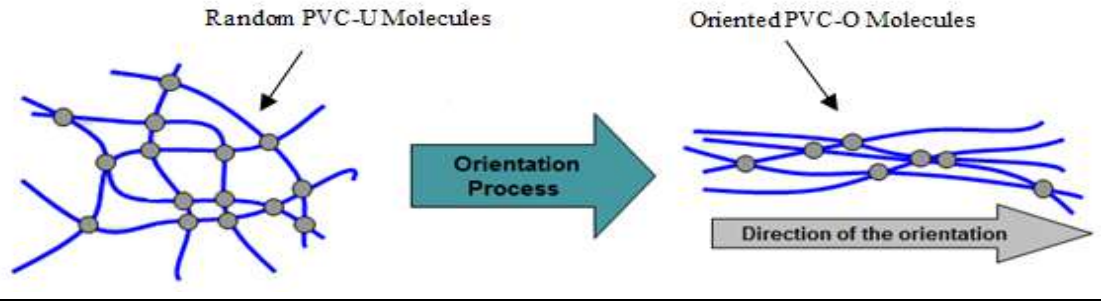

Figure 1. Molecular orientation process (PromainsTOM®, 2012).

2.MATERIALS AND METHODS

In this work-oriented (PVC-O) with a minimum required strength (MRS) of 50MPa and design stress of 25MPa, usually designated as PVC-O 500 has been used as a pipe material with a size of 110 mm diameters and 3.8 mm thickness and nominal working pressure of 25bar as shown in figure (2a). The PVC-O 500 pipe is sourced from Molecor company-Spain, which is specialized in molecular orientated pipe materials. The pipe is sectioned to prepare tensile specimens and hydrostatic test. For the tensile test, nine specimens were machined according to ISO 6259-2: 1997, as shown in figure (2b) with a width of 6mm and a gauge length of 25mm. The samples were cut from three different directions with respect to the pipe axis (0°) (X-axis - longitudinal direction), (45°) (XY - plane), and (90°) (Y-axis - circumferential direction). The samples were conditioned for 24hrs in the Lab at 23^{o}C, according to ASTM D618. Then, the samples were tensile tested at a rate of 5mm/min using a computerized universal testing machine of 30KN capacity, as shown in figure (2c).

The hydrostatic test has been done according to ISO 1167-1, 2, and ASTM D1599 using a computerized hydrostatic testing machine capable of full monitoring and controlling water temperature and pressure rate during the test. The hydrostatic test has been performed in a water bath maintained at 20^{o}C using two samples of the pipe with a length of 700 mm and two types of end caps [end closures] type (A and B) as presented in figure (3a). Both pipes are subjected to hydrostatic pressure gradually at a rate of 1MPa / second until the failure, as shown in figure (3b). The two samples burst at 6.2MPa.

(a) - PVC-O 500 pipes.

(b) - Tensile test specimen (ISO 6259-2: 1997).

(c) - Universal tensile test machine (XWW-30KN).

Figure 2. Tensile testing procedures.

(a) - The pipe under hydrostatic pressure.

(b) - Pipe failure due to hydrostatic pressure.

Figure 3. Failure shape during the hydrostatic pressure test.

2.1Numerical analysis

For the numerical analysis, SolidWorks 2018, with a built-in simulation tool, has been employed based on Von Mises failure criteria theory (Kurowski, 2018). The pipes have been modeled with a length of 700 mm and dimensions similar to the samples of the experimental part and subjected to a uniform hydrostatic pressure of 6.2 MPa for both types of end caps. Type (A) end caps are gripped to the pipe body, which provides free movement in the longitudinal direction. While type (B) end caps, which are attached to pipe ends through a steel bar passing inside the pipe, which restrict movement in the longitudinal direction. A linear elastic study was performed with solid curvature elements shown in figure (4) and with high-quality curvature mesh type of 39948 elements and 79644 nodes and with parameters shown in table 1. The FE analysis conducted using boundary conditions similar to the one observed or recorded during the experimental work and the resulted are tabulated in table 2.

Table 1. The mechanical property of PVC-O in different directions.

Angle with respect to the pipe axis	Modulus (MPa)	Poisson's ratio	Shear Modulus (MPa)	Mass Density (Kg/m^3)	Tensile Strength (MPa)	Compressive Strength (MPa)
0°	3000	0.35	1500	1410	49	66
45°	3500	0.35	1500	1410	61	66
90°	4000	0.35	2000	1410	91	66

Table 2. Experimental and numerical analysis of test results.

Properties	Exp. results	FE Stress analysis Results		ΔR (%) Experimental Vs FE	
	Measured value the average	End cap type A	End cap type B	End cap type A	End cap type B
Tensile strength at yield in the longitudinal direction MPa@23°C Direction 0°	49	46.57	26.66	4.96	45.6
Tensile strength at yield in the direction of 45°@23°C (MPa)	61	57.848	48.514	5.16	20.47
Tensile strength at break in the Circumferential direction MPa@23°C	91	91.057	90.149	0.06	0.93

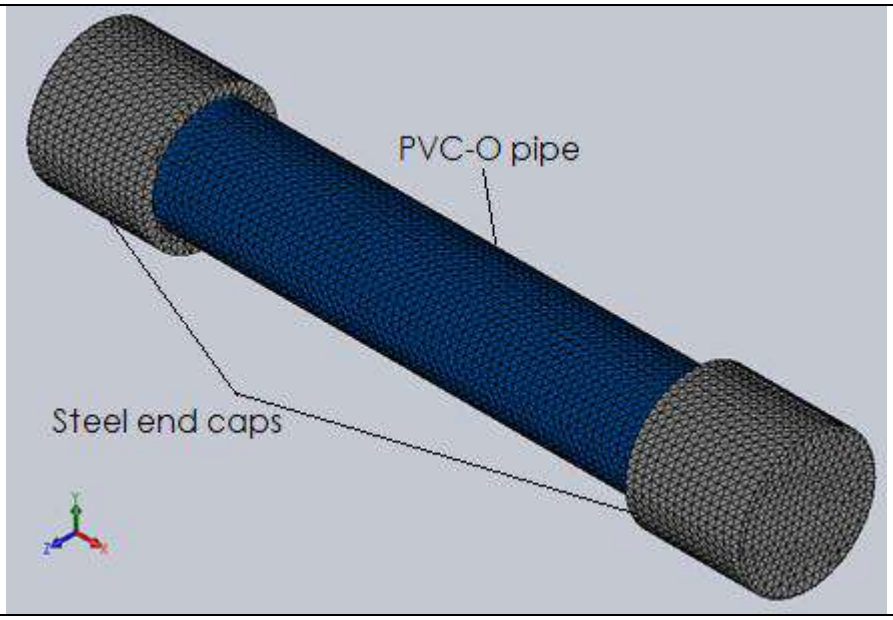

Figure 4. Finite element mesh of PVC-O pipe with end caps.

3.RESULTS AND DISCUSSION

3.1Tensile Test

From the tensile test curves shown in figure (5), it's clearly shown that the material behavior and mechanical properties of PVC-O greatly depend on the test direction, i.e., the material is showing un-isotropy (William D. Callister). The tensile strength increases with increasing molecular orientation from the nearly zero orientation in the 0^o direction (Longitudinal direction) to high orientation in the 90^o direction (Hoop direction). This behavior is attributed to the fact that at an angle (0^o) (longitudinal direction), the molecular are just tangled and can easily slip over each other and entangled (Mulapeer et al, 2016). So at 0^o direction, the yield point is clearly visible due to the slip of the tangled molecular over each other, as in the case of metals where the yield point occurs due to the motion of freed dislocations of atoms in the crystal lattice (Hall.E.O, 1970). In polymers, yielding occurs due to molecular movement out of the entanglement (Bauer, 1994) as shown in figure 1. At angle (45^o) (XY-plane) because of a certain amount of orientation, which is estimated to be around 50%, the yield point is higher but not clearly visible compared with the yield point of (0^o) direction. At angle (90^o) (hoop direction), all the molecular are nearly 100% aligned and oriented, and therefore, the yield point is not clear at all since there is no more un-entanglement or slipping. The reason for showing the yield point is due to the un-entanglement of molecular chains and the orientation phenomena (Mulapeer et al, 2016). The results from figure 5 and more clearly from the figure (6 a & b) show that while the tensile strength at yield increases with increasing molecular orientation, the ductility or the percent elongation at fracture decreases. The tensile strength of 91MPa has been recorded at the direction of (90^o), but the percent elongation is decreased to only 61%. While at (45^o) and (0^o), the tensile strength at yield was 61MPa and 49MPa, and the percent elongation was 76% and 200%, respectively. The elastic modulus significantly increased from 3000 MPa at (0^o) to 4000MPa at (90^o).

These results are very important and significant because the hydraulic capacity and hydrostatic strength of pipes depend mainly on the material strength in the hoop direction (Ahmad et al., 2010). Increasing hoop stress results in increasing the nominal working pressure of the pipes which saves material, and reduces the cost.

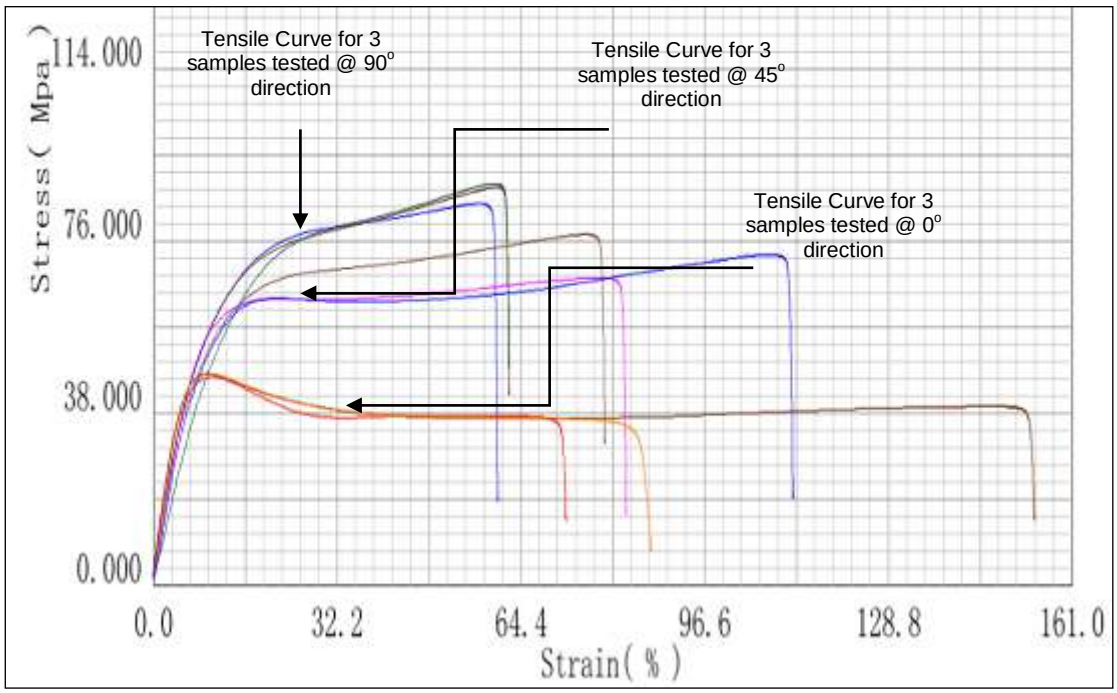

Figure 5. Stress-Strain diagram of (PVC-O) tested at (0°, 45°, 90°).

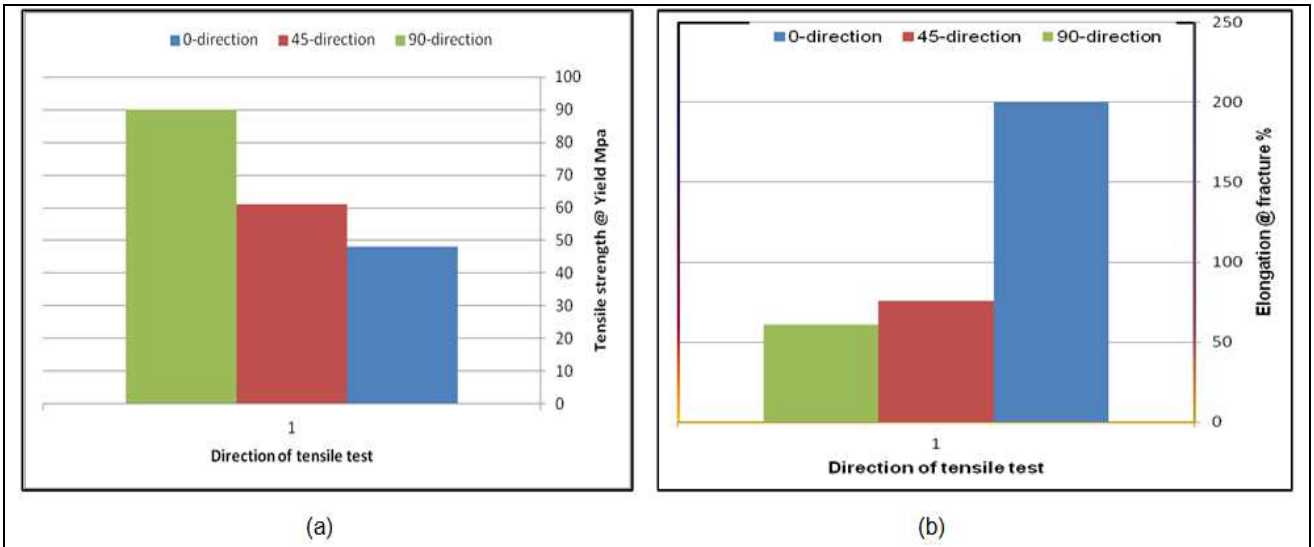

Figure 6. Variation of tensile strength at yield and Percent elongation as a function of test direction and molecular orientation

3.2 Hydrostatic Test

To experimentally characterize the effect of molecular orientation on hydrostatic of strength and behavior of PVC-O material, both pipes were individually and separately subjected to a gradually increasing hydrostatic pressure till the failure. Both pipes burst at the same pressure of 6.2MPa regardless of the type of end cap used. All thin-walled vessels, when subjected to hydrostatic pressure, undergo two types of static stresses longitudinal (axial) and circumferential (hoop) stresses (Shigley, 2011). Most of the failure occurs under the hoop stress since its magnitude is twice compared with axial stresses, as shown by the basic equations 1 and 2.

$$\sigma_H = \frac{Pd}{2t} \quad (1)$$

$$\sigma_L = \frac{Pd}{4t} \quad (2)$$

σ_H - Hoop stress in MPa
σ_L - Longitudinal stress in MPa
P – Internal pressure in Pa
d – Cylinder diameter mm
t – Wall thickness in mm

Increasing the design stresses from 12.5 MPa with a safety factor of 2 for PVC-U pipes to 25 MPa with the same safety factor for PVC-O pipes, led the plastic pipe technology a step forward to move to a higher design stress. From the hydrostatic test results shown in figures (3a) and (3b) it can be observed that in both pipes, failure has initiated in the areas close to the end caps because of the stress concentration from the sharp edges of the end caps that prevent the pipe in these areas from the expansion as well as the presence of scratches due to gripping effect of type A end cap. It was also observed that the failure due to hydrostatic pressure proceeds at 45^o with respect to the pipe axis, and this is not the usual case of PVC-U pipes. This behavior may be attributed to the percent of molecular orientation. There is almost around 50% orientation in the 45^o direction and is usually weaker than the hoop direction where the maximum stress occurs.

3.3 Finite Element Analysis

The objective of the numerical analysis was to investigate and visualize the effect of hydrostatic pressure on the PVC-O pipe material in the three directions (0^o, 45°, and 90^o) and the stress distribution along the pipe. The analysis evaluated according to the Von Mises stress failure criterion, also known as the shear-energy theory or the maximum distortion energy theory as expressed by equation (3) (Shigley, 2011) . Numerical results of stresses are tabulated in the table (2) and compared with the experimental results. From the results obtained, it is shown that the experimental results show a good agreement with the FEA results for both pipes of different end caps. The relative difference is expressed by equation (4) (Nazhad et al, 2020) at locations where the effect of end caps is not considered.

$$\sigma_v = \sqrt{\frac{1}{2}[(\sigma_1 - \sigma_2)^2 + (\sigma_2 - \sigma_3)^2 + (\sigma_3 - \sigma_1)^2]} \geq \sigma_y \quad (3)$$

$$\Delta R = \left|\left(\frac{Exp. - FEA}{Exp.}\right) 100\%\right| \quad (4)$$

σ_v = Von Mises stress (MPa).

σ_1, σ_2, σ_3 = Principle stresses (MPa).

For thin wall cylinder $\sigma_3=0$.

σ_y = Yield stress (MPa).

ΔR = Relative difference

From the FE analysis of the hydrostatic test shown in figure (7), it can be seen that the type of the end cap has a great influence on the magnitude of stress in the 0^o and 45^o directions as shown in figure 7a through 7d except for the stress in hoop direction which remain very close to each other for both types of end caps as shown in figures (7e) and (7f). Comparing the longitudinal stresses in figures (7a) and (7b), it can be seen that for type (A) end cap, the longitudinal stress has increased by 42.75% compared with type (B) end cap since there is no longitudinal thrust involved in the type B end cap. Similar behavior is observed for figures (7c) and (7d), and the stress at angle 45^o for type A end cap is greater by the amount of 16.13% compared with type B end cap. While for the circumferential direction, the magnitude of stress for type A end cap is larger by an amount of only 1% compared with Type B.

Stress distribution along the pipe length and the effect of stress concentration due to end caps can be clearly seen in figures (8), (9), and (10) in all the three directions. It's very obvious that end caps affect the stress intensity around the pipe, especially in the 0^o and 45^o. Pipe failure during the hydrostatic test shown in figure 3b is believed to be initiated from the points of stress concentration near the edges of the end caps and propagated at angle of 45^o with respect to the pipe axis.

There is a good agreement between FE stress analysis especially for type A end cap and the tensile test results as shown in table 2, the relative difference is 4.96, 5.16, and 0.06 in the 0^o, 45^o, and 90^o respectively. While for type B end caps the relative difference is much higher except in the 90^o direction which is almost near 1%. This is attributed to the fact that both types of end caps act differently on the pipe when it's under pressure. The restricted longitudinal movement of the pipe when using type B end cap has greatly affected stress distribution along the pipe body especially in the 0^o and 45^o direction and led to increase the relative difference when compared with experimentally determined tensile strength at those directions. While for Type A end cap, the pressure thrust acting on both ends of the pipe when its under its ultimate internal pressure capacity of 6.2MPa; resulted in the proper stress distribution and minimized the relative difference due the fact that the stress reached its maximum permissible value in all the directions.

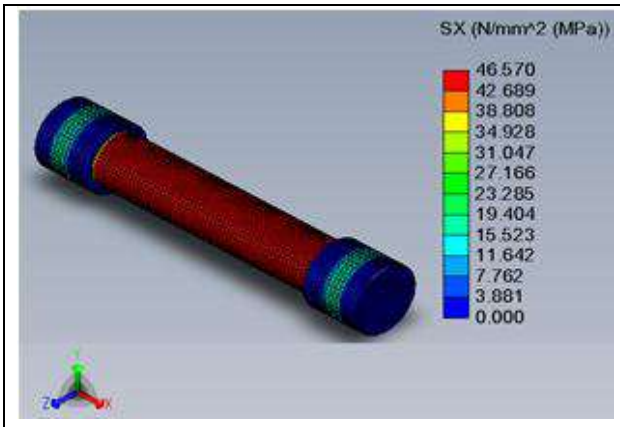

(a) - Longitudinal stress (Type A end cap).

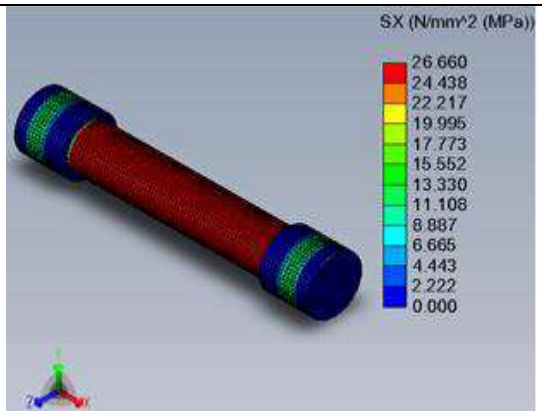

(b) - Longitudinal stress (Type B end cap).

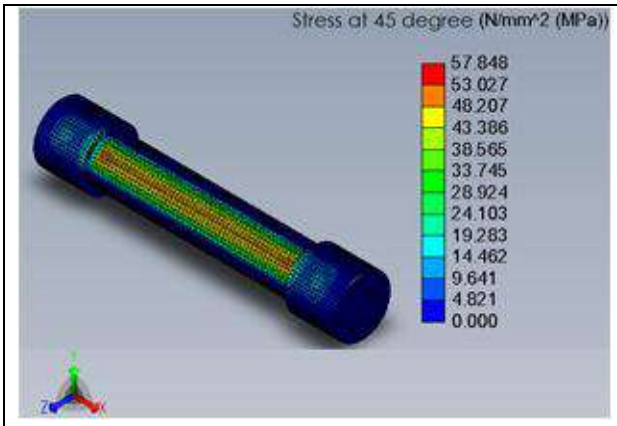

(c) - Stress at 45^{o} angle (Type A end cap).

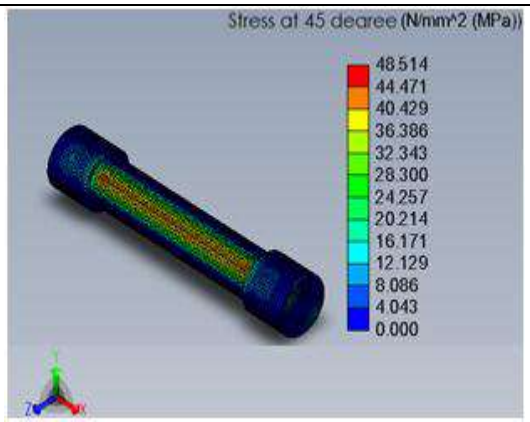

(d) - Stress at 45^{o} angle (Type B end cap).

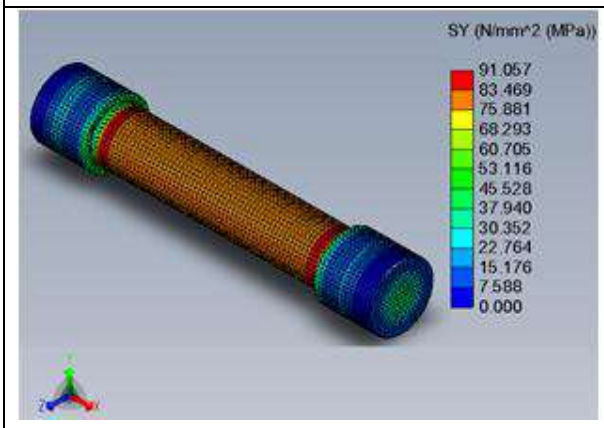

(e) - Circumferential stress (Type A end cap).

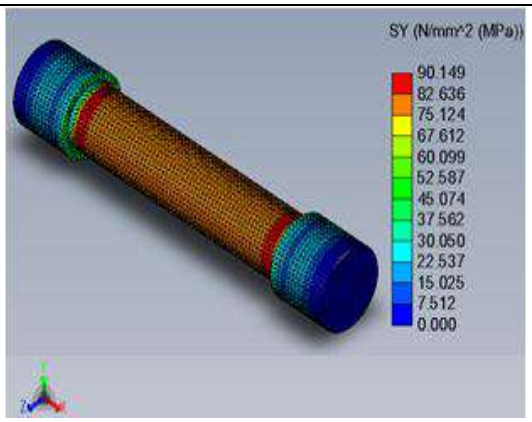

(f) - Circumferential stress (Type B end cap).

Figure (7). Finite element analysis of stress distribution during the hydrostatic test at 6.2MPa internal pressure.

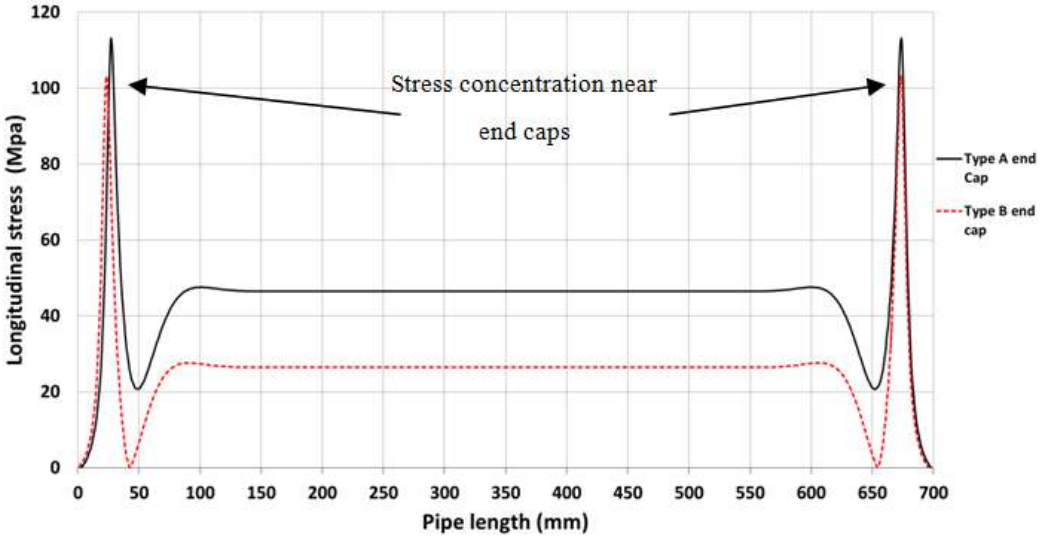

Figure (8). Distribution of longitudinal stress along the pipe (0^{o}- direction).

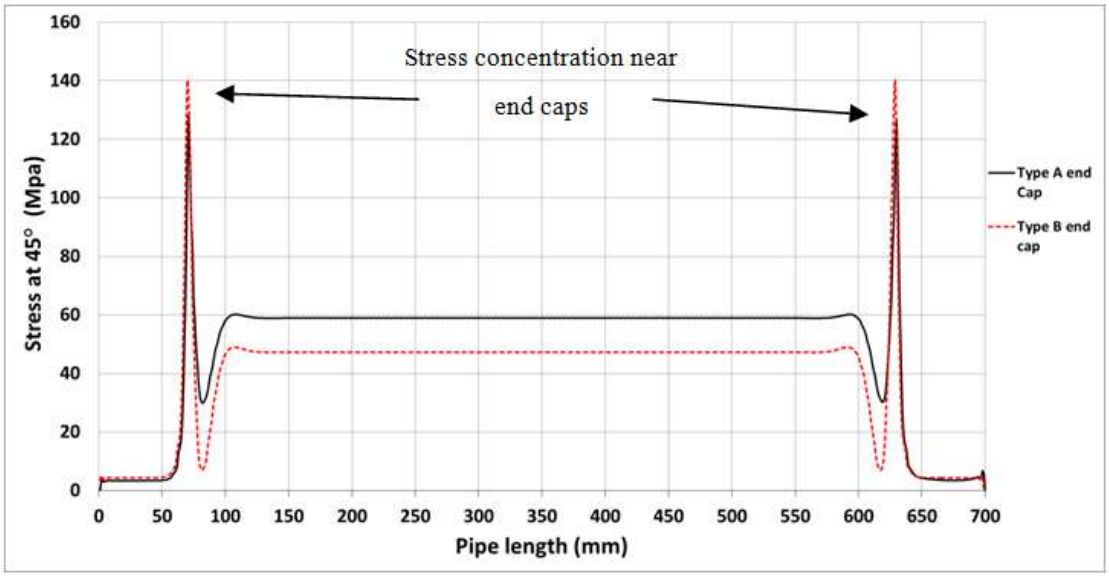

Figure (9). Distribution of Stress at an angle of 45° along the pipe.

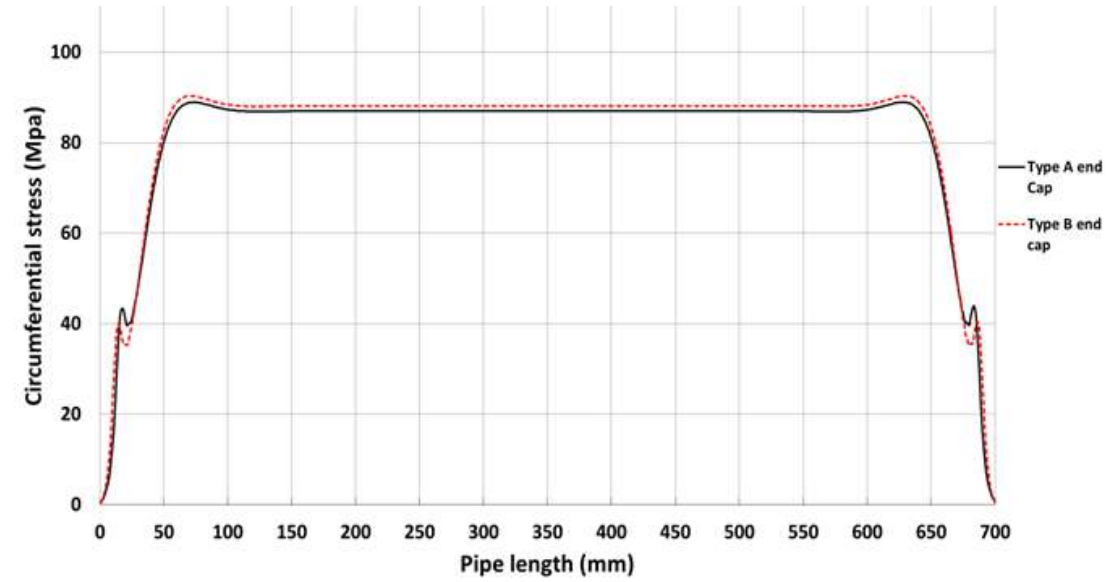

Figure (10). Distribution of circumferential (hoop) stress along the pipe (90^{o}-direction).

4.CONCLUSIONS

Tensile properties and hydrostatic behavior of PVC-O 500 pipes with two different end caps types (A and B) have been investigated experimentally and numerically. The core of the present work is to examine the effect of molecular orientation on the mechanical properties (tensile strength, circumferential resistance, and elongation). Numerical and experimental results exposed that:

1- Molecular orientation has a significant impact on the pipe strength. By increasing

the molecular orientation in the direction of the hoop, the strength increased to 91MPa compared with the traditional strength of PVC-U pipes of 49MPa.

2- The ductility has dropped dramatically with increasing the percent of molecular orientation.

3- The FEA has showed a good agreement with experimental results with a maximum difference of about 5.16% in the direction 45^o angle for type A end cap.

4- The FE results also showed that end caps affect stress distribution around the pipe during the hydrostatic test with a maximum difference occurred when using type B end caps.

5- It's also concluded that both types of end caps cause stress concentration near the edges of the caps which may affect experimental results and the actual burst pressure value of the pipe. Pipe failure during the hydrostatic test is believed to be initiated from the points of stress concentration near the edges of the end caps and propagated at angle of 45^o with respect to the pipe axis.

Finally, further research is recommended to study the effect of pipe diameter and pipe thickness of such material on hydrostatic behavior.

Acknowledgments
The authors feel grateful to the Mechanical and Energy Engineering Department – Erbil Polytechnic University for supporting this work.

Conflict of interests
The author declares that they have no competing interests.

Funding
The author declares that this paper does not have any funder.

REFERENCES

AWWA Manual. 2002. PVC Pipe Design and Installation, AWWA Manual M23, Second Edition.

Soran Saleem ALKAKI, Mete Onur KAMA N and Mohammedtaher MULAPEER . *1st International Conference on Engineering Technology and Applied Sciences Afyon Kocatepe University, Turkey 21-22 April 2016, PP785-792.*

ISO 16422:2006. Pipes and joints made of oriented unplasticized poly(vinyl chloride) (PVC-O) for the conveyance of water under pressure — Specifications

Molecor Tecnología. (2017), S.L., MOLECOR: Orienting the future, <www.molecor.com>.

UK Water Industry. 1999. Information Guidance Note, IGN 4-37-02, Design against surge and fatigue conditions for thermoplastic Pipes.

FERRANTE, M., CAPPONI, C., BRUNONE, B. & MENICONI, S. 2015. Hydraulic characterization of PVC-O pipes by means of transient tests. *Procedia Engineering,* 119**,** 263-269.

BAUER, D. E. 1994. Oriented pvc pipe (PVCO): experience and research. *Buried Plastic Pipe Technology: 2nd Volume.* ASTM International.

Purdue ECT Team. 2017. Technology to manufacture oriented PVC (PVC-O) pipes.

AWHAM, M. & SALIH, Z. G. M. 2011. A study of some mechanical behavior on a thermoplastic material. *Al-Nahrain Journal of Science,* 14**,** 58-65.

AHMAD, M., RAHMAT, A. R. & HASSAN, A. 2010. Mechanical properties of unplasticised PVC (PVC-U) containing rice husk and an impact modifier. *Polymers and Polymer Composites,* 18**,** 527-536.

ONITIRI, M. & ADENIYI, J. 2015. Effects of temperature on the compressive properties of extruded recycled unplasticized polyvinylchloride (uPVC) plastics under transverse compressive loading. *Journal of Raw Materials Research,* 2.

NIRMALA, R. & RAJKUMAR, R. 2016. Finite element analysis of buried UPVC pipe. *Indian Journal of Science and Technology,* 9**,** 1-5.

KUROWSKI, P. 2018. *Engineering Analysis with SolidWorks Simulation,* SDC publications.

WILLIAM D. CALLISTER, Jr. *Materials Science and Engineering An Introduction,* John Wiley &
Sons, Inc. EIGHTH E DITION 2015, p 643-650.

HALL, E.O, 1970. *Yield point phenomena in Metals and Alloys,* Plenum press, NEW YORK, p 18-26.

SHIGLEY, J. E. 2011. *mechanical engineering design,* Tata McGraw-Hill Education.

NAZHAD, A. H, ABDULLAH, S. S., HOSSEINI-HASHEMI, S., HUSSEIN, N. A., R. 2020b. Thermal stress and magnetic effects on nonlinear vibration of nanobeams embedded in nonlinear elastic medium. Journal of Thermal Stresses, 1-17.

Promains TOM PVC-O. (2012). Technical Guide AS/NZS 4441.

Figure captions:

ZANCO Journal of Pure and Applied Sciences
The official scientific journal of Salahaddin University-Erbil
https://zancojournals.su.edu.krd/index.php/JPAS

ISSN (print):2218-0230**, ISSN (online):** 2412-3986**, DOI: http://dx.doi.org/10.21271/zjpas**

RESEARCH PAPER

EFFECT OF COATING ON THE SPECIFIC PROPERTIES AND DAMPING LOSS FACTOR OF ULTEM 1010

SARA M. AHMAD*, SAFEEN Y. EZDEEN

Mechanical Department, College of Engineering, Salahaddin University-Erbil, Erbil, Iraq

A B S T R A C T:

The dynamic analysis of the fused deposition modeling (FDM) products is one of the most important topics in investigation of 3D manufacturing nowadays. The purpose of this paper to present the dynamic properties of FDM parts made from ULTEM 1010 with different coating layer thicknesses. The coating process consists of two stages: physical vapor deposition (PVD) to pre-coat the samples with a thin layer of Cu and Cr to prepare samples for the next step, electroplating different layer thickness Cu an outer layer of Ni. COMSOL Multiphysics software is used for finite element analysis of the models for free and forced vibration. The results showed an increase in ultimate tensile strength and Young's modulus with increasing coating thickness. The effect of different coating layer thickness on the natural frequency and damping loss factor was studied. The scanning electron microscope was used to investigate the coating layers in tensile specimens after failure.

KEY WORDS: ULTEM 1010; Fused Deposition Modeling; Physical Vapor Deposition; Electroplating; Damping Loss Factor;
DOI: http://dx.doi.org/10.21271/ZJPAS.33.2.10
ZJPAS (2021) , 33(2);105-116 .

1. INTRODUCTION :

3D printing of polymers is widely used as a new cost-effective, efficient technology to produce a complex geometry structure (Singh, 2011, Bikas et al., 2016). In order to increase the quality and the flexibility of the prototype made by 3D printing the material properties must be improved. One of the methods to increase the strength of 3D parts is electroplating with different metal layers on the printed materials (Yang et al., 2015, Kannan and Senthilkumaran, 2014, Saleh et al., 2004). (Wang and Inman, 2013, Liu et al., 2017) mentioned that one of the essential properties that must be considered with increasing the strength of 3D printed parts is vibration suppression. Early mechanical failure by resonant vibration excepted in structures with lower damping. Therefore, stiffness and damping study of the systems are essential during the strengthening process of materials. (Taylor et al., 2018) studied the mechanical properties of ULTEM1010 to investigate of flexural behavior of ULTEM 1010. Different storage modulus and damping loss factor was presented by (Reichl and Inman, 2018), for various types of 3D printed materials. (Cuan-Urquizo et al., 2019, Mohamed et al., 2016, Bellini and Güçeri, 2003, Domingo-Espin et al., 2014) demonstrated the effect of the process condition on dynamic properties of the 3D printed product by FDM process using the theoretical model and experimental work. Many researchers have reported studies of the theoretical and empirical investigation of damping properties and natural frequencies of materials. They presented the effect of different parameters such as Poisson's ratio and modulus of elasticity on the natural frequencies and damping loss factor (Vitaliy et al., Vergassola et al., 2018, Al-Jumaily and Jameel,

* **Corresponding Author:**
SARA M. AHMAD
E-mail: sara.ahmad@su.edu.krd
Article History:
Received: 26 / 10/2020
Accepted: 07/11/2020
Published: 18 /04 /2021

2000, Xu and Deng, 2016, Chirikov et al., 2020, Abbasloo and Maheri, 2018, Mohammed, 2017).
(Ge et al., 2020), studied the damping properties of a 3D printed photopolymer. They used impact loading that was caused by extreme damping. (Gietl et al., 2018), investigated 3D printed parts' damping properties measured and compared with the manufacturer's values. They use the COMSOL Multiphysics software to design samples by predicting eigenvalues or bending modes for cantilever beams.
This work present the effect of coating on the samples of ULTEM 1010 manufactured by fused deposition modeling. The mechanical properties were obtained from the tensile test for all models. The data from the experimental work used in the COMSOL Multiphysics software for determining the damping loss factor of the coated samples. The vibration tests were performed for pieces of the base material to validate the COMSOL Multiphysics software results.

2. EXPERIMENTAL METHODOLOGY

ULTEM 1010 samples for tensile and vibration tests were manufactured using a fused deposition manufacturing process by the 3D-Fabrica company (Turkey). Fifty tensile test specimens were made in x and y directions according to ASTM D638 type v. The beams with a dimension of 300×20×5 mm were produced for vibration analysis test. The experimental part of this study includes five experiments.

- First, the coating processes were performed on the sample groups, as indicated in Table 1. The coating process consists of two stages spattering physical vapor deposition (PVD) to pre-coat samples with thin layers of Cr(30nm) and Cu(200nm) and electroplating of the models with different layer thickness Cu and an outer layer of 2μm Ni. The PVD process and electroplating were performed by the FHR Centrotherm group and Galvanoform Companies in Germany.
- The second experiment was the tensile tests. A tensile test machine type "Karmmrath & Weiss Dortmund" with 10 kN capacity was used to perform tensile tests.
- In the third experiment, a field emission gun scanning electron microscope was used to study the specimens' coating layer. All second and third experiments were conducted at Freiberg University-Germany.
- The fourth and fifth experiments were free and forced vibration analysis of the provided samples. An impact hammer type 8206 B&K and an exciter type 5961 B&K were used to carry out free and moved vibration tests. An accelerometer type 4507 B&K and load cell type 8230 B&K used to measure acceleration and force. Then all data transmitted through a Module type 3560 B&K for analyzing as shown in figure 1.

Table 1. Sample sets for coating process

Thickness of coating (μm)		No of specimens		
Cu layer	Ni layer	x-direction	y-direction	z-direction
0	0	5	5	5
100	2	5	5	0
150	2	5	5	0
200	2	5	5	0
250	2	5	5	0

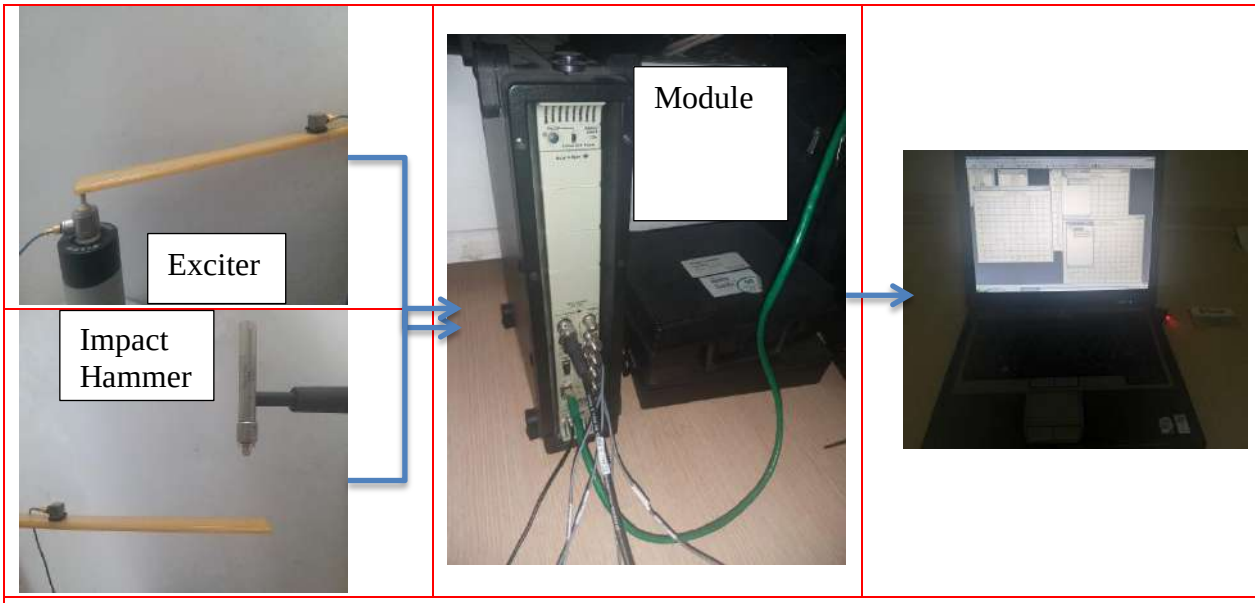

Figure 1 The experimental setup of a beam in free and forced vibration

3. FINITE ELEMENTMODELING

The finite element modeling FEM was performed using the COMSOL Multiphysics software for free and forced vibration analysis. A beam of 300mm long, 20mm width, and 5mm thickness with geometry properties of total surface area 0.015m^2 and center of mass (0.15, 0.01, 0.0025)m was created. The material properties were obtained from the experimental procedure for ULTEM 1010. Eight thousand two hundred sixty-eight elements with 41415 degrees of freedom were made in the beam's meshing, as shown in figure 2. The left end of the beam was constrained to satisfy the cantilever beam's boundary condition. A nodal force applied on the free end of the beam with a frequency variation of 0.1 Hz/Sec during forced vibration analysis. The damping loss factor was obtained from the results using the half-power bandwidth method.

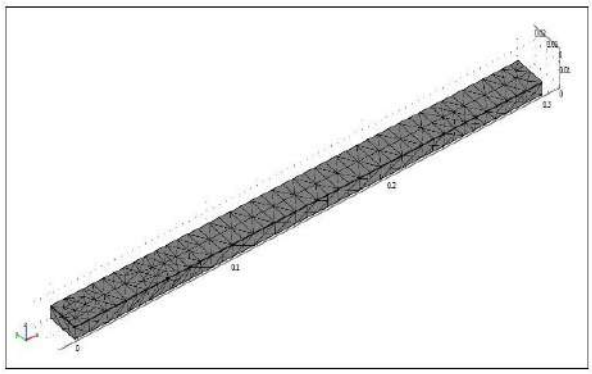

Figure 2.a The finite element model of a beam in COMSOL multiphysics software

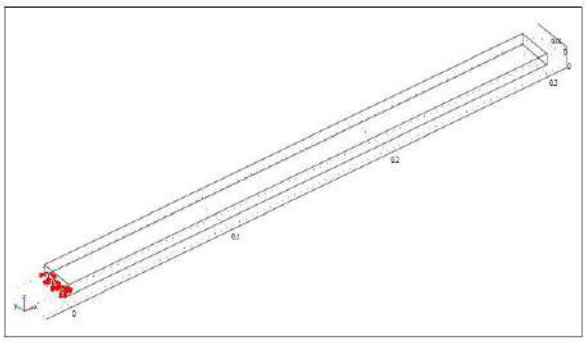

Figure 2.b The boundary condition of a beam in COMSOL multiphysics software

4. RESULTS AND DISCUSSION

Figure 3 shows the stress-strain diagram for ULTEM 1010 samples made by fused deposition modeling in x, y, and z-directions. It resulted from the stress-strain charts that the strength in x and y-directions were high in comparison with the samples made in the z-direction. The production of parts in the z-direction is more time-consuming and costly than the manufacturing in the x and y-directions.

The stress-strain diagrams for the coated samples were shown in figures 4 and 5 for the models made in x and y-directions, respectively. Ultimate tensile strength, modulus of elasticity, Poisson's ratio, and ductility can be obtained from the stress-strain diagrams for all cases. The five samples were electroplated for each coating thickness then tested.

The coating thickness layer's effect on the ultimate tensile strength of ULTEM 1010 is presented in figure 6. The results were conducted in the increasing of maximum tensile strength with an increasing layer thickness of Cu. The strength of ULTEM 1010 was increased by 175% for samples made in the x-direction and 162% for models in the y-direction, where the pieces coated by 250 μm Cu and 2μm Ni.

Figure 7 illustrates the effect of electroplated thickness on Young's modulus. The modulus of elasticity increased with the increasing of coating layers. The largest value of coating layer thickness resulted in the highest modulus of elasticity.

The scanning electron microscope images for the tensile tested samples' fracture surface are shown in figure 8. Good adhesion between the layers and the base materials that effected in high strength of the coated pieces can be observed. Also, it was apparent that the thickness of copper and nickel layers decreased due to the plastic deformation when indicated the high ductility of the coated samples in comparison with the base material ULTEM 1010.

Table 2 presented Young's modulus's values, and Poisson's ratio was obtained from the tensile test. These results were used for the finite element modeling in the COMSOL Multiphysics software. Damping loss factor (DLF) was determined using the half-power bandwidth method. The natural frequency must be determined firstly in the procedure of calculating the damping loss factor. In the COMSOL Multiphysics software, Eigen-frequency solution was used to find the natural frequency of all samples. The natural frequency obtained from the experimental impact hammer test was used to validate the COMSOL Multiphysics software results. The natural frequencies for base materials were brought in practical tests were 13.7 and 14 Hz for samples made in x and y-direction, respectively. These results agreed with the COMSOL Multiphysics software results, 13.4 and 13.6 Hz, for the models in x and y-directions. Frequency response solutions used to determine the damping loss factor in the COMSOL Multiphysics software — the data from the COMSOL Multiphysics software transferred to MATLAB the damping loss factor calculated using the half-power bandwidth method.

The results from forced vibration in the experimental method obtained and damping loss factor calculated in the same way used in finite element modeling in the COMSOL Multiphysics software. The damping loss factor for the base material ULTEM 1010 obtained from the COMSOL Multiphysics software was 0.004418 for samples made in the x-direction and 0.006096 for the models in the y-direction. The damping loss factor for the same material obtained in experimental tests was 0.004599for samples in the x-direction and 0.006475 for models in the y-direction. By comparing the results, a good agreement between the results from COMSOL Multiphysics software and experimental work can be observed. Table 3 shows the coated samples obtained from the COMSOL Multiphysics software for all models in x and y-directions. Damping loss factor increases for the coated pieces concerning the base material illustrated in figure 9. These results showed that the samples with a thickness of 150μm copper had the highest percentage value. Damping loss factor depended on mechanical properties such as modulus of elasticity, Poisson's ratio, and materials density. The variation of all aspects during the coating process caused in the most considerable value for samples with a 150μm copper thickness.

Table 2. Modulus of elasticity and Poisson's ratio for different samples.

The thickness of Cu coating (μm)	E-x direction (MPa)	E-y direction (MPa)	υ-x direction	υ-y direction
100	3215	3346	0.424	0.476
150	3912	3570	0.497	0.515
200	4121	4176	0.551	0.543
250	4319	4582	0.565	0.565

Table 3. First and second lateral frequencies from the COMSOL Multiphysics software.

Thickness of Cu coating (μm)	f1-x direction (Hz)	f1-y direction (Hz)	DLF-x direction	DLF-y direction
100	12.7	13.1	0.011142	0.007687
150	13.4	13.4	0.028687	0.011769
200	12.9	12.7	0.009147	0.008008
250	12.6	12.9	0.005302	0.008271

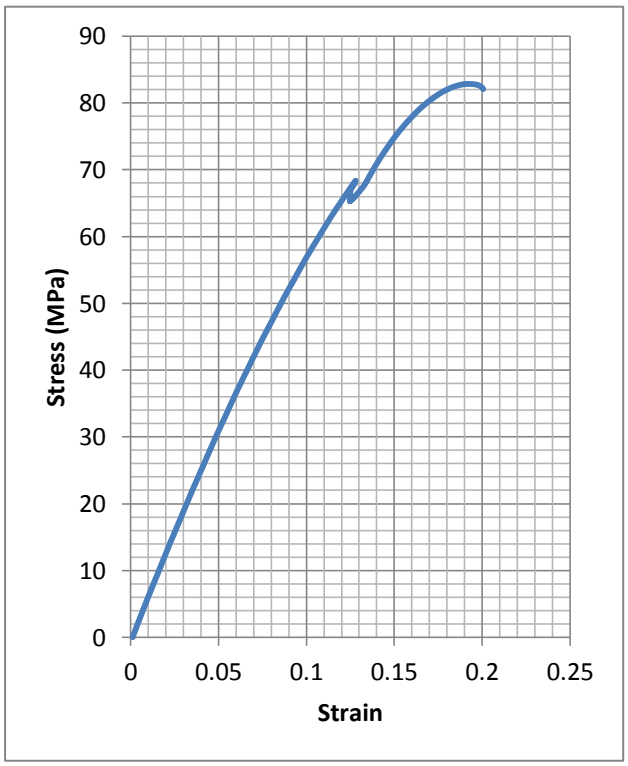

Figure 3-a. Strain-stress diagram for uncoated samples made in the x-direction.

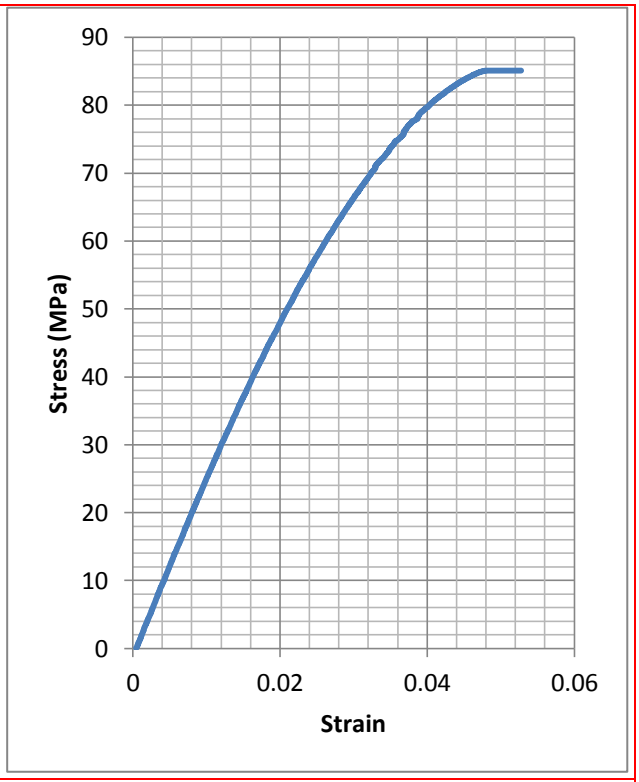

Figure 3-b. Strain-stress diagram for uncoated samples made in the y-direction

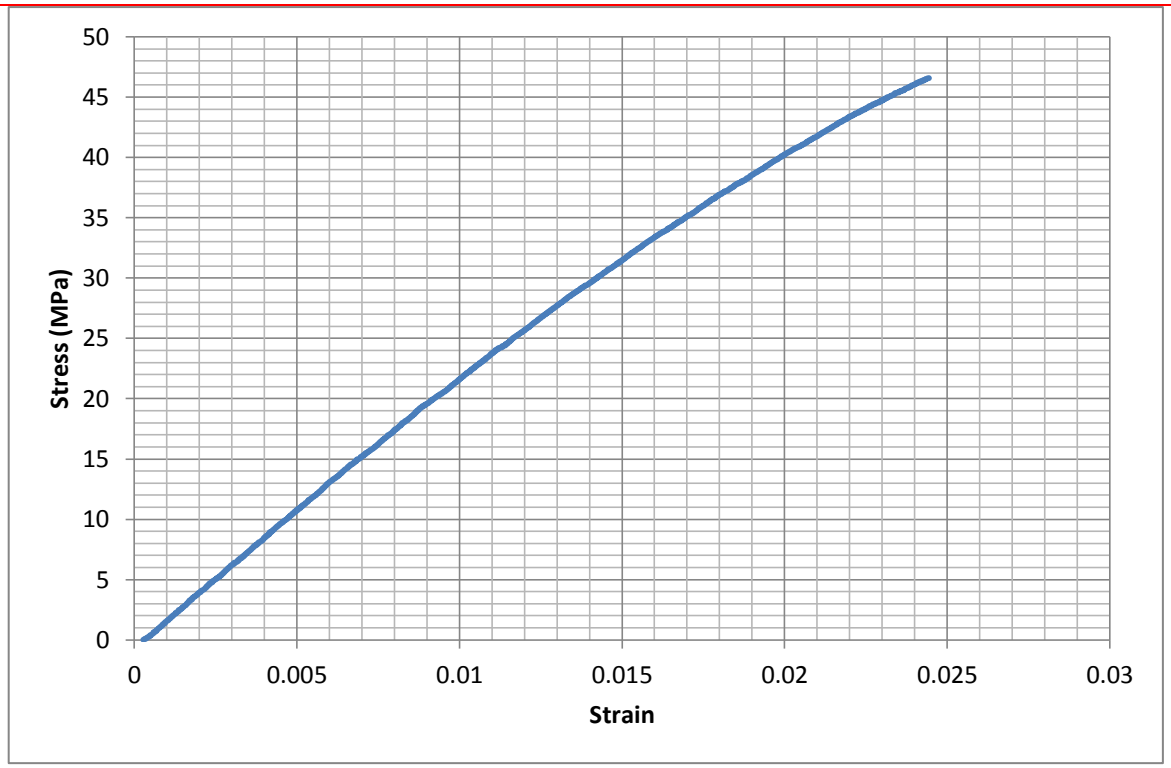

Figure 3-c. Strain-stress diagram for uncoated samples made in the z-direction

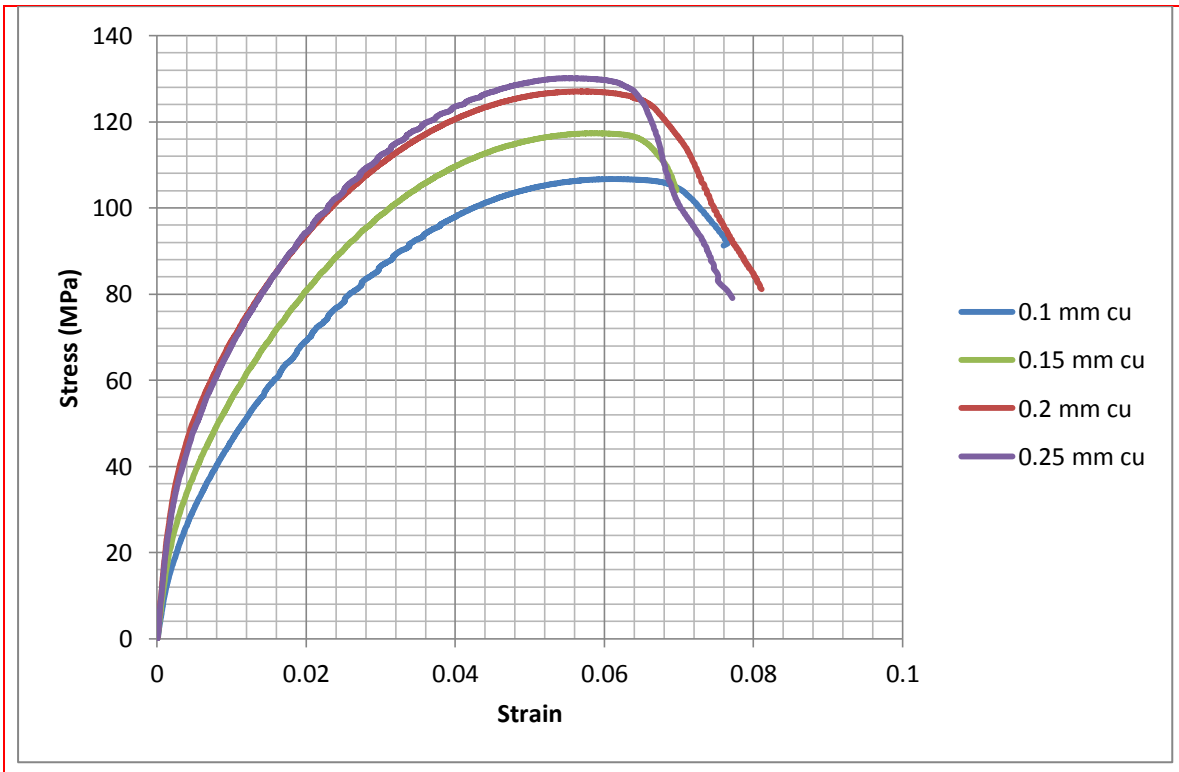

Figure 4. Strain-stress diagram for coated samples made in the x-direction

.

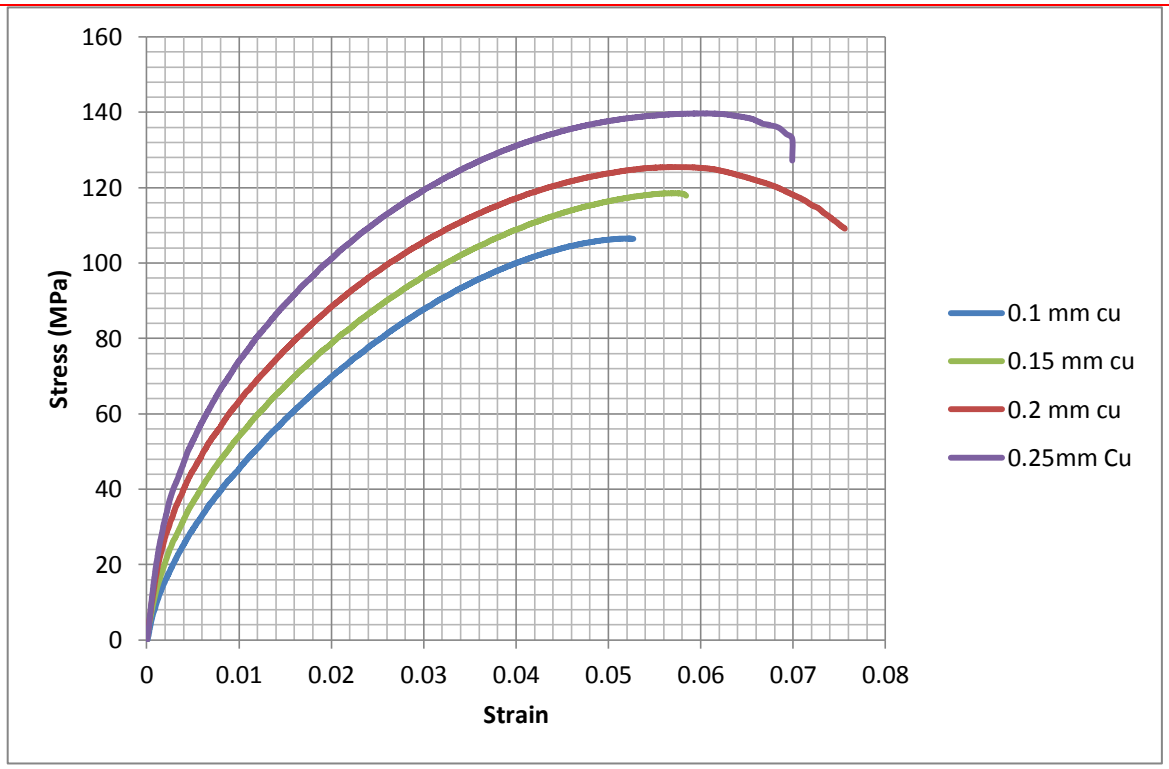

Figure 5. Strain-stress diagram for coated samples made in the x-direction.

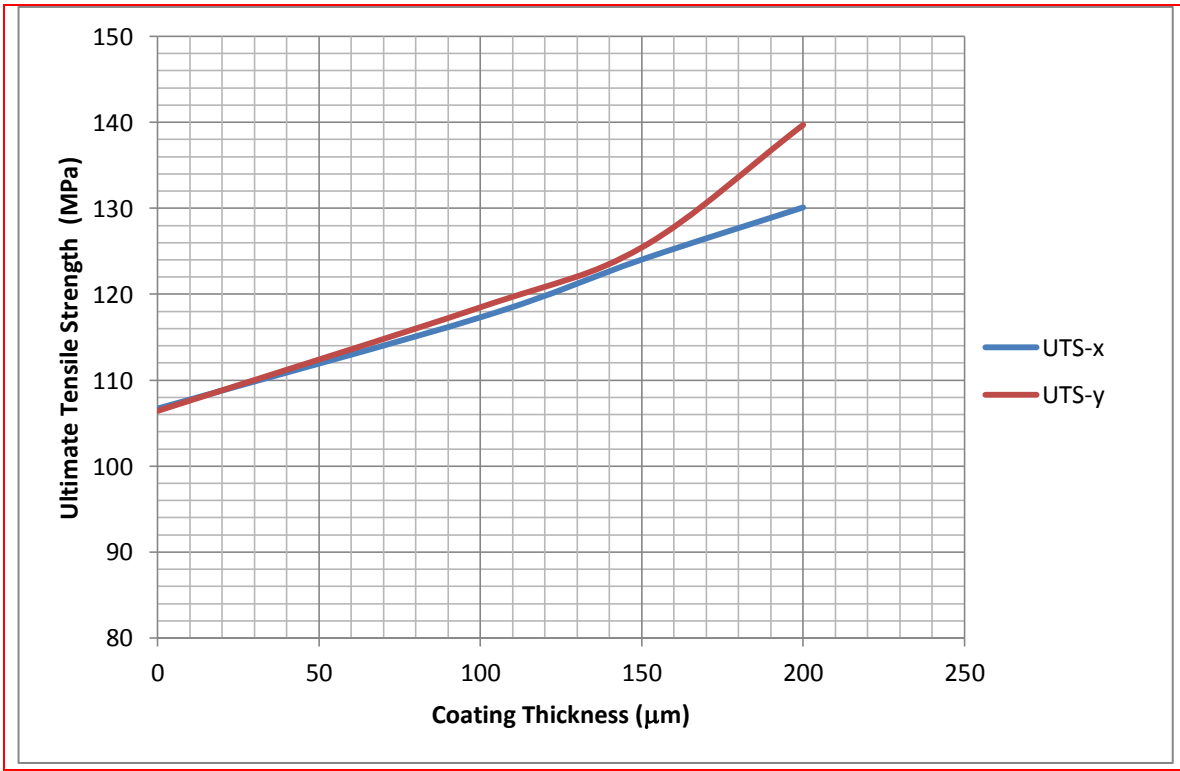

Figure 6. Ultimate tensile strength of samples with different coating thickness made in x and y-direction

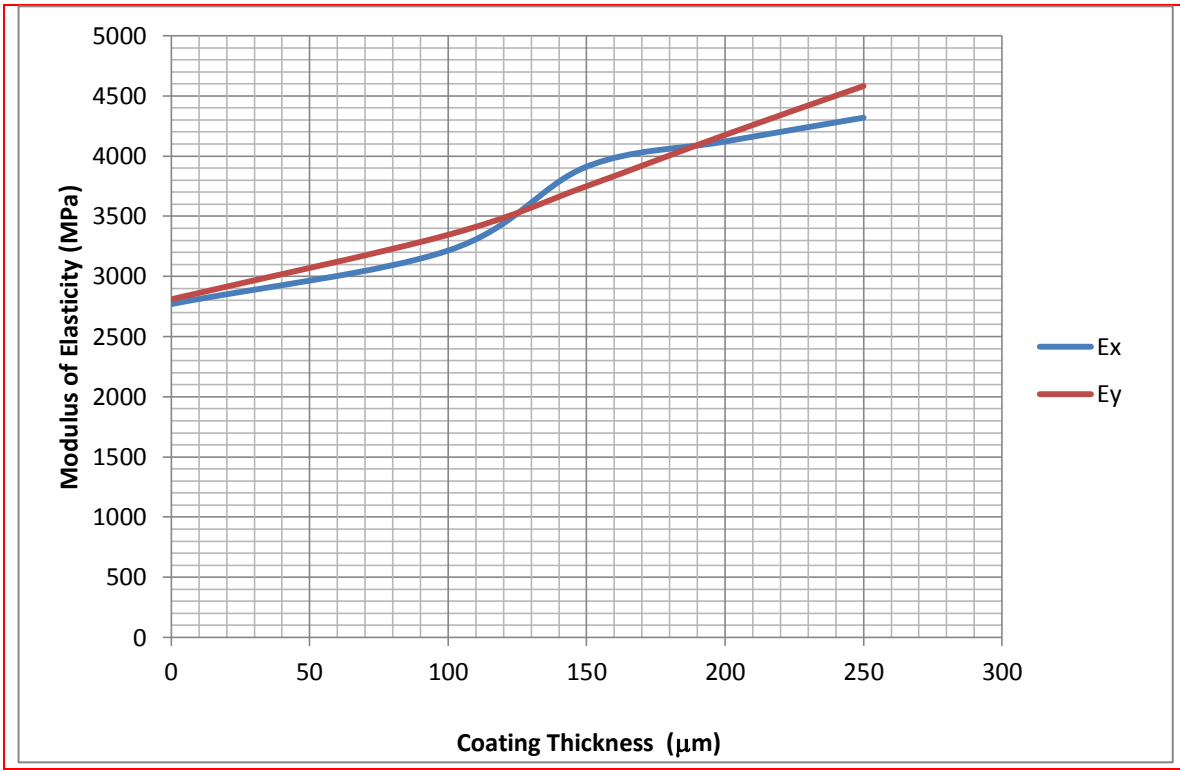

Figure 7. Modulus of elasticity for samples with different coating thickness made in x and y-direction

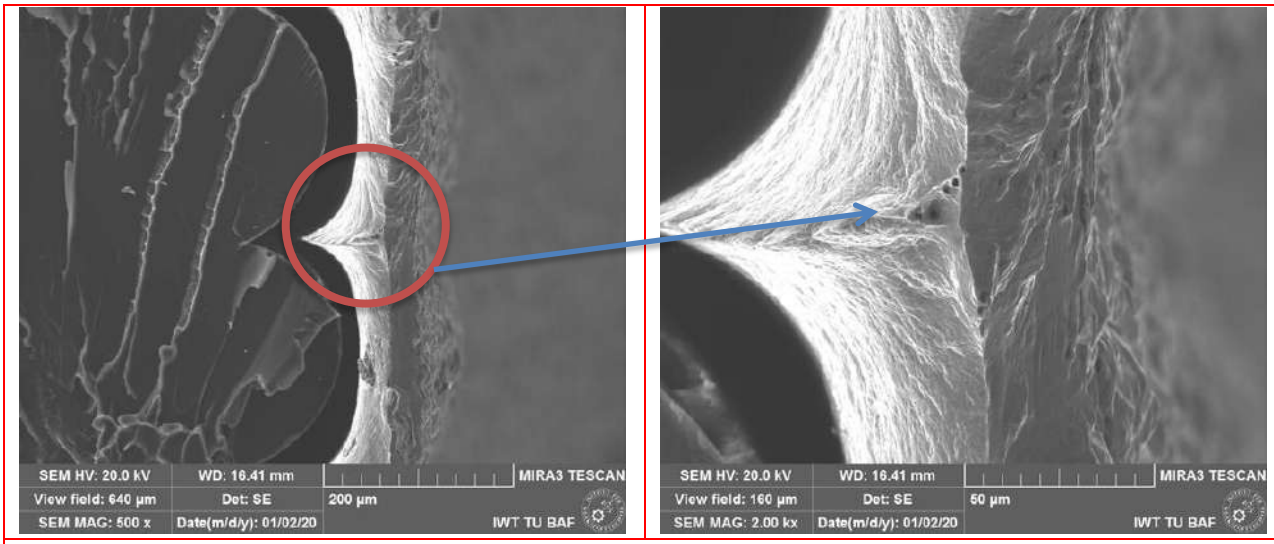

Figure 8-a. SEM image of the ULTEM 1010 coated with 100 µm Cu and 2 µm Ni.

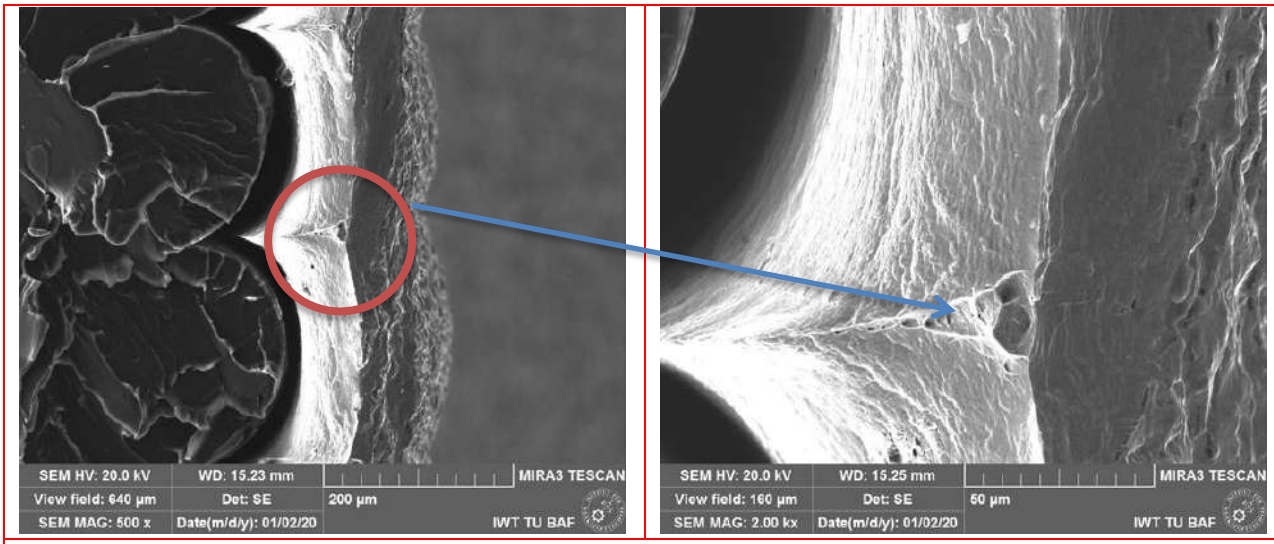

Figure 8-b. SEM image of the ULTEM 1010 coated with 150 µm Cu and 2 µm Ni.

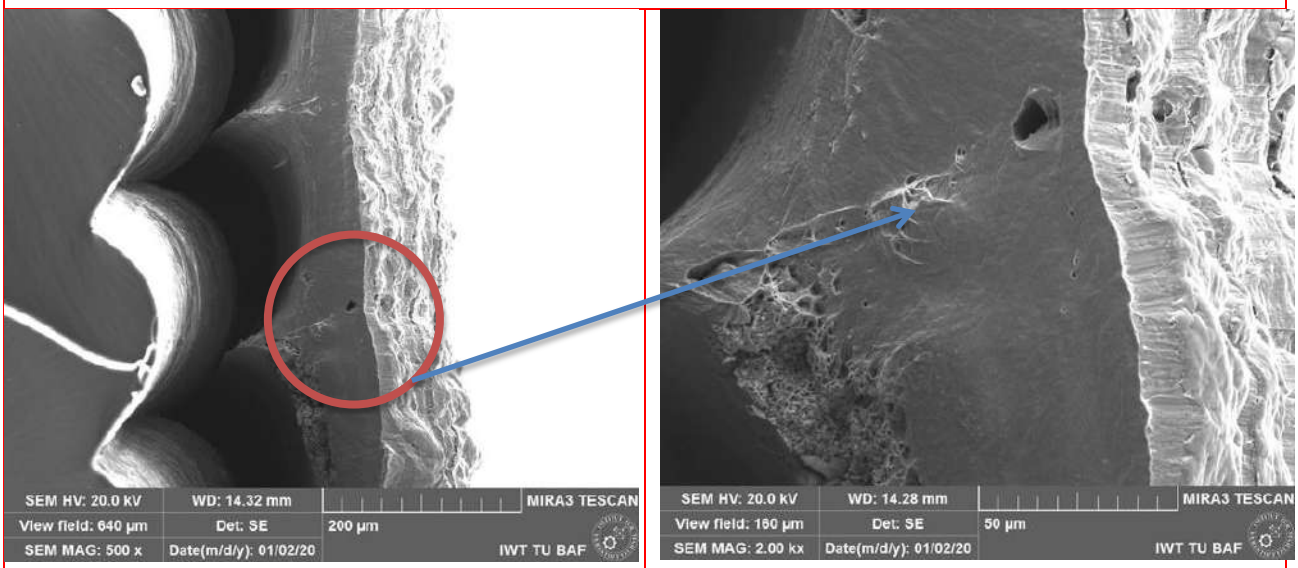

Figure 8-c. SEM image of the ULTEM 1010 coated with 200 µm Cu and 2 µm Ni.

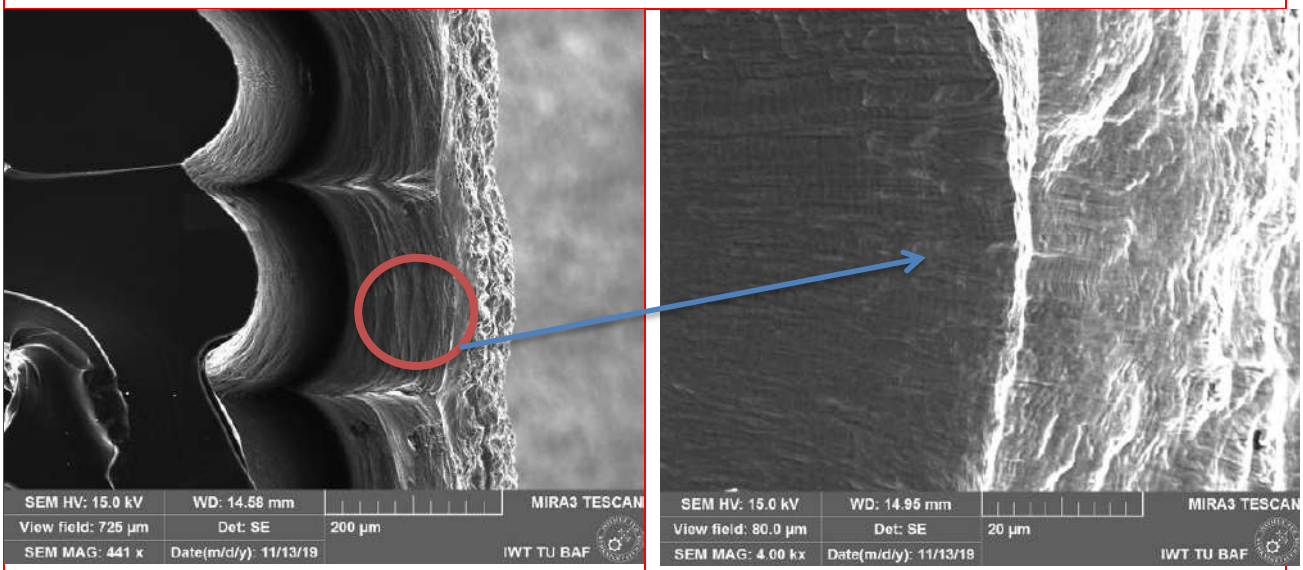

Figure 8-d. SEM image of the ULTEM 1010 coated with 250 μm Cu and 2 μm Ni.

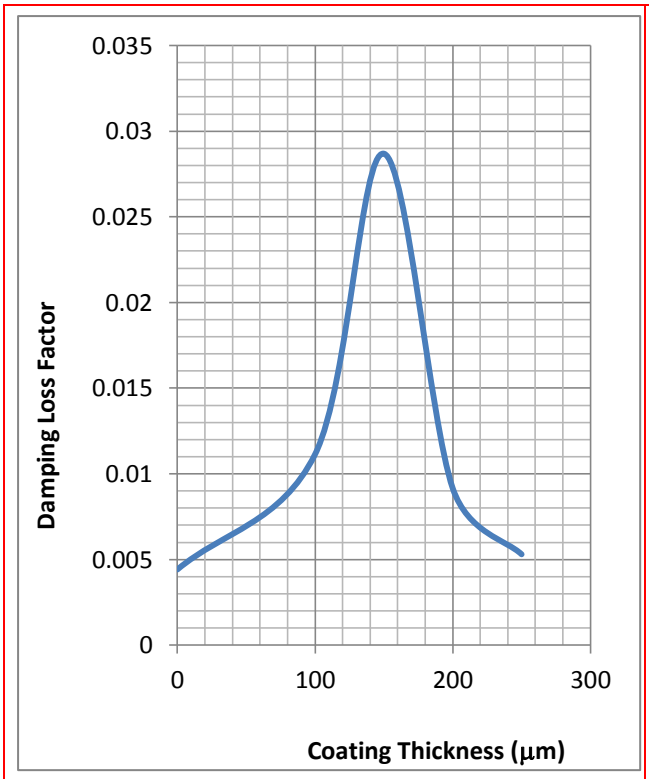

Figure 9.a Damping loss factor of coated samples made in the x-direction.

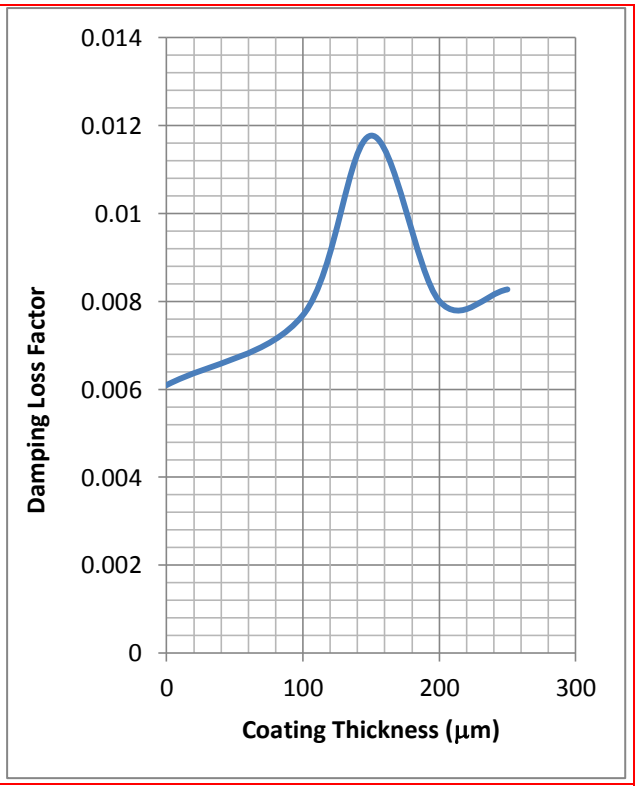

Figure 9.b Damping loss factor of coated samples made in the y-direction.

Figure captions

Figure 1 The experimental setup of a beam in free and forced vibration

Figure 2-a The finite element model of a beam in COMSOL

Figure 2.b The boundary condition of a beam in COMSOL multiphysics software

Figure 3-a. Strain-stress diagram for uncoated samples made in the x-direction.

Figure 3-b. Strain-stress diagram for uncoated samples made in the y-direction.

Figure 3-c. Strain-stress diagram for uncoated samples made in the z-direction.

Figure 4. Strain-stress diagram for coated samples made in the x-direction.

Figure 5. Strain-stress diagram for coated samples made in the y-direction.

Figure 6. Ultimate tensile strength of samples with different coating thickness made in x and y-direction.

Figure 7. Modulus of elasticity for samples with different coating thickness made in x and y-direction.

Figure 8-a. SEM image of the ULTEM 1010 coated with 100 μm Cu and 2 μm Ni.

Figure 8-b. SEM image of the ULTEM 1010 coated with 150 μm Cu and 2 μm Ni.

Figure 8-c. SEM image of the ULTEM 1010 coated with 200 μm Cu and 2 μm Ni.

Figure 8-d. SEM image of the ULTEM 1010 coated with 250 μm Cu and 2 μm Ni.

Figure 9-a. Damping loss factor of coated samples made in the x-direction.

Figure 9-b. Damping loss factor of coated samples made in the y-direction.

5. CONCLUSIONS

The results of tensile tests for the specimens of ULTEM 1010 manufactured by FDM were conducted in low mechanical properties in z-directions in comparison with x and y-directions. Therefore, the study performed on the samples in x and y-directions. PVD process was used to pre-coat the models with thin layers to prepare for electroplating materials with Cu and Ni layers. The tensile tests resulted in the highest ultimate tensile strength and modulus of elasticity for the layer thickness of 250 μm Cu and 2μm Ni. The data from the tensile tests used in the COMSOL Multiphysics software analyzed free and forced vibration to find the natural frequencies and damping loss factor. The maximum damping loss factor was obtained for the thickness of 150μm Cu and 2μm Ni. A comparison between the COMSOL Multiphysics software results and experimental tests showed a good agreement between the works.

Acknowledgments

The authors are grateful to the Freiberg University-Germany and Salahaddin University - Erbil for supporting this work.

Conflict of interests

The author declares that they have no competing interests.

Funding

The author declares that this paper does not have any funder.

References

ABBASLOO, A. & MAHERI, M. R. 2018. On the mechanisms of modal damping in FRP/honeycomb sandwich panels. *Science and Engineering of Composite Materials,* 25**,** 649-660.

AL-JUMAILY, A. & JAMEEL, K. 2000. Influence of the Poisson ratio on the natural frequencies of stepped-thickness circular plate. *Journal of sound and vibration,* 234**,** 881-894.

BELLINI, A. & GÜÇERI, S. 2003. Mechanical characterization of parts fabricated using fused deposition modeling. *Rapid Prototyping Journal*.

BIKAS, H., STAVROPOULOS, P. & CHRYSSOLOURIS, G. 2016. Additive manufacturing methods and modelling approaches: a critical review. *The International Journal of Advanced Manufacturing Technology,* 83**,** 389-405.

CHIRIKOV, V. A., DIMITROV, D. M. & BOYADJIEV, Y. S. 2020. Determination of the Dynamic Young's Modulus and Poisson's Ratio Based on Higher Frequencies of Beam Transverse Vibration. *Procedia Manufacturing,* 46**,** 87-94.

CUAN-URQUIZO, E., BAROCIO, E., TEJADA-ORTIGOZA, V., PIPES, R. B., RODRIGUEZ, C. A. & ROMAN-FLORES, A. 2019. Characterization of the mechanical properties of FFF structures and materials: A review on the experimental, computational and theoretical approaches. *Materials,* 12**,** 895.

DOMINGO-ESPIN, M., BORROS, S., AGULLO, N., GARCIA-GRANADA, A.-A. & REYES, G. 2014. Influence of building parameters on the dynamic mechanical properties of polycarbonate fused deposition modeling parts. *3D Printing and Additive Manufacturing,* 1**,** 70-77.

GE, C., CORMIER, D. & RICE, B. 2020. Damping and cushioning characteristics of Polyjet 3D printed photopolymer with Kelvin model. *Journal of Cellular Plastics***,** 0021955X20944972.

GIETL, J., VIGNOLA, J., STERLING, J. & RYAN, T. Characterization of Damping Properties in 3D Printed Structures. Journal of Physics: Conference Series, 2018. IOP Publishing, 012002.

KANNAN, S. & SENTHILKUMARAN, D. 2014. Investigating the influence of electroplating layer thickness on the tensile strength for fused deposition processed ABS thermoplastics.

International Journal of Engineering and Technology, 6**,** 1047-1052.

LIU, Y., YI, J., LI, Z., SU, X., LI, W. & NEGAHBAN, M. 2017. Dissipative elastic metamaterial with a low-frequency passband. *AIP Advances*, 7**,** 065215.

MOHAMED, O. A., MASOOD, S. H. & BHOWMIK, J. L. 2016. Experimental investigations of process parameters influence on rheological behavior and dynamic mechanical properties of FDM manufactured parts. *Materials and Manufacturing Processes*, 31**,** 1983-1994.

MOHAMMED, D. 2017. Effect of Fiber Angles on Dynamic Response of Cantilever Composite Beams. *ZANCO Journal of Pure and Applied Sciences*, 29**,** 157-163.

REICHL, K. & INMAN, D. 2018. Dynamic mechanical and thermal analyses of Objet Connex 3D printed materials. *Experimental Techniques*, 42**,** 19-25.

SALEH, N., HOPKINSON, N., HAGUE, R. J. & WISE, S. 2004. Effects of electroplating on the mechanical properties of stereolithography and laser sintered parts. *Rapid prototyping journal*.

SINGH, R. 2011. Process capability study of polyjet printing for plastic components. *Journal of mechanical science and technology*, 25**,** 1011-1015.

TAYLOR, G., WANG, X., MASON, L., LEU, M. C., CHANDRASHEKHARA, K., SCHNIEPP, T. & JONES, R. 2018. Flexural behavior of additively manufactured Ultem 1010: experiment and simulation. *Rapid Prototyping Journal*.

VERGASSOLA, G., BOOTE, D. & TONELLI, A. 2018. On the damping loss factor of viscoelastic materials for naval applications. *Ships and Offshore Structures*, 13**,** 466-475.

VITALIY, P., VYACHESLAV, F., IBRAHIM, G. & VICTOR, S. THEORETICAL-EXPERIMENTAL METHOD FOR INVESTI-GATING THE DAMPING PROPERTIES OF MATERIALS.

WANG, Y. & INMAN, D. J. 2013. Finite element analysis and experimental study on dynamic properties of a composite beam with viscoelastic damping. *Journal of Sound and Vibration*, 332**,** 6177-6191.

XU, X.-J. & DENG, Z.-C. 2016. Closed-form frequency solutions for simplified strain gradient beams with higher-order inertia. *European Journal of Mechanics-A/Solids*, 56**,** 59-72.

YANG, S., TANG, Y. & ZHAO, Y. F. 2015. A new part consolidation method to embrace the design freedom of additive manufacturing. *Journal of Manufacturing Processes*, 20**,** 444-449.

ZANCO Journal of Pure and Applied Sciences
The official scientific journal of Salahaddin University-Erbil
https://zancojournals.su.edu.krd/index.php/JPAS

ISSN (print):2218-0230**, ISSN (online):** 2412-3986**, DOI: http://dx.doi.org/10.21271/zjpas**

RESEARCH PAPER

Shear Strength of Reinforced High-Performance Concrete Wide Beams

BARZAN OMAR MAWLOOD[1], AHMED HEIDAYET MOHAMMAD[2], NAWAL M. ABDULRAZZAQ[3], and KAMARAN S. ISMAIL[4]

[1]Department of Civil Engineering, College of Engineering, Salahaddin University-Erbil, Kurdistan Region, Iraq
[2]Department of Civil Engineering, College of Engineering, Salahaddin University-Erbil, Kurdistan Region, Iraq
[3]Department of Civil Engineering, College of Engineering, Salahaddin University-Erbil, Kurdistan Region, Iraq
[4]Department of Civil Engineering, College of Engineering, Soran University, Kurdistan Region, Iraq Iraq

A B S T R A C T:
Wide shallow beams have become more common among structural designers since having more space for utility services under the floor. However, the provisions of codes of practice need to be evaluated against an experimental data to evaluate their margin of safety for this type of structural element. This paper is an experimental and theoretical investigations on the shear behavior and capacity of wide shallow beams. A total of seven beam specimens were tested to assess the effect of beam width to height ratio (b/h) which ranged from 0.67 to 3; shear reinforcement ratio ranging from 0 to 0.222%; and carbon fiber content ranging from 0 to 0.53%. The results show that with increasing width to height ratio, the shear strength of the beam decreased and the provisions of codes of practice (ACI318-14 and EC2) might not lead to accurate results when they are used to predict the shear capacity of wide shallow beams.

KEY WORDS: Shear strength; wide shallow beam; web reinforcements; high strength concrete; width to height ratio; fibers.
DOI: http://dx.doi.org/10.21271/ZJPAS.33.2.11
ZJPAS (2021), 33(2);117-127.

1. INTRODUCTION:

Although the utilization of wide shallow beams in structural buildings is not new, in recent years its use is more common. The main idea of using this type of structural member is to have more space for utility services such as ventilation ducts, sewage pipes, and water supply pipes. Flat slab is also useful for these purposes, but it has punching shear problems when encounter for heavy loadings. For heavily loaded slab, beams are normally used between columns to control bending and deflection. However, for normal depth beams, sometimes, the utility services need to pass through the section due to height limitations. These holes could weaken the beam in shear or bending. Therefore, the answer is to use wide shallow beams to compensate for all aforementioned problems. Additionally, using wide shallow beams means decreasing story height, which in turns decreases the overall height of the building.

In the literature, different researchers tried to investigate the behavior of wide beams experimentally and theoretically. Based on the experimental results of wide beams, Sherwood et al (Sherwood et al., 2006) concluded that member width has no significant effect on shear stress at failure. Depending on their experimental works on wide beam, Lubell et al (Lubell et al., 2009) concluded that stirrup efficiency decreased significantly as the stirrup legs spacing across the width is increased. They also concluded that, the capacity of the members with well distributed shear reinforcement could be safely predicted by ACI shear model. Shuraim and Al-Negheimish

* **Corresponding Author:**
BARZAN OMAR MAWLOOD
E-mail: barzan.mawlood@su.edu.krd
Article History:
Received: 15/09/2020
Accepted: 08/12/2020
Published: 18/04 /2021

(Shuraim & Al-Negheimish, 2011) concluded that the distribution of the moments in wide beam was found to not match what is usually assumed in the design practice, as indicated in ACI-318 and EC-2. Therefore, a new evaluation of the moment distribution is needed to satisfy strength and serviceability criteria. Working on the high strength concrete were the efforts of many researchers that concluded and gave advantages on this type of material (Yousif et al., 2004; Saeed et al., 2007). The contribution of web reinforcement in shear strength of wide beam using normal and high strength concrete was studied by Hanafy el al (Hanafy et al., 2012), the results showed that, the effect of web reinforcement on the shear strength is more pronounced in beams with normal concrete compressive strength than beams made from high strength concrete. Lubell et al (Lubell et al., 2009), Shuraim and Al-Negheimis (Shuraim & Al-Negheimish, 2011) and Lotfy et al (Lotfy et al., 2014) found that the configuration of the stirrups (beams with constant stirrups ratio) has an influence on the shear strength, four legs configuration showed high increase in its efficiency to resist shear force over stirrups with two legs configurations.

Conforti and Plizzari (Conforti et al., 2013) demonstrated experimentally that, the effect of wide beam with relatively low steel fiber content increase significantly the shear capacity and ductility. So, the fibers were more prominent in wide shallow beams than in deep beams. Conforti el al (Conforti et al., 2015; Conforti et al., 2017) conducted an experimental investigation on wide and deep beams examining the effect of shear reinforcement and polypropylene fibers. The result showed that the polypropylene fiber can be used to totally replace the shear reinforcement in wide beams.

Self-compacting concrete (SCC) is a special type of concrete which consolidate (i.e., compacting) under its own weight, has a high flowability property during freshen stage, eliminating external mechanical vibration process during filling of forms, which in turns reducing labors cost. This type of concrete is very suitable for areas with congestion reinforcements (like beam-columns joints), permit the concrete to fill complex formwork. The additional works can be faced during casting is induced of voids that occur in the normal concrete especially in columns; this can be reduced or eliminated by SCC.

For design and analysis purposes, structural engineers and designers follow the procedure and provisions of building codes of practice such as ACI 318-14 (ACI Committee 318, 2014) and EC2 (Eurocode-2, 2004). However, the shear provisions of these codes are based on experimental and theoretical investigations that conducted primarily on beams with normal depth to height ratio. These provisions need to be evaluated to examine their margin of safety when applied to wide shallow beams made with high strength concrete. Thus, the current research is to provide an experimental investigation of the shear behavior of wide shallow beams made with high performance concrete (HSC and SCC). Additionally, it tries to assess the aforementioned codes provisions experimentally for wide shallow beams based on experimental results from this and other researches.

2. SPECIMENS PREPARATION AND TEST SETUP

A total of seven beam specimens were cast using ready mix concrete. Five of these specimens were cast with targeted compressive strength of 90 MPa and without discrete fibers. The other two specimens were cast with discrete fibers (low and medium content), more details, can be found in Table 1.

The investigated parameters are: width to overall height ratio (b/h) of the beams; shear reinforcement ratio and ration of discrete fibers. The reinforcements were positioned so that the beams tested as propped cantilever beams as shown in Fig.1. The main flexural reinforcement $\emptyset 20$ mm was used at the top of the cross section and cross bars were welded to the end of the longitudinal bars to prevent bond failure prematurely at end the test. All the specimens were cast without shear reinforcement except WB-4 and WB5 which they reinforced with $\emptyset 8@200$ mm and $\emptyset 8@100$ mm, respectively. The steel properties are given in Table 2. The beams were designed to fail in shear; therefore, the flexural reinforcement ratios used were higher than the maximum permissible ratio (i.e., ε_t less than 0.004) according to ACI 318-14 to prevent flexural failure.

Table (1) Beam properties with variable included in experimental works.

Specimen No.	*b* (mm)	*b/h*	Stirrups	V_f (%)	Top longitudinal bars	ρ_w (%)
WB-1	100	0.67	0	0	2-Ø20mm	5.50
WB-2	300	2	0	0	4-Ø20mm	3.67
WB-3	450	3	0	0	6-Ø20mm	3.67
WB-4	450	3	Ø8@200mm	0	6-Ø20mm	3.67
WB-5	450	3	Ø8@100mm	0	6-Ø20mm	3.67
WB-6	450	3	0	0.254	6-Ø20mm	3.67
WB-7	450	3	0	0.53	6-Ø20mm	3.67

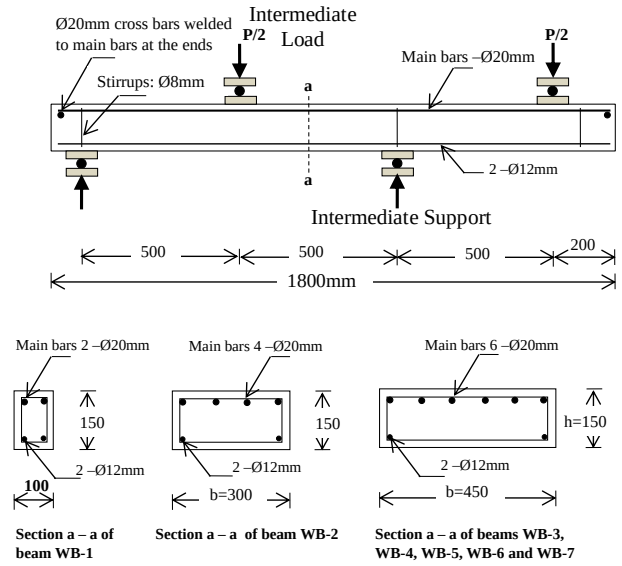

Figure 1: Reinforced details of WB beams.

The reinforcement cages were put in its location inside the wooden mold and the covers were guaranteed by using 20 mm plastic clear covers. All the beams and control specimen with and without fibers were cast at the same time using ready mix concrete.

Before casting WB-6, WB-7 and their control specimens, the specified amount of chopped carbon fibers (length 20 mm, fiber diameter 7 to 8 µm, with tensile strength 2840 MPa, modulus of elasticity 235 GPa, and density 1780 kg/m3) were added to the concrete, mixed for three minutes after fiber addition.

Table (2) Properties of steel used.

Nominal diameter (mm)	Area (mm^2)	Yield strength (MPa)	Ultimate Strength (MPa)
Ø8	50	485	587
Ø12	110	390	562
Ø20	308	478	780

The specimens were cured for about 56 days, then they were air dried in the laboratory.

Before testing they were painted with white paint for crack tracing during the loading stages. The free end deflection; mid-span (the point load between the two supports) deflection, strain of the concrete above the support were recorded (Fig. 2) every 5 kN throughout loading history.

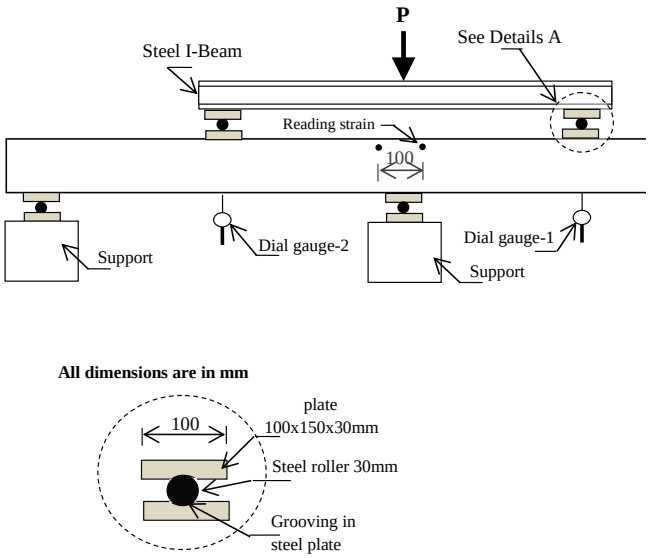

Figure 2: Details of loading and supporting points.

A universal testing machine with maximum capacity of 2500 kN were used to test the beams. The control specimens which are six cubes 150x150x150 mm for compressive strength, three prisms 75x75x380 mm for flexural strength, and two cylinders 100x200 mm for splitting tensile strength were tested at the same day of the beam tests. The failure load of beam specimens and control specimens are presented in Table 3.

3. TEST RESULTS

The failure load of tested beams and control specimens are presented in Table 3. Discussion of test results is given in the sections to follow:

Table (3) The failure load of beam specimens and control specimens.

Specimen No.	f'_{cu}	f'_c (MPa)	f'_r	f'_{ct}	V_u, EXP (kN)	Change** (%)	Deflection at Free end (mm)
WB-1					80	-71.3	9.50
WB-2					195	-30.1	9.59
WB-3	107.6	91.5*	5.8	9.14	279	0.0	11.30
WB-4					320	14.7	13.71
WB-5					372	33.3	17.70
WB-6	62.6	53.2	6.89	6.77	212.5	-23.8	11.05
WB-7	42.5	36.1	3.79	6.73	181	-35.1	9.03

*Cylindrical compressive (f'_c) test result taken as equivalent to 0.85 cubes (f'_{cu}) test results.
**The negative sign (-) indicates reduction of the shear strength of WB relative to reference beam (WB-3).

3.1 Cracks and Cracks Propagations

Cracks occurrence, distribution, and propagation present the respond of reinforced concrete beams under the loads, cracks happen when the internal tensile strength due to applied external load reached tensile strength of the material at that position. After the specimen was loaded, the first visible cracks were observed at location 1 (Fig. 3). In this stage the beams have one or two major cracks that have limited length which is less than quarter of the beam depth, these flexural cracks are mostly vertical and straight, started at top toward bottom, at maximum negative moment (i.e., the intermediate support). The loading procedure was continued during which no cracks were appeared in the web of the section, until the loading reached to about more than 90% of failure load, the shear cracks were appeared at location 2 (Fig. 3), mid-height of the beam. These cracks are almost horizontal, with increasing load, they extended diagonally towards location 3 and 4 (Fig. 3). Further increasing of loads produced semi-parallel crack 5 around path 3-2-4 at the top and bottom of first shear cracks.

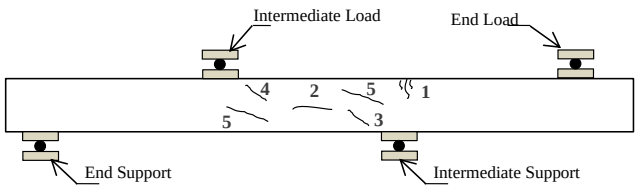

Figure 3: Sequence of cracking appearance.

The majority of the main shear cracks were observed between intermediate loading (see Fig. 1) and intermediate support, while the cracks on other side of intermediate support were observed to be less critical as shown in Fig. 4. With the test progress the cracks width and length increased and final failure were triggered due to splitting shear failure of the cracks.

Figure 4: Crack patterns of the specimens at failure.

The appearance of shear cracks was delayed significantly by the presence of stirrups (Ø8@200 and Ø8@100 mm c/c). The same thing is also noticed in beams with fibers especially the beams with higher fiber content. The specimen with 0.53% fiber content failed in more ductile manner compared to other beams without fibers.

3.2 Control Specimens

High strength self-compacted concrete prepared by truck mixer from central batch plant under the authors' order. The average cubes compressive strength (150x150x150 mm) of the concrete reached to 107.6 MPa, while adding of wet carbon fiber polymer (microfiber) by 0.254% and 0.530%, led to strength reduction by 42% and 61%, respectively, these results may be attributed due to the mix design was just done for HS SCC,

but at the practical work, we added two specimens with fiber without mix design (HS SCC with fiber) The same trend was observed for tensile strength of the concrete. The reason behind this reduction may be that high strength self-compacted concrete is more sensitive to addition of micro fiber than high strength concrete with steel fiber (Wafa & Ashour, 1992); this means that it's required a new mix design for using microfiber with SCC. The tensile strength of the concrete was obtained using indirect tensile test on prisms (modulus of rapture) and cylinders (splitting test).

The results indicated that adding 0.254% fiber led to an increase of the flexural tensile strength by 18.8%, while adding 0.53% of fiber led to reduction of the flexural tensile strength by 34.7%. The same conclusion as discussed earlier for compressive strength is also true for the tensile strength. The other indirect test (Splitting strength) undergoes 25.9% and 26.4% reduction on strength for both fiber contents, respectively. The reasons may be, adding fibers led to increase the friction between the ingredients of fresh concrete, so less workability obtained and during the cast, the balling of fiber observed at 0.53% fiber content, as a result, influenced on the final strength.

4. INVESTIGATED PARAMETRS

4.1 Beam Width to Height Ratio

The effect of width to height ratio (b/h) on the shear strength of the beams is shown in Fig. 5. As the beam (b/h) ratio increases from 0.67 to 2 and 3, the area of concrete contribution (of the beam section) in shear strength are increased 3 and 4.5 times with respect to control specimen WB-3. While the reduction of shear strength of beam reached 30.1% and 71.3% respectively. It can be seen that with increasing b/h the shear strength decreased. This could be attributed to the fact that the area of the cross-section becomes larger with increasing width of the beam, and the probability of encounter for weak point is higher when the area is larger. This eventually leads to lower shear strength due to releasing more fracture energy throughout loading history.

4.2 Stirrups

As the shear reinforcement increase from 0 to Ø8 at 200 mm c/c and Ø8 at 100 mm c/c, the shear strength increased by 14.7% and 33.3%, respectively, relative to WB-3, as shown in Fig. 6. It is clear from the figure, that the stirrups have limited effect on the shear strength of the beams as most of the applied stress is resisted by concrete. However, during the test, it was observed that the presence of stirrups is very essential for restricting width and length of shear cracks at final stages of loading.

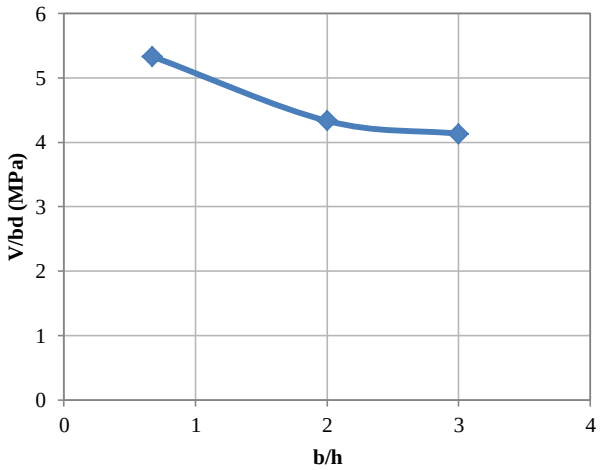

Figure 5: Effect of (b/h) on the shear strength of the specimens.

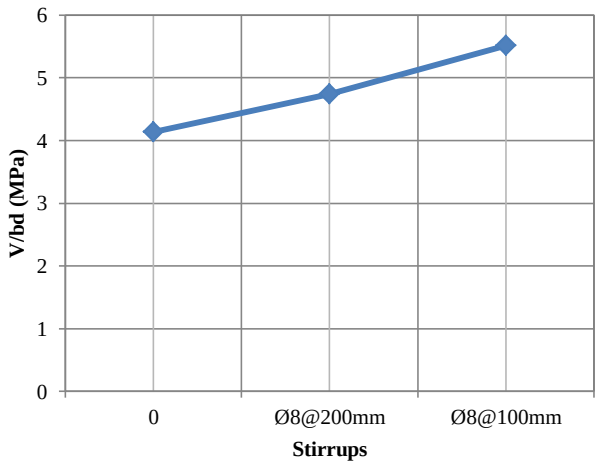

Figure 6: Effect of shear reinforcement on the shear strength of the specimens.

4.3 Fiber Content

Adding microfiber to fresh mix led to significant decrease in the compressive strength of the concrete. The reductions were 42% and 61% for 0.254% and 0.53% fibers contents, respectively. This reduction in strength reflected on all properties of concrete, including shear strength. This is probably the reason that only slight increases in shear strength can be seen in Fig. 7, which shows the effect of fiber content on

the normalize shear strength $\left(V/\sqrt{f_c'}\,bd\right)$ of the beams.

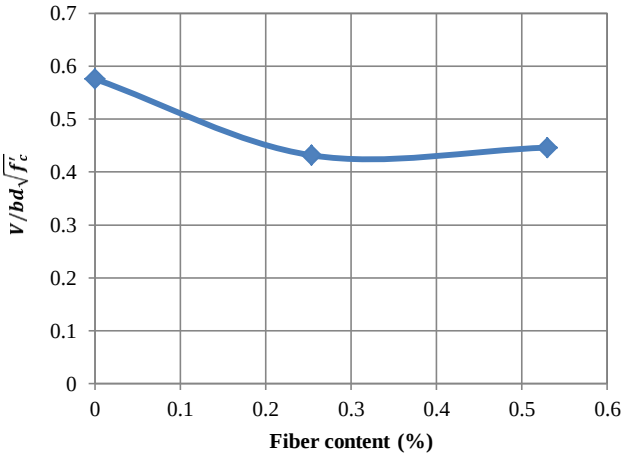

Figure 7: Effect of fiber content on the normalized shear strength of the specimens.

4.4 Load-Displacement Relationship

The vertical displacements were recorded at mid-span between the supports (under intermediate load) and at free end (under the end load). The intermediate load displacement is very small compared to the free end displacement, therefore, the main focus here is the displacement of the free end. Fig. 8-10 show the load deflection relationship of the beams which grouped based on different investigated parameters. Fig. 8 shows the relationship for beams with different (b/h). As can be seen in the figure, by decreasing beam width, the final deflection decreased by 15.9% and 15.1% for (b/h) 0.67 and 2, respectively. In addition, the stiffness of the beam (slope of the curve) is decreased clearly as the width decreased.

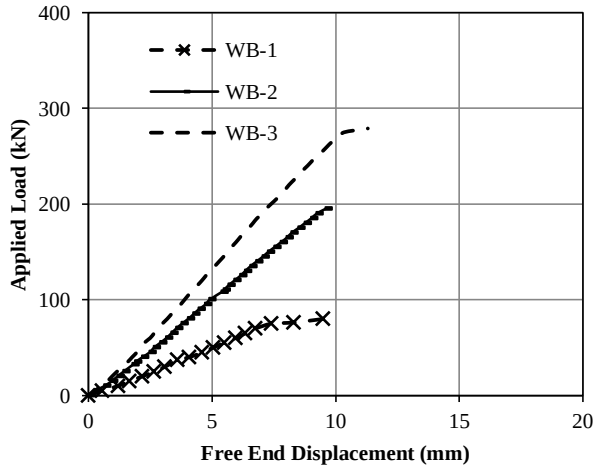

Figure 8: Load-displacement relationship (effect of b/h).

Fig. 9 shows the load deflection of beams with different shear reinforcement, the final displacement of WB-3 reached to 11.3 mm while with increasing stirrups reached to 13.7 mm and

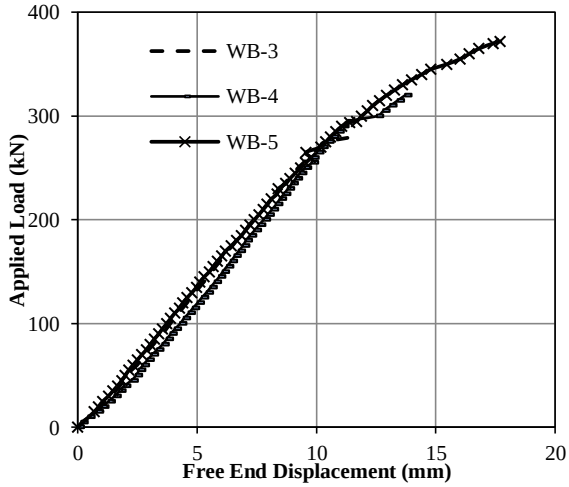

Figure 9: Load-displacement relationship (effect of shear reinforcement).

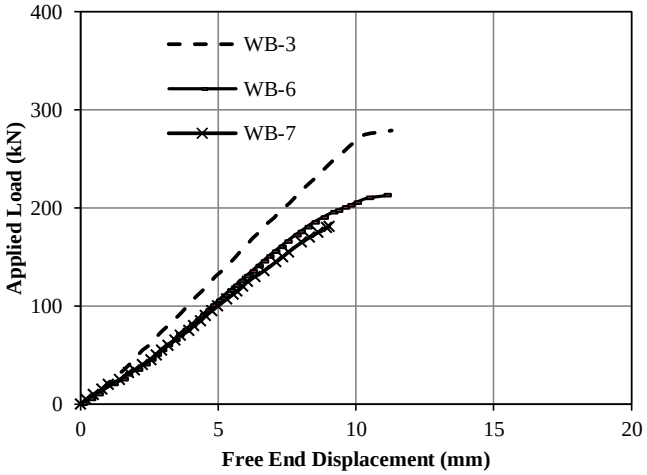

Figure 10: Load-displacement relationship (effect of fiber content).

17.7 mm for WB-4 and WB-5 respectively. It is clear that the shear reinforcement has no influence on the load deflection behavior, except it enhanced the load capacity of the beam. It is also obvious from the figure that the presence of shear reinforcement leads to more ductile behavior (the final displacement) after shear crack development.

The deflection at all loading stages and final deflection were noticed decreased relative to WB-3, as shown in Fig. 10. The reason can be attributed to bad results of existence of fibers relative to control specimens.

5. SHEAR STRENGTH THEORIES

Up until now, there is no unified shear theory among researchers and codes of practice. ACI Code (ACI Committee 318, 2014) divided the shear resistance of a concrete member into two components, concrete resistance, V_c, and shear

reinforcement resistance, V_s; while EURO Code (Eurocode-2, 2004), shear resistance approach neglects the concrete contribution to the shear resistance in the presence of shear reinforcement.

The nominal shear strength of ACI Code adopted by V_n, when strength done by two contributions as follow:

$$V_n = V_c + V_s \quad (1)$$

Where, V_c is concrete strength contribution and simplified shear strength of concrete equals to

$$V_c = 0.17\sqrt{f_c'}b_w d \quad for\ \sqrt{f_c'} \leq 8.33\ \text{MPa} \quad (2a)$$

Additionally, for simplified equation, another case was considered without $\sqrt{f_c'} < 8.33$ restriction to check the equation for concrete compressive strength higher than 70 MPa.

$$V_c = 0.17\sqrt{f_c'}b_w d \quad (2b)$$

ACI also permits to use more accurate equation, include the effect of applied shear and moment and has also effects of dowel action of the longitudinal bars.

$$V_c = \left(0.17\sqrt{f_c'} + 17\rho_w \frac{V_u d}{M_u}\right) b_w d \quad (3)$$

The value of $V_u d/M_u$ in Eq. (3) must be equals or less than 1. Also, V_s is the steel contribution and equals to:

$$V_s = \frac{A_v f_{yv}\, d}{s} \quad (4)$$

Euro Code (EC-2) adopted variable strut inclination method to find shear strength of a member. This method takes the diagonal strut as a concrete strut, D_c, the ties act as a vertical stirrup V_T, and the longitudinal reinforcement acts as a bottom chord, B_T, where the angle θ, has varying between 22 to 45 degree, shown in Fig. 11.

The EC-2, design shear resistance of a member without shear reinforcement is $V_{Rd,c}$ as given

$$V_{Rd,c} = \left[0.18\left(1 + \sqrt{200/d}\right)(100\rho_w f_{ck})^{1/3}\right] b_w d \quad (5)$$

But not less than

$$V_{Rd,c} = \left[0.035\left(1 + \sqrt{200/d}\right)^{3/2}\sqrt{f_{ck}}\right] b_w d \quad (6)$$

Where $1 + \sqrt{200/d} \leq 2$

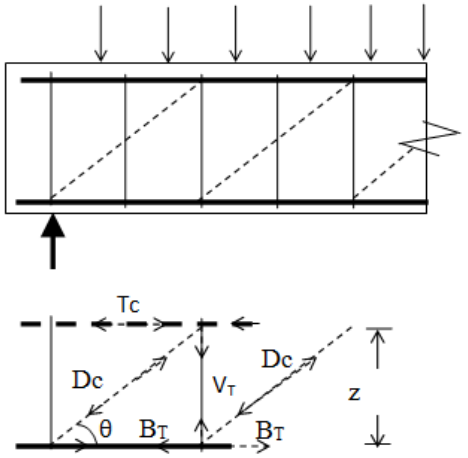

Figure 11: Strut and tie mechanism.

Where $V_{Rd,c}$ is the design shear strength of a member governed by the yielding of web bars (kN), $A_{sw}$is the area of web bars (mm^2),f_{ywd}: is the design yield strength of web bars (MPa), θ is the angle between the concrete strut and the longitudinal axis of the beam (rad), and f_{ck}: is the cylinder compressive strength of concrete ($= \sqrt{f_c'}$), (MPa).

The external applied shear V_{ED} is greater than resisting shear of concrete, $V_{Rd,c}$, all the applied shear is resisted by stirrups (neglecting the effect of concrete contribution), so the shear resistance of the web reinforcement $V_{Rd,c}$ is given by (EC-2, Clause (6.2.3))

$$V_{Rd,s} = \frac{A_{sw}}{s} f_{ywd} \cot\theta \quad (7)$$

$$\theta = 0.5 \sin^{-1}\left(\frac{V_{Rd,E}/b_w d}{0.153 f_{ck}(1 - f_{ck}/250)}\right) \quad (8)$$

A shear strength formula is proposed based on the 65 experimental data of the current paper and other six literatures (Sherwood et al., 2006; Lubell et al., 2009; Shuraim, 2012; Hanafy et al., 2012; Lotfy et al., 2014; Mohammadyan-Yasouj et al., 2015) for wide beams. The proposed shear strength equation composed of three parts which are concrete strength contribution (V_c), shear reinforcement contribution (V_{vs}) and longitudinal reinforcement contribution (V_{LS}). The following equations are proposed:

$$V_R = V_c + V_{vs} + V_{Ls} \quad (9)$$

$$V_c = 0.75\ \theta\ f_c^{'}\ b_w d \quad (10)$$

$$V_{vs} = \frac{A_v\, z\, f_{yv}}{20\ s \tan\theta} \quad (11)$$

$$V_{Ls} = \left(A_s \rho - \frac{M_u}{z}\right) tan\theta \quad (12)$$

Where:

$$\theta = 0.5\ \sin^{-1}\left(\frac{2\ V_u}{b\ z\ f_c^{'}}\right) \quad (13)$$

$$19 \le \theta \le 60$$

6. THEORETICAL MODEL ASSESSMENT

The efficiency of the proposed model is compared to the provisions of ACI 318-14 and EC2 using 65 wide beams from the literatures (5 wide beams from (Sherwood et al., 2006), 13 from (Lubell et al., 2009), 16 from (Shuraim, 2012), 12 from (Hanafy et al., 2012), 10 from (Lotfy et al., 2014), 4 from (Mohammadyan-Yasouj et al., 2015), and 5 from the authors, the results are shown in Fig. 12, 13 and 14; and statistical details are presented in Table 4. The majority of the considered beams were made from normal strength concrete (NSC) while eleven of them are made from high strength concrete (HSC) (i.e., compressive strength is equal to or higher than 70 MPa). For ACI 318-14 and EC2, no safety factors and material partial safety factors were used.

Fig. 12 shows the influence of concrete compressive strength on the shear strength prediction using ACI 318-14, EC2 and proposed equation. It can be seen that ACI 318-14 prediction is more conservative and more scatters compared to EC2; however, EC2 conservatism does not change with increasing concrete compressive strength as the ACI 318-14 becomes extremely conservative and uneconomic when concrete compressive strength is higher than 70 MPa. The proposed equation leads to more accurate results with the least coefficient of variation.

The second considered parameter on the shear strength prediction of wide beams using aforementioned codes of practice and the proposed equation is width to depth ratio (b/h) of the beam as shown in Fig. 13. It is clear from the figure that the degree of conservatism for both ACI318-14 and EC2 decreases as the width of the beam increases and becomes very unsafe when b/h is higher than 3, this is more pronounced in the EC2 prediction than ACI318-14. This is probably because the provisions of these codes of practice were drawn mainly on beams with normal b/h and could lead to very unsafe results when applying to wide shallow beams.

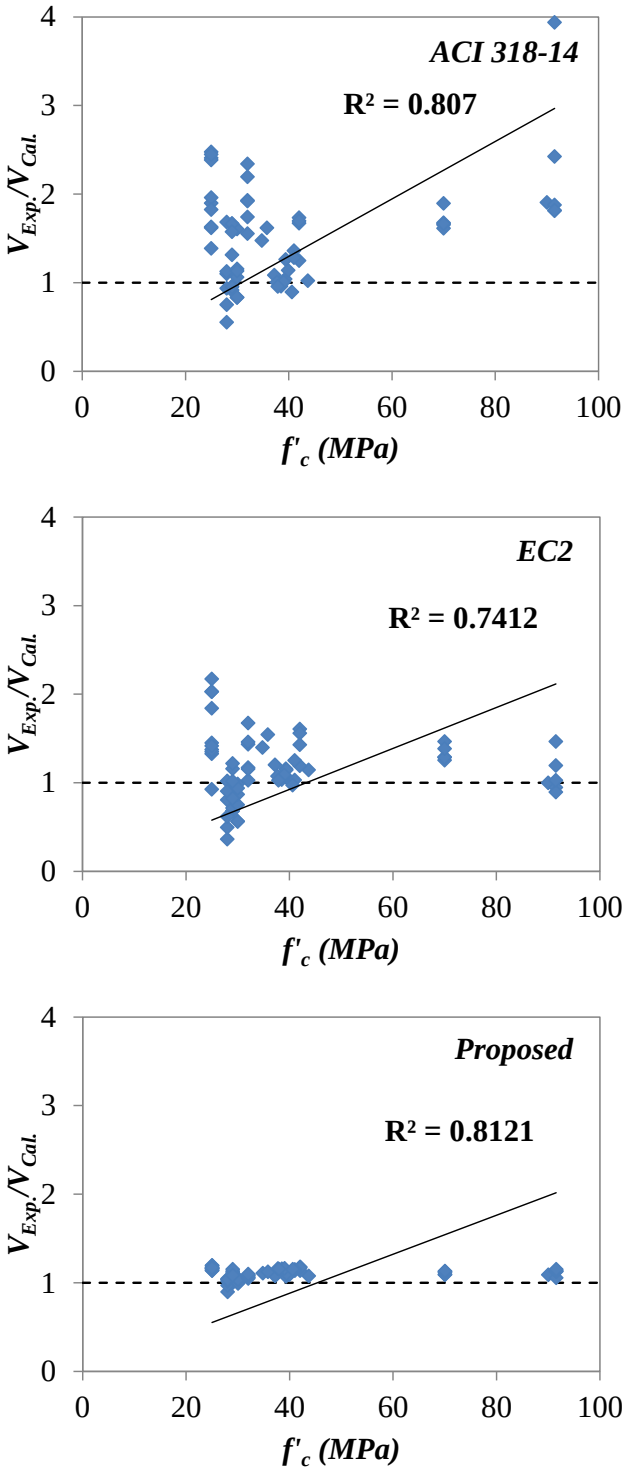

Figure 12: Influence of concrete compressive strength on the predicted shear capacity of wide beams by different approaches.

Table (4) Experimental to theoretical shear strength results for different methods.

Equations	$V_{EXP}/V_{Theor.}$			
	Average	**SD**	**COV**	**R^2**
ACI (1): Eq. (1), (2) and (4)	1.53	0.57	37.01	0.807
ACI (2): Eq. (1), (2) and (4) without $\sqrt{f`_c} < 8.333$	1.5	0.52	34.75	0.788
ACI (3): Eq. (1), (3) and (4)	1.38	0.48	34.50	0.802
Euro (EC-2): Eq. (5), (6), (7) and (4)	1.16	0.36	31.33	0.741
Proposal: Eq. (9), (10), (11), (12) and (13)	1.10	0.06	5.69	0.812

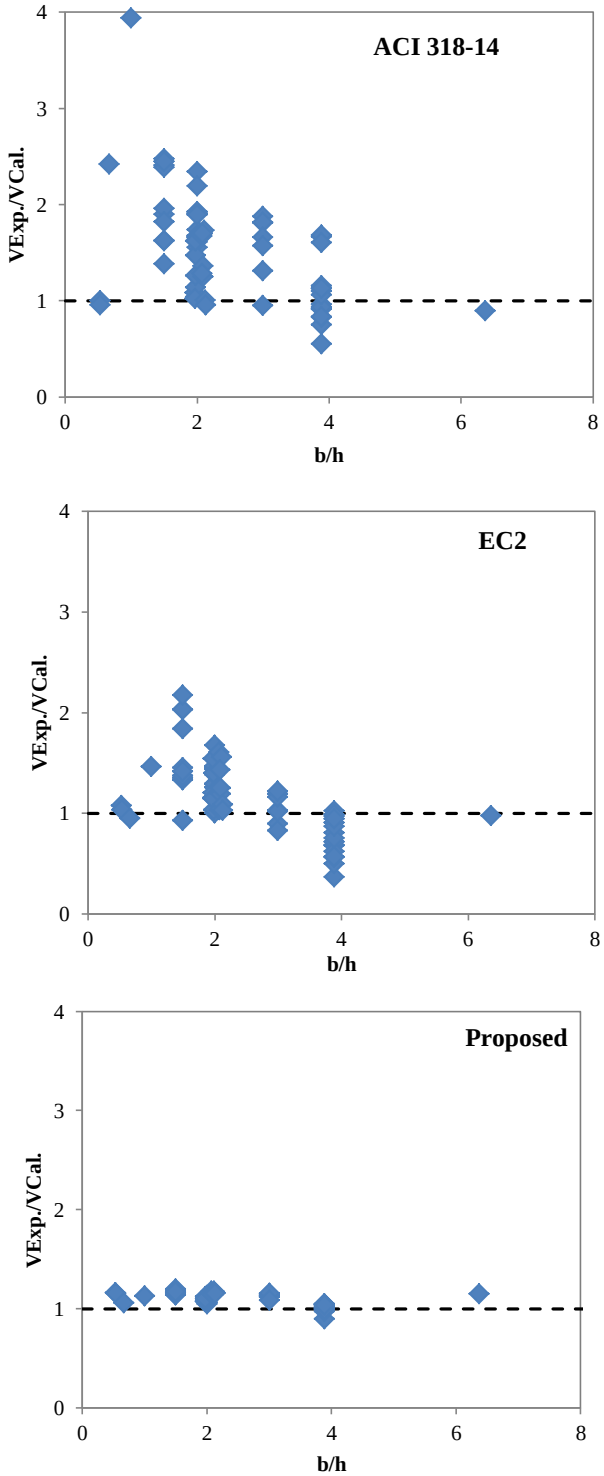

Figure 13: Influence of b/h on the predicted shear capacity of wide beams by different approaches.

The influence of shear reinforcement index ($\rho_V f_{yv}$) on the shear strength prediction of the considered approaches are shown in Fig. 14. Once more the codes of practice do not have a constant margin of safety for beams with different shear reinforcement ratio. Shear reinforcement ratio has limited effect on the shear capacity of the beam; it could enhance the capacity when shear reinforcement is increased up to a limit, any increase after that has a negligible effect on the shear capacity. This cannot be fulfilled with the provisions of EC2, since it neglects the effect of concrete contribution which in turn could lead to very unsafe results for beams with high shear reinforcement ratio as can be seen in Fig. 14. For beams with shear reinforcement index more than 1.0 MPa, ACI318-14 code is more conservative compared to EC2, since ACI 318-14 accounts for concrete contribution in the shear strength prediction.

The experiment result of 65 WB available in the literatures are divided by calculated result (V_{EXP}/V_{cal}) are showed that, the average values are as follows: from smallest to highest 1.0, 1.16, 1.38, 1.50 and 1.53 for proposal, EC-2, ACI-Eq. (3), ACI-Eq. (2b) without $\sqrt{f_c'}$ restriction, and ACI-Eq.(2a) with $\sqrt{f_c'}$ restriction. The COV has same ascending order are 5.69%, 31.3%, 34.5%, 34.75%, and 37.0%, respectively (Table 4). From these results of average, SD and COV, it can be concluded that ACI (3) accurate is better that ACI-Eq. (2) for wide beam.

This means that $\sqrt{f_c'}$ restriction is conservative, can be worked with HSC, and can be removed from ACI. EC-2 Code depends on struts and tie model but has little difference with ACI (3) in all three statistical assessments. The proposed method depends on strut and tie model but incorporated with some changeable in the

factor and got more close result to unity for (V_{EXP}/V_{cal}) as shown in Table 4.

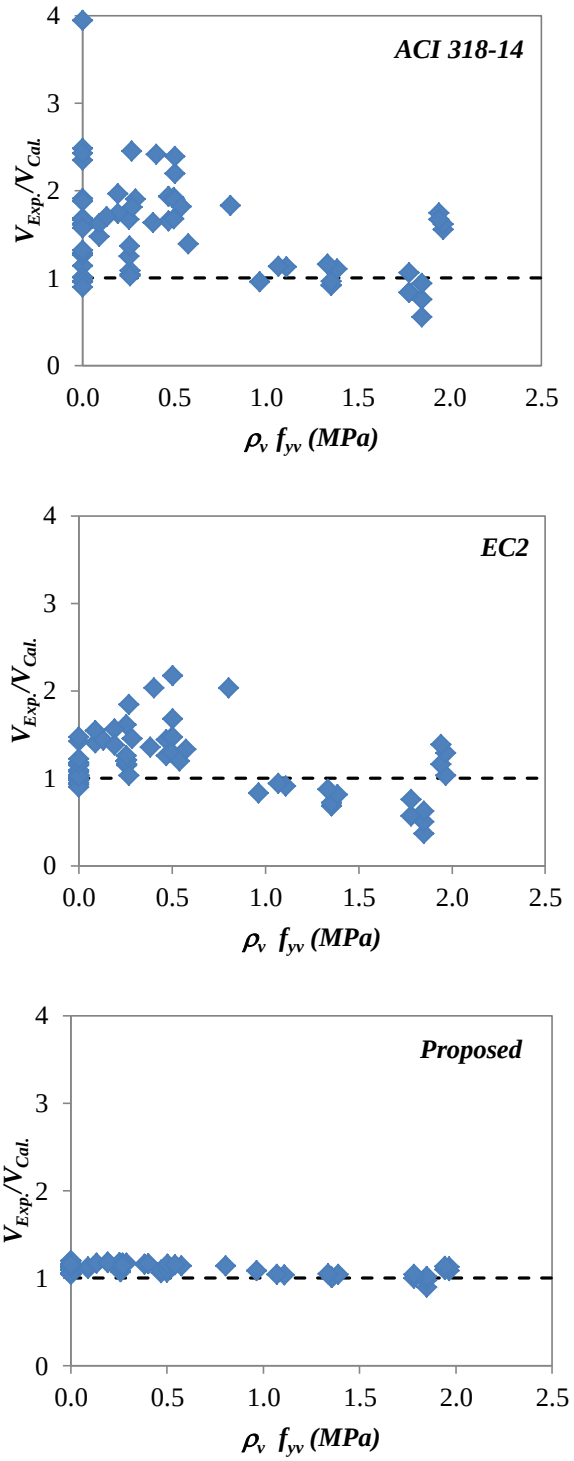

Figure 14: Influence of shear index on the predicted shear capacity of wide beams by different approaches.

The proposed equation could account for all aforementioned parameters and predict the shear behavior of wide shallow beams very accurately. However, it needs further investigation and validations against more experimental data, since the equation was proposed using best fit analysis for the same database. Therefore, the authors of this paper recommend more experimental investigation on wide shallow beam and validating the proposed approach.

7. CONCLUSION

The following conclusion can be drawn based on the experimental and theoretical work of the current paper:

- For high strength self-compacted concrete, adding of wet carbon fiber polymer (microfiber) could lead to reduction in the compressive strength. This is because high strength self-compacted concrete is more sensitive to add micro fiber than high strength concrete with steel fiber, it's required a new mix design for using microfiber with SCC.
- As the beam (b/h) ratios decrease from 3 to normal depth, the reduction of shear strength of beam reached 30.1% and 71.3% respectively. It is noted that, the relation between (b/h) ratios and the shear strength are somewhat proportion linearly.
- The WB with and without stirrups has no effect on load-displacement relationship during most loading increment. The exitance of the stirrups lets to delay the final failure of the beams, then increased the final deflection. The final deflection increased as the stirrups increased from 0 (WB-3) to 8Ø@200 mm c/c (WB-4) and 8Ø@100 mm c/c (WB-5), changed from 11.3 mm (WB-3) to 13.7 mm and 17.7 mm, respectively.
- ACI equations has a limit in calculation of shear strength with concrete compressive strength (f_c') up to 70 MPa. This means that the restriction is conservative. The experimental results showed the ACI equation can be worked with HSC with f_c' more than 70 MPa. The restriction can be removed from ACI.
- The experiment results with respect to calculated results (V_{EXP}/V_{cal}) of 65 WB available in the literatures are showed that, the average values are as follows: from smallest to highest 1.0, 1.16, 1.38, 1.50 and 1.53 for proposal, EC-2, ACI-Eq. (3), ACI-Eq. (2b), and ACI-Eq. (2a). From these results, it can be concluded that ACI code equations gave conservative results relative to Euro code for WB.

Acknowledgements

The authors gratefully acknowledge the staff of concrete laboratory in Civil Engineering Department of Salahaddin University-Erbil.

Conflict of Interest

The authors declare no conflict of interest regarding the publication of this paper.

References

ACI Committee 318, 2014. *Building code requirements for structural concrete (ACI 318-14) : an ACI standard : commentary on building code requirements for structural concrete (ACI 318R-14), an ACI report*. Farmington Hills: American Concrete Institute. Available at: https://books.google.iq/books?id=Z-LGrQEACAAJ.

Conforti, A., Minelli, F. & Plizzari, G.A., 2013. Wide-shallow beams with and without steel fibres: A peculiar behaviour in shear and flexure. *Composite Part B: Engineering*, 51(1359-8368), pp.282-90. Available at: http://www.sciencedirect.com/science/article/pii/S1359836813001352.

Conforti, A., Minelli, F., Tinini, A. & Plizzari, G.A., 2015. Influence of polypropylene fibre reinforcement and width-to-effective depth ratio in wide-shallow beams. *Engineering Structures*, 88(0141-0296), pp.12-21. Available at: http://www.sciencedirect.com/science/article/pii/S0141029615000528.

Conforti, A. et al., 2017. Structural applicability of polypropylene fibres: Deep and wide-shallow beams subjected to shear. In *FRC 2014 JOINT ACI- FIB INTERNATIONAL WORKSHOP*. Montreal, 2017. Polytechnique Montreal.

Eurocode-2, 2004. *Desgin for Buildingssign of Concrete Structures, Part 1-1; General Rules ans Rules for Buildings(EN 1992-1-1)*. Brussels, Belgium: European Committee for Standardization.

Hanafy, M.M., Mohamed, H.M. & Yehia, A.B., 2012. On the Contribution of Shear Reinforcement in Shear Strength of Shallow Wide Beams. *Life Science Journal*, 9(3), pp.484-98.

Lotfy, E.M., Mohamadien, H.A. & Hassan, M., 2014. Effect of Web Reinforcement on Shear Strength of Shallow Wide Beams. *International Journal of Engineering and Technical Research (IJETR)*, 2(11), pp.98-107.

Lubell, A.S., Bentz, E.C. & Collins, M.P., 2009. Shear Reinforcement Spacing in Wide Members. *ACI Structural Journal*, 106(2), pp.205-14.

Mohammadyan-Yasouj, S.E., Marsono, A.K., Abdullah, R. & Moghadasi, M., 2015. Wide beam shear behavior with diverse types of reinforcement. *ACI Structural Journal*, 112(2), pp.199-208.

Saeed, J.A., Muhammad, A.H. & H., D.K., 2007. Properties Of High Strength Concrete Using Locally Available Low-Cost Materials. *The Scientific Journal of Salahaddin University*, 19(2).

Sherwood, E.G., Lubell, A.S., Bentz, E.C. & Collins, M.P., 2006. One-Way Shear Strength of Thick Slabs and Wide Beams. *ACI Structural Journal*, 103(6), pp.794-802.

Shuraim, A.B., 2012. Transverse stirrup configurations in RC wide shallow beams supported on narrow columns. *Journal of Structural Engineering*, 138(3), pp.416-24. Available at: https://doi.org/10.1061/(ASCE)ST.1943-541X.0000408.

Shuraim, B. & Al-Negheimish, A.I., 2011. Design Considerations for Joist Floors with Wide-Shallow Beams. *ACI Structural Journal*, 108(2), pp.188-96.

Wafa, F. & Ashour, S.A., 1992. Mechanical Properties of High-Strength Fiber Reinforced Concrete. *ACI Material Journal*, 89(5), pp.449-55.

Yousif, A.R., A., O.Q. & M., H., 2004. Size Effect On Shear Failure Of High Strength Reinforced Concrete Corbels Without Stirrups. *The Scientific Journal of Salahaddin University*, 16(1).

ZANCO Journal of Pure and Applied Sciences
The official scientific journal of Salahaddin University-Erbil
https://zancojournals.su.edu.krd/index.php/JPAS

ISSN (print):2218-0230**, ISSN (online):** 2412-3986**, DOI: http://dx.doi.org/10.21271/zjpas**

RESEARCH PAPER

Comparison Between Measured and Empirically Predicted Radio Wave Pathloss in Rural Environment

[1] Sevan Siyyah Abdullah, [2]Sattar Othman Hasan

[1&2]Physics Department, College of Education, Salahaddin University-Erbil, Kurdistan Region, Iraq.

A B S T R A C T:

In this study a comparative analysis of various empirical models for estimating radio wave propagation path losses with those measured experimentally for the rural area in Erbil city is presented. In Gazna village near the center of the Erbil city, one of the Korek telecommunication towers is selected for the purpose of comparative analysis and seven different empirical models were utilized. The implemented models are free space model, Electronic Communication Committee (ECC-33), Stanford Interim University (SUI), Optimization Cost-231, Okumura-Hata, Egli, and Ericson models. The data were collected at operating frequencies of 1800 MHz and 2100 MHz using drive test equipment with Sony-Ericson mobile phone to measure received signal strength. Generally, the analyzed results, which are based on the Mean Absolute Percentage Error (MAPE) values, shows that the Egli and ECC-33 overestimated while both FSPL and Okamura-Hata are underestimated path loss values. In addition, the SUI and Optimized-Cost-231 models are providing minimum MAPE path loss values which are 0.49 and 0.55 at 1800 MHz and 0.07 and 0.16 at 2100 MHz, respectively. Therefore, in order to improve network performance and accurate estimation of financial feasibility, these two models especially SUI model can be used successfully and confidently in the design of the wireless communication system in the rural area of Erbil city in Kurdistan region of Iraq.

KEY WORDS: Network planning: path loss: received signal strength: radio wave propagation.
DOI: http://dx.doi.org/10.21271/ZJPAS.33.2.12
ZJPAS (2021) , 33(2);128-138 .

1.INTRODUCTION:

Erbil town is the capital city of Kurdistan region in Iraq. It is an urban city characterized by sites placed near to moderate and tall mountains, commercial and residential buildings as well as small size industries with large offices. Here, the access to Global System for Mobile Communication (GSMC) has become an active area of interest since 2005 up to now.

The GSM service providers in the town are Asia cell, Korek Telecom, and Zain operating at 900MHz, 1800 MHz and 2100MHz, but the quality of their services is poor due to several factors such as high-rise building, trees, location and height of the antenna towers. The investigation and specification of the possible factors and proper treatments through scientific research became necessary towards solving problems faced by the customers (Singh, 2012). One of the main factors that makes the mobile communication systems to provide their services with a suitable quality and with a high data rate capacity, is accurate estimation of the signal strength in the region under consideration.

In wireless communication systems, the signals are transferred between transmitter and receiver antennas using electromagnetic waves. The propagated signals usually reduced in its strength

* **Corresponding Author:**
Sevan Siyyah Abdullah
E-mail: sevan.abdullah@su.edu.krd
Article History:
Received: 12/11/2020
Accepted: 06/02/2021
Published: 18/04 /2021

with distance away from the transmitting tower due to terrain factors such as buildings height, mountain, tall trees and location of the antennas (Singh, 2012). This reduction in radio wave power signals as it propagates from transmitter to the receiver is called path loss (Singh, 2012), (Akande et al., 2017). The factors that lead to path losses in radio wave propagation are mainly due to free space, absorption, diffraction, scattering and multipath signal losses as well as type of environment (urban, sub-urban and rural), height of transmitter and receiver antennas and carrier frequencies (Omolaye et al., 2015). Basically, the path loss is defined as the ratio of the transmitted power P_t to the received power P_r and mathematically is expressed as:

$$PL(dB) = 10 \log \frac{P_t}{P_r} \qquad (1)$$

Estimation of radio wave path losses are very important in predicting signal strength power at the receiver, link budget design analysis, interference optimization analysis and cell size estimation. There is different model for path loss estimation and for different types of environments such as urban, suburban, and rural.

Generally, the evaluation of radio wave propagation path losses is determined by different models, such as deterministic, stochastic and empirical models (Akande et al., 2017) and (Mardeni & Priya, 2010). In deterministic model all the objects in the mediums must be defined accurately and then the physical laws of Maxwell equations is implemented to specify the mechanisms of radio wave propagation in a particular location (Akinwole & J.J, 2013). The accuracy of deterministic models is very high but it needs high computation complexity due to requirement of 3D data about the propagation environment. In Stochastic models the environment is considered as a series of random variables that are least accurate but require few information about the area of wave propagation and employ less processing power to generate predictions (Ghosh et al., 2012). On the other hand, empirical models which is based on the observed and extensive measurements data are usually used in practice than statistical and deterministic propagation models for estimating path loss. Generally, empirical models are simple in nature, low cost and require less calculation effort to predict path losses with acceptable accuracy (Akinwole & J.J, 2013).

Different empirical prediction models have been adapted to different environment and at different frequency operation. The classification of these models for use into urban, suburban and open (rural) areas has been addressed in (Kamboj et al., 2011) and (Sharma, 2011). These models include the free space model, Stanford University Interim (SUI), COST 231, Okumura Hata, Lee, Walfish-Ikegami, ECC-33 model and others. Some wireless network providers use the COST 231-Hata and Okumura-Hata models for radio wave propagation network designing. However, the accuracy of the available models is limited when they are used for an environment of different geographical characteristic formation from that for which they have been proposed. Therefore, the network performance is mostly relying on the accuracy of the prediction model that implemented for the planning designation (Imoize & Oseni, 2019).

Free space and Okumura - Hata models has been employed to estimate broadcasting radio wave signal strength for a television station in Akure Ondo State, Nigeria. This work reveals that the performance of Okumura–Hata model is reliable for good signal prediction in the Akure metropolis (Imoize & Oseni, 2019). Moreover, the modified Ericson model which is proposed by (Akande et al., 2017) at 2100MHz for the Alagbado axis of Lagos, Nigeria showed best performance in compare to the measured path loss data. On the other hand, there are a lot of researches on radio wave propagation path loss measurements and channel modeling, especially for rural environments but we are not been able to decide which of them is suitable for the prediction of radio wave path losses in the environment of Erbil city.

Therefore, this work is established to investigate different empirical path loss models against measured radio wave propagation path loss in rural environment of Erbil city. For this purpose, one of the Korek telecom cellular sites operating at frequencies 1800 MHz and 2100 MHz is selected and various empirical models have been tested. This site is located at Gazna village which is a small size village located near to the center of the city under consideration. The

procedure of the measured and calculated results is described in the following sections.

2.EMPIRICAL MODELS

As previously mentioned, the radio wave propagation path loss greatly affected on the quality of services delivered by mobile communication systems. Therefore, accurate estimation of radio wave propagation path loss may lead to the development of efficient design and operating at high quality with high-capacity network. There are a lot of empirical path loss models employed by previous researchers which are helpful in the planning of best Global System for Mobile Communication (GSM) networks.

This work is established to predicting radio wave propagation path loss in rural area of Erbil city in Kurdistan region of Iraq by comparing measured data with those estimating by the different available empirical models. For this, seven models have been utilized namely, free space, ECC-33, Stanford Interim University (SUI), Optimized Cost-231, Okumura-Hata, Egli and Ericson models (Akande et al., 2017). A brief description for each of these models are presented in the following subsections.

2.1 FREE SPACE PATH LOSS MODEL

The free space path loss is a theoretical estimation for the prediction of RF signal strength at a particular distance away from the transmitting tower neglecting losses which need to be accounted for while estimating the signal at a location. However, the Free Space Path Loss (FSPL) is a reliable approximation for predicting the signal losses as propagating through the space and is expressed mathematically as (Akande et al., 2017):

$$\mathrm{PL_{FSPL}} = 32.45 + 20\log_{10}(d) + 20\log_{10}(f_c) \qquad (\mathbf{2})$$

d: Transmitter to receiver distance in km, f_c: operating frequency in MHz.

2.2 OKUMURA –HATA MODEL

The Okumura-Hata model is a set of empirical formula obtained on the bases of signal power measurements and data extrapolations from curves derived by Okumura and is valid between 150 MHz to 1500 MHz. In this model the profile terrain, such as hills or other obstacles between the transmitter and receiver are neglected. This assumption is considered by Hata and Okumura due to the fact that the transmitter would normally be placed on hills (Oluwafemi & Femi-Jemilohun, 2018). Okumura-Hata's equations for rural environment is expressed as:

$$\begin{aligned}\mathrm{PL(dB)} = {} & 69.55 + 26.16\log_{10}(f_c) - 13.82\log_{10}(h_t) + \left(44.9 - 6.55\log_{10}(h_t)\right)\log_{10}(d) \\ & -4.78\left(\log_{10}(f_c)\right)^2 + 18.33\log_{10}(f_c) - 40.94 - (1.1\log_{10}(f_c) - 0.7)h_r \\ & -(1.56\log_{10}(f_c) - 0.8) \qquad (\mathbf{3})\end{aligned}$$

Generally, in all models, the following parameter symbols have the same meaning and are as follows (P. Akinyemi et al., 2015):

h_t: height of transmitter antenna in m, h_r: height of receiver antenna in m,
d: Transmitter to receiver distance in km, f_c: operating frequency in MHz.

2.3 ELECTRONIC COMMUNICATION COMMITTEE (ECC-33) MODEL

The ECC-33 path loss model is developed by Electronic Communication Committee (ECC) which is based on Okumura model and is regarded as one of the most suitable models for estimating path losses. This model has been extended to be applicable for predicting path losses for the frequencies up to 3.5 GHz by the International Telecommunication Union (ITU). In this model path loss is given by (Akinyemi et al., 2015) and (Khan & Kamboh, 2012) and the terms are defined as:

$$\mathrm{PL(dB)} = \mathrm{A_{fs}} + \mathrm{A_{bm}} - \mathrm{G}_t - \mathrm{G}_r \quad (4)$$

where, A_{fs}: attenuation due to free space attenuation [dB], A_{bm}: basic median path loss [dB], G_t: transmitter antenna gain factor, G_r: receiver antenna gain factor.

The mathematical formula for each of these parameters is given by (Sharma, 2011) and (Chebil et al., 2013) and are expressed as:

$$\mathrm{A_{fs}} = 92.4 + 20\log_{10}(d) + 20\log_{10}(f_c) \quad (5)$$

$$\mathrm{A_{bm}} = 20.41 + 9.83\log_{10}(d) + 7.894\log_{10}(f_c) + 9.56[\log_{10}(f_c)]^2 \quad (6)$$

$$\mathrm{G}_t = \log_{10}\left(\frac{h_t}{200}\right)(13.958 + 5.8[\log_{10}(d)]) \quad (7)$$

$$\mathrm{G}_r = [42.57 + 13.7\log_{10}(f_c)][\log_{10}(h_r) - 0.585] \quad \text{for rural and medium city} \quad (8)$$

$$\mathrm{G}_r = 0.759(h_r) - 1.862 \quad \text{for large city} \quad (9)$$

2.4 STANFORD INTERIM UNIVERSITY (SUI) MODEL

This model is proposed by the IEEE 802.16 which is an extension of the Hata model by taking into account a correction parameter for frequencies above 1900 MHz. The SUI model is developed as a solution for network planning of the WiMAX at 3.5 GHz band. This model is applicable for base station antenna height between 10 m to 80 m, receiving antenna height between 2 m to 10 m (Bola & Saini, 2013) and (Chebil et al., 2013). In this model different mathematical equation are proposed for predicting path losses in different propagation environments. The hilly areas with moderate or dense vegetation is considered as an urban, while a hilly area with low vegetation and heavy trees densities is regarded as a sub-urban and a flat area with light vegetation and low-density trees is assumed as a rural terrain.

Generally, the path loss formula that are proposed by this model for each mentioned environment along with its correction factors are expressed as:

$$\mathrm{PL(dB)} = \mathrm{A} + 10\,\gamma\log_{10}\left(\frac{d}{d_o}\right) + \mathrm{X}_f + \mathrm{X}_h + \mathrm{s} \quad \text{for} \quad d > d_o \quad (10)$$

where, (d_o) is the reference distance $(d_o = 100\,m)$, (d) is the distance between transmitter and receiver antennas in meters, (X_f) is the frequency correction factor for frequency above 2 GHz, (X_h) is the correction factor for receiving antenna height and (s) is a parameter used to account for tree and clutter shadowing and its values are between 8.2 dB to 10.6 dB (Mardeni & Priya, 2010).

$$\mathrm{X}_f = 6.0\log_{10}\left(\frac{f_c}{2000}\right) \quad (11)$$

$$\mathrm{X}_h = -10.8\log_{10}\left(\frac{h_r}{2000}\right) \quad \text{for Terrains 1 and 2} \quad (12)$$

$$\mathrm{X}_h = -20.0\log_{10}\left(\frac{h_r}{2000}\right) \quad \text{for Terrain 3} \quad (13)$$

The parameter (γ) is called path loss exponent and it is values is determined by the equation:

$$\gamma = \mathrm{a} - \mathrm{b}\,h_t + \frac{c}{h_t} \quad (14)$$

where, a , b and c are constants and their values are given in Table 1 which are vary according to the types of the environments (Milanovic et al., 2007). The value of the exponent parameter is $(\gamma = 2)$ for LOS propagation area, $(3< \gamma < 5)$ for urban NLOS environment and $(\gamma > 5)$ for indoor propagation medium (Sharma & Singh, 2010). Finally, the parameter A in the above equation is called as the intercept factor and is expressed as:

$$\mathrm{A} = 20 \log_{10}\left(\frac{4\pi d_o}{\lambda}\right) \qquad (\mathbf{15})$$

where, (λ) is the wavelength in (m),

Table 1: Parameter values in different environments for SUI model (Milanovic et al., 2007).

Model Parameter	Terrain 3	Terrain 2	Terrain 1
a	3.6	4.0	4.6
b (m^{-1})	0.0050	0.0065	0.0075
c (m)	20.0	17.1	12.6
s	8.2	9.6	10.6

2.5 OPTIMIZED COST-231 MODEL

The Optimization COST 231-Hata model is the extension of Cost-231 and it considered as an improvement version of the Hata model restricted to the frequency ranges from 1500 MHz to 2000 MHz, transmitter antenna height of 30 m to 200 m, receiver antenna height is between 1 m to 10 m and the distance between them is 1 km to 20 km. Mathematically, the Optimization Cost-231 model as given by the (Akande et al., 2017) is expressed as:

$$\mathrm{PL(dB)} = 41.42 + 33.9 \log_{10}(f_c) - 13.82 \log_{10}(h_t) - \mathrm{a}(h_r) + [44.9 - 6.55 \log_{10}(h_r)] \log_{10}(d) + \mathrm{C_K} \qquad (\mathbf{16})$$

where,

$$\mathrm{a}(h_r) = (1.11 \log_{10}(f_c) - 0.7)\, h_r - (1.56 \log_{10}(f_c) - 0.8) \quad \text{in dB} \qquad (\mathbf{17})$$

The value of the correction factor $(\mathrm{C_k})$ is $(0\ \mathrm{dB})$ for medium city and suburban areas whereas its values for urban or large cities is $(3\ \mathrm{dB})$ (Shebani et al., 2013).

2.6 EGLI MODEL

Egli model is also an empirical model that is used for estimating radio wave propagation path losses and is suitable for use in the frequency bands of 3 MHz to 3 GHz. This model is normally applicable when there is Line of Sight (LOS) between the base station transmitting antenna and mobile receiving antenna (Chebil et al., 2013). Egli path loss is calculated using the following equations (Mardeni & Priya, 2010) and (Imoize & Ogunfuwa, 2019):

$$\mathrm{PL(dB)} = 20 \log_{10}(f_c) + \mathrm{P_o} + 76.3 \qquad h_r \leq 10 \qquad (\mathbf{18})$$

$$\mathrm{PL(dB)} = 20 \log_{10}(f_c) + \mathrm{P_o} + 83.9 \qquad h_r > 10 \qquad (\mathbf{19})$$

where, $$\mathbf{P_o}(\mathrm{dB}) = 40 \log_{10}(d) - 20 \log_{10}(h_t) - 10 \log_{10}(h_r) \qquad (\mathbf{20})$$

2.7 ERICSON MODEL

The Ericson model also based on the modification of Okumura-Hata model which allow the change in parameters according to the radio wave propagation terrain. The calculation of the path loss values according to this model is obtained by the use of the following equations (Mardeni & Priya, 2010) and (Imoize & Ogunfuwa, 2019).

$$\mathrm{PL(dB)} = \mathrm{a_o} + \mathrm{a_1}\log_{10}(d) + \mathrm{a_2}\log_{10}(h_t) + \mathrm{a_3}\log_{10}(h_t).\log_{10}(d) - 3.2\,[\log_{10}(11.75\,h_r)^2] + \mathrm{g}(f_c) \quad (\mathbf{21})$$

Where,

$$\mathrm{g}(f_c) = 44.49\log_{10}(f_c) - 4.78[\log_{10}(f_c)]^2 \quad (\mathbf{22})$$

The values of the parameters $(\mathrm{a_o}, \mathrm{a_1}, \mathrm{a_2}\ and\ \mathrm{a_3})$ for different types of terrain environments are presented in Table 2 (Zakaria et al., 2015).

Table 2: Parameter values of $(\mathrm{a_o}, \mathrm{a_1}, \mathrm{a_2}\ and\ \mathrm{a_3})$ for different environment area (Zakaria et al., 2015).

Environment	$\mathrm{a_3}$	$\mathrm{a_2}$	$\mathrm{a_1}$	$\mathrm{a_o}$
Urban	0.1	12.0	30.20	36.20
Rural	0.1	12.0	100.6	45.95
Suburban	0.1	12.0	68.93	43.20

3.MATERIALS AND METHOD

In order to predict the path loss model of cellular transmission, actual data measured on site is required. Here, a downlink data was collected on a given site of the Korek telecom transmitter antennas located at Gazna village near center of the Erbil city which is characterized by desert land region with small sized building and low population. The materials that are used for this study included Ericsson Test Mobile System (TEMS) investigator software, mobile phone handset complete with charger and other require equipment with a laptop. Moreover, the signals frequencies operating in 1800 MHz and 2100 MHz were taken into consideration in this work. The experimental data were obtained by locating the drive tests on the mentioned sites located in rural environment near the Erbil city. The procedure for measuring signal strength for both GSM operation frequencies were obtained through these drive tests
conducted along a given selected route in the mentioned village and is topographically shown in Figure 1.

The mobile phone handset was used to identify the signal strength during the data collection steps. The received power signal strength was recorded starting from a distance of 250 m from the mobile base station and along the displayed route from the site up to a distance of about two kilometers. The equipment for the drive test was placed in a vehicle maintained at an average speed of 30 $\frac{km}{h}$ and mobile antenna height of the order of 1.5 m. The measured signal power is transferred to the TEMS log file in the laptop by using Ericsson mobile phones. Measurement was conducted in the company of Korek telecom technique team in November 2019. The coordinate for the tower site with its height, transmitting power as well as its antenna type are presented in Table 3.

Table 3: Simulation parameters of the selected Korek tower site.

Parameters	Antenna type	Tower location	Operation frequency (f)	Mobile antenna height (h_r)	Transmitter antenna height (h_t)	Base station transmitter power (P_t)
Specification	K-80010485	Gazna-B	**1.8** GHz **2.1** GHz	**1.5** m	**23** m	**43** dBm

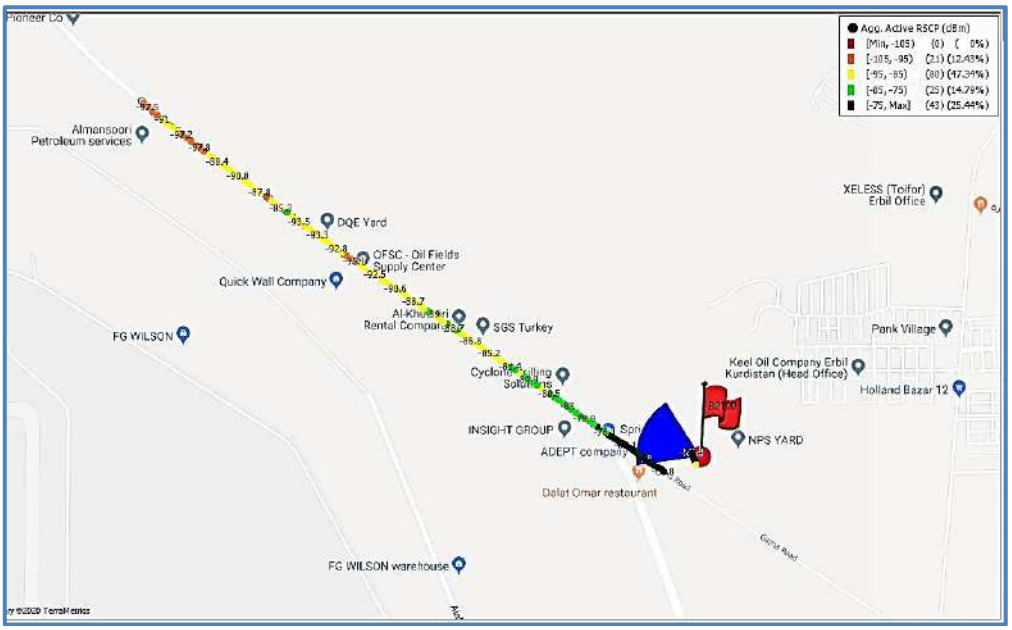

Figure 1. Log file representing the received signal level distribution in Gazna area.

4.RESULTS

The measured received signal strength values during the drive test in the mentioned environment and at both operating frequencies are presented in Figure 2. On the other hand, the signal path loss values was also evaluated through the measured received signal strength power using eq.(1) and the results are displayed in Figure 3. In addition, the path loss value that is measured by (Akinyemi et al., 2015) in Nigeria for the similar environment are also presented on the same figure.

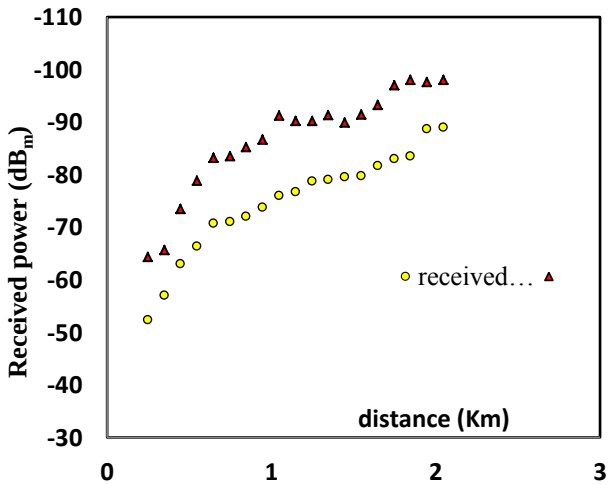

Figure 2. Measured signal strength versus distance from the transmitting tower of height h_t =23 m.

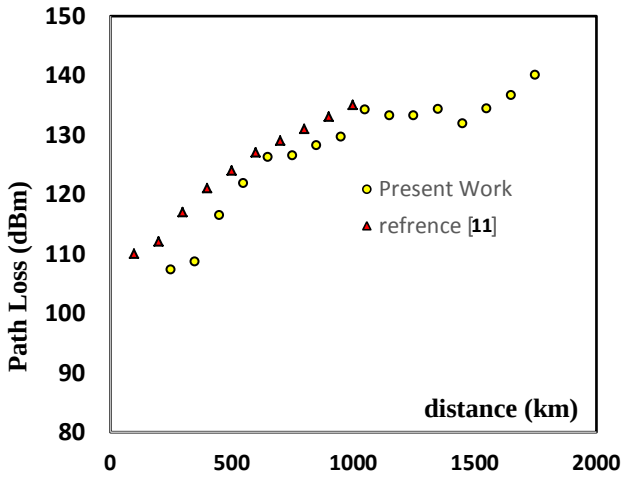

Figure 3. Variation of measured path loss with distnace away from the base station at frequency operation of 2100 MHz

Moreover, specification of the suitable employed empirical model also has been performed by comparing their predicted pathloss to those measured practically. For this purpose, all of the mentioned models with their formula equations have been unified together in a MATLAB computer program. The computed values for the mentioned path loss prediction models were identified using equations (2), (3), (4), (10), (16), (18) and (21). The computation results of the path loss values estimated by these models and those measured practically by equation (1) are determined through a developed MATLAB code simulation and are shown together on the path loss distributed graph as shown in Figures 4a and 4b for frequency operation of 1800 MHz and 2100 MHz, respectively.

Furthermore, the most accurate identification of the reliable model for predicting path loss in this environment can be identified more accurately by calculating the root means square error (RMSE) and mean absolute percentage error (MAPE) for each model against measured values. These two parameters were evaluated by using the following mathematical expression as given by (Erceg et al., 1999). and the results of the comparison are presented in Table 4.

$$\mathbf{RMSE} = \frac{\mathbf{1}}{\mathbf{n}}\sum_{\mathbf{t=1}}^{\mathbf{n}}\sqrt{(\mathbf{P}_{mt} - \mathbf{P}_{Rt})^{\mathbf{2}}} \qquad (\mathbf{24})$$

$$\mathbf{MAPE} = \frac{\mathbf{1}}{\mathbf{n}}\sum_{\mathbf{t=1}}^{\mathbf{n}}\left|\frac{(\mathbf{P}_{mt}-\mathbf{P}_{Rt})}{\mathbf{P}_{mt}}\right| \times \mathbf{100}\% \qquad (\mathbf{25})$$

where: P_{mt} is the mean value of measured data, P_{Rt} is the mean value of predicted path loss values and (n) is the number of data points (Fesseha, 2018). The computed results of these two parameters are also displayed in the form of histogram as shown in Figures 5.

Table 4: Performance of different path loss models at operating frequency of [1.8 and 2.1] GHz

No.	Model	[1.8] GHz		[2.1] GHz	
		RMSE	MAPE	RMSE	MAPE
1.	FS-Model	39.65	1.31	29.04	0.95
2.	ECC-33	37.91	1.27	29.48	0.97
3.	SUI	12.06	0.49	1.85	0.07
4.	Opt. Cost231	14.00	0.55	4.31	0.16
5.	Okumura - Hata	15.30	0.74	26.4	1.33
6.	Egli	112.71	2.56	102.10	2.31
7.	Ericson	31.28	1.17	20.20	0.78

5.DISCUSSION

The results of figures 2 and 3 indicate that the signal strength power and path loss values decrease with increasing distance from the tower and also with increasing frequency of operation. In addition, it is evident to note from these two figures that there was no signal reception beyond 2 km. In addition, the comparison of the measured path loss values in our region and those measured by (Akinyemi et al., 2015) at the operation frequency of 2100 MHz indicate the accuracy of our measurement procedure.

Figures 4a & 4b, display that the path loss is seen to increase with distance away from the base station and with the use of all investigated models but in different behavior. Generally, the computed results presented in these two figures implies that the path loss that estimated by Egli and ECC-33 models are overestimated while those obtained by Okamura-Hata and FSPL models are underestimated compare to path loss values measured experimentally. Moreover, it is clearly seen from Figure 4 that the path loss values obtained with SUI and Optimized-Cost-231followed by Ericson models are very close to those measured experimentally at both operating frequencies. From the results presented in Table 4, and those shown in Figure 5, one clearly observes that the SUI and Optimized-Cost-231 are provide the lowest percentage error values at both operational frequencies regarded in this investigation. In addition, the Egli models followed by free space model showed the highest RMSE and MAPE value. Hence the SUI model which provide minimum error percentage can be considered as a best candidate and most reliable model for use in rural environment of Erbil city in the Kurdistan region of Iraq for planning and designation of any network system for such areas.

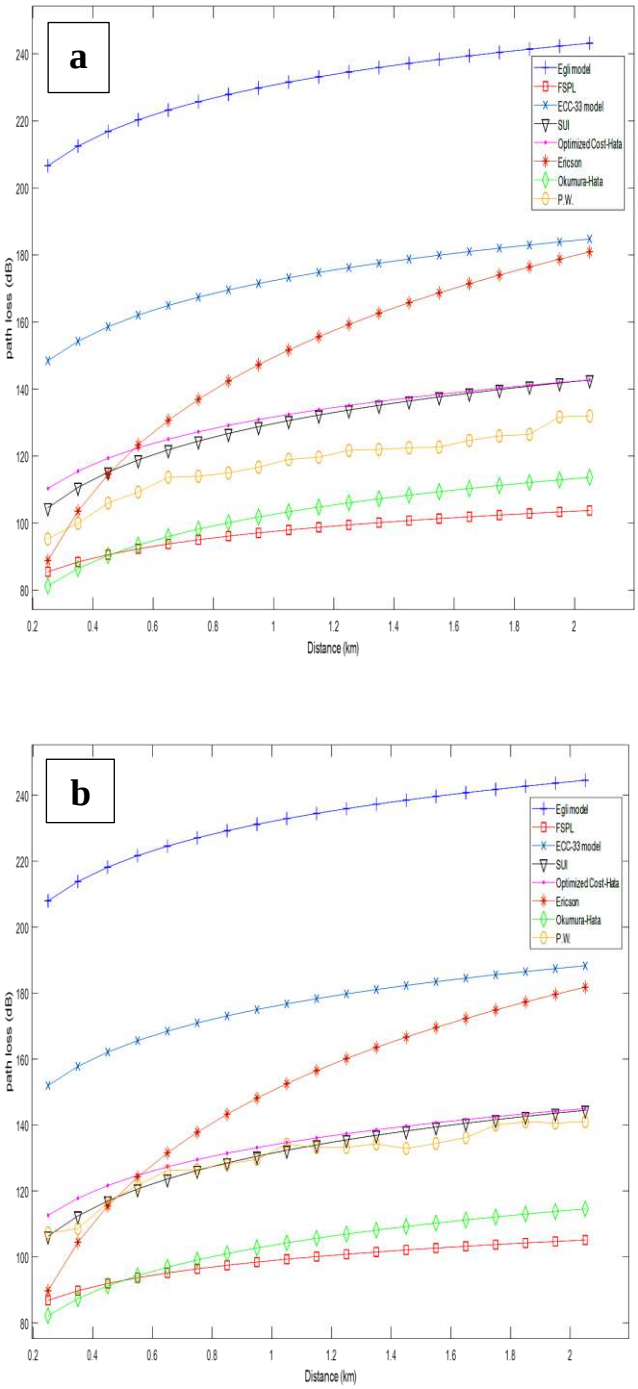

Figure 4. Comparison between measured and different empirical path loss model calculation versus distance from the transmitting tower antenna operating at: (a) 1.8 GHz and (b) 2.1 GHz.

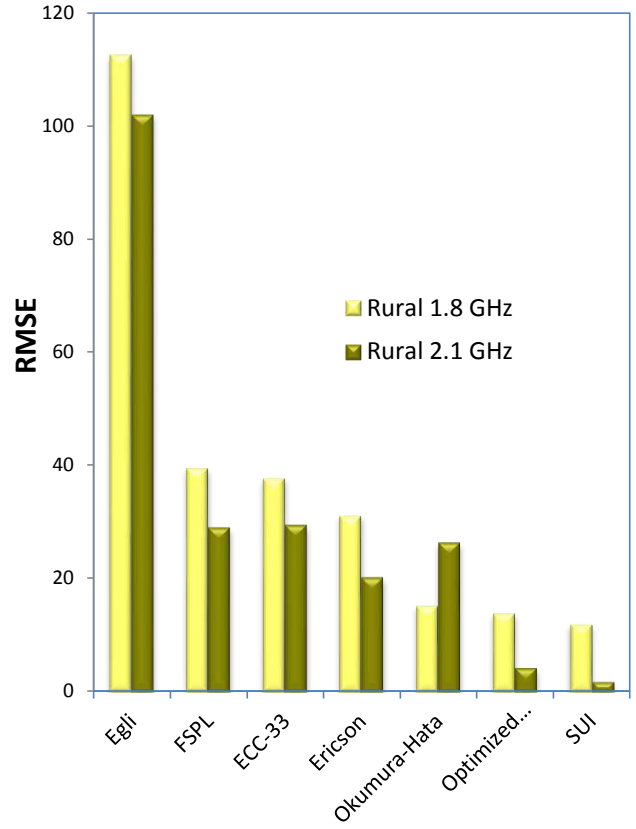

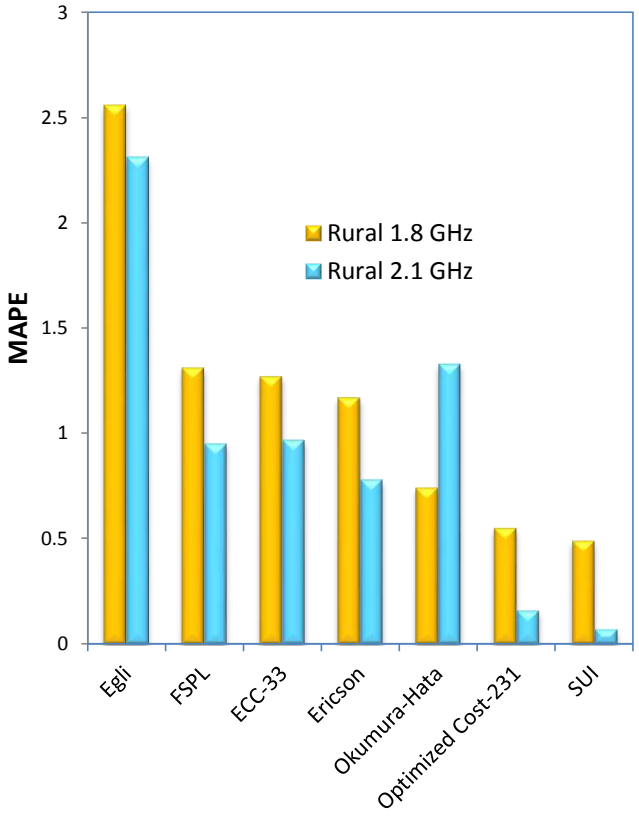

Figure 5. Histogram representation of RMSE and MAPE with the use of different path loss models and at 1800 MHz and 2100 MHz

6.CONCLUSIONS

It was clearly seen from the results of this investigations that the radio wave propagation path loss increases with increasing distance away from the base station and operational frequencies. In addition, the measurement results indicate that the signal strength is dropped completely beyond about 2 km far from the base station. It is also evident from the computed results that the path loss values that predicted by SUI followed by Optimized-Cost-231 were in good agreement with those measured experimentally. Since, the MAPE values provided by SUI are 0.49 and 0.07, while for Optimized-Cost-231 are 0.55 and 0.16 at operation frequencies 1800 MHz and 2100 MHz, respectively. In addition, the computed results indicate that the Egli followed by ECC-33 models are generally overestimated path losses while FSPL and Okamura-Hata models are underestimated path loss values.

Therefore, it can be said that the SUI followed by Optimized-Cost-231 are best candidate models for predicting signal path loss successfully and

can be employing them confidently in the network planning and designing problems for wireless communication system in rural area of the city under consideration.

Acknowledgements

I would like to thank "**Korek Telecom company"** with their test derive technical team staff which helping us in measuring signal strength in the area under consideration with all necessary equipment required for this purpose.

Conflict of Interest

There is no any conflict of interest and any funding sources of this research

7.REFERENCE

Singh, Y., 2012. Comparison of Okumura, Hata and COST-231 Models on the Basis of Path Loss

and Signal Strength. International Journal of Computer Applications, pp.37-41.

Akande, A.O., Semire, F.A. & Adeyemo, Z.K., 2017. Performance Analysis and Optimization of Cost-231 - Hata Model for Mobile Communication in Nigeria. International Journal of Computer Applications, 173(6), pp.4-9.

Omolaye, O.P., Igwue, G.A., Akpakwu, G.A., 2015. Okumura-Hata: A Perfect Model For Driving Route UHF Investigation, American Journal Of Engineering Research, 4(9), pp.139-147.

Mardeni, R. & Priya, T.S., 2010. Optimised Cost-231 Hata Models for WiMAX Path Loss Prediction in Suburban and Open Urban Environments. Modern Applied Science, 4(9), pp.75-89.

Kamboj, V., Gupta, D.K. & Birla, N., 2011. Comparison Of Path Loss Models For Wimax In Rural Environment At 3.5 GHZ. International Journal of Engineering Science and Technology, 3(2), pp.1432-37.

Akinwole, B.O.H. & J.J, B., 2013. Comparative Analysis of Empirical Path Loss Model for Cellular. American Journal of Engineering Research (AJER), 02(08), pp.24-31.

Ghosh, P.M., Hossain, M.A., Abadin, A.Z., Karmakar, K.K., 2012. Comparison Among Different Large Scale Path Loss Models for High Sites in Urban, Suburban and Rural areas, International Journal of Soft Computing and Engineering (IJSCE), 2(2), pp. 287-290.

Sharma, P.K., 2011. Comparative Study of Path Loss Models Depends on Various Parameters, International Journal of Engineering Science and Technology, 3(6), pp.4683-4690.

Imoize, A.L. & Oseni, A.I., 2019. Investigation And Path loss Modeling Of Fourth Generation Long Term Evolution Network Along Major Highways In Lagos Nigeria. Ife Journal Of Science, 21(1), pp.039-60

Oluwafemi, I.B. & Femi-Jemilohun, O.J., 2018. Suburban Area Path Loss Propagation Prediction and Optimization at 900 and 1800 MHz. Journal of Engineering and Applied Sciences, 13(9), pp.2521-29.

Akinyemi, P., Azi, S.O., Ojo, J.S. & Abiodun, C.I., 2015. Evaluation for suitable propagation model to mobileCommunications in South-South Nigeria urban terrain. American Journal of Engineering Research (AJER), 4(4), pp.1-5.

Khan, I. & Kamboh, S.A., 2012. Performance Analysis of Various Path Loss Models for Wireless Network in Different Environments. International Journal of Engineering and Advanced Technology (IJEAT), 2(1), pp.161-65.

Bola, G.S. & Saini, G.S., 2013. Path Loss Measurement and Estimation Using Different Empirical Models For WiMax In Urban Area. International Journal of Scientific & Engineering Research, 4(5), pp.1421-28.

Chebil, J., Lawas, A.K. & Rafiqul Islam, M.D., 2013. Comparison Between Measured and Predicted Path Loss for Mobile Communication in Malaysia. World Applied Sciences Journal (Mathematical Applications in Engineering), 21, pp.123-28.

Milanovic, J., Rimac-Dirlje, S. & Bejuk, K., 2007. Comparison of Propagation Model Accuracy for WiMax on 3.5GHz. 14th IEEE International Conference on Electronic Circuits and Systems, 8(7), pp.111-14.

Sharma, P.K. & Singh, R.K., 2010. Comparative Analysis of Propagation Path loss Models with Field Measured Data. International Journal of Engineering Science and Technology, 2(6), pp.2008-2013.

Fesseha, N., 2018. Fine-tuning of Cost-231 Hata Path Loss Model for LTE Network: The Case of 4 Kilo Area. Ethiopia: Addis Ababa University.

Erceg, V., Greenstein, L.J. & Tjandra, S.Y., 1999. An Empirically Based Path Loss Model for Wireless Channels in Suburban Environments. IEEE Journal On Selected Areas In Communications, 17(7), pp.1205-11.

Shebani, N.M., Mohammed, A.E., Mosbah, M.A. & Hassan, Y.A., 2013. Simulation and Analysis of Path Loss Models for WiMax Communication System. In Conference: The 3rd International Conference on Digital Information Processing and Communications. Dubai, UAE, January 2013. SDIWC.

Imoize, A.L. & Ogunfuwa, T.E., 2019. Propagation Measurements of a 4G LTE Network in Lagoon Environment. Nigerian Journal of Technological Development, 16(1), pp.1-9.

Oudira, H., Djouane, L. & Garah, M., 2019. Optimization of Suitable Propagation Model for Mobile Communication in Different Area. International Journal of Information Science & Technology, 3(3), pp.10-19.

Zakaria, Y., Hosek, J. & Misurec, J., 2015. Path Loss Measurements for Wireless Communication in Urban and Rural Environments. American Journal of Engineering and Applied Sciences, 8(1), pp.94-99.

ZANCO Journal of Pure and Applied Sciences
The official scientific journal of Salahaddin University-Erbil
https://zancojournals.su.edu.krd/index.php/JPAS

ISSN (print):2218-0230**, ISSN (online):** 2412-3986**, DOI: http://dx.doi.org/10.21271/zjpas**

RESEARCH PAPER

Darboux and rational first integrals for a family of cubic three dimensional system

Sarbast H. Mikaeel [1], Azad I. Amen [2,*,⋆]

[1] Department of Mathematics, Faculty of Science, Soran University, Kurdistan Region, Iraq.
[2] Department of Mathematics, College of Basic Education, Salahaddin University, Kurdistan Region, Iraq.
[*]Department of Mathematics, Faculty of Science, Soran University, Kurdistan Region, Iraq.
[⋆]Department of Mathematics, College of Basic Education, University of Raparin, Kurdistan Region, Iraq.

A B S T R A C T:
In this paper, we investigate the first integrals of the following system

$$\dot{x} = y, \quad \dot{y} = z, \qquad \dot{z} = b_1 x + b_2 y x^2 + b_3 z^3 \tag{1}$$

where $b_1 \in \mathbb{R}$ and $b_2,\ b_3 \in \mathbb{R}/\{0\}$. This kind of system is a special case of three-dimensional polynomial cubic differential systems. Generally, several methods can be used to investigate the first integrals, but unfortunately, most of them are not enabled for finding first integrals. In this study, the Darboux method has been used to study the first integrals for the generalized system for all parameters. We characterize all its invariant algebraic surfaces and all its exponential factors of that system. We have shown that the above system does not admit a polynomial, rational, and Darboux first integrals for any values of the parameters.

KEY WORDS: Draboux First Integral; Invariant Algebraic Surfaces; Exponential Factor; Rational First integral.

DOI: http://dx.doi.org/10.21271/ZJPAS.33.2.13
ZJPAS (2021) , 33(2);139-146 .

1.INTRODUCTION

Investigating the first integrals is one of the most famous problems in qualitative theory for three-dimensional polynomial differential systems, because the knowledge of first integrals of a differential system can be very useful in order to understand and simplify the study of the dynamics of the system. In 1878, Darboux (Darboux, G., 1878a, Darboux, G., 1878b) presented a new simple method to construct first integrals and integrating factors for the planar polynomial vector field using their invariant algebraic curves. The author showed how the first integrals of polynomial vector fields in $\mathbb{R}^2$ or $\mathbb{C}^2$ possessing sufficient invariant algebraic curves which can be constructed.

In 1979 Jouanolou expanded the planar polynomial differential system into higher-dimensional, especially for rational first integrals. Existencing first integrals of Draboux type based on the existence of invariant algebraic surfaces and exponential factors. This kind of integrability has been successfully applied to study some physical models (see for instance(Jalal, A.A. et al., 2020, Barreira, L., et al., 2020, Llibre, J. and Zhang, X., 2009b, Llibre, J. and Valls, C., 2005a Llibre, J. and Valls, C., 2010c Llibre, J. and Valls, C., 2005a, Llibre, J. and Valls, C., 2007b, Valls, C., 2005)), limit cycles, centers and bifurcation problems of polynomial differential systems (see for instance (Giné, J. and Llibre, J., 2005, Llibre, J. and Rodrıguez, G., 2004, Schlomiuk, D., 1993)). The key existing and non existing of Darboux first integrals depend on exponential factors and

* **Corresponding Author:**
Sarbast H. Mikaeel
E-mail: sarbast.mikael@soran.edu.iq
Article History:
Received: 12/11/2020
Accepted: 17/02/2021
Published: 18/04/2021

invariant algebraic surfaces. More information about this method can be found in (Llibre, J. and Zhang, X., 2009a, Llibre, J. and Zhang, X., 2009a).

Now we apply the Darboux method for investigating the existence of analytic first integrals in one of the families of differential systems which for some values of the parameters exhibit chaos. More precisely, we study the Darboux first integral of the following three-dimensional differential system

$$\begin{aligned} \dot{x} &= y, \\ \dot{y} &= z, \\ \dot{z} &= b_1 x + b_2 y x^2 + b_3 z^3, \end{aligned} \tag{3}$$

where $b_1 \in \mathbb{R}$ and $b_2, b_3 \in \mathbb{R}/\{0\}$.
The above system has been reported in (Sprott, J.C., 1997), the author verifies the chaotic behaviours for system (3), where $0 < b_1 < 1$ and $b_2 = b_3 = -1$. The existence of sufficiently first integrals determines completely its phase portrait in a complete way for differential equations. Many different methods have been used for studying the existence of first integrals for polynomial systems. Generally, for a given differential system, it is a difficult problem to determine the existence or nonexistence of a first integral. For a given polynomial system. This paper aims to study the polynomial, rational, and the Darboux integrability of the system (3). This kind of integrability will be studied by using the Darboux theory of integrability, for more details see (Dumortier, F., et al. 2006) and (Llibre, J. and Zhang, X., 2009a, Llibre, J. and Valls, C., 2005a).

2. PRELIMINARIES

Firstly, we denote a vector field for the differential system (3) as follows

$$X = y\frac{\partial}{\partial x} + z\frac{\partial}{\partial y} + (b_1 x + b_2 y x^2 + b_3 z^3)\frac{\partial}{\partial z}.$$

Suppose that $\mathcal{W}$ be an open dense subset of $\mathbb{R}^3$. Let $\mathcal{H}: \mathcal{W} \to \mathbb{R}$ be $\mathcal{C}^1$. Then $\mathcal{H}$ is the first integral of vector field X in $\mathcal{W}$ if $\mathcal{H}$ is a constant on the solutions of system (3) contained in $\mathcal{W}$; i.e. if

$$X\mathcal{H} = y\frac{\partial \mathcal{H}}{\partial x} + z\frac{\partial \mathcal{H}}{\partial y} + (b_1 x + b_2 y x^2 + b_3 z^3)\frac{\partial \mathcal{H}}{\partial z} = 0, \tag{4}$$

for all $(x, y, z) \in \mathcal{W}$.

We say that $h(x, y, z) = 0$ is an invariant algebraic surface (Darboux polynomial) of the system (3) where $h \in \mathbb{C}[x, y, z]\backslash\mathbb{C}$ if there exists $\mathcal{K} \in \mathbb{C}[x, y, z]$ such that

$$Xh = y\frac{\partial h}{\partial x} + z\frac{\partial h}{\partial y} + (b_1 x + b_2 y x^2 + b_3 z^3)\frac{\partial h}{\partial z} = \mathcal{K}h \tag{5}$$

where $\mathcal{K}$ is called the cofactor of degree at most two.
A non-constant function $E = e^{g/h}$ is called an exponential factor of the polynomial system (3) if the following equation is satisfied

$$XE = y\frac{\partial E}{\partial x} + z\frac{\partial E}{\partial y} + (b_1 x + b_2 y x^2 + b_3 z^3)\frac{\partial E}{\partial z} = \mathcal{L}E \tag{6}$$

where $g, h \in \mathbb{C}[x, y, z]$ are coprime polynomail and $\mathcal{L}$ is cofactor of the exponential factor with the degree of cofactors is almost two.

The next result explaining that how to find Darboux first integrals. The prove of the following theorem can be found in (Dumortier, F., et al. 2006).

Theorem 1. Assume that a polynomial vector field X of degree d in $\mathbb{C}^3$ admits p irreducible invariant algebraic surfaces $h_i = 0$; such that the h_i they are pairwise relatively coprimes with cofactors $\mathcal{K}_i$ for $i = 1, \dots, p$ and q exponential factors $E_i = e^{\frac{g_j}{h_j}}$ with cofactors $\mathcal{L}_j$ for j 1, … , q.
There exist λ_i and μ_j not all zero such that

$$\sum_{i=1}^{p} \lambda_i \mathcal{K}_i + \sum_{j=1}^{q} \mu_j \mathcal{L}_j = 0 \tag{7}$$

if and only if the (multi-valued) function

$$h_1^{\lambda_1} h_2^{\lambda_2} \dots h_p^{\lambda_p} \left(E_1^{\mu_1} E_2^{\mu_2} \dots E_q^{\mu_q}\right) \tag{8}$$

is a first integral for X.

Darboux first integral is the first integral that can be obtained from equation (8). A polynomial first integral in the polynomial form. A rational function is called rational first integral if it is satisfied equation (4).

The following theorem has been proven in (Llibre, J. and Zhang, X., 2009a, Llibre, J. and Valls, C., 2005a) will be helpful to investigate the exponential factor of the system (3).

Theorem 2. The following statements hold.

a. If $e^{\frac{g}{h}}$ is an exponential factor for the polynomial differential system (1) and g is not a constant polynomial, then h = 0 is an invariant algebraic surface.
b. Ultimately e^{g} can be an exponential factor, derived from the multiplicity of the infinity invariant plane.

Theorem 3. Let X be a polynomial vector field defined in $\mathbb{C}^n$ of degree $d > 0$. Then X admits $\binom{d+n-1}{n} + n$ irreducible invariant algebraic hypersurfaces if and only if X has a rational first integral.

3. RESULTS AND THEIR PROOF

In this section, we will prove that the system has no Darboux first integral nither rational first integral. The existence and nonexistence of invariant algebraic surfaces play an important role in studying the Darboux type of the first integral for any differential system. Finally, we have found that the system (3) has no Draboux polynomial nither rational first integral.

Proposition 4. System (3) does not admit Draboux polynomials.

Proof. Let $h = \sum_{i=1}^{n} h_i\ (x, y, z)$ be a Darboux polynomial of the system (3), and $h_i(x, y, z)$ be a non zero homogeneous polynomial of degree i, for $i = 1, \dots, n$. Since the system is cubic, then we can assume $\mathcal{K}$ of the following form $\mathcal{K} = k_0 + k_1x + k_2y + k_3z + k_4x^2 + k_5xy + k_6xz + k_7y^2 + k_8yz + k_9z^2$, for some $k_i \in \mathbb{R}$, and $j = 0, \dots, 9$. Then, equation (5) must satisfy the following equation

$$y\frac{\partial h}{\partial x} + z\frac{\partial h}{\partial y} + (b_1x + b_2yx^2 + b_3z^3)\frac{\partial h}{\partial z} = (k_0 + k_1x + k_2y + k_3z + k_4x^2 + k_5xy + k_6xz + k_7y^2 + k_8yz + k_9z^2)h \quad (9)$$

Counting the terms of degree $n + 2$ in equation (9), we have

$$(b_2yx^2 + b_3z^3)\frac{\partial h_n}{\partial z} = (k_4x^2 + k_5xy + k_6xz + k_7y^2 + k_8yz + k_9z^2)h_n.$$

Solving the above differential equation, we obtain

$$h_n = S_n(x,y)\,(b_2x^2y + b_3z^3)^{\frac{k_9}{3b_3}} \left(\frac{\sqrt{z^2 - z\sqrt[3]{\frac{b_2yx^2}{b_3}} + \left(\sqrt[3]{\frac{b_2yx^2}{b_3}}\right)^2}}{z + \sqrt[3]{\frac{b_2yx^2}{b_3}}}\right)^{A(x,y)} \quad (10)$$

$$exp\left(\frac{1}{\sqrt{3}}arctan\left(\frac{2}{3}\frac{\sqrt{3}z}{\sqrt{\frac{b_2yx^2}{b_3}}} - \frac{\sqrt{3}}{3}\right)\frac{k_6x\sqrt[3]{\frac{b_2yx^2}{b_3}} + k_8y\sqrt[3]{\frac{b_2yx^2}{b_3}} + k_4x^2 + k_5xy + k_7y^2}{b_3\left(\sqrt[3]{\frac{b_2yx^2}{b_3}}\right)^2}\right)$$

where $S_n(x, y)$ is an arbitrary polynomial and

$$A(x,y) = \frac{k_6x\sqrt[3]{\frac{b_2yx^2}{b_3}} + k_8y\sqrt[3]{yx^2} - k_4x^2 - k_5xy - k_7y^2}{b_3\left(\sqrt[3]{\frac{b_2yx^2}{b_3}}\right)^2}.$$

Since h_n is a polynomial of degree n, it is required that $k_4 = k_5 = k_6 = k_7 = k_8 = 0$ and $k_9 = 3mb_3$, for some positive integer m. Now, we give terms of degree $n + 1$ in equation (9) and we find that

$$(b_2yx^2 + b_3z^3)\frac{\partial h_{n-1}}{\partial z} = (k_1x + k_2y + k_3z)h_n + (3mb_3z^2)h_{n-1}.$$

Solving the above differential equation we obtain

$$h_{n-1} = \frac{P(x,y,z)T(x,y)}{\sqrt{3}}$$

$$arctan\left(\frac{1}{\sqrt[3]{\frac{b_2yx^2}{b_3}}}\left(-2z+\sqrt[3]{\frac{b_2yx^2}{b_3}}\right)\right)$$

$$-3\mathrm{P}(x,y,z)\ b_3\ S_{n-1}(x,y)$$

$$\left(\sqrt[3]{\frac{b_2yx^2}{b_3}}\right)^2 + \frac{P(x,y,z)V(x,y)}{2}$$

$$\ln\left(\frac{z^2 - z\sqrt[3]{\frac{b_2yx^2}{b_3}} + \left(\sqrt[3]{\frac{b_2yx^2}{b_3}}\right)^2}{\left(z+\sqrt[3]{\frac{b_2yx^2}{b_3}}\right)^2}\right)$$

where

$$P(x,y,z) = -\frac{(b_2yx^2+b_3z^2)}{3b_3\left(\sqrt[3]{\frac{b_2yx^2}{b_3}}\right)^2}$$

$$T(x,y) = S(x,y)\left(k_1x + k_2y + k_3\sqrt[3]{\frac{b_2yx^2}{b_3}}\right)$$

$$V(x,y) = S(x,y)\left(k_1x + k_2y - k_3\sqrt[3]{\frac{b_2yx^2}{b_3}}\right)$$

and $S_{n-1}(x,y)$ is an arbitrary polynomial. Since h_{n-1} is a polynomial then either $S_n(x,y) = 0$, or $k_1 = k_2 = k_3 = 0$. If $S_n(x,y) = 0$, then we obtain $h_n = 0$, which is a contradiction, they must be $k_1 = k_2 = k_3 = 0$. Thus we have

$h_{n-1} = (b_2x^2y + b_3z^3)^m\ S_{n-1}(x,y)$.

Finally, calculating the terms of degree n in equation (9) gives the following equation

$$y\frac{\partial h_n}{\partial x} + z\frac{\partial h_n}{\partial y} + b_1x\frac{\partial h_n}{\partial z} + (b_2yx^2 + b_3z^3)\frac{\partial h_{n-2}}{\partial z} = k_0\,h_n + 3mz^2h_{n-2}.$$

Solving the above differential equation, we have

$$h_{n-2} = (3mb_1yx^2 - mxz^2 - 2my^2z)$$

$$S_n(x,y)A_1(x,y,z) - \frac{1}{3}x\sqrt[3]{\frac{b_2yx^2}{b_3}}A_2(x,y,z)$$

$$A_1(x,y,z)\left(S_nm + 3y\frac{\partial S_n}{\partial y}\right)(b_2x^2y + b_3z^3)$$

$$+\left(k_0xy - \frac{4m}{3}y^2 - xy^2\frac{\partial S_n}{\partial x}\right)A_1(x,y,z)$$

$$A_3(x,y,z) + (b_2x^2y + b_3z^3)^m S_{n-2}(x,y),$$

where $S_{n-2}(x,y)$ is an arbitrary polynomial and

$$A_1(x,y,z) = \frac{(b_2x^2y+b_3z^3)^{m-1}}{3\,b_3xy\left(\sqrt[3]{\frac{b_2yx^2}{b_3}}\right)^2},$$

$$A_2(x,y,z) = \sqrt{3}\arctan\left(\frac{2}{\sqrt{3}}\frac{z}{\sqrt[3]{\frac{b_2yx^2}{b_3}}} - \frac{1}{\sqrt{3}}\right) + ln\left(\frac{\sqrt{z^2 - z\sqrt[3]{\frac{b_2yx^2}{b_3}} + \left(\sqrt[3]{\frac{b_2yx^2}{b_3}}\right)^2}}{z+\sqrt[3]{\frac{b_2yx^2}{b_3}}}\right),$$

$$A_3(x,y,z) = \sqrt{3}\,arctan\left(\frac{2}{\sqrt{3}}\frac{z}{\sqrt[3]{\frac{b_2yx^2}{b_3}}} - \frac{1}{\sqrt{3}}\right) + ln\left(\frac{z+\sqrt[3]{\frac{b_2yx^2}{b_3}}}{\sqrt{z^2 - z\sqrt[3]{\frac{b_2yx^2}{b_3}} + \left(\sqrt[3]{\frac{b_2yx^2}{b_3}}\right)^2}}\right).$$

Since $h_{n-2}(x,y,z)$ is a homogeneous polynomial, then we must have

$$k_0xy - \frac{4m}{3}y^2 - xy^2\frac{\partial S_n}{\partial x} = 0, \qquad (11)$$

and

$$S_n m + 3y\frac{\partial S_n}{\partial y} = 0. \qquad (12)$$

From equation (11) , we obtain

$$S_n(x,y) = \frac{S(y)e^{\frac{k_0x}{y}}}{\left(\sqrt[3]{x}\right)^{4m}}\ , \qquad (13)$$

where $S(y)$ is an arbitrary function. Now, by substituting equation (13) in equation (10) we obtain

$$h_n(x,y) = \frac{S(y)(b_2x^2y + b_3z^3)^m e^{\frac{k_0x}{y}}}{\left(\sqrt[3]{x}\right)^{4m}}$$

Since h_n is homogeneous polynomial, then we have $k_0 = m = 0$, then $k_9 = 0$. Thus $k_j = 0$, for $j = 0, 1, \dots, 9$. This gives that the system has no Darboux polynomial.

Proposition 5. System (3) has no polynomial first integrals.

Proof. Let $\mathcal{H}(x,y,z)$ be a polynomial first integral of the degree n of the system (3). We can write $\mathcal{H} = \sum_{i=1}^{n}\mathcal{H}_i\,(x,y,z)$, where each $\mathcal{H}_i$ is a homogenous polynomial in the variables x, y, and z and $\mathcal{H}_i \neq 0$ for $n \geq 1$. Thus, $\mathcal{H}$ is satisfied equation (4). Then by calculating the terms of degree n + 2 in equation (4), we obtain

$$(\,b_2yx^2 + b_3z^3)\frac{\partial \mathcal{H}_n}{\partial z} = 0.$$

Since b_2, b_3 are not zero, then form above differential equation we obtain $\mathcal{H}_n = \mathcal{H}_n(x,y)$. The terms of degree $n+1$ in equation (4), we have

$$(\,b_2yx^2 + b_3z^3)\frac{\partial \mathcal{H}_{n-1}}{\partial z} = 0,$$

Since b_2, b_3 are not zero, then we obtain $\mathcal{H}_{n-1} = \mathcal{H}_{n-1}(x,y)$. Again, computing the terms of the degree n in equation (4), we have

$$y\frac{\partial \mathcal{H}_n}{\partial x} + z\frac{\partial \mathcal{H}_n}{\partial y} + (b_1x + b_2yx^2 + b_3z^3)\frac{\partial \mathcal{H}_{n-2}}{\partial z} = 0.$$

Solving the above differential equation, we obtain

$$\mathcal{H}_{n-2} = A_4(x,y,z)\left(\frac{y}{\sqrt[3]{\frac{b_2yx^2}{b_3}}}\frac{\partial \mathcal{H}_n}{\partial x} + \frac{\partial \mathcal{H}_n}{\partial y}\right) + A_5(x,y,z)\left(\frac{\partial \mathcal{H}_n}{\partial y} - \frac{y}{\sqrt[3]{\frac{b_2yx^2}{b_3}}}\frac{\partial \mathcal{H}_n}{\partial y}\right) + S_1(x,y).$$

where $S_1(x,y)$ is an arbitrary polynomial and

$$A_4(x,y,z) = \frac{-1}{\sqrt{3}b_3\sqrt[3]{\frac{b_2yx^2}{b_3}}}\, arctan\left(\frac{1}{\sqrt{3}}\left(\frac{2z}{\sqrt[3]{\frac{b_2yx^2}{b_3}}} - 1\right)\right),$$

$$A_5(x,y,z) = \ln\left(\frac{\sqrt[3]{z + \sqrt[3]{\frac{b_2yx^2}{b_3}}}}{\sqrt[6]{z^2 - z\sqrt[3]{\frac{b_2yx^2}{b_3}} + \left(\sqrt[3]{\frac{b_2yx^2}{b_3}}\right)^2}}\right)^{\frac{1}{b_3\sqrt[3]{\frac{b_2yx^2}{b_3}}}}.$$

Since $\mathcal{H}_{n-2}\ (x,y)$ is a homogeneous polynomial. Then it must be

$$\frac{\partial \mathcal{H}_n}{\partial y} - \frac{y}{\sqrt[3]{\frac{b_2yx^2}{b_3}}}\frac{\partial \mathcal{H}_n}{\partial y} = 0,$$

then $\mathcal{H}_n = S\left(ln\ \frac{\left(b_2^2x^5 + b_2x^2y\left(\sqrt[3]{\frac{b_2yx^2}{b_3}}\right)^2\right)^{\frac{3}{5}}}{x^2}\right)$

This is a contradiction to our assumption that $\mathcal{H}_n$ be a homogeneous polynomial. This ends the proof of the proposition.

Proposition 6. The exponential factors of the system (3) are e^x, e^y, e^{x^2}, e^{y^2} and e^{xy} with cofactors y, z, $2xy$, $2yz$, and $y^2 + xz$, respectively.

Proof. From Proposition (4) and Theorem (2), we can write exponential factors of the system (3) by $= e^{g(x,y,z)}$, where $g(x, y, z)$ is a polynomial of its variables. Since system (3) is cubic, we must have a cofactor of the form $\mathcal{L} = s_0 + s_1x + s_2y + s_3z + s_4x^2 + s_5xy + s_6xz + s_7y^2 + s_8yz + s_9z^2$ for some $s_j \in \mathbb{C}$ and $j = 0,1, \dots, 9$. We write $g = \sum_{i=1}^{n} g_i(x, y, z)$, where each g_i is a homogeneous polynomial of degree i and assume that $g_n \neq 0$ for $n \geq 3$. Then E satisfy the following partial differential equation

$$y\frac{\partial e^g}{\partial x} + z\frac{\partial e^g}{\partial y} + (b_1x + b_2yx^2 + b_3z^3)\frac{\partial e^g}{\partial z} = \mathcal{L}e^g. \quad (14)$$

We simplify equation (14) to obtain

$$y\frac{\partial g}{\partial x} + z\frac{\partial g}{\partial y} + (b_1x + b_2yx^2 + b_3z^3)\frac{\partial g}{\partial z} = \mathcal{L}. \quad (15)$$

We compute the terms of degree n + 2 in equation (15) to obtain

$$(b_2yx^2 + b_3z^3)\frac{\partial g_n}{\partial z} = 0,$$

since $b_2, b_3 \in \mathbb{R}/\{0\}$, this implies that $g_n = g_n(x, y)$.

The terms of degree $n + 1$ in equation (15) give that

$$(b_2yx^2 + b_3z^3)\frac{\partial g_{n-1}}{\partial z} = 0,$$

since $b_2, b_3 \in \mathbb{R}/\{0\}$, then obtain $g_{n-1} = g_{n-1}(x, y)$.

Again we calculate the terms of the degree n in equation (15) to obtain

$$y\frac{\partial g_n}{\partial x} + z\frac{\partial g_n}{\partial y} + b_1x\frac{\partial g_n}{\partial z} + (b_2yx^2 + b_3z^3)\frac{\partial g_{n-2}}{\partial z} = 0.$$

Solving the above equation for g_{n-2}, we obtain

$$g_{n-2} = A_4(x,y,z)\left(\frac{y}{\sqrt[3]{\frac{b_2yx^2}{b_3}}}\frac{\partial g_n}{\partial x} + \frac{\partial g_n}{\partial y}\right) + A_5(x,y,z)\left(\frac{\partial g_n}{\partial y} - \frac{y}{\sqrt[3]{\frac{b_2yx^2}{b_3}}}\frac{\partial g_n}{\partial y}\right) + S_0(x,y),$$

where $S_0(x, y)$ is an arbitrary polynomial and

$$A_4(x,y,z) = \frac{-1}{\sqrt{3}b_3\sqrt[3]{\frac{b_2yx^2}{b_3}}} arctan\left(\frac{1}{\sqrt{3}}\left(\frac{2z}{\sqrt[3]{\frac{b_2yx^2}{b_3}}} - 1\right)\right),$$

$$A_5(x,y,z) = \ln\left(\frac{\sqrt[3]{z + \sqrt[3]{\frac{b_2yx^2}{b_3}}}}{\sqrt[6]{z^2 - z\sqrt[3]{\frac{b_2yx^2}{b_3}} + \left(\sqrt[3]{\frac{b_2yx^2}{b_3}}\right)^2}}\right)^{\frac{1}{b_3\sqrt[3]{\frac{b_2yx^2}{b_3}}}}.$$

Since g_{n-2} is a homogeneous polynomial. Then it must be

$$\frac{\partial g_n}{\partial y} - \frac{y}{\sqrt[3]{\frac{b_2yx^2}{b_3}}}\frac{\partial g_n}{\partial y} = 0,$$

then $g_n = S\left(ln\frac{\left(b_2^2x^5 + b_2x^2y\left(\sqrt[3]{\frac{b_2yx^2}{b_3}}\right)^2\right)^{\frac{3}{5}}}{x^2}\right)$.

Since g_n is a homogenous polynomial of degree n, then it must be $g_n = 0$, which is a contradiction. Then g must be a polynomial of the degree two satisfying equation (15). Suppose that

$$g(x,y,z) = \beta_0 + \beta_1 x + \beta_2 y + \beta_3 z + \beta_4 x^2 + \beta_5 xy + \beta_6 xz + \beta_7 y^2 + \beta_8 yz + \beta_9 z^2,$$

for some $\beta_k \in \mathbb{R}$, and $k = 0, \dots, 9$. Equation (14) yields

$$y\frac{\partial g}{\partial x} + z\frac{\partial g}{\partial y} + (b_1 x + b_2 y x^2 + b_3 z^3)\frac{\partial g}{\partial z} = s_0 + s_1 x + s_2 y + s_3 z + s_4 x^2 s_5 xy + s_6 xz + s_7 y^2 + s_8 yz + s_9 z^2,$$

solving the above equation when $b_2, b_3 \in \mathbb{R}/\{0\}$, then we have

Hence, $e^{s_2 x + s_3 y + \frac{1}{2}s_5 x^2 + \frac{1}{2}s_8 y^2 + s_7 xy}$ is the exponential factor with cofactor $s_2 y + s_3 z + s_5 xy + s_8 yz + s_7 y^2 + s_7 xz$. Then the result follows.

Theorem 7. System (3) has no Darboux first integrals.

Proof. Suppose that system (3) has a Darboux first integral. In viewing Proposition (4), system (3) does not admit invariant algebraic surface with non-zero cofactors and by Proposition (6) we have that system (3) has only five exponential factors e^x, e^y, e^{x^2}, e^{y^2} and e^{xy} with cofactors $y, z, 2xy, 2yz,$ and $y^2 + xz$, respectively. From equation (7), there exists $\mu_i \in \mathbb{R}$ not all zero for $i = 1, \dots, 5$ such that

$$\mu_1 y + \mu_2 z + 2\mu_3 xy + 2\mu_4 yz + \mu_5 (y^2 + xz) = 0,$$

the above equation has only one solution which is $\mu_1 = \mu_2 = \mu_3 = \mu_4 = \mu_5 = 0$. This is a contradiction to the Darboux theorey. Hence system (3) has no Darboux first integrals.

Corollary 8. System (3) has no rational first integrals.

Proof. Suppose that system (3) has a rational first integral. Observably, the vector filed associated system (3) is defined in $\mathbb{R}^3$ with degree (d = 3). By utilizing Theorem (3), we must have $\binom{5}{3} + 3$, invariant algebraic surfaces. According to Proposition (4), system (3) has no invariant algebraic surfaces. This means that the system has no rational first integrals.

4. CONCLUSION

In this paper, we have applied a Darboux method for studying polynomial, rational, and Darboux first integrals of a three-dimensional jerk cubic system (3). According the definitions of invariant algebraic surfaces and exponential factors, we found all invariant algebraic surfaces and exponential factors of that system. We have shown that system (3) has no invariant algebraic surface. Moreover, this system has five exponential factors. Depending on the Darboux theory, we proved that the system has no polynomial, rational, and Draboux first integrals.

5. REFERENCES

Barreira, L., Llibre, J. and Valls, C., 2020. Integrability and zero-Hopf bifurcation in the Sprott A system. *Bulletin des Sciences Mathématiques*, p.102874.

Dumortier, F., Llibre, J. and Artés, J.C., 2006. *Qualitative theory of planar differential systems*. Berlin: Springer.

Darboux, G., 1878a. Mémoire sur les équations différentielles algébriques du second ordre et du premier degré. *Bulletin des Sciences Mathématiques et Astronomiques*, *2*(1), pp.123-144.

Darboux, G., 1878b. De l'emploi des solutions particulières algébriques dans l'intégration des systèmes d'équations différentielles algébriques. *CR Math. Acad. Sci. Paris*, *86*, pp.1012-1014.

Giné, J. and Llibre, J., 2005. A family of isochronous foci with Darboux first integral. *Pacific journal of mathematics*, 218(2), pp.343-355.

Jalal, A.A., Amen, A.I. and Sulaiman, N.A., 2020. Darboux integrability of the simple chaotic flow with a line equilibria differential system. *Chaos, Solitons & Fractals*, 135, p.109712.

Jouanolou, J.P., 1979. Eouations de Pfaff algebriques sur un espace projectif. In *Equations de Pfaff algébriques* (pp. 80-135). Springer, Berlin, Heidelberg.

Llibre, J. and Rodrıguez, G., 2004. Configurations of limit cycles and planar polynomial vector fields. *Journal of Differential Equations*, 198(2), pp.374-380

Llibre, J. and Zhang, X., 2009a. Darboux theory of integrability in C^n taking into account the multiplicity. *Journal of Differential Equations*, *246*(2), pp.541-551.

Llibre, J. and Valls, C., 2005a. Integrability of the Bianchi IX system. *Journal of mathematical physics*, *46*(7), p.072901.

Llibre, J. and Valls, C., 2007b. On the integrability of the Einstein–Yang-Mills equations. *Journal of mathematical analysis and applications*, *336*(2), pp.1203-1230.

Llibre, J. and Valls, C., 2010c. The Michelson system is neither global analytic, nor Darboux integrable. Physica D: *Nonlinear Phenomena*, 239(8), pp.414-419.

Llibre, J. and Zhang, X., 2009b. Darboux theory of integrability for polynomial vector fields in R^n taking into account the multiplicity at infinity. *Bulletin des sciences mathematiques*, *133*(7), pp.765-778.

Schlomiuk, D., 1993. Algebraic particular integrals, integrability and the problem of the center. *Transactions of the American Mathematical Society*, 338(2), pp.799-841.

Sprott, J.C., 1997. Some simple chaotic jerk functions. *American Journal of Physics*, *65*(6), pp.537-543.

Valls, C., 2005. Rikitake system: analytic and Darbouxian integrals. *Proceedings of the Royal Society of Edinburgh Section A: Mathematics*, *135*(6), pp.1309-1326.